Conference proceedings

(book 5)

RGNF

5th congress in 2024
(biennial)

"Theory and application in geomathematics 2024"

5th Croatian geomathematical scientific congress

Geomatematička teorija i primjena 2024

V. hrvatski geomatematički kongres

održan na Rudarsko-geološko-naftnom fakultetu
Sveučilišta u Zagrebu

21. listopad 2024. godine

Skup su priredili:

Rudarsko-geološko-naftni fakultet
Sveučilišta u Zagrebu

Geomatematički odsjek
Hrvatskoga geološkog društva

Theory and application in geomathematics 2024

5th Croatian geomathematical congress

held on Faculty of Mining, Geology and Petroleum Engineering,

University of Zagreb

21st October 2024

Organised by:

RGNF

Facuty of Mining, Geology and Petroleum Engineering of the University of Zagreb

Geomathematical Section of the Croatian Geological Society

Geomatematička teorija i primjena 2024

ZBORNIK RECENZIRANIH RADOVA

IZDAVAČ:

Sveučilište u Zagrebu

RGNF

Rudarsko-geološko-naftni fakultet

Zagreb, 2024.

Theory and application in geomathematics 2024

PROCEEDINGS OF REVIEWED PAPERS

PUBLISHER:

University of Zagreb

RGNF

Faculty of Mining, Geology and Petroleum Engineering

Zagreb, 2024

Urednici

dr. sc. Zoran Kovač, izv. prof.

dr. sc. Tomislav Malvić, red. prof. u trajnom izb.

Izdavač
Sveučilište u Zagrebu Rudarsko-geološko-naftni fakultet

Za nakladnika
dr. sc. Vladislav Brkić, izv. prof. (dekan RGNF-a) ;

Programski i znanstveni odbor

Naklada u
obliku e-knjige

ISSN 3043-9736

Zbornik će biti indeksiran u bazama Petroleum Abstracts (Sveučilište u Tulsi),te u Google Schoolar (preko Hrvatske znanstvene bibliografije). Bit će predložen i za indeksaciju u bazi Scopus. Autori su odgovorni za jezični sadržaj, lekturu priloga i postupanje prema uputama autorima.

Zbornik je u cjelosti pripremljen korištenjem instalacije alata Open Monograph Press dostupnog na Portalu hrvatskih znanstvenih i stručnih časopisa Hrčak.

Editors

Dr. Zoran Kovač, Assoc. Prof.

Dr. Tomislav Malvić, Full Prof. tenured

Publishers

University of Zagreb Faculty of Mining, Geology and Petroleum Engineering

For publishers

Dr. Vladislav Brkić, Assoc. Prof.(Dean)

Copies
as e-book

ISBN 3043-9736

The proceedings will be indexed in Petroleum Abstracts (University of Tulsa) and Google Scholar (via Croatian scientific bibliography). It will be also proposed for indexation in the Scopus. Authors are solely responsible for contents, Croatian/English proofreading and formatting according to author's instruction.

The proceedings were prepared using the Open Monograph Press tool available on the Portal of Croatian scientific and professional journals HRČAK.

SADRŽAJ / CONTENT

5th Croatian geomathematical congress
UDC: 622.1; category: original scientific paper

Manual interpolation of different subsurface structures and application of numerical integration methods in volume calculations

Lorena Birko[1*]; Ivana Brajnović[1]; Maria Rudec[1]; Marko Uzelac[1]
[1] University of Zagreb, Faculty of Mining, Geology and Petroleum Engineering, Pierottijeva 6, HR 10000 Zagreb, Croatia ORCID: 0009-0009-5415-3954; 0009-0003-2296-5444; 0009-0000-6559-7213; 0009-0000-9261-9449
Corresponding author: lorena.birko@rgn.unizg.hr

Abstract

The two analysed hydrocarbon reservoirs in this paper were targets for creating the structural maps, which includestructural maps of the reservoir layers, isochore and isopach maps (from the hydrocarbon - water contact to both the reservoir's top and bottom). Each of the maps includes the base elements such as the title, corresponding scale, equidistance, legend, and an arrow pointing north. In addition to calculating the final reservoir volume, geological sections were made along the maps. Detailed analyses have shown which of the parameters affect the differences shown on the maps and how, while simultaneously pointing towards their similarities. The surface area was defined using linear interpolation with partial extrapolation, which in turn was used to calculate the total volume of the reservoir structure. These methods are based on numerical integration, two of which were used in this paper, namely the Simpson's and Trapezoidal rules. The analysed structures are described as irregular brachianticlines, which had to be identified both in the maps and in calculations to get the desired results.

Keywords: interpolation; volume; reservoir; brachianticline; Simpson's rule, Trapezoidal rule.

1. Introduction

A reservoir is a geomorphological structure saturated with oil, gas or geothermal water, which can be characterized by numerous conditions of genesis, the most significant of which are depth, temperature, pressure and surrounding layers whose primary purpose is to create traps preventing fluid migration. Furthermore, in the case of strctural traps the shapes of reservoirs can considerably vary, from the simplest domes to more irregular anticlines and ultimately brachianticlines. The goal of the paper is to create, analyse and compare two similar but not identical brachiantiklines using the structural maps of reservoirs's top and bottom, isochore and isopach maps, along with a geological sections. Volume calculations are made based on the aforementioned isopach maps. The maps were manually interpolated, for example like interpolation made on similar structures in Šapina (**2016**). One of the key characteristics of a reservoir structure is its volume, which requires extensive and detailed calculations. Since geological structures are generally not simple geometric shapes whose parameters can be interpreted with basic, primitive functions, to calculate their volume approximation methods based on numerical integration are used. Such methods have a vast role in numerous areas of mathematics, statistics, economics and engineering, with the two most prominent, the Simpson's rule and the Trapezoidal rule (e.g., **Malvić et al.**, **2014**). To improve the accuracy of reservoir volume calculation, both of the methods are used simultaneously, and their difference must not exceed 20 %. Volumes of the productive part of the layers are used in different cases, e.g. when calculating the storage capacity of CO_2 in sandstone in the western part of the Sava Depression (**Podbojec and Cvetković, 2015)** or other applications.

2. Methods

In the process of making and analysing the structural maps, numerous methods from the field of technical and natural sciences can be applied, with interpolation, planimetry and volume calculation being the most significant. Each of the methods is crucial for each step in the making of the maps and study in general. Initially, a certain number of specially distributed point data representing wells were given, the values of which were then interpolated to create structural maps mentioned above. Planimetry is a method which is directly linked to interpolation and is a technique used for measuring the surface area of a cross-section by tracing the bordering line of a section with a planimeter (e.g., **Malvić, 2015**). The last and perhaps the most important step, involves two approximation methods based on numerical integration, the Simpson's rule and the Trapezoidal rule, in an subsurface reservoir volume calculation. The shape of a geological structure such as a reservoir is usually approximated geometrically as a truncated cone, and the two taforementioned methods are used to calculate a similar a structure, with the goal of minimising errors of the final result.

2.1. Interpolation

Interpolation is, in the physical sense, defined as an approximation of numerical values of a function in a set points based on known surrounding values. Evaluation or interpolation is possible in one to three dimensions and applies to numerous scientific fields such as the natural sciences (**e.g., Grezio and Pinardi, 2006**), biotechnical sciences (e.g., **Galić, 2021**) and even in the humanistic sciences (e.g., **Čimin, 2013**). In underground mapping, interpolation is primarily used to draw lines connecting equal values on a map by allocating specific values to point data in an inter-well space (e.g., **Malvić, 2008).** For interpolation to be successful, it must be assumed that the values of surrounding, known points are sufficient to to accurately represent the value of a new, unknown point (**Davidović, 2016)**.

What is further, depending on the number of known data and their purpose, the same can be applied in geostatistics, where the most common applications are Inverse distance and Kriging. Linear interpolation is a multitude of methods, that provides the most accurate values of unknown points for the largest number of tested profiles of natural fields (e.g., **Kovač, 1982**). The Kriging is commonly, the most reliable method of interpolation when there is a known number of data on a narrow field (more than 20) and their relatively even spatial arrangement (**Malvić, 2008**). This interpolation method was developed by mining engineer D.G. Krige with the help of statistician H.S. Sichel for the needs of the mining industry in the early 1950s to improve the assessment of the ore reserves (e.g., **Davidović, 2016**). However, ths particular method requires compensation for the effects of data clustering, known as declusterization (e.g., **Mesić Kiš & Malvić, 2014**).

Considering all that was formerly mentioned and in terms of simplicity, the method of classic interpolation was used to analyse the maps in this paper. The spatial distribution of the wells was pre-determined, and in both cases almost equal, with 42 wells in structure 1 and 45 wells in structure 2. By increasing the number of input point data, errors in drawing the isolines are less likely to happen. To go along with interpolation, the method of extrapolation should not be overlooked. Similarly, it is a method based on approximation of point data values outside of the inter-well area.

2.2. Planimetry

The following method is planimetry, the method of determining the surface area of a bordered cross-section using a planimeter. It is typically used in basic planning when a selected cross-section is divided into equal elements whose surface areas are determined separately, and the final value is the sum of those elements (e.g., **Cindori Kovačević, 2016**). In this case, the surface area of our structural figure is defined by lines of equal thickness called isopachs, which are shown on isopach maps from contact to the reservoir's top and bottom.

A planimeter is an instrument that directly measures relative values (e.g., **Malvić, 2015**) by tracing the isolines bordering a specific figure, the absolute difference of which, multiplied by the conversion factor represents the surface area of the said figure. In this paper, planimetry is done using a polar planimeter (**Figure 1**) whose polar arm rotates around a weighted-down unmoving pole. The relative values are then read from the wheel brim and collected before and after the process.

The readings make up a four-digit number, each in the range 0-9 in a set order: the first digit is read from the biggest wheel and is measured between two digits pointed by an arrow, the smaller of which is chosen; the second digit is read on the perpendicular wheel, where the recorded value is a number pointed to by a zero on a perpendicular wheel; the third digit is read from the same wheel as the second and is a value od a fine line observed on a subscale from the perpendicular wheel, and finally the fourth digit which is read from the so-called nonius, a perpendicular wheel where the chosen value is shown on a corresponding line in a perpendicular subscale. As already stated, the absolute difference between the two relative values was calculated, which is finally multiplied by a conversion factor, defined by the scale of a map. The final numerical value is the surface area of the said figure from which the reservoir volume was calculated using numerical integration.

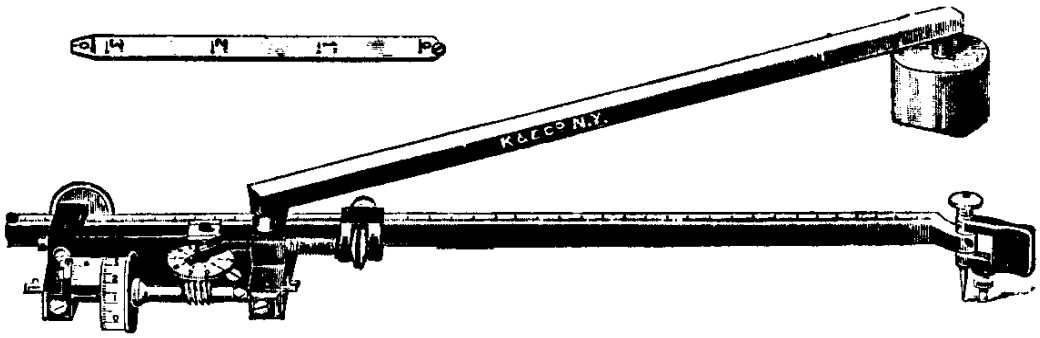

Figure 1: Polar planimeter (available at: https://www.leinweb.com/snackbar/planimtr/wheatley/s10-4.html).

2.3 Volume calculations

Calculation of the volume of an underground structure is one of the primary tasks in the reservoir geology and petroleum engineering. The shapes of all geological structures are irregular which greatly impacts their analytical and geometrical analysis. Generally, specific integration methods are used when calculating the surface area and volume of a geological structure,. Analytically speaking, integration is a method of determining a value using bordering parameters of a basic function. As it was previously stated, geological structures are not simple geometric shapes whose parameters can be defined using a basic function. This means that in order to calculate their volume based on numerical integration, methods must be applied that use a set, definite number of numerical values when integrating.

Historically, the term numerical integration was first used in 1915 in a study by David Gibbs (**Uddin & Kowsher, 2019**) which only notes its value in the mathematical field. Moreover, numerical integration is a simple term whose numerous methods are applicable in countless fields, such as mathematics, statistics, economics and engineering, but its value is the most notable for the field of geosciences. The two of the most notable numerical integration methods used in geosciences are the Simpson's rule and the Trapezoidal rule. Both of these methods originated from the fundamental and long-term Newton-Cotes method (**Uddin & Kowsher, 2019**). Newly developed methods such as the Simpson's and the Trapezoidal rule were developed to correct the errors of the previously used methods.

The Trapezoidal rule is an approximation of an integral using polynomials of the first order, or in geometric terms, it is an approximation of a surface area framed by the function's graph, a trapezoid with defined points. To eliminate large errors when applying the above rule, certain intervals are divided into smaller segments that are separately approximated. In this paper, the Trapezoidal rule is used in the case of an odd number of segments (or even case for the toppest segement), or an even number of isopachs for the calculation of the last, top segment of the structure. Everything withstanding, it is primarily used as a verification method in the final volume calculation.

Simpson's method, on the other hand, depending on the number of chosen segments, uses the polynomial of the second order (Simpson 1/3 rule, even number of segments). In this paper, the method is used with both an even and an odd number of segments and isopachs seeing as its accuracy is superior compared to the Trapezoidal method. These two methods are applicable in reservoir volume calculations when their irregular shape can be geometrically interpreted as a prismoidal, a figure whose points lie in one or two parallel planes, and when their values are equal across (**Malvić, 2015**). When considering the conventional structural traps, that approximating geometric figure is a truncated cone.

An acceptable difference in the calculation of reservoir volume, is considered to be a maximum of 20 %. This is the absolute difference between volumes calculated using both approximation methods.

3. Interpolation, planimetry and calculation of structure 1

Based on the given data, the following maps were created: a structural map of the reservoir's top and bottom, an isochore map, isopach maps from contact to the top and bottom, as well as a geological section, and finally the reservoir volume was calculated.

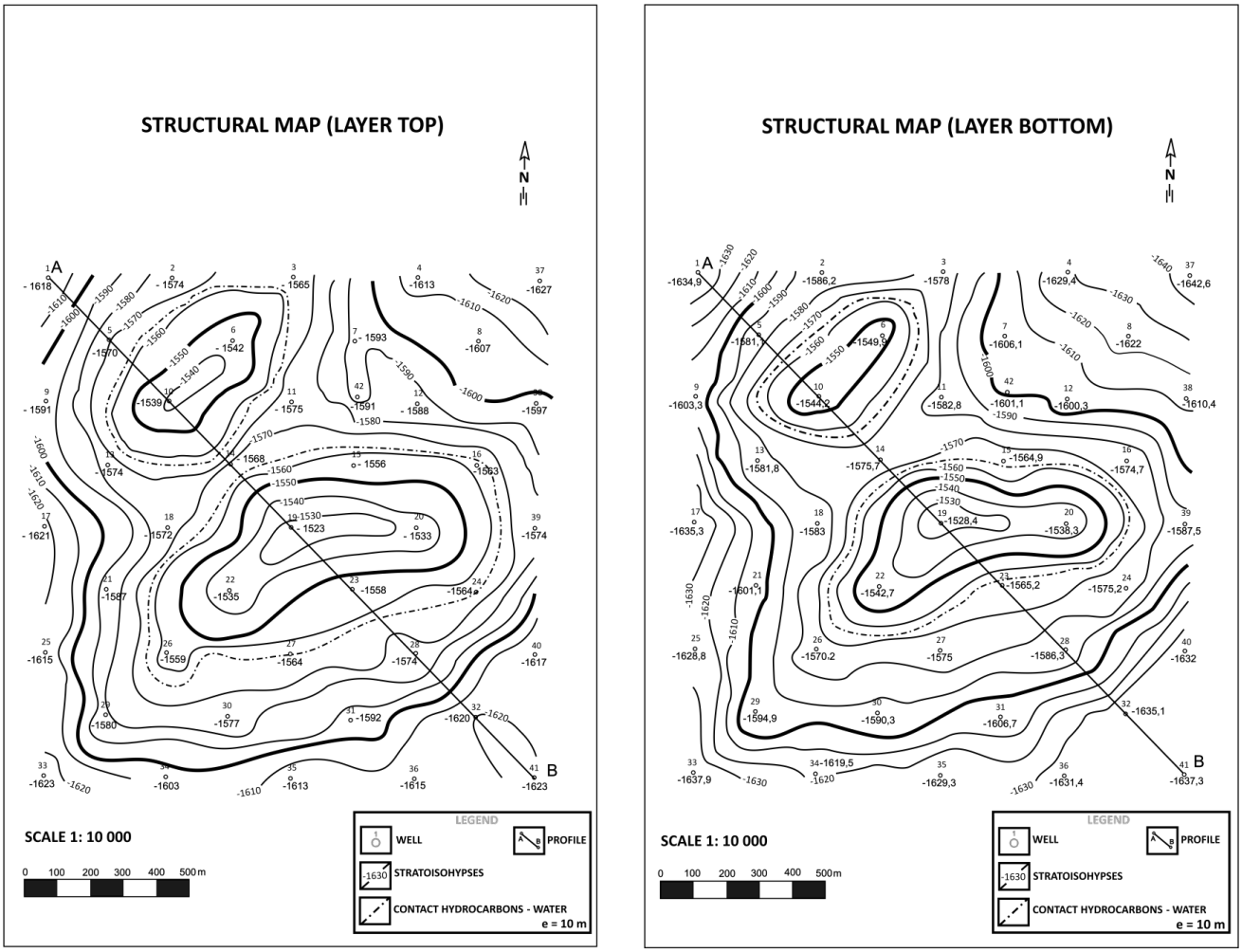

a b

Figure 2: (a) Structural map (layer top) - equidistance 10 m; (b) Structural map (layer bottom) - equidistance 10 m.

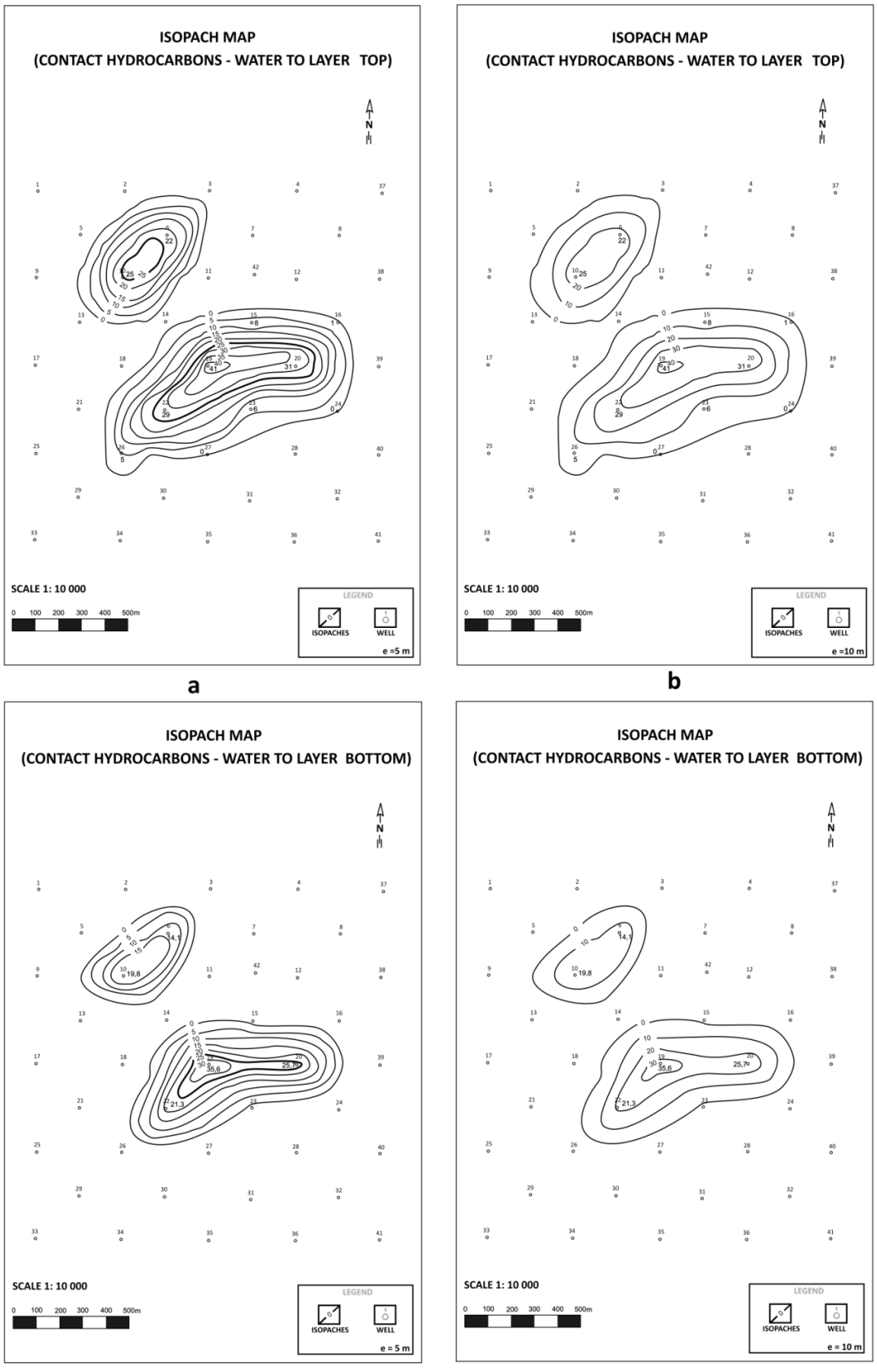

Figure 3: (a) Isopach map (HC - layer top) - equidistance 10 m; (b) Isopach map (HC - layer top) - equidistance 5 m; (c) - Isopach map (HC - layer bottom) - equidistance 5 m; (d) Isopach map (HC - layer bottom) - equidistance 10 m.

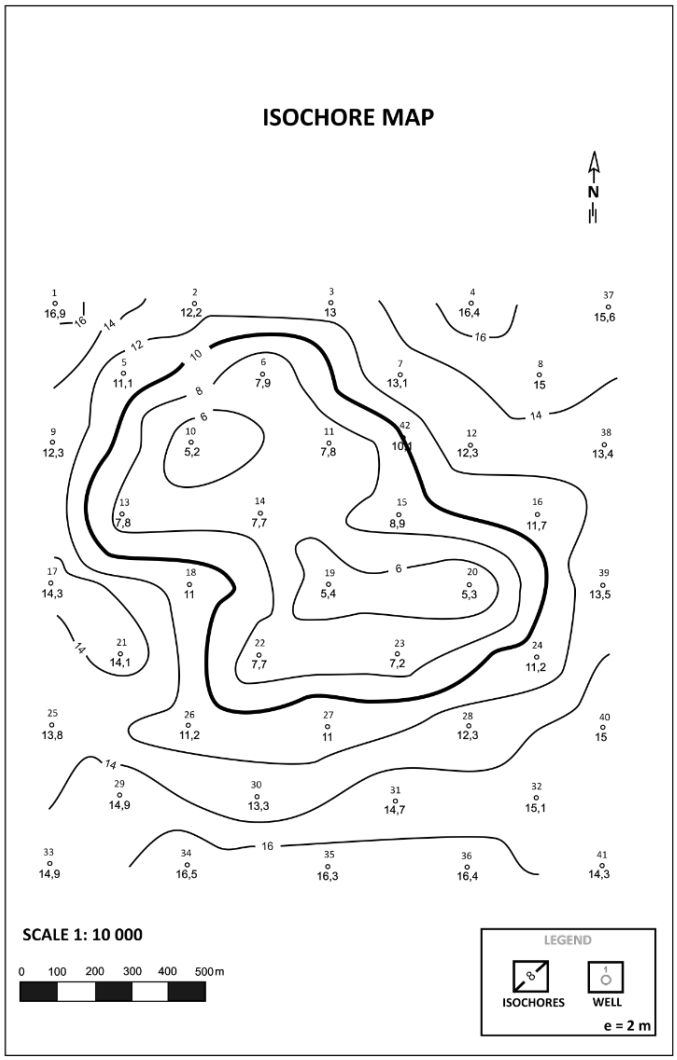

Figure 4: Isochore map - equidistance 2 m

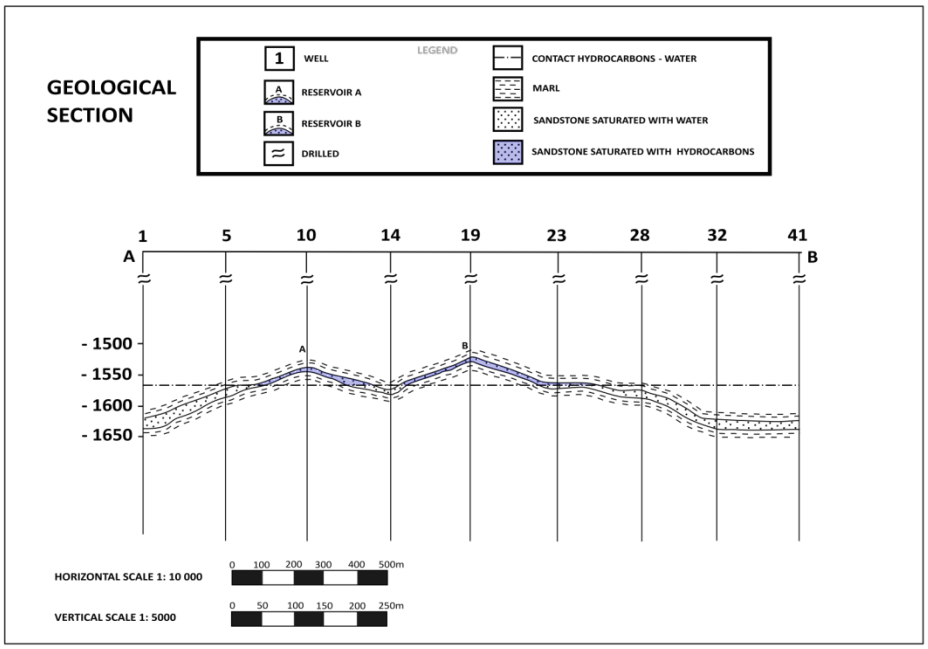

Figure 5: Geological section

Structural maps are defined as maps that show structural relations on a specific chosen layer. The structural maps of both the top and bottom layers were formed based on the absolute depths and the lines shown on the map connecting points of equal, real depths of the top and bottom layers are called stratoisohypses. The scale used for making the above-mentioned maps is larger meaning that the structure itself is significantly reduced in size, resulting in lesser calculated reservoir volume. Generally speaking, when selecting a scale of similar size, greater equidistance interval of 10 meters is applied to avoid the clustering of stratoisohypses. The mapping is done based on said table parameters and equidistance results in a descriptive, i.e., interpretative map. Given the positive results, the next step was to analyse the finished structure. To achieve greater data visibility every fiftieth isoline was thickened..

At first glance, the structure shown in **Figure 2a** does not have a defined shape seeing as the morphological diversity is quite severe. However, after further analysis, it was concluded with certainty that the structure is an irregular anticline, also known as a brachianticline. The highest isolines create tops of an anticline. The hydrocarbon-to-water contact line cuts the top las it is interpolated on the map itself. Seeing as the contact itself is not connected via the saddle form, we can conclude that the structure consists of two separate reservoirs. Again, because of the greater geomorphological diversity presented, it can be approximated that the volume calculations will result in a larger error. Despite that, it was concluded that the errors will fall within the maximum appropriate error limit and that the assignment can be continoued. Based on the interpolated, hydrocarbons-to-water contact line, as shown in **Figure 2a**, the isopach maps were created with contact to both top and bottom layers. By creating the above maps, the first official step to volume calculations has been taken. The isopach map showcasing contact to the top layer has been created by setting the reservoir layer thickness zero in places where specific points cut the top layer. This cutting line is now defined as the "new" isopach zero point from with all others are interpolated, using equidistance of 10 metes. The preceding map is shown in **Figure 3b**.

However, the created map presents an issue with the final volume calculation; it does not provide enough segments or isopachs to approximate the volume using the Simpson's and the Trapezoidal rule (**Eq. 1 and 2**) :

$$V_{trap} = \frac{h}{2} (a_0 + 2a_1 + 2a_2 + \ ... + a_n) \quad (1)$$

Where are:
V_{trap} - Trapezoidal volume
a_n - area bounded with the isopach
h - equidistance.

$$V_{simp} = \frac{h}{3} (a_0 + \ 4a_1 + 2a_2 + 4a_3 + \ ... + 4a_{n-1} + a_n) \quad (2)$$

Where are:
V_{simp} - Simpson's volume
a_n - area bounded with the isopach
h - equidistance.

For that reason, the equidistance was "thickened" and changed to 5 meters, from which we have secured enough segments for the shown calculation. The comparison between the original isopach map with an equidistance of 10 meters, and the map with an equidistance of 5 meters is shown in **Figures 3a** and **3b**.

By doubling the equidistance, enough segments have been created to continue with the volume calculation process accorting to Simpson's and Trapezoidal rules. The reservoir was cut every 5 meters with isopach planes and the cross-section surface areas were measured with a planimeter. For ease of understanding, the two separate reservoir structures will from now onward be reffered to as „reservoir A“ (upper, left corner) and „reservoir B“ (right). The planimetry results are shown in **Table 1**, while the surface areas are applied in **Eq. 1 and 2.**

Table 1: Planimeter results for section crossing (Isopach map contact hydrocarbons - water to layer top - Figure 3a). Multiplicative constant is 800.

Isopach no. („reservoir A“)	1st starting point of planimeter	2nd finishing point of planimeter	|1st -2nd|	Absolute area [m^2]
0	5259	5446	187	149 600
5	5518	5694	176	140 800
10	5714	5863	149	119 200
15	5889	5991	102	81 600
20	5006	5038	32	25 600
25	5051	5068	17	13 600
Isopach no. („reservoir B“)	1st starting point of planimeter	2nd finishing point of planimeter	|1st -2nd|	Absolute area [m^2]
0	6991	7651	660	528 000
5	7632	8151	519	415 200
10	8139	8557	418	334 400
15	8548	8868	320	256 000
20	0242	0448	206	164 800
25	0434	0572	138	110 400
30	0567	0663	96	76 800
35	0651	0699	48	38 400
40	0688	0691	3	2400

Reservoir "A“ includes an even number of isopach and an odd number of segments. Moreover, Simpson's rule (**Eq.1**) is only applicable in cases with an odd number of isopach and an even number of segments. A similar issue has been discussed in the paper where a new approach to the was presented (**Malvić et al., 2014**). In that case, the combination of both the Simpson's rule and the Trapezoidal rule is to be used as follows: the Simpson's volume equation ise used to calculate the second to last isopach (**Eq. 2**), while the Trapezoidal rule is applied to calculate the last isopach (**Eq. 3**).

$$V_{trap} = \frac{h}{2} (a_{n-1} + a_n) \quad (3)$$

Where are:
V_{trap} - Trapezoidal volume
a_n - area bounded with the isopach
h - equidistance.

The volume of the cap is added at the very end itself, seeing as the total volume is increased by the addition, however minor it is. This particular volume, above the final isopach, has very little impact on the total volume, in fact only a few percentages, nevertheless, it is not negligible. The volume itself is defined by a height that is lesser than the equidistance. If there is point data in the area defined by the highest isopach, the undefined height can be approximated from the difference between the last known isopach height and the number associated with the specific point data. In another case, if no point data exists in that area, the height can be arbitrarily determined, and it usually varies between 1 and 2 meters. Furthermore, that specific height is calculated using

the pyramid and sphere approximation given in **Eq. 5** and **Eq. 6**. Finally, the total volume is presented as the arithmetic mean of the two values (**Eq. 7**).

$$V_p = \frac{h_n a_n}{3} \quad (5)$$

Where iare:
V_p - pyramidal approximation
a_n - area bounded with the last isopach
h_n - distance from the last isopach to the top of the structure.

$$V_{sf} = \frac{h_n^3 \pi}{6} + \frac{a_n h_n}{2} \quad (6)$$

Where are:
V_{sf} - spherical approximation
a_n - area bounded with the last isopach
h_n - distance from the last isopach to the top of the structure.

$$V_{top} = \frac{1}{2}(V_p + V_{sf}) \quad (7)$$

Where are:
V_{sf} - spherical approximation
V_p - pyramidal approximation
V_{top} - top volume.

The total volume, for „reservoir A“, is a sum of all three mentioned volumes, the results of which are shown in **Table 2** below. Contrastingly, „reservoir B“ is made up of an odd number of isopachs, as well as an even number of segments. This make sit possible to use only Simpson's equation (**Eq. 2**) in combination with the formula for the cap volume (**Eq. 7**) for the total volume calculation. Repeatedly, the overall volume is the sum of both, as shown in **Table 2.**

Table 2: Volume results (Figure 3a - Isopach map contact hydrocarbons - water to layer top)

Reservoir	e (m)	V_p (m^3)	V_{sf} (m^3)	V_T (m^3)	Number of sections	Used areas	Total volume (m^3)	Volume calculated with Trapezoidal formula (m^3)
„A“	5	4533.33	6800.53	5666.93	5	a_0, a_5, a_{10} a_{15}, a_{20}, a_{25}	Simpson’s (first n-1 sections) + Trapezoidal (n-th section) + top (above n-th section) 2275666.93	2244000
„B“	5	800	1200.52	1000.26	8	a_0, a_5, a_{10} a_{15}, a_{20}, a_{25} a_{30}, a_{35}, a_{40}	Simpson’s + top formulas 8271666.927	8306000

Similarly, the bottom layer structural map was made using the absolute depths of the top layer and subtracting it from the drilled layer thickness. The formed map, as shown in **Figure 2b**, also showcases the hydrocarbons-to-water contact line meaning that the same mapping procedure can

be applied. Moreover, on an isopach map to the bottom layer, the contact line is now the new starting, isopach zero interpolated using equidistance of 10 meters. Still, the original equidistance does not produce a map with enough structural elements for the volume approximation. Thus, the equidistance is altered and thickened to 5 meters, which successfully ensures the use of Simpson's and Trapezoidal rule in volume calculatons. The comparison between the original isopach map with an equidistance of 10 meters, and the map with an equidistance of 5 meters is shown in **Figures 3c** and **3d**.

The planimetry results for the isopach map to the bottom layer are shown in **Table 3**. The equations of „reservoir A“ and „reservoir B“, calculations are the same as shown in the case of the isopach map to the top layer, since „reservoir A“ has an even number of isopachs, and „reservoir B“ has an odd number of isopachs (**Table 4**).

Table 3: Planimeter results for section crossing (Isopach map contact hydrocarbons - water to layer bottom - Figure 3c). Multiplicative constant is 800.

Isopach no. („reservoir A“)	1st starting point of planimeter	2nd finishing point of planimeter	|1st -2nd|	Absolute area [m^2]
0	6287	6435	148	118 400
5	6392	6491	99	79 200
10	6481	6532	51	40 800
15	6517	6561	44	35 200
Isopach no. („reservoir B“)	1st starting point of planimeter	2nd finishing point of planimeter	|1st -2nd|	Absolute area [m^2]
0	3766	4166	400	320 000
5	4153	4467	314	251 200
10	4461	4678	217	173 600
15	4665	4810	145	116 000
20	4801	4897	96	76 800
25	4883	4925	42	33 600
30	4911	4922	11	8800

Table 4: Volume results (Figure 3c - Isopach map contact hydrocarbons - water to layer bottom)

Reservoir	e (m)	V_p (m^3)	V_{sf} (m^3)	V_T (m^3)	Number of sections	Used areas	Total volume (m^3)	Volume calculated with Trapezoidal formula (m^3)
„A“	5	56320	84537.91	70428.955	3	a_0, a_5 a_{10}, a_{15}	Simpson’s (first n-1 sections) + Trapezoidal (n-th section) + top (above n-th section) 1053762.285	984000
„B“	5	16426.67	24731.95	20579.31	6	a_0, a_5, a_{10} a_{15}, a_{20}, a_{25} a_{30}	Simpson’s + top formulas 4075245.997	4078000

To meet the designated maximum fault requirements, the calculations need to have their absolute difference below 20%. The difference contained in the percentage includes the total

volume calculated using Simpson's rule versus the overall volume calculated using the Trapezoidal rule. The percentage results are shown in **Table 5**.

Table 5: Simpson's and Trapezoidal total volumes difference

Map	Isopach map contact hydrocarbons - water to layer top	Isopach map contact hydrocarbons - water to layer bottom
Difference (%)	$\frac{\lvert V_T - V_S \rvert}{V_T} \cdot 100$	$\frac{\lvert V_T - V_S \rvert}{V_T} \cdot 100$
„Reservoir A“	1.41	7.09
„Reservoir B“	0.41	0.07

The error is more significant in „reservoir A“ compared to reservoir B, but is still below the the permissible error limit of 20%. In „reservoir B“, the error is barely noticeable and quite insignificant meaning that the approximation is virtually ideal. The difference is relatively small and within the boundary which signifies the acceptance of the calculated volume. Based on drilled layer thickness intervals, an isochore maps likewise constructed. Unlike the formerly analysed isopach maps, the isochore maps showcase lines of equal, drilled layer thickness (**Figure 4**).

The terms isopach and isochore are often incorrectly used in the petroleum industry as synonyms for thickness measurements, although they are fundamentally different. The isochore map refers to the actual thickness of the drilled layer, whereas the isopach maps illustrate thickness measured perpendicularly to the layer's top and bottom or to the fluid contact.

It is important to note that the thickness values presented on an isochore map are the result of a subtraction between absolute depths of the top and bottom layers, while the actual thickness is presented in **Figure 3a** and **Figure 3c**. Isopach and isochore maps are comparable if the layer is perfectly horizontal. Isochore maps show what can be seen when analysing a cross-section of a structure, namely a geological section, which is created using a definite number of wells to better determine the structure. The chosen profile connects wells 1 to 41 all the while cutting across the structure from northwest to southeast, which is shown in **Figure 5**. However, an issue that was encountered when constructing the profile was the inter-well space. In practice, the problem is solved by correlating the from carottage readings or measurements with the seismology being the one that solves the inter-well space. Seismology can, likewise, be used to view and examine a particular layer while it is not able to detect a reservoir, which is why to correlation between the different geophysical methods is of great significance. In this instance, when making the geological profile, the solution to the uncertainty of the inter-well space is resolved using stratoisohypses that pass through the area in question. The hydrocarbons-to-water contact line intersects both the top and bottom layers at two different points, indicating the existence of two separate reservoir structures. Seeing as the contact line is non-continuous the layer shown can be defined as a brachianticline, although the shape is generally not easily detectible when looking only at the geological section alone.

One can easily be misled when analysing the profile and conduct that the reservoir consists of two perfect domes, which is why it is particularly important to use multiple geological profiles to correctly determine the final shape. The chosen profiles must cut across the structure in different directions. For that reason, in this paper, structural maps of the top and bottom layers are used to to create the said profile we used (**Figure 2a and Figure 2b**). The deepest of stratoiohypses represent the determining factor in defining the final shape of an underground structure. Looking at a profile, such as the one shown in **Figure 5**, it is easily ascertainable that both of the brachianticlines show a level of symmetry from their tops, and that both flanks are continuous in their deeping. The slope of the structure is uniform and somewhat continuous. Additionally,

when speaking of tops, the structure consists of two, which directly points to great geomorphological diversity. The thickness of the layer shown on the geological section is apparent, but not actual and can vary throughout the structure. The main purpose of a section is to obtain a better visual understanding of an subsurface structure and to confirm the assumptions made from structural maps.

4. Interpolation, planimetry and calculation of structure 2

As already explained in the introduction to this work, as well as for structure 1, it was also necessary to create structural and thickness maps (isohypses, isopachs, and isochores maps) based on the different numerical data, to construct a characteristic geological profile, to calculate the surfaces of isopachs with the help of a planimeter and calculate the volume of the productive part of the layer.

The input number of wells was 45, and the greatest depth was -920 meters on well-9. Backed up by given numerical data, the frist map was created, a structural map (layer top) which is visible in **Figure 6a**. When looking at the map, it is noticeable that there are seven stratoisohypses divided into two parts at the lowest absolute depth of -800 meters. The map shows how the isolines together form an elliptical shape that represents elongated brachyanticline, a structure that runs regularly from north to south and is almost centrally symmetrical. In addition, it is visible that the hydrocarbons-water contact at -870 meters marked with a "dash-dot-line" intersects the roof layer top, as the contact itself is interpolated on the map. A scale of 1: 5000 with an equidistance of 20 meters was chosen for the structure, based on evaluation of of the input data. The geological section A-B, which was later used to create the section itself, can be seen on the structure map alongside the boreholes and the stratoiso hypses with the corresponding depths.

The values of the absolute depths of the top slab of the productive layer were read directly from the input data, while the values of the depth of the bottom slab were obtained by the absolute addition of the depth of the roof slab to the perforated permeable interval. Tha data was used to create the subsurface depth map of the layer, which is visible in **Figure 6b**. The input number of wells was 45, with the greatest depth being -924.8 meters at the Well-9. The values of the stratisohypsies, of which there are seven in total, fall regularly from the edge towards the center, i.e. from -900 meters to -800 meters deep, surrounding a body as in the case of the structural map (layer top). Together, the isolines form an ellipse, the shape of which is characteristic of the structural trap called brachnianticline, which is elongated and symmetrical, just like in the case of the structural map (layer top). In addition, there are also so-called extrapolated lines, i.e. assumed lines that are shown as interrupted on the map and were created due to a smaller amount of data in this part of the terrain. The hydrocarbons-water contact is indicated at an absolute depth of -870 meters, which is highlighted on the map with a "dash-dot-line", incicaring that the contact intersects the subsurface of the layer. The map was made at a scale of 1:5000 with an associated equidistance of 20 meters. Just as in the case of the structural map (layer top), the section A-B is visible, which was used to obtain the vertical reservoir visualisation.

When creating the layer thickness map in **Figure 8**, the values of the drilled permeability interval in meters were used. The isoline representing the thinnest permeable interval is marked with "2” on the map, while the isoline representing the thickest interval is marked with "12". In addition, due to the reduced amount of data and the reduced number of wells, part of the sixth line on the map has been extrapolated, which indicates the assumption of further expansion. A scale of 1:5000 was used in the creation, but the equidistance was reduced to obtain a sufficient number of isolines. Accordingly, an equidistance of two meters was used.

The principle of creating an isopach map (contact hydrocarbons-water to layer top), which is visible in **Figure 7a**, is similar to the creation of a structural map (layer top), but in this case, the wells that were located at a greater depth than the hydrocarbons-water contact were omitted. Wells

that are located at a shallower depth than the absolute depth at which the hydrocarbons-water contact is located are assigned a recalculated value. The new values correspond to the absolute difference between the contact distance and the structural map (layer top). This map shows eight isolines that are equidistant at a distance of ten meters. The highest isopach on the map is indicated as 70, and is simultaneously divided into two structures. The upper, more elongated and larger isoline and the lower, smaller and more regular isoline. In places and in wells where the reservoir intersects the roof, the thickness of the reservoir part is zero. It is precisely for the reason that this isopach is marked with zero on the isopach map (contact hydrocarbons-water to layer top), and represents the hydrocarbons-water contact itself, which is at -870 meters. By separating the bottom from the contact to the roof surface of the layer, the brachianticline was again obtained, which confirms the assumption about the geological structure. A scale of 1:5000 with the already mentioned equidistance of ten meters was used to create the map. The equidistance is reduced in contrast to the equidistance used in the creation of structural maps (roof and bottom layer) as there is a reduction in the number of isopachs.

Analogous to creating an isopach map (contact hydrocarbons-water to layer top), an isopach map (contact hydrocarbons-water to layer bottom) was created (**Figure 7b**). In this case, the wells that were located at a shallower depth than the hydrocarbons-water contact were given new values representing the absolute difference between the contact distance and the depth of the bottom surface of the layer. Seven isopachs are visible on the map, with the highest isopach at 60 meters and the lowest at zero meters. The 'zeroth' isopach simultaneously represents the oil-water contact, which in this case, just as in creation of an isopach map (contact hydrocarbons-water to layer top), is the reference depth that has been given a new value, zero. By separating the bottom itself from the contact to the bottom layer, the previously stated hypothesis on a structural trap brachyanticline is confirmed. The assumption about the mentioned geological structure is confirmed by the isolines that shape the ellipse. A scale of 1:5000 was used for the creation, but in this case with an equidistance of 10 meters due toa reduced number of isopachs.

The structural map (layer top) (**Figure 6a**) and the structural map (layer bottom) (**Figure 6b**) were used to create the geological profile. The above-mentioned line A-B was placed on them, passing through the points of the Well- 2, -6, -12, -18, -24, -30, -37, and Well-42 with the aim of transferring as many points as possible to make the curve of the geological profile more precise. To check the accuracy of the transmission of the distance and the geological profile obtained, the number of the corresponding points of the roof surface of the layer was lowered by the value of the drilled interval. Its value should correspond to the points determined for the subsurface curve of the layer. The profile (**Figure 9**) shows that the hydrocarbons-1qwater contact, marked as a "dash-dot-line", is located at -870 meters. At the same time, it intersects both the roof surface and the bottom surface of the layer, so the bed itself is therefore located between them. Furthermore, observing the given section, almost continuous thickness of the layer can be concluded. The permeable layer is marked with the sandstone hatch, with only formation water saturation below the oil-water contact, while above the contact there is oil saturation, marked in green. The hatch for the marl represents an impermeable layer that has the role of preventing fluid migration from the deposit, therefore in this case the marl is located above the roof surface and at the same time below the bottom surface of the layer. The scale is visible in the lower left corner, which is the same in both the horizontal and vertical parts, and in this case, it is 1:5 000.

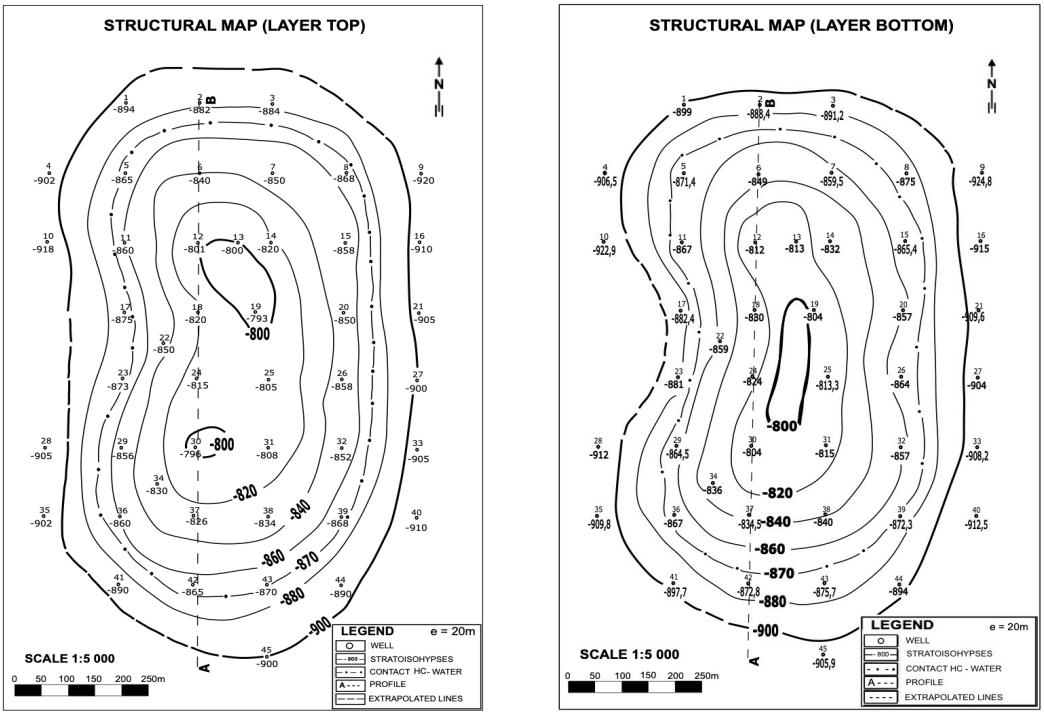

Figure 6: (a) Structural map (layer top) ; (b) Structural map (layer bottom)

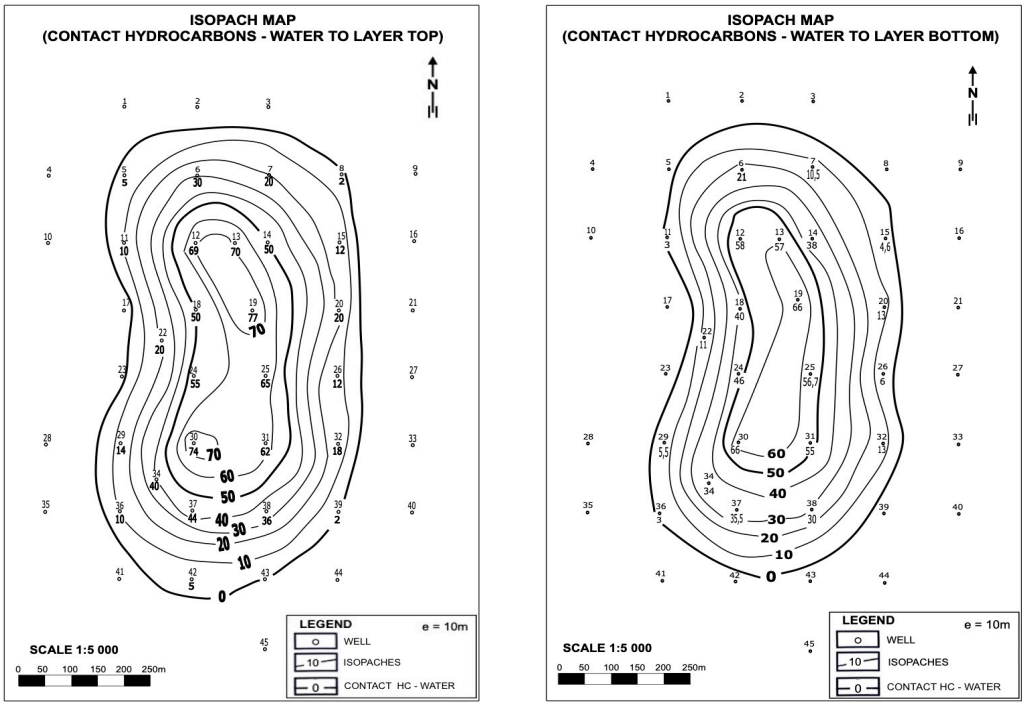

Figure 7: (a) Isopach map (HC - layer top); (b) - Isopach map (HC - layer bottom)

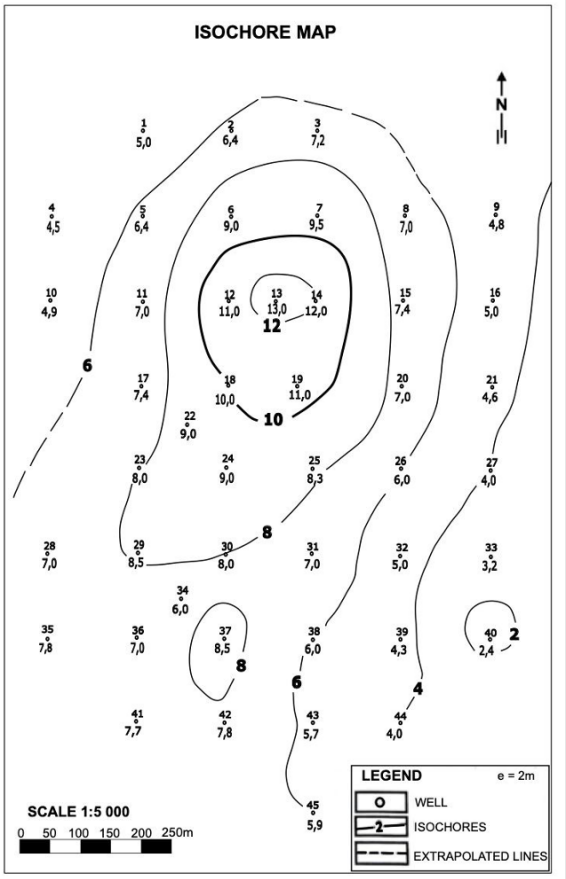

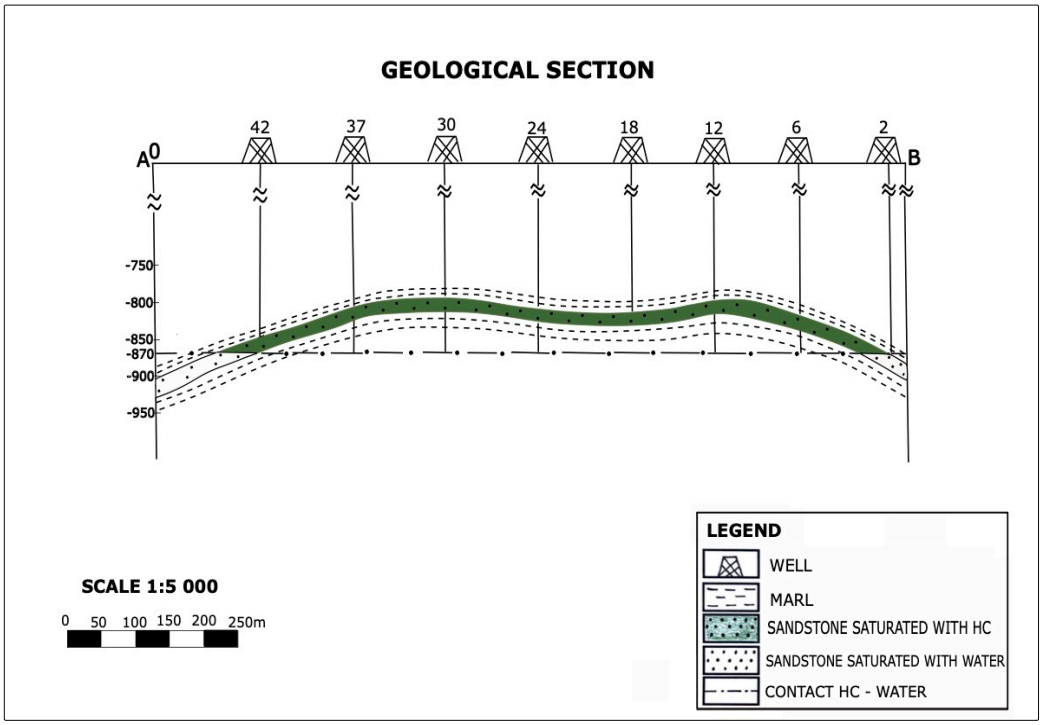

Figure 8: Isochore map
Figure 9: Geological section

To enable a better understanding of the obtained data and its processing to estimate the available hydrocarbon volume, the calculation of the reservoir volume is a key process. For assessment and calculation of this volume, it is necessary to know the area obtained by planimetry of the isopach map (contact hydrocarbons-water to layer top) and on the isopach map (contact hydrocarbons-water to layer bottom). The data obtained by planimetry for the isopach map (contact hydrocarbons-water to layer top) are given in **Table 6**, where when calculating the area of the "70" isopach, it was necessary to measure the surfaces separately and then add them up and observe the specified isopach as a whole in the further calculation. Accordingly, the data obtained for the isopach map (contact hydrocarbons-water to layer bottom) can be seen in **Table 7**. In the tables, the absolute difference between the first and second measurements represents the relative surface, converted into an actual surface by multiplying by a factor of 200, respecting the scale 1: 5000, which was given as a constant in the planimeter instructions. The correct choice of volume estimation method also depends on the number of interpolated isosurfaces on the maps. In the example of volume calculation for structure 2, the isopach map (contact hydrocarbons-water to layer top) has an even number of isopachs, and an odd number of isopachs for the subsurface, which is why the procedure itself will differ.

Table 6: Planimeter results for section crossing (Isopach map contact hydrocarbons – water to layer top). Multiplicative constant is 200.

Isopach no.	1st starting point of planimeter	2nd finishing point of planimeter	|1st -2nd|	Absolute area [m^2]
0	2873	5029	2156	431 200
10	5081	6752	1671	334 200
20	6763	8091	1328	265 600
30	8095	9148	1053	210 600
40	9131	9971	840	168 000
50	1798	2433	635	127 000
60	2418	2771	353	70 600
70_1	2596	2701	105	21 000
70_2	2766	2782	16	3 200
70 (70_1 + 70_2)	/	/	121	24 200

Table 7: Planimeter results for section crossing (Isopach map contact hydrocarbons - water to layer bottom). Multiplicative constant is 200.

Isopach no.	1st starting point of planimeter	2nd finishing point of planimeter	|1st -2nd|	Absolute area [m^2]
0	5858	7601	1743	348 600
10	7582	8931	1349	269 800
20	8933	9978	1045	209 000
30	1265	2139	874	174 800
40	2162	2718	556	111 200
50	2741	3081	340	68 000
60	3096	3251	155	31 000

Accordingly, in the isopach map, contact hydrocarbons-water to layer top (**Figure 7a**) even number of isopachs appear, which is why it is necessary to use a combination of the two already mentioned formulas, the Simpson's and the Trapezoidal formulas, in the calculation. The Simpson's formula (**Eq. 2**) was used to calculate the structure 2 for the first six sections under the condition

that the equidistance is 10 meters (h=10 m), and to calculate the volume of the last section, the Trapezoidal formula (**Eq. 3**) was used with the same equidistance of 10 meters (h=10 m).

The volume of the cap was obtained by **Eq. 5** and **Eq. 6** from which the final volume (**Eq. 7**) of the cap was calculated as the mean value of the results obtained using these two formulas. Within the formula, it is necessary to determine the height from the last isopach to the top of the structure, which on the isopach map (contact hydrocarbons-water to layer top) is 7 meters (h_7=7 m), as there is a well with actual thickness of 77 meters within the last isopach. The final volume (**Eq. 8**) was obtained by summing the volumes obtained from Simpson's formula, the Trapezoidal formula, and the cap volume formula.

$$V_{total} = V_{simp} + V_{trap} + V_{top} = 14\,065\,339.8\ m^3 \quad (8)$$

To be able to check the accuracy of the calculation and find a possible error, the total volume was calculated only with the help of the Trapezoidal formula (**Eq. 9**), again using an equidistance of 10 meters (h=10 m).

$$V_{trap} = \frac{h}{2}\,(a_0 + 2a_1 + 2a_2 + 2a_3 + 2a_4 + 2a_5 + 2a_6 + a_7) = 14\,037\,000 m^3 \quad (9)$$

As already stated, the calculation error must be less than 20 %, and it refers to the absolute difference between the obtained results (**Eq. 10**). Since the accuracy of the calculation depends on the equidistance, the choice of scale, the number of isopachs and the area's thinning, in the case of the isopach map (contact hydrocarbons-water to layer top), the absolute difference in the results is very small, i.e. it is only 0.3 %. The map was made with a smaller scale, i.e., 1:5000, with an equidistance of 10 meters used, which ensured the number of isopachs on the map. Accordingly, a sufficient number of segments was provided for a full call of Simpson's and Trapezoidal formulas. As shown on the map (**Figure 7a**) an elongated brachnianticline negatively affects the accuracy while numerous other, already mentioned parameters, preserve the smaller error percentage.

$$\left|\frac{V_{trap} - (V_{simp} + V_{trap})}{V_{trap}}\right| = 0{,}003 = 0{,}3\% \quad (10)$$

After calculating the volume of the isopach map (contact hydrocarbons-water to layer top), the isopach map is calculated (contact hydrocarbons-water to layer bottom). An odd number of isopachs is visible on the map (**Figure 7b**), which is why the calculation can be carried out using only Simpson's formula (**Eq. 2**) for all six sections, i.e. all seven isopachs with an equidistance of 10 meters (h=10 m).

The value of the volume of the cap was obtained in the same way as for the calculation of the roof area of the layer, using the formulas **Eqs. 5, 6**, and **7**. The main difference is the height between the last isopach and the top of the structure, which in this case is 6 meters (h_6=6 m) as there is a well at 66 meters of actual thickness inside the last isopach. The final volume was obtained by summing the volumes obtained from Simpson's formula and the cap calculation formula (**Eq. 11**).

$$V_{uk} = V_{simp} + V_{top} = 10\,312\,223.22\ m^3 \quad (11)$$

Again, as in the case of the volume of the roof surface, the volume was finally calculated using only the Trapezoidal formula (**Eq. 12**) with an equidistance of 10 meters (h=10 m).

$$V_{trap} = \frac{h}{2}\,(a_0 + 2a_1 + 2a_2 + 2a_3 + 2a_4 + 2a_5 + a_6) = 10\,226\,000\ m^3 \quad (12)$$

The obtained volume calculated by only the Trapezoidal formula served to check the accuracy of the results and to determine their mutual deviations, which must not exceed the already mentioned 20 %. It is also within the permissible deviations for the calculation of the subsurface area, namely 0.08 %, which is shown in Eq. 13.A major influence on the accuracy of the calculation is again the reduced scale of 1:5000 with the used equidistance of 10 meters, which enabled a sufficient number of isopachs. In addition, the small separation of the area with only one head contributed to the accuracy of the results.

$$\left|\frac{\mathrm{v}_{trap}-\mathrm{v}_{simp}}{\mathrm{v}_{trap}}\right| = 0{,}0008 = 0{,}08\% \quad (13)$$

5. Comparison of mapping and volume calculations

As was already determined, the goal of this paper was to identify and record the similarities and differences between Structure 1 and Structure 2 after analysing them in detai. The comparison is based, in its entirety, on created structural maps.

Firstly, starting with structural maps of the top layers (**Figures 2a and 6a**), it has been noticed that they have been interpolated with a similar number of input data. In the case of structure 1 the number of input point data, or rather wells is 42, and in case of structure 2, 45 wells. The main difference is in the absolute depths, both defining the well depths and the hydrocarbons-to-water contact line. Namely, in structure 1 the contact line is at an absolute depth of -1564 m, and in structure 2 at -870 m. In both structures, the contact line intersects the top layer. By observing both structures, the similarities regarding the shape were spotted and it was concluded that both of them can be described as brachianticlines, formed by isolines to an ellipse-like shape. The next perceived difference lies in the uniformity of the structures formed by stratoiohypses, with two distinct peaks in the case of structure 1, and a single peak in structure 2. Specifically, the first („reservoir A“), smaller of the two peaks is more spheric, and in the case of a second, bigger peak („reservoir B“) is elliptic in shape. Contrastingly, the single peak making up the structure 2, can be described as an elongated ellipse. The third biggest difference is the scale: structure 1 has a scale of 1:10 000, and structure 2 has a scale of 1: 5 000, resulting in the difference in equidistance, which is 10 meters for structure 1, and 20 meters for structure 2. The reduction or increase of the equidistance in both structures is a direct result of the scale choice, dictating the number of isolines.

Analogous differences and similarities are observed In the matter of the structural map of the bottom layer (**Figures 2b and 6b**). The main difference is again in the absolute depths of the specific wells and contact line. Both contact lines for structures 1 and 2 intersects the bottom layer. The presence of two peaks in structure 1 indicates a greater level of geomorphological diversity than in the case of structure 2, which consists of a single top. Furthermore, the structure shape is an irregular anticline, or rather brachianticline which can negatively affect the volume calculations. The difference is again observed in the scale and equidistance. When speaking of structure 1, due to the greater number of stratoisohypses, a larger scale is selected, namely 1:10 000, with a 10 m equidistance. For structure 2, whose depths and isoline numbers are smaller, the selected scale is 1: 5000, with an equidistance of 5 meters.

In the comparison of the layer thickness maps (**Figures 4 and 8**), a correlation with the number of isochores is observed, where their numbers in both maps are almost equal. One of the differences is in maximum thickness, which is 16 meters in structure 1, and 12 meters in structure 2. Secondly, they differ in the minimal thickness of the drilled intervals, whicj is 2 m in the case of the second structure, and 6 meters in the case of the first structure. The equidistance used in both maps is the same, namely 2 m, in order to display as many isolines as possible. Even with the same

equidistance, the scales differ and correspond to the scales used for the respective maps in previous analyses.

Regarding the isopach maps from contact to the top layer (**Figures 3a and 7a**), the first noted similarity is in the referential zero, or an isopach determining the hydrocarbon-to-water contact. The greatest thickness in structure 1 between the top layer and the contact is 25 m in „reservoir A“, and 40 m in „reservoir B“. In the case of structure 2, the greatest difference is 70 m. It can be likewise notice that the second structure is non-continuous, and the 70-th isopach is divided into two separate peaks, while the first structure has single top. In the first structures, multiple isolines represent the same thickness and are scattered across the map. The scale is also different when comparing the two maps, 1:5000 for structure 2, and 1:10 000 for structure 1. The equidistances are also different, 5 m in structure 1, and 10 meters in structure 2.

A omparison between the isopach maps from contact to the bottom layer follows (**Figures 3c and 7b**). In both structures, the hydrocarbon-to-water contact is taken as the reference depth, i.e. the new starting point, with the value of 0. Furthermore, the values are positive because they represent layer thickness, not layer depths. in structure 2, the thickness from the contact line to the bottom layer is 60 meters, and in structure 1 it is much less at just 15 meters for „reservoir A“, and 30 meters in „reservoir B“. The scale in structure 1 is again 1:10 000, with an equidistance of 5 meters. Similarly, the scale for the second structure is 1:5 000, with an equidistance of 10 meters.

In the last comparison, before the volume analysis, two characteristic geological sections, i.e. profiles were observed (**Figures 5 and 9**). It is to be noted that in the two cases, the hydrocarbons-to-water contact lines intersects both the top and bottom layers of the oil-saturated sandstone. The saturated sandstone layer is surrounded from the top and bottom by impermeable layers of marl. The main purpose of the marl is to prevent fluid migration, specifically the hydrocarbons. The second structure shows a continuous reservoir, while the second structure has two separate reservoirs within the sandstone layer, reservoirs „A“ and „B“. Due to an unusual geomorphological diversity shown in the structural maps of the top and bottom layers, the thickness of the permeable layer in structure 1 is variable. Structure 2 showcases even thickness across the entire layer. Vertical scales are the same in both cases and are 1: 5000. The horizontal differentiates, in structure 1 it is 1: 10 000, and in structure 2 it is once again 1: 5 000.

After analysing all the structural maps in detail and identifying and observing possible correlations, the final volume results are presented. Finally, it was determined which parameters are most likely to have an impact and change and in what way. After carefully examining and analysing the **Tables 2** and **4** and **Eq. 8, 9, 11** and **12**. it is clear that the total volume figure is greater for structure 2, with the main deciding perimeter being the smaller scale, 1:5 000. Contrastingly, the total volume figure in structure 1 is significantly smaller, partly due to the bigger scale of 1:10 000. Separating the two reservoirs making up the total of structure 1, it can be concluded that „reservoir B“ has a greater contribution in volume than „reservoir A“. The reason lies in the overall number of segments used in the calculations, with „reservoir B“ having twice as many segments as „reservoir A“.

There is a certain analogy that can be drawn between the two approximation methods, **Table 8** shows the absolute difference in Simpson's and Trapezoidal volumes. As was already established, the absolute difference must not exceed the limit of 20 % recommended in the literature The figures shown in the table below meet the criteria.

Table 8: Simpson's and Trapezoidal total volumes difference

Map	Isopach map contact hydrocarbons - water to layer top	Isopach map contact hydrocarbons - water to layer bottom
Difference (%)	$\frac{\lvert V_T - V_S \rvert}{V_T} \cdot 100$	$\frac{\lvert V_T - V_S \rvert}{V_T} \cdot 100$
Structure 1: „Reservoir A“	1.41	7.09
Structure 1: „Reservoir B“	0.41	0.07
Structure 2	0.30	0.08

From the table above it can been seen that the second structure renders smaller faults compared to the first. The parameters that have greatly contributed to such a result are primarily the scale of 1:5 000 in combination with its selected equidistance of 10 meters. Further, these two parameters, namely the smaller apparent scale and equidistance interval help to achieve a sufficient amount of segments to approximate the volume of the structures using Simpson's rule and Trapezoidal rule. When observing the geomorphological diversity, it was concluded that it only affected one structure, creating two separate reservoirs from structure 1 and consequently creating a bigger overall error in volume. Even though both structures can be described as brachianticlines, and the faults in volume results vary, they ultimately come under 10 %. it can also be noted that, even though the most "regular" shape in structure can be observed in „reservoir A“ of structure 1, it shows the biggest fault in volume compared to both structure 2 and „reservoir B“ of structure 1. That is due to the chosen scale of 1:10 000 which resulted in a smaller amount of segments and isopachs, and finally in greater error. To conclude, the final results depends on multiple different parameters, none of which can be ignored in volume calculations.

6. Conclusions

The main goal of this study was to examine and compare two papers analysing constructed structural maps, in addition to volume calculations, using fundamental knowledge of physical and mathematical laws combined with the knowledge of petroleum geology and engineering acquired during our present education. Analysing the input data, and comparing it to the structural maps it is easily ascertainable that the overall reservoir volume depends on numerous parameters. In one respect, when studying the structures against their respective maps, it is clear that the first structure consists of two separate reservoirs, while structure 2 can be considered as a whole. The shape of both deciding structures can be described as irregular anticline, or brachianticline. The shape of the structure alone can be a very decisive factor for volume calculations, where a greater number of reservors or peaks result in a huger overall error. Furthermore, the predetermined input data is specific to each of the maps making up the two fundamental studies and is founded on different scales and equidistance. The productive, reservoir part of structure 1 was supposed to be interpolated according to an equidistance of 10 meters. However, that equidistance in combination with the scale of 1:10 000, results in only two segments, three isopachs in „reservoir A“, and four segments, five isopachs in „reservoir B“, as is shown in **Figure 3b**. In the case of a map shown in **Figure 3d**, that same equidistance results in only one segment, two isopach in „reservoir A“, and three segments, four isopachs in „reservoir B“. However, as it was previously mentioned, the number of resulting isopachs and segments is not considered adequate for the use of Simpson's and Trapezoidal equations in volume calculations. Taking that into consideration, the equidistance was

thickened to 5 meters which resulted in five segments, six isopachs for „reservoir A“, and eight segments, nine isopachs with „reservoir B“ of structure 1, shown in **Figure 3a**. With the same new equidistance of 5 meters, shown in **Figure 3c**, there are now three segments, four isopachs in „reservoir A“, and six segments, seven isopachs in „reservoir B“. With structure 2, however, the initial set equidistance of 10 meters, as shown in **Figure 7a**, resulted in six segments, and seven isopachs. Finally, seven segments and eight isopachs are given in **Figure 7b**. Similarly, the results displayed in **Table 8**, for both structures, show that the final volume fault is significantly smaller, seeing as there is a greater number of isopachs compared to structure 1. The fault percentage is greater in structure 1, which is due to the greater geomorphological diversity, namely the two separate reservoirs which ultimately contribute to the irregularity of the structure. Equidistance is also one of the parameters for controlling the number of segments and isopachs, and indirectly the volume fault. In relation to the layer thickness, a larger equidistance in thinner layers does not equate to an adequate number of segments used in volume calculations and on the other hand, that same equidistance, but with thicker layers, can result in the expected number of segments. Accuracy and errors of the volume result heavily depend on the equidistance, with a smaller equidistance lesading to a greater number of results, segments thus diminishing the need for approximation. According to the convention of admissible equidistance, the optimum equidistance at which accuracy is greatly improved, is only 1 or 2 meters. Simpson's method requires at least four segments, otherwise, the results would not be permissible. In the case of „reservoir A“ of the structure 1, the error percentage is quite high at more than 7 %, and even using a more suitable equidistance does not result in an acceptable number of segments. It is important to note that the overall error does not exceed the permissible one of 20 %, and the approximation of reservoir volume is accurate. Using the example of „reservoir A“ in structure 1, it can be deduced that the number of isopachs particularly affects accuracy. A a certain percentage of error is still present, but it is greatly reduced when increasing the number of applied subintervals. Lastly, the scale is also important factor in calculations. The larger the scale, the larger the overall reservoir volume, as is seen in this paper.

7. References

1. Cindori Kovačević, M. (2016): Priručnik za projektiranje cesta (*Manual for road design*). Graditeljska tehnička škola, Zagreb, 78 p.
2. Davidović, M., M. Petrovič, V., Borisov, M. (2016): Analysis of the Display of Digital Terrain Models using Different Interpolation Methods. Geod. list, 70, 3, 267–282.
3. Husanović, E., Malvić, T., (2014) : Pregled dosadašnjih determinističkih geostatističkih kartiranja ležišta ugljikovodika u Republici Hrvatskoj te prednosti takvoga pristupa (*Overview of deterministic geostatistical mapping of hydrocarbon deposits in the Republic of Croatia and the advantages of such an approach*). Nafta, 65, 1, 64-68. (in Croatian)
4. Ivšinović, J. (2019): Odabir i geomatematička obrada varijabli za skupove manje od 50 podataka pri kreiranju poboljšanog dubinskogeološkoga modela na primjeru iz zapadnog dijela Savske depresije (*Selection and geomathematical calculation of variables for sets with less than 50 data regarding the creation of an improved subsurface model, case study from the western part of the Sava Depression*). University of Zagreb, Faculty of Mining, Geology and Petroleum Engineering, Zagreb, 160 p.
5. Ivšinović, J., Malvić, T. (2022): Comparison of mapping efficiency for small datasets using inverse distance weighting vs. moving average, Northern Croatia Miocene hydrocarbon reservoir. Geologija, 65, 1, 47-57.
6. Jashim Uddin, Md., Moheuddin Mir, Md., Kowsher, Md. (2019): A new study of trapezoidal, Simpson’s 1/3 and Simpson’s 3/8 rules of numerical integral problems. An International Journal (MathSJ), 6, 4, 13 p.

7. Kovač, I. (1982): Digitalni model reljefa hrvatske - izrada i upotreba za planimetriranje mreža odašiljača i pretvarača (*Digital model of the relief of Croatia - creation and use for planimetry of transmitter and converter networks*). Geod. list, 36, 10 - 12. (in Croatian)
8. Malvić, T. (2015): Upute za uporabu planimetra (*Instructions to measure with planimeter*). University of Zagreb, Faculty of Mining, Geology and Petroleum Engineering, University script, Zagreb, 20 p. (in Croatian)
9. Malvić, T. (2008): Primjena geostatistike u analizi geoloških podataka (*Application of geostatistics in geological data analysis*). University of Zagreb, Faculty of Mining, Geology and Petroleum Engineering, Manualia Universitatis studiorum Zagrabiensis,, Zagreb, 87 p. (in Croatian)
10. Malvić, T., Rajić, R., Slavinić, P., Novak Zelenika, K. (2014): Numerical integration in volume calculation of irregular anticlines. Rudarsko-geološko-naftni zbornik (The Mining-Geological-Petroleum Engineering Bulletin), 28, 2, 1-8.
11. Medved, I., Pribičević, B., Medak, D., Kuzmanović, I. (2010): Usporedba metoda interpolacije batimetrijskih mjerenja za praćenje promjena volumena jezera (*Comparison of methods of interpolation of bathymetric measurements for monitoring lake volume changes*). Geod. list, 64, 2, 71–86. (in Croatian)
12. Mesić Kiš, I., Malvić, T. (2014): Zonal estimation and interpolation as simultaneous approaches in the case of small input data set (Šandorovac field, Nothern Craotia). Rudarsko-geološko-naftni zbornik (The Mining-Geological-Petroleum Engineering Bulletin), 29, 1 , 9-16.
13. Pavičić, J., Andreić, Ž., Malvić,T., Rajić, R., Velić, J. (2018): Application of Simpson´s and trapezoidal formulas for volume calculation of subsurface structures - recommendations. Zbornik recenziranih radova, Faculty of Mining, Geology and Petroleum Engineering of the University of Zagreb, 15-26.
14. Podbojec, M., Cvetković, M. (2015): Preliminary estimate of CO2 storage capacity by petrophysical modelling in Upper Miocene Poljana Sandstones in the western part of the Sava Depression. Rudarsko-geološko-Naftni Zbornik (The Mining-Geological-Petroleum Engineering Bulletin), 31, 1, 31–43.
15. Šapina, M. (2016): A Comparison of Artificial Neural Networks and Ordinary Kriging depth maps of the Lower and Upper Pannonian stage border in the Bjelovar Subdepression, Northern Croatia. Rudarsko-geološko-Naftni Zbornik (The Mining-Geological-Petroleum Engineering Bulletin), 31, 3, 75–86.

Internet sources:

URL no.1: https://www.leinweb.com/snackbar/planimtr/wheatley/s10-4.html (accessed on 7 June, 2024.)

Acknowledgment

This work is motivated by support expressed from Tomislav Malvić, tenured Full Professor, on the University of Zagreb, Faculty of Mining, Geology and Petroleum Engineering.

Abstract in Croatian

Klasična interpolacija i izračun volumena dviju usporedivih ležišnih struktura - metodološke i interpretacijske sličnosti i razlike

Analizirana su dva ležišta ugljikovodika na temelju strukturnih i karata debljina koje su obuhvatile - karte dubina krovinske i podinske plohe sloja, debljine sloja te debljina od kontakta ležišta do krovinske i podinske plohe sloja. Svaka karta potkrijepljena je osnovnim elementima kao što su njezin naziv, odgovarajuće mjerilo i ekvidistancija, oznaka sjevera te pripadajuća legenda. Uz navedeno, izrađeni su i geološki profili ležišta te je proveden proračun volumena produktivnog dijela sloja. Detaljnom usporedbom detektirano je koji parametri i na koji način utječu na

postojanje razlika, a istovremeno na mogućnost korelacije između istih. Klasičnom ručnom interpolacijom i djelomičnom ekstrapolacijom dobivene su površine za planimetriranje kao ulazi za izračun volumena struktura. Te metode se temelje na numeričkoj integraciji, a u radu su korištene one najpoznatije, Simpsonova i Trapezna jednadžba. Dvije uspoređene strukture su brahiantiklinale, svaka sa svojim specifičnostima, koje su trebale biti prepoznate na kartama i volumetrijskom izračunu kako bi oba pristupa dala konkretna rješenja.

Ključne riječi: interpolacija; volumen; ležište; brahniantiklinala; Simpsonova jednadžba, Trapezno pravilo.

Authors contribution

Maria Rudec (undergraduate student) supervised abstract, introduction and comparison of mapping and volume calculations. **Marko Uzelac** (undergraduate student) provided the interpolated maps, tables, equations, planimeter results and calculations under the title interpolation, planimetry and calculation of the structure 1 and style. **Ivana Brajnović** (undergraduate student) provided the interpolated maps, tables, equations, planimeter results and calculations under the title interpolation, planimetry and calculation of the structure 2. **Lorena Birko** (undergraduate student) supervised methods, conclusions, style and translation of this work.

5th Croatian geomathematical congress
UDC: 628.1; category: original scientific paper

Assessing the natural vulnerability of the recharge area of the Velika Gorica well field

Marin Validžić[1]; Jelena Parlov[2*]; Dario Perković[3]
[1]University of Zagreb Faculty of Mining, Geology and Petroleum Engineering, Pierottijeva 6, Zagreb, Croatia
[2]University of Zagreb Faculty of Mining, Geology and Petroleum Engineering, Pierottijeva 6, Zagreb, Croatia; https://orcid.org/0000-0002-2862-7222
[3]University of Zagreb Faculty of Mining, Geology and Petroleum Engineering, Pierottijeva 6, Zagreb, Croatia; https://orcid.org/0000-0003-2625-6568
Corresponding author: jelena.parlov@rgn.unizg.hr

Abstract

Groundwater is an important natural resource and plays a crucial role in the preservation of ecosystems, providing potable water and the supply of various industries in the Republic of Croatia. Therefore, it represents a major challenge of utmost importance for hydrogeologists dedicated to the protection of its qualitative and quantitative integrity. Thus, one of the most common methods used in groundwater protection projects, namely the assessment of the natural vulnerability of aquifers, is applied in this study. The study focuses on the recharge area of the Velika Gorica well field, located in the Zagreb aquifer, which is composed of alluvial deposits. The natural vulnerability assessment of the Velika Gorica well field recharge area was determined using the parametric SINTACS method. This method includes the assessment of seven parameters and is applied for two different scenarios. The final vulnerability index is determined by multiplying the parameter values by weighting coefficients. The result is a map illustrating the natural vulnerability of the Velika Gorica well field recharge area. This map shows different zones with varying degrees of natural vulnerability. The assessment shows that the entire observed area falls into a groundwater vulnerability class greater than high in both scenarios. This indicates a significant risk of groundwater contamination in the recharge area of the Velika Gorica well field.

Keywords: vulnerability index; SINTACS method; alluvial aquifer; Velika Gorica well field

1. Introduction

Groundwater is a vital natural resource in the Republic of Croatia, playing a crucial role in maintaining ecosystems, supplying drinking water, and supporting various industrial sectors. However, with the increasing population, urbanization, and intensified agricultural activities, there is growing pressure on these waters. Sustainable management and protection of this vital resource are essential, not only to ensure long-term water supply but also to preserve ecological balance and protect human health. In this context, legal frameworks such as the Sustainable Development Strategy of the Republic of Croatia (**URL1**), Water Management Strategy (**URL2**) and the Water Act (**URL3, URL4** and **URL5**) play a crucial role in water management. Furthermore, adherence to European Union guidelines, such as the Water Framework Directive (**URL6**), becomes increasingly important as it promotes sustainable water management and the protection of natural resources.

Assessing aquifer vulnerability is crucial for protecting groundwater. It helps us identify potential sources of contamination, plan land use, and take measures to protect drinking water supplies. Additionally, vulnerability assessment enables us to assess environmental impacts and respond promptly to accidental pollution. In this context, using the SINTACS method to assess groundwater vulnerability in Velika Gorica recharge area is crucial. This method allows for a detailed analysis of vulnerability and the identification of areas with higher or lower vulnerability. The application of geographic information systems (GIS) facilitates the preparation of input data, analysis, and interpretation of results.

In this study focus is on the recharge area of the Velika Gorica well field, which is supplied with water from the Zagreb aquifer composed of alluvial deposits from the Sava River. The aim is to conduct a detailed analysis of groundwater vulnerability in this area to better understand its susceptibility to contamination and contribute to the preservation of water quality for future generations.

The boundaries of the recharge area of the Velika Gorica well field were determined using the particle tracking model (with an assumed pumping rate of Q = 850 l/s) defined for the delineation of the sanitary protection zones of the Velika Gorica well field (**Bačani & Posavec, 2009**). **Figure 1** shows the results of the groundwater flow simulation and particle tracking for high and low water periods and thus defines the study area for natural vulnerability assessment. In addition, the wells of the Velika Gorica well field are shown in relation to the adopted second sanitary protection zone and the selected research domain. The Sava River forms the boundary of the recharge area of the well field on the northern side, while the southern boundary is formed by the Sava-Odra Canal. The study frame on the eastern side fully follows the groundwater flow model, while on the western side it also follows the boundary of the flow model, but up to a certain point where a part of the particle tracking route is excluded to avoid an overly irregular shape of the study frame. Thus, in line with the "European approach", the wells are actually reference sites or points where groundwater contamination should not occur under any circumstances, while the groundwater flow paths are routes that can transport contaminated fluid from the potential pollution source, defined by the well field recharge area, to the destination.

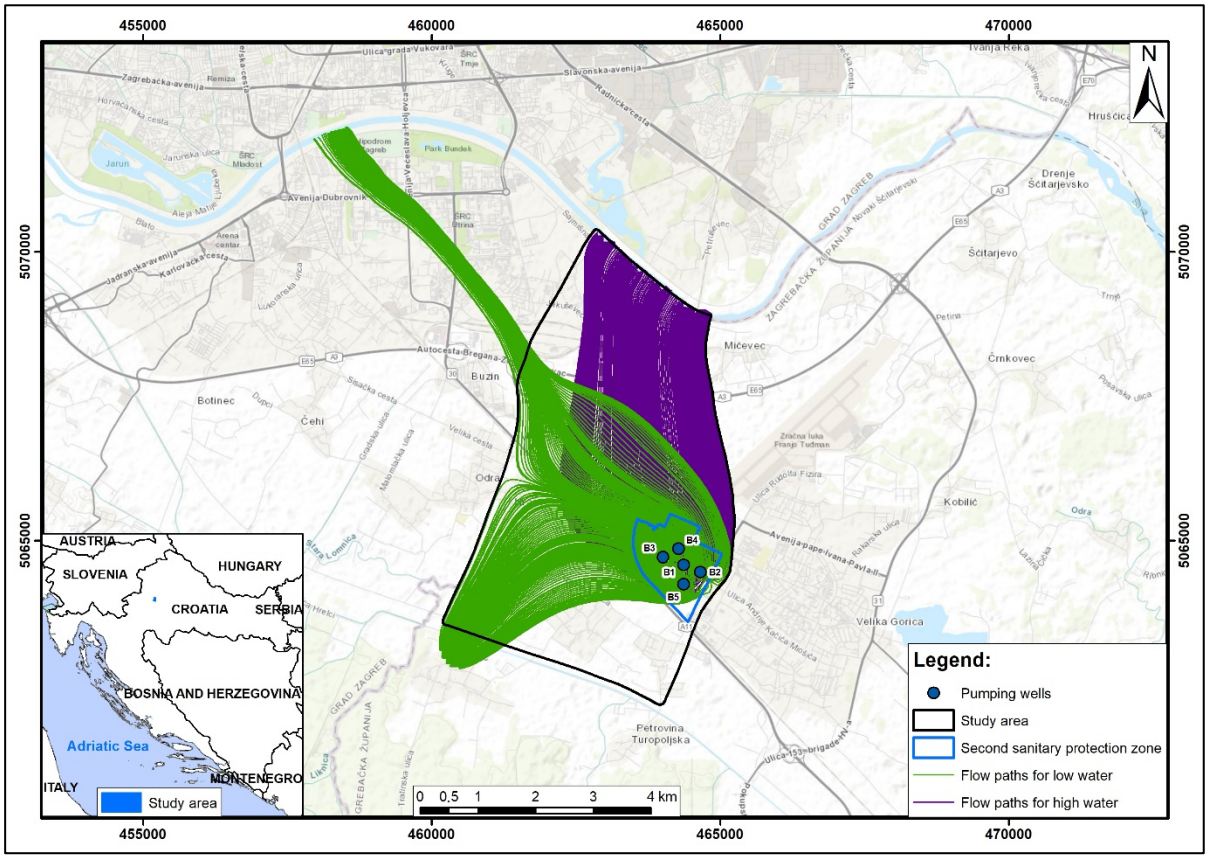

Figure 1. The study area with simulated flow paths for low and high water (according to **Bačani & Posavec, 2009**)

2. Characteristics of the study area

The average annual air temperatures measured at the Zagreb-Pleso meteorological station for the period from 1997 to 2019 are shown in **Figure 2a**. The average annual air temperature for

the selected period is 11.8°C, with fluctuations ranging from the lowest value of 10.4°C in 2005 to the highest of 13.1°C in 2012.

Figure 2b shows the distribution of annual precipitation for the Zagreb-Pleso meteorological station from 1997 to 2019. Annual precipitation ranges from 560.3 to 1459.5 mm, with the multi-year average value for the twenty-two-year period being 961.5 mm. On a monthly basis, the highest rainfall occurs in September (108.9 mm), while the lowest occurs in January (59.1 mm).

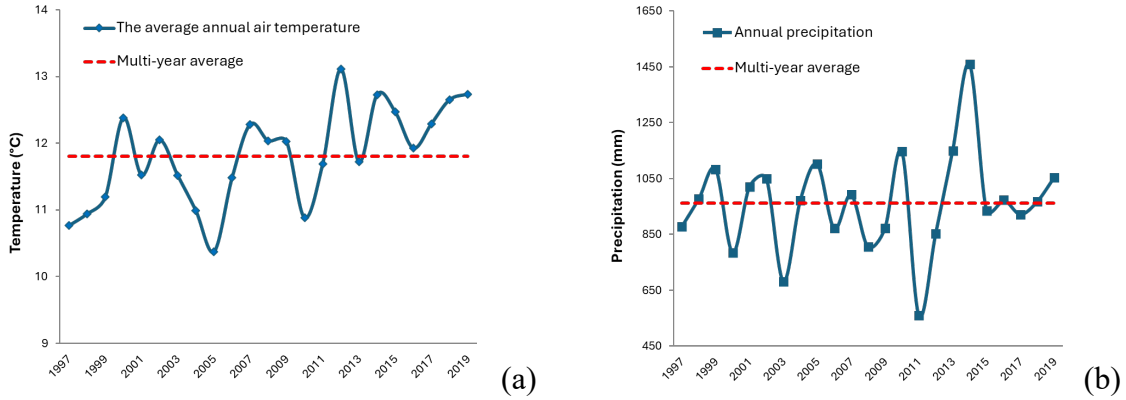

Figure 2. The average annual air temperatures (a) and annual precipitation (b) measured at the Zagreb-Pleso meteorological station (from 1997 to 2019)

The study area consists of four pedological units, which are, in order of prevalence: Fluvisoil, Eutric Cambisoil on Holocene deposits, Pseudogley-gley, and water bodies (**Figure 3a**). **Fluvisoil** is a hydromorphic soil type formed by increased moisture due to unrestrained flooding. Such soils occur along watercourses and rivers. It is characteristic of the Zagreb area that they have not been flooded for many years, but are categorised as alluvial soils due to their underdevelopment. **Eutric Cambisoil on Holocene deposits** is classified as an automorphic soil, as it was formed exclusively by precipitation without water stagnation. It is only developed on alluvial clayey deposits in the area of the Zagreb aquifer. The texture of this soil varies from powdery-clayey to, less frequently clayey-loamy. **Pseudogley-gleys** soils are hydromorphic soils characterised by alternating dry and wet periods and thus by reduction and oxidation processes. They contain a horizon where clayey making them impermeable and highly compacted (**Ružičić, 2013**).

Figure 3b illustrates the relationship between the geological deposits of the study area based on the 1:100,000 scale geological base maps, sheet Zagreb (**Šikić et al., 1977**), with the corresponding legend for the geological map of the Zagreb sheet (**Šikić et al., 1979**), and the Ivanić Grad sheet (**Basch, 1981**), with the corresponding legend for the geological map of the Ivanić Grad sheet (**Basch, 1983**). The study area is characterised by a simple geological structure consisting of alluvial deposits of the second Sava terrace – a2 (gravel and sand), floodplain sediments – ap (clayey silts), oxbow alluvium – am (clayey silts and silty clays) and recent alluvial deposits – a (sand and gravel).

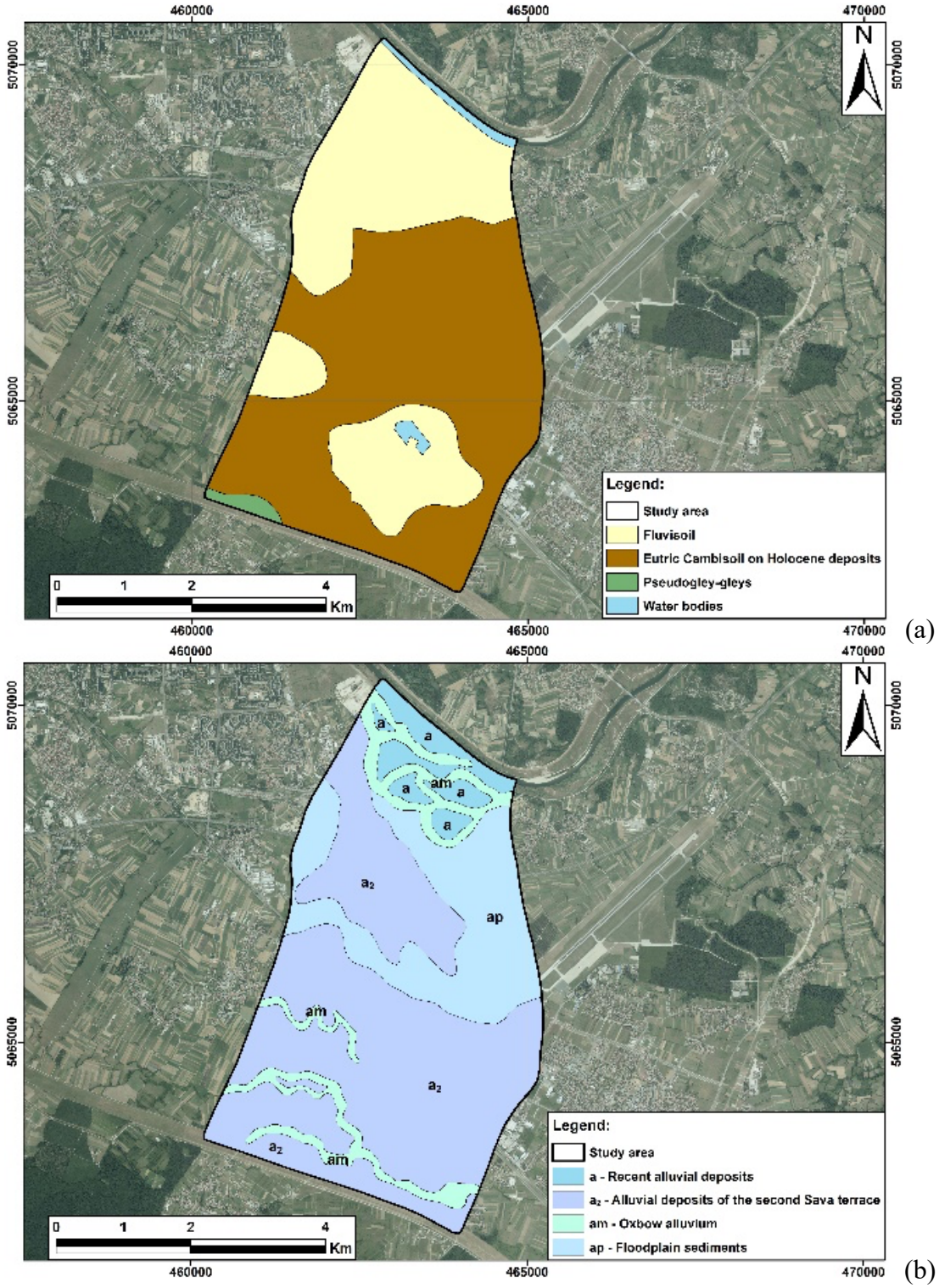

Figure 3. Pedological (a) and geological (b) map

The aquifer is an unconfined type with a regional groundwater flow direction from north-west to south-east (**Bačani & Posavec, 2009**). It consists of two layers, with the first layer consisting mainly of alluvial deposits of the Sava River, mostly consisting of gravels and sands, while the second layer consists mainly of lacustrine-marshy deposits. The layers are hydraulically connected. On the surface there are very thin covers of poorly permeable deposits of clay and silt, which are often absent. The aquifer is recharged mainly by infiltration from the Sava River and by precipitation (**Posavec, 2006**).

3. Method

The SINTACS method (**Civita, 1994**) is classified as a parametric method for assessing aquifer vulnerability. It can be considered as a certain upgrade to the American DRASTIC method (**Aller et al., 1987**), as it was developed with the aim of correcting deficiencies related to the ranges of values of individual parameters and assigning appropriate points. Additionally, the authors aimed to create a new method that would provide greater flexibility and applicability throughout Italy regardless of the aquifer type. Over the years, the original version of the SINTACS method evolved and changed with an increasing number of tests and grounded experiences (over 500 applications in various areas) until the year 2000 when the SINTACS R5 version was proposed (**Civita & De Maio, 2000**). According to this version, vulnerability assessment is based on scoring seven parameters and possesses five weighting systems that depend on the hydrogeological structure of the aquifer and surface conditions due to anthropogenic loading. For the purposes of this study, the SINTACS R5 method will be applied, which assesses vulnerability based on the evaluation of the following seven parameters:

1 Parameter S1 - depth to groundwater,
2 Parameter I - effective infiltration,
3 Parameter N - attenuation capacity in the unsaturated zone,
4 Parameter T - attenuation capacity in soil/cover layers,
5 Parameter A - hydrogeological characteristics of the aquifer,
6 Parameter C - hydraulic conductivity of the aquifer, and
7 Parameter S2 - slope of the terrain.

The assessment parameters in the model are converted into SINTACS parameters using certain tables, diagrams, ranges, and calculations, with each parameter ranging from 1 to 10, where a higher value indicates a greater vulnerability of the aquifer (**Civita & De Maio, 2004**). The final vulnerability is obtained by calculating the vulnerability index according to the **Equation1**:

$$I_{SINTACS} = \sum_{i=1}^{7} P_i \cdot W_i \quad (1)$$

where are:
- the P_i is the rating of each of the seven parameters that the method considers and
- W_i is the relative weight.

In **Figure 4**, the basic steps and processes of data preparation and processing involved in creating a vulnerability map are shown. GIS technology, specifically ArcMap 10.1, was utilized for preparing and analysing parameters using the SINTACS method to evaluate the natural vulnerability of the Velika Gorica well field recharge area. It is important to emphasise that the entire GIS analysis was performed in the official coordinate system of the Republic of Croatia, HTRS96/TM, while the GIS basemap layers are represented by the digital orthophoto map at a scale of 1:25,000 and the topographic map at a scale of 1:25,000 from the Geoportal of the State Geodetic Administration (**URL7**). Microsoft Excel was used to create a database and calculate certain values required for the preparation of the SINTACS parameters.

The vulnerability index is useful at a regional scale to priorities area of very extreme, extreme, high, moderate, low and very low vulnerability regions.

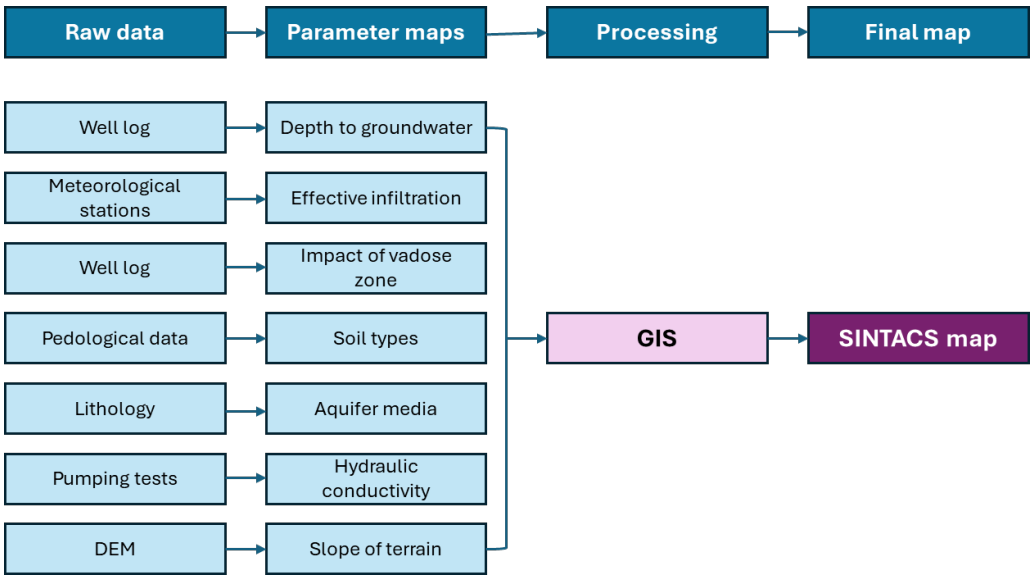

Figure 4. Flow chart of steps and processes in creating a vulnerability map

4. Results

The depth to the groundwater (parameter S1) was determined based on measurements from 18 piezometers during the period from 1997 to 2012. Maps of the highest high groundwater levels and the lowest low groundwater levels were created (**Figure 5a** and **Figure 5b**), and with the use of weighting factors, maps of parameter S1 for scenario 1 (**Figure 5c**) and parameter S1 for scenario 2 (**Figure 5d**) were produced.

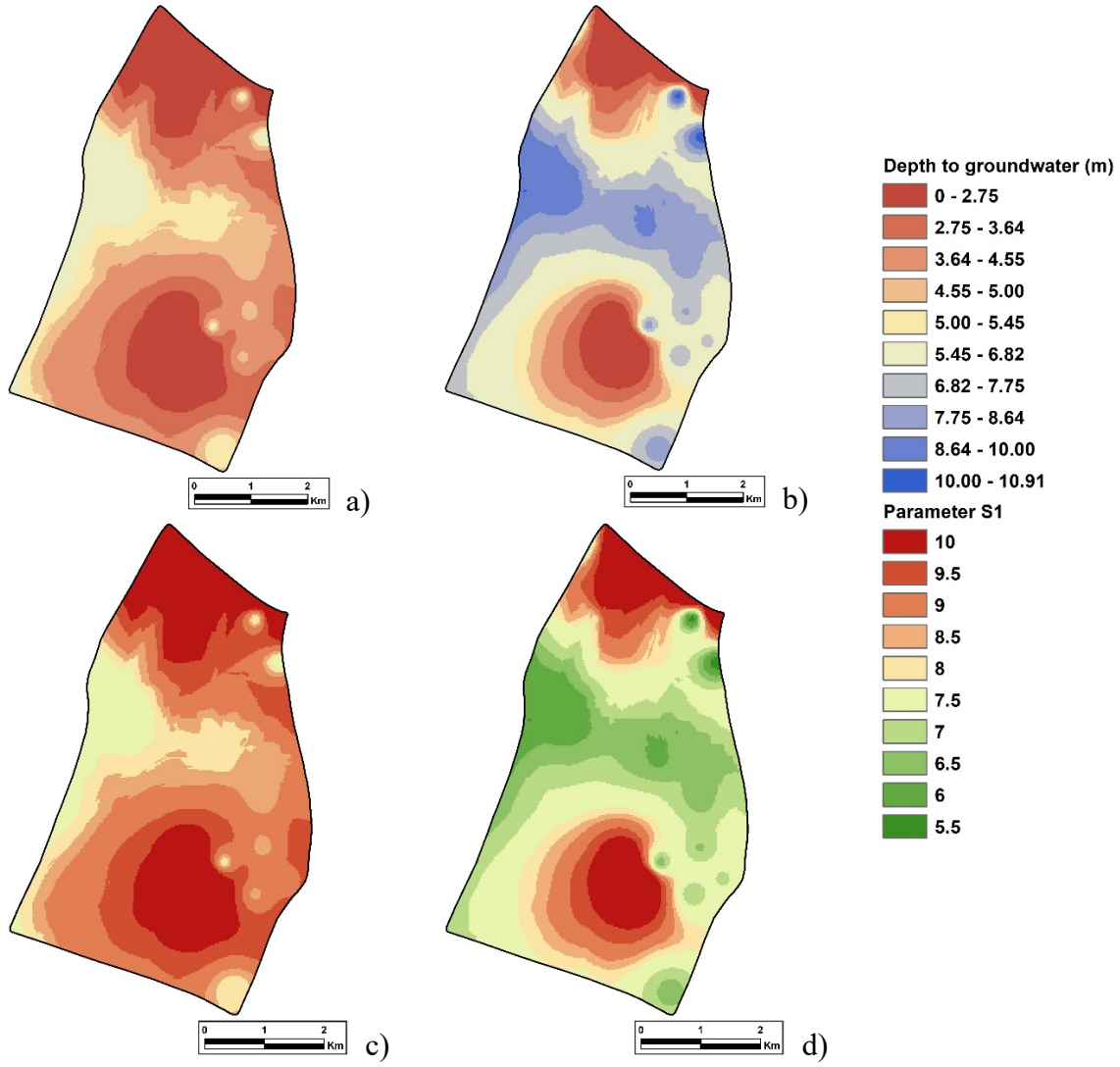

Figure 4. Spatial distribution of the parameter S1 for scenario 1 and scenario 2

The effective infiltration (parameter I) represents the amount of water per unit area that penetrates the soil surface and reaches the groundwater. The role that effective infiltration plays in assessing the vulnerability of aquifers is very significant as contaminants are entrained at the surface but are also diluted, first as they travel through the unsaturated zone and then within the saturated zone. The effective infiltration was analysed for two scenarios for the period from 1997 to 2019. The first case refers to the year with the highest precipitation (2014), in which the calculated actual evapotranspiration was also the highest for the observed period, while the second case considers the year with the lowest precipitation (2011). Table 1 shows the associated values of the parameter x (depending on the texture and hydraulic properties of the soil; for each soil type present in the recharge area) and the calculated values of effective infiltration for two scenarios.

Table 1. The effective infiltration (I) for scenario 1 and scenario 2

		Scenario 1 (Year 2014)			Scenario 2 (Year 2011)		
Soil type	**X**	**(P-Et)**	**I (mm/year)**	**Parameter *I***	**(P - Et)**	**I (mm/year)**	**Parameter *I***
Eutric Cambisoil on Holocene deposits	0.2	806	161	6.5	117	23	1.0
Fluvisol	0.3	806	242	9.0	117	35	1.5
Pseudogley-gley	0.1	806	81	4.0	117	12	0.0
Water body	1.0	806	806	10.0	117	1	10.0

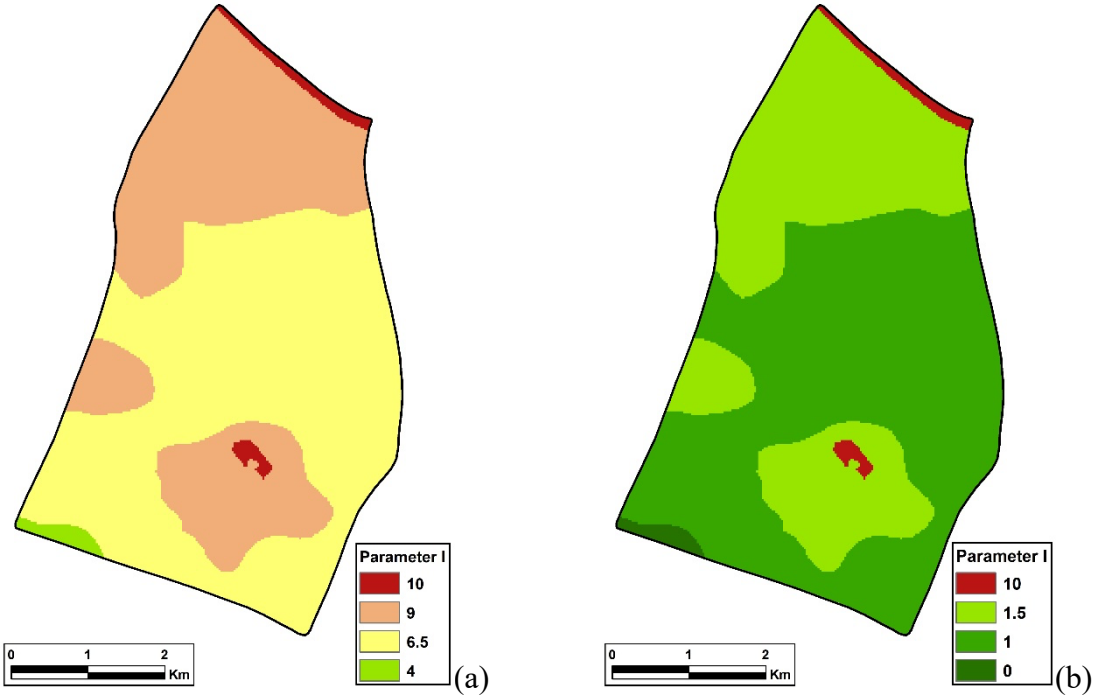

Figure 5. *Spatial distribution of the parameter I for scenario 1 (a) and scenario 2 (b)*

The unsaturated zone is described as the zone below the typical soil horizon and above the water table, which is unsaturated or discontinuously saturated. The unsaturated zone is the “second line” of defence" of the hydrogeological system against fluids or water-borne contaminants. Therefore, the **attenuation capacity of the unsaturated zone (parameter N)** is crucial. The thickness of the unsaturated zone at high (**Figure 6a**) and low (**Figure 6b**) groundwater levels led to a spatial distribution of the associated parameter N for scenario 1 (**Figure 6c**) and scenario 2 (**Figure 6d**).

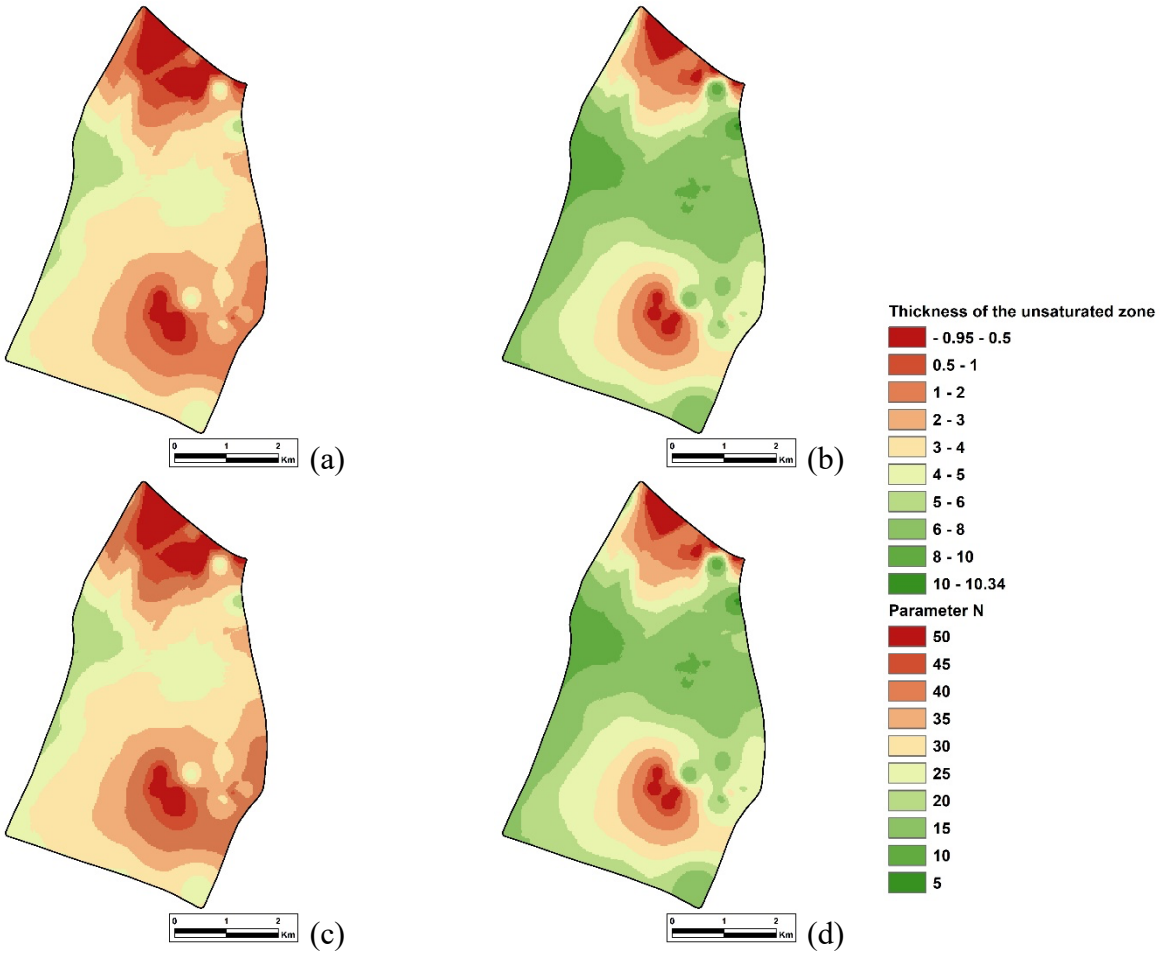

Figure 6. Thickness of the unsaturated zone at high (a) and low (b) groundwater levels and spatial distribution of the parameter N for scenario 1 (c) and scenario 2 (d)

The parameter T represents the attenuation capacity of the soil/cover layers to retain contaminants. When assessing the vulnerability of the aquifer, the soil is considered separately from the unsaturated zone and independently as the first line of defence of the aquifer against potential contamination, as it is able to slow down or retain the movement of the contaminated fluid through the hydrogeological system. **Figure 7** shows all possible values of the parameter T assigned to the different soils based on their granulometric composition, as well as the spatial distribution of the parameter T within the recharge area of the Velika Gorica well field.

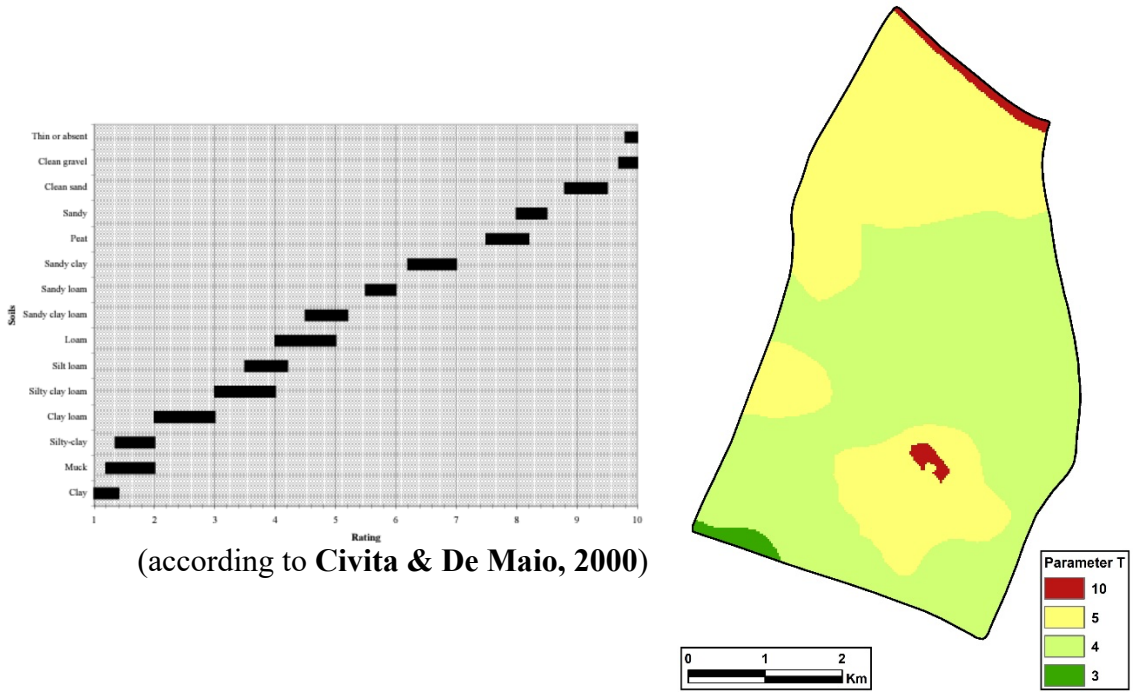

(according to **Civita & De Maio, 2000**)

Figure 7. Spatial distribution of the parameter T

The hydrogeological characteristics of the aquifer (parameter A) depend on the properties of the rocks of which it is composed. The Zagreb aquifer consists of medium to coarse-grained alluvial deposits, i.e. gravel and sand particles predominate in its lithological composition, with small amounts of fines. For the purposes of the SINTACS classification, the aquifer is generally categorised as consisting of coarse-grained alluvial deposits, and the entire thematic layer is given a score of 8 according to **Civita & De Maio (2000)**.

The hydraulic conductivity range of the aquifer (parameter C) represents the ability of the groundwater to move within the aquifer. To create this thematic layer, data on the hydraulic conductivity of the aquifer was collected from pumping tests of 11 different wells. The values are between 0.01 and 0.05 m/s (**Figure 8**), and the entire study area was assigned a value of 10 according to **Civita & De Maio (2000)**.

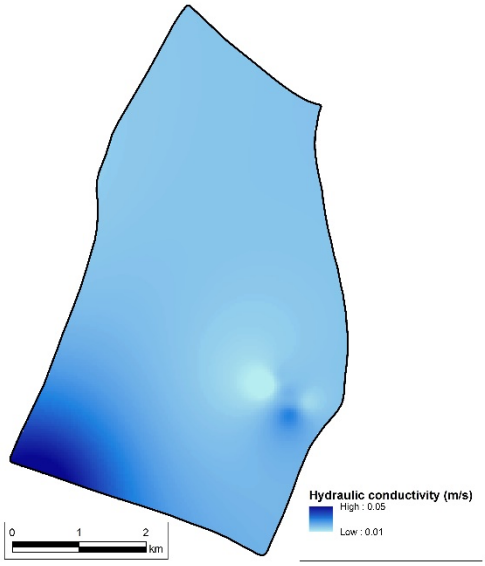

Figure 8. Spatial distribution of the hydraulic conductivity

The hydrological role of the topographic slope (parameter S2) is an important factor in vulnerability assessment, as it determines the amount of surface runoff that is generated. A digital elevation model (DEM) with a resolution of 25 metres was used to determine this parameter. Since the entire study area is located in the alluvial plain of the Sava River, a lowland relief with terrain slopes of less than 1% predominates. Accordingly, the slope map was reclassified into a single class (0-2%) with a parameter S2 value of 10 according to **Civita & De Maio (2000)**. After defining the values of all parameters, the vulnerability index was calculated using the following **Equation 2**:

$$I_{SINTACS} = 5S1 + 5I + 4N + 5T + 3A + 2C + 2S2 \quad (2)$$

Since the study area is almost entirely covered by agricultural and urbanized surfaces, i.e., intensive land use, the "Severe impact" group of weighting coefficients was selected (**Civita, 1994**). The parameter maps extracted above were overlaid in the GIS environment, and the vulnerability index maps of the study area was derived by using **Equations 1** and **2**. From the obtained vulnerability map of the recharge area of the Velika Gorica wellfield for scenario 1 (**Figure 9a**), it is evident that the study area is divided into two classes: extreme and very extreme aquifer vulnerability. The largest area of the study area is occupied by the class of very extreme vulnerability (21.2 km^2), while almost five times smaller area (4.3 km^2) belongs to the class of extreme vulnerability. Furthermore, in the case of low water levels (Scenario 2), the vulnerability index values in the considered area range from 144 to 364. From the obtained vulnerability map of the recharge area of the Velika Gorica wellfield for Scenario 2, as shown in **Figure 9b**, it is visible that the study area is divided into four classes: high, very high, extreme, and very extreme aquifer vulnerability. It can be observed that the classes are fairly evenly distributed within the study area, with the high vulnerability class covering an area of 7.3 km^2, the very high vulnerability class 5.7 km^2, the extreme vulnerability class 7.06 km^2, while the very extreme vulnerability class occupies the smallest area of 5.4 km^2.

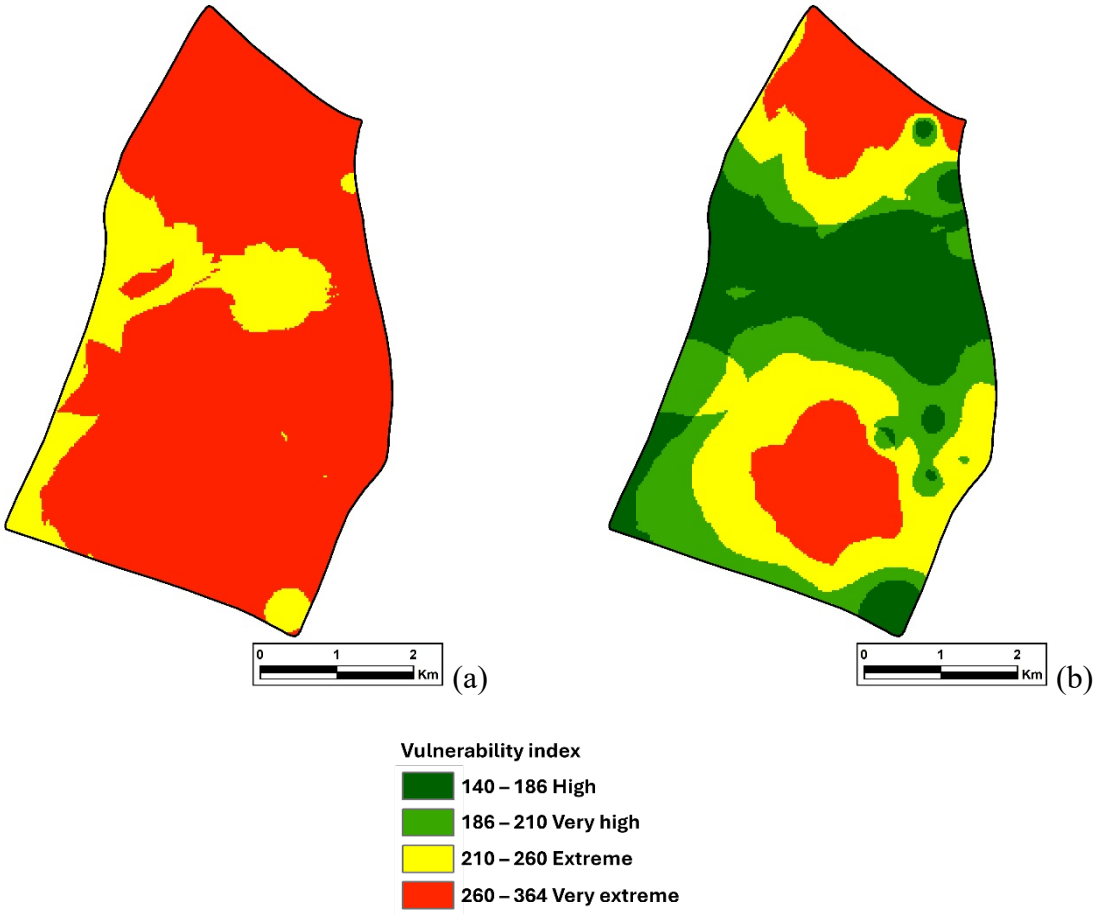

Figure 9. Spatial distribution of the vulnerability index in case of scenario 1 (a) and scenario 2 (b)

5. Discussion and conclusions

The determination of the aquifer vulnerability using the SINTACS method for scenario 1 resulted in values exceeding the extreme vulnerability threshold for the entire investigated area, which emphasises that the recharge area of the Velika Gorica well field is significantly vulnerable to contamination in case of a high groundwater level. These results were also to be expected, as the studied area is located in the alluvial valley of the Sava River. It is therefore a lowland area with gentle slopes and relatively shallow depth to groundwater, while the subsurface consists of alluvial deposits of medium to coarse texture with high hydraulic conductivity. In addition, the Zagreb aquifer is an unconfined aquifer with a weakly developed overburden that is exclusively associated with floodplains and thus directly linked to surface activities. Numerous factors have a negative impact on the vulnerability of the aquifer. Almost every parameter of the SINTACS method was evaluated with values above 5 in scenario 1, which leads to high vulnerability index values.

In the case of the second scenario, there was greater diversity in vulnerability degrees. The maximum vulnerability indices remained the same in both scenarios, while the minimum indices varied significantly. This is primarily due to significant differences in parameter I, as effective infiltration due to large precipitation amounts increased the aquifer vulnerability level for the same type of surface deposits. Furthermore, differences arose due to greater depths to groundwater (parameter S1) and thickness of the unsaturated zone (parameter N), while parameters T, A, C, and S2 remained unchanged in both scenarios. Therefore, in conditions of low water levels, areas with very extreme aquifer vulnerability are located near surface waters – the Sava River and Lake

Lomnica southwest of the Velika Gorica well field, while the area with high vulnerability, representing the class with the lowest vulnerability index values in these conditions, is around Velika Mlaka, where the greatest depths to groundwater were actually measured, further indicating the importance of unsaturated zone thickness in assessing aquifer vulnerability.

Although there are no previously published works on vulnerability assessment for such a narrow research area, the vulnerability analysis of the Velika Gorica well field recharge area can be considered reliable, as vulnerability analyses have been conducted at the national level, covering the entire Zagreb aquifer, where similarly high vulnerability (extreme and very high) characteristic of alluvial aquifers with very good hydraulic properties, relatively shallow depth to groundwater, and weak protective function of the unsaturated zone and soil were also observed (**URL8**).

For future research, the use of a digital elevation model (DEM) with higher resolution compared to that applied in this study, at least 5 meters for this large research scale, is recommended. Among other things, a denser network of structural-piezometric boreholes is desirable, since the boreholes used to determine soil thickness are unevenly distributed; they are more densely positioned in the northern part of the research area, while almost absent in the southwest, and a similar situation applies to piezometers, which certainly affects the accuracy of determining some parameters of the SINTACS method. Furthermore, it is recommended to have at least one pedological profile for each soil type, as this will enable safer determination of soil characteristics crucial for parameter assessment, especially through granulometric analysis.

In conclusion, this study conducted a natural vulnerability assessment of the Velika Gorica well field recharge area as part of the Zagreb aquifer. The Zagreb aquifer is an alluvial aquifer composed of gravel and sand of Quaternary age, divided into upper and lower aquifer layers, with relatively weakly developed cover layers in the upper aquifer layer, in certain areas. Therefore, due to its geological structure and intensive land use, the risk of aquifer contamination is significantly increased, which is why vulnerability analysis was conducted in this area. For the purpose of aquifer vulnerability assessment, the parameter SINTACS method was selected, which considers seven parameters: depth to groundwater (S1), effective infiltration action (I), dilution capacity in the unsaturated zone (N), dilution capacity in soil/cover layers (T), hydrogeological characteristics of the aquifer (A), hydraulic conductivity of the aquifer (C), and hydrological role of slope (S2). To determine and analyse each of these parameters, it was necessary to collect quality input data and manipulate them skilfully within the ESRI ArcGIS software package. Since a larger amount of spatial input data was not available for some parameters, e.g., soil data, decisions about values had to be made based on theoretical values, and as interpolation method was applied for point data, the reliability of applying the SINTACS method in some segments may be considered low. However, ultimately, there are weighting factors that improve the analytical process and provide an additional dimension of adaptation to the prevailing conditions in the research area. In addition to the above, the SINTACS method includes seven parameters in its evaluation, which presents a challenge in situations with a lack of sufficient input data. To precisely assess the parameters, it is necessary to have high-quality input data, which is not always easy to collect. After collecting input data, it is essential to carefully analyse their relevance, and for quality analysis and precise approximation, it is important to have a detailed knowledge of the hydrogeological and environmental characteristics of the researched area.

From the obtained maps of natural vulnerability of the Velika Gorica well field recharge area, it is visible that the entire observed area in both scenarios is characterized by aquifer vulnerability index greater than large, highlighting the vulnerability to groundwater contamination in this area. Finally, it is clear that the right approach to the management and protection of groundwater resources can minimise the risk of aquifer contamination in such a sensitive area. The large number of consumers and the resulting high demand for groundwater from the Zagreb aquifer emphasise the importance of protecting the recharge area of the Velika Gorica well field and all other well fields within the Zagreb aquifer.

6. References

1. Aller, J.R., Bennet, T., Feheer, J.H., Petty R.J. & Hackett G. (1987): DRASTIC, a standardised system for evaluating groundwater pollution potential using hydrogeological settings. US EPA 600/2-87-035.
2. Bačani, A. & Posavec, K. (2009): Elaborat zaštitnih zona vodocrpilišta Velika Gorica. Fond stručnih dokumenata Zagrebačke županije. 2-39.
3. Basch, O. (1981): Osnovna geološka karta SFRJ 1:100 000. List Ivanić Grad L33-81 [Basic geological map of SFRY 1:100 000, Ivanić Grad sheet - in Croatian] - Geološki zavod, Zagreb, Savezni geološki zavod, Beograd.
4. Basch, O. (1983): Osnovna geološka karta SFRJ 1:100 000. Tumač za list Ivanić Grad L33-81 [Basic geological map of SFRY 1:100 000, Geology of the Ivanić Grad sheet - in Croatian] - Geološki zavod, Zagreb, Savezni geološki zavod, Beograd, 66 p.
5. Civita, M. (1994): Le carte della vulnerabilità degli acquiferi all'inquinamento: teoria e pratica. Quaderni di tecniche di protezione ambientale, Pitagora Editrice Bologna, 7, pp. 325.
6. Civita, M. & De Maio, M. (2000): SINTACS R5, a new parametric system for the assessment and automating mapping of groundwater vulnerability to contamination. Pitagora Editor, Bologna, 226 p.
7. Civita, M. & De Maio, M. (2004): Assessing and mapping groundwater vulnerability to contamination: The Italian “combined” approach. Geofísica Internacional, 43, 513-532.
8. Posavec, K. (2006): Identifikacija i prognoza minimalnih razina podzemne vode zagrebačkog aluvijalnog vodonosnika modelima recesijskih krivulja. [Identification and prediction of minimum ground water levels of Zagreb alluvial aquifer using recession curve models] Doktorska disertacija. Sveučilište u Zagrebu Rudarsko-geološko-naftni fakultet. 89 p.
9. Ružičić, S. (2013): Model transporta potencijalno toksičnih elemenata kroz nesaturiranu zonu na području regionalnog vodocrpilišta Kosnica. [Transport model of potentially toxic elements through unsaturated zone at regional wellfield Kosnica] Doktorska disertacija. Sveučilište u Zagrebu Rudarsko-geološko-naftni fakultet. 183 p.
10. Šikić, K., Basch, D. & Šimunić, A. (1977): Osnovna geološka karta SFRJ 1:100.000. List Zagreb: l 38-80 [Basic geological map of SFRY 1:100 000, Zagreb sheet - in Croatian] – Institut za geološka istraživanja, Zagreb (1972), Savezni gelolološki zavod, Beograd.
11. Šikić, K., Basch, D. & Šimunić, A. (1979): Osnovna geološka karta SFRJ 1: 100.000. Tumač za list Zagreb, l 38-80 [Basic geological map of SFRY 1:100 000, Geology of the Zagreb sheet - in Croatian] – Institut za geološka istraživanja, Zagreb (1972), Savezni geološki zavod, Beograd, 81 p.

Internet sources:

URL1: https://narodne-novine.nn.hr/search.aspx?sortiraj=4&kategorija=1&godina=2009&broj=30&rpp=200&qtype=1&pretraga=da (accessed 5th June 2024)

URL2: https://narodne-novine.nn.hr/search.aspx?sortiraj=4&kategorija=1&godina=2008&broj=91&rpp=200&qtype=1&pretraga=da (accessed 5th June 2024)

URL3: https://narodne-novine.nn.hr/search.aspx?sortiraj=4&kategorija=1&godina=2019&broj=66&rpp=200&qtype=1&pretraga=da (accessed 5th June 2024)

URL4: https://narodne-novine.nn.hr/search.aspx?sortiraj=4&kategorija=1&godina=2021&broj=84&rpp=200&qtype=1&pretraga=da (accessed 5th June 2024)

URL5: https://narodne-novine.nn.hr/search.aspx?sortiraj=4&kategorija=1&godina=2023&broj=47&rpp=200&qtype=1&pretraga=da (accessed 5th June 2024)

URL6: https://www.voda.hr/sites/default/files/dokumenti/propisi-i-obrasci/01_-_directive_2000-60-ec.pdf (accessed 5th June 2024)

URL7: https://geoportal.dgu.hr/wms (accessed 5th June 2024)

URL8: https://narodne-novine.nn.hr/search.aspx?sortiraj=4&kategorija=1&godina=2023&broj=84&rpp=200&qtype=1&pretraga=da (accessed 5th June 2024)

SAŽETAK

Procjena prirodne ranjivosti priljevnog područja crpilišta Velika Gorica

Podzemna voda je važan prirodni resurs i igra ključnu ulogu u očuvanju ekosustava, osiguravanju pitke vode te opskrbi različitih industrija u Republici Hrvatskoj. Stoga predstavlja veliki izazov od iznimne važnosti za hidrogeologe posvećene zaštiti njihove kvalitativne i kvantitativne cjelovitosti. U ovom se radu primjenjuje jedna od najčešćih metoda korištenih u projektima zaštite podzemnih voda, a to je procjena prirodne ranjivosti vodonosnika. Fokus je na priljevnom području crpilišta Velika Gorica, koje se nalazi u zagrebačkom vodonosniku građenom od aluvijalnih naslaga. Procjena prirodne ranjivosti priljevnog područja crpilišta Velika Gorica provedena je korištenjem parametarske metode SINTACS. Ova metoda uključuje procjenu sedam parametara i primijenjena je za dva različita scenarija. Konačni indeks ranjivosti određen je množenjem vrijednosti parametara s težinskim koeficijentima. Rezultat je karta koja ilustrira prirodnu ranjivost priljevnog područja crpilišta Velika Gorica. Ova karta prikazuje različite zone s različitim stupnjevima prirodne ranjivosti. Procjena pokazuje da cijelo promatrano područje spada u klasu ranjivosti podzemnih voda veću od visoke u oba scenarija. To ukazuje na značajan rizik od onečišćenja podzemnih voda u priljevnom području crpilišta Velika Gorica.

Ključne riječi: indeks ranjivosti; SINTACS metoda; aluvijalni vodonosnik; crpilište Velika Gorica

Author's contribution

Marin Validžić (1) (mag. ing. geol.) made data analysis and vulnerability analysis. **Jelena Parlov (2)** (full professor) participated in the evaluation of the input data and vulnerability analysis. **Dario Perković (3)** (associated professor) contributed to data processing and interpretation of the spatial analysis.

5th Croatian geomathematical congress
UDC: 622.3; category: original scientific paper

Possibilities of analysing the pressure build-up test in the vertical oil well with decreased production

Sonja Koščak Kolin[1]; Vladislav Brkić[1]; Nikola Jukić[2]; Sonja Buti Njie[3]
[1] University of Zagreb, Faculty of Mining, Geology and Petroleum Engineering, Pierottijeva 6, 10 000 Zagreb, Croatia, ORCID 0000-0003-0056-4466
[1] University of Zagreb, Faculty of Mining, Geology and Petroleum Engineering, Pierottijeva 6, 10 000 Zagreb, Croatia, ORCID 0000-0003-2075-1832
[2] AGS Hrvatska d.o.o.. Zagrebačka avenija 100A, 10 000, Zagreb, Croatia
[3] INA - Industrija nafte, d.d., Avenija Većeslava Holjevca 10, 10 020 Zagreb, Croatia
Corresponding author: sonja.koscak-kolin@rgn.unizg.hr

Abstract

The paper describes the pressure build-up test analysis of the vertical oil well using the Saphir programme. The main objective is to determine the permeability of the rock and the skin factor. In order to obtain the most reliable results, three cases are analysed depending on the PVT properties of the fluid. In the first case, the fluid is assumed to be single-phase, in the second case two-phase and in the third case multiphase. Although the Bourdet log-log diagram method did not reach the transient phase in any of three cases because there was no complete overlap of the measured data and modelled curves, the results can be accepted with sufficient accuracy according to the descriptions in the discussion. The most reliable result is obtained in the first analysis. The permeability of the rock is determined to be 0.18 mD (1.78E-16 m^2) and the corresponding skin factor is 3.7.

Keywords: Pressure build-up test analysis; rock permeability; skin effect

1. Introduction

Well testing represents an important segment of oil and gas production and reservoir engineering. Analysis of the well test data indicates the possibility that the reservoir rock can produce reservoir fluids. The interpretation of the measured data can reveal the permeability of the reservoir rock, reservoir pressure, skin effect, radius of the stimulation, hydrodynamic connection of reservoir parts or boundaries of the reservoir (**Bourdarot, 1998**). Information about the reservoir and the well is collected throughout the life of the well in order to obtain the most accurate descriptions of the changes in production conditions in the well and in the reservoir by means of pressure analyses. The most common method for well testing is pressure build-up test, as it provides the necessary data for well models that continuously monitor, describe and forecast well production. A pressure build-up test is performed by allowing the well to produce at a constant flow rate and then shutting it down for a certain period of time. During the entire process, the pressure in the well is monitored and recorded. In this way, pressure build-up curve is obtained over a certain period of time, which is then analysed using the Saphir computer programme, that is part of the KAPPA Workstation software package (University Licence #9643) (www.kappaeng.com). During the analysis, the software first transforms the dimensionless solutions of the diffusion equation according to the principle of superposition (**Houze, et al., 2022**). The resulting solutions are then used to create a model that is compared by the programme with the measured values. In this way, matching points are obtained from which certain properties of the reservoir can be determined (**Koščak Kolin, 2018**). The main purpose of such tests is mainly to determine the permeability of the reservoir rock (k) and the skin factor (s) as well as the reservoir pressure.

The pressure build-up test of vertical well X, located on reservoir Y, is analysed with the Saphir programme. Three analyses of the pressure build-up test are performed assuming a single-phase, two-phase and multiphase fluid in order to compare the results and determine the permeability of the reservoir rock (k) and the skin effect (s) as accurately as possible. After entering the input data

and describing the analytical model for each case, a discussion of the results obtained is carried out.

2. Methods

The fluid flow in the reservoir is the theoretical basis for analysing the pressure increase test in the vertical well, since the corresponding solutions of the diffusion equation for radial flow are used, as in production tests, but assuming a constant flow, which is 0 because the well is closed during the test (**Čikeš, 2015**). Based on these solutions, the equations are adapted to determine certain properties such as the permeability of the reservoir rock (k) and the skin effect (s). The final form of the diffusion equation in the radial system is shown by **Equation 1**:

$$\frac{\partial^2 p}{\partial r^2} + \frac{1}{r}\frac{\partial p}{\partial r} = \frac{\phi \mu c_t}{k}\frac{\partial p}{\partial t} \tag{1}$$

where are:
p – pressure (Pa),
r – radius (m),
ϕ – porosity (%),
μ – viscosity (Pa·s),
c_t – total compressibility (Pa^{-1}),
k – rock permeability (m^2),
t – time (s).

In the analysis of the pressure build-up test, the dimensionless form of the diffusion equation is used, which is expressed with dimensionless variables: dimensionless pressure (p_D), dimensionless time (t_D) and dimensionless radius (r_D). With initial and boundary conditions, the solution of the dimensionless form of the diffusion equation for transient flow is in an infinite reservoir (**Čikeš, 2015**):

$$p_D(t_D) = \frac{1}{2}(\ln t_D + 0.80907) \tag{2}$$

Using the dimensionless variables, type curves are defined for the analysis of production tests and pressure build-up tests in the method called Bourdet log-log diagram, (**Figure 1**), that is integrated into the Saphir programme as well. The analysis of the pressure build-up test is based on the PTA theory or Pressure Transient Analysis. The reason for this is that the well must be kept closed for the measurement until the pressure in the well stabilises, and stabilisation is achieved when the infinite acting radial flow (IARF) is reached. The wellbore storage effect occurs after closing and manifests as a left asymptote, which has a slope of one during the entire storage effect. This Bourdet diagram is solved by grouping dimensionless variables, where the dimensionless pressure (p_D) is a function of the dimensionless group (t_D/C_D) and the curves are described by the value of the parameter (C_De^{2s}) (**Bourdet, 1989**). At the beginning, all curves asymptotically approach the line with the slope of value one, and after the initial phase, the solution of the diffusion equation for an infinite reservoir is applied. In the further development of the typical curves, the derivative of the pressure (p_D') is introduced. Initially, the given curves in the log-log system have a unit slope, while the curves become horizontal at the moment the IARF is reached and have a value of 0.5. If the measurement data in the log-log diagram correspond to the second asymptote at the end of the measurement, this means that pressure stabilisation has been achieved (**Gringarten, 2008**). The application of the typical curve method consists of overlapping the

measured data with typical curves. After overlapping, matching points are selected and used to calculate the rock properties (**Liu et al., 2018**; **Jirjis and Abdulaziz, 2019**).

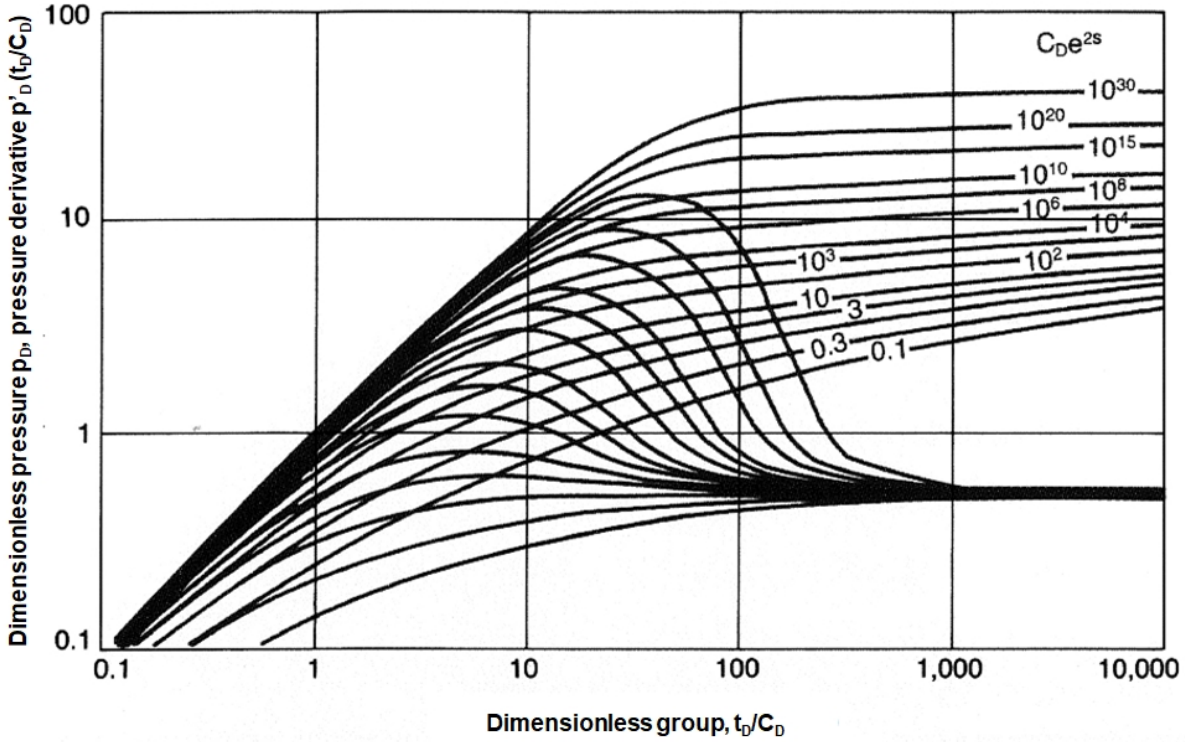

Figure 1: Bourdet diagram with type curves for an infinite reservoir (**Economides and Nolte, 2000**)

In the following, an analysis of the pressure build-up test of a vertical oil well was carried out using the Saphir programme (**Houze et al., 2022**). All reservoir and well parameters are taken from INA's technical documentation (**INA, 2014**). The actual name of the well or oil field is not given, as the name of the field is labelled Y and the well is labelled X.

3. Basic technical data of a well X

The well is located on a reservoir Y in the north-west of Croatia. The altitude in this area is between 150 and 250 metres. The reservoir is completely saturated with oil, and well X, which is located in the centre of reservoir Y, is a production well. Oil field Y has been exploited continuously since 1989, with the exception of six months in 1997, when it was temporarily shut down due to high transport costs (**INA, 2014**).

The length of well is 2283 m (TMD-True Measured Depth). The bottom of the column is at 1460 metres. The top of the cement plug is at 1460 metres and there are three open intervals in the well. The first interval is at a depth of 1425 metres to 1431 metres (TMD), the second interval is at a depth of 1433 metres to 1441 metres (TMD) and the third interval is at a depth of 1445 metres to 1488 metres (TMD). Well X is producing with the aid of down hole pump.

4. Main results of pressure build-up test analyses

The pressure build-up test in the vertical oil well X, which is analysed using the Saphir programme (University Licence #9643), lasted a full 360 hours (**Jukić, 2022**). The dynamic pressure at the bottom of the oil well was 31.8 bar at the time of closure and rose to 118.5 bar, after pressure stabilisation at the end of the measurement (**Figure 2**).

At the beginning of the analysis, the data required for the interpretation and calculation of the results are entered into the programme (**Houze et al., 2022; Kappa-Workstation, 2024**). These are the well radius of 0.03016 m, the thickness of the production layer, which in this case is effectively 6.9 m, the compressibility of the rock of 4.9E-10 Pa^{-1}, the porosity of 22.3% and the depth of the production layer of 1425 m. In the next step, the properties of the fluid are entered, such as the volume factor of oil 1.285 m^3/m^3, viscosity 7E-4 Pas, and total compressibility 1.26E-9Pa^{-1}.

When defining the parameters for the analytical model in the final step of entering the input data, four key conditions are selected to determine the output model in analysis of the pressure build-up test. These are Wellbore storage, which is constant in this case, the Well model, i.e. the vertical well, the Reservoir model, for which homogenity is assumed, and the Boundary model, in which the reservoir is assumed to be infinite (**Kappa-Workstation, 2024)**.

In accordance with the flow and pressure measurement data before and after closing the well for the build-up test, the entire test is shown in **Figure 2**, which is analysed with the change in PVT data. This means that the test is first analysed assuming a single-phase fluid, then for a two-phase fluid and finally for a multiphase fluid (**Valjak, 2021**). This case analyses are performed to determine the most accurate properties of the reservoir, i.e. the results for rock permeability (k) and skin factor (s), because after the long-term operation of the well since 1989, the hydrodynamic state of the reservoir has also changed significantly, which affects the results of such analyses. Therefore, the overlap of the measured data with the typical curves in the log-log diagram can hardly be fully realised, which is discussed by presenting the results of individual cases (**Azi et al., 2008**).

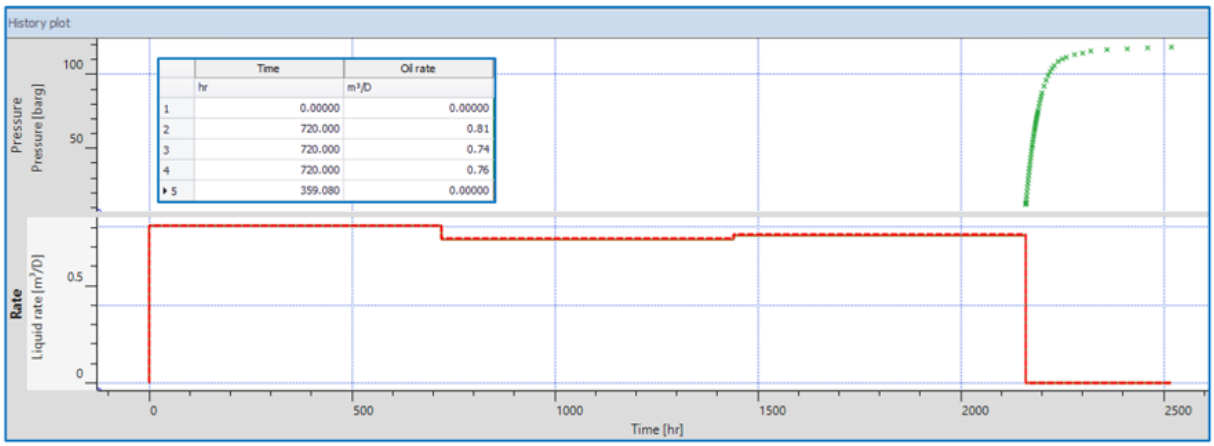

Figure 2: History plot

Figure 2 shows that the well was stabilised over a long period of time before it was closed in order to obtain more accurate results during interpretation (**Jukić, 2022**). An attempt was made to maintain a constant flow, which strongly influences the accuracy of the application of theoretical solutions. The diagram shows three phases of well stabilisation, i.e. stabilisation of flow, prior to the actual shut-in, initially producing at a constant oil flow of 0.81 m^3/day for a period of 720 hours, then at a constant flow of 0.74 m^3/day for the next 720 hours and finally at a flow of 0.76 m^3/day for the next 720 hours. As mentioned earlier, this was followed by a 360-hour pressure build-up test, during which the measurement curve increased from a dynamic pressure of 31.8 bar at the time the well was closed to a static pressure of 118.5 bar at the end of the test. In **Figure 2**, these pressure measurement data are marked with green crosses. Although the build-up test for a conventional reservoir type theoretically lasted long enough in terms of permeability, the results for all three analysis cases show that pressure stabilisation could not be fully achieved even though all production requirements for well operation were met. This is shown by the insufficient overlap of the curve of the pressure derivative with the typical curves, i.e. with the modelled curves in the log-log diagram, which is discussed later. At this point, it should be noted that the test conducted

was carried out in 2007, when the well reached a relatively low flow rate and was a potential candidate for future hydraulic fracturing. For this reason, it was necessary to carry out such detailed tests because the success of the stimulation procedure design to increase the productivity of the well, i.e. the success of the hydraulic fracturing procedure (**Sun and Schechter, 2015**), depends largely on the required results for rock permeability (k) and skin factor (s).

The 'History plot' in **Figure 2** refers to the first case of analysis of the pressure build-up test for a single-phase fluid, where it is assumed that the well produces only oil, the flow of which is shown with a red line before closing.

4.1. Pressure analysis for a case of a single-phase fluid

Figure 3 shows the log-log diagram for the first case of the analysis, where the fluid is assumed to be single-phase, and **Figure 4** shows the corresponding results of this analysis, where the key to the comparison with the other two cases for two-phase and multiphase fluid are the rock permeability (k) and the skin factor (s). In the diagram, the measured pressure data are marked with green crosses and their derivatives with red circles, while the solid red and black lines refer to type curves, i.e. modelled pressure values and derivatives that the programme approximates, achieving maximum accuracy when the curves overlap. The theoretical conditions must be satisfied that the beginning of the measured and derived data coincides with the first dashed direction of slope 1, which indicates the period of fluid storage in the well, which is fulfilled, and that the final derived pressure values coincide with the second dashed direction, i.e. with an asymptote of 0.5, which is not completely fulfilled. The reason for this could be the possible proximity of the fault (**Koščak Kolin, et al., 2013**), as a result of which the pressure response does not enter the stabilisation, but it can be concluded that the scattering of the data around the asymptote of 0.5 indicates a slight anomaly, the influence of which could not have been known before the measurement.

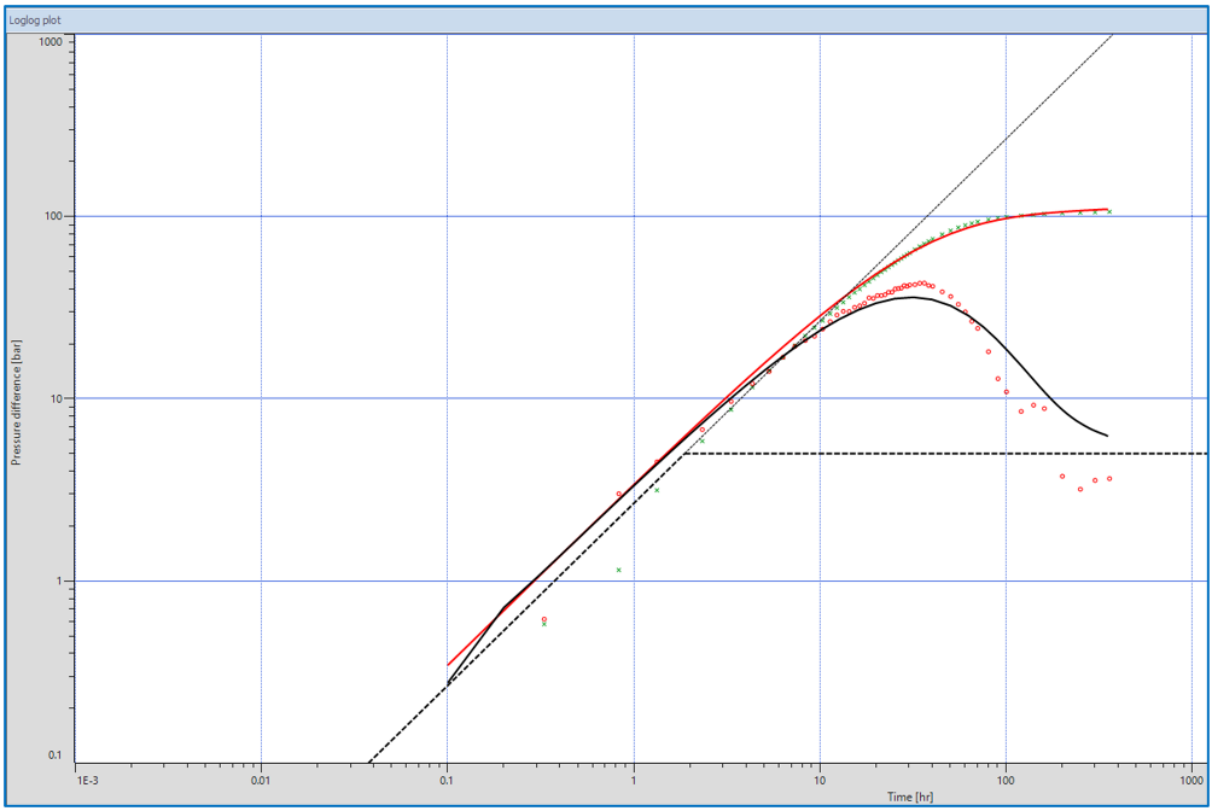

Figure 3: The first analysis for a single-phase fluid

When displaying the results in **Figure 4**, the programme lists the conditions selected when creating the analysis model. The most important results for all three analyses are presented together in **Table 1**. In addition to the results for reservoir pressure (p_i), permeability (k) and skin factor (s) already mentioned, the product of permeability and effective reservoir thickness (kh) and the storage constants (C) are also given.

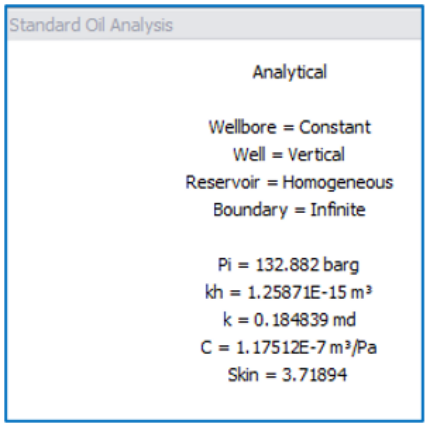

Figure 4: Results of the first analysis

4.2. Pressure analysis for a case of a two-phase fluid

Figure 5 shows the log-log diagram for the second analysis, in which the data had to be supplemented with additional laboratory parameters for the two-phase fluid compared to the first analysis, which unfortunately were not all known, as additional laboratory tests have to be carried out. Since some of them are not available, they are assumed in accordance with software corellation, in order to obtain the first insight into the evaluation of the results of the second analysis. For this reason, in practise only the analysis for a single-phase fluid is usually carried out. As it can be seen, the overlap of measured and modelled data has not improved compared to the first analysis, but there were differences in the results (**Figure 6**), which are discussed according to **Table 1**.

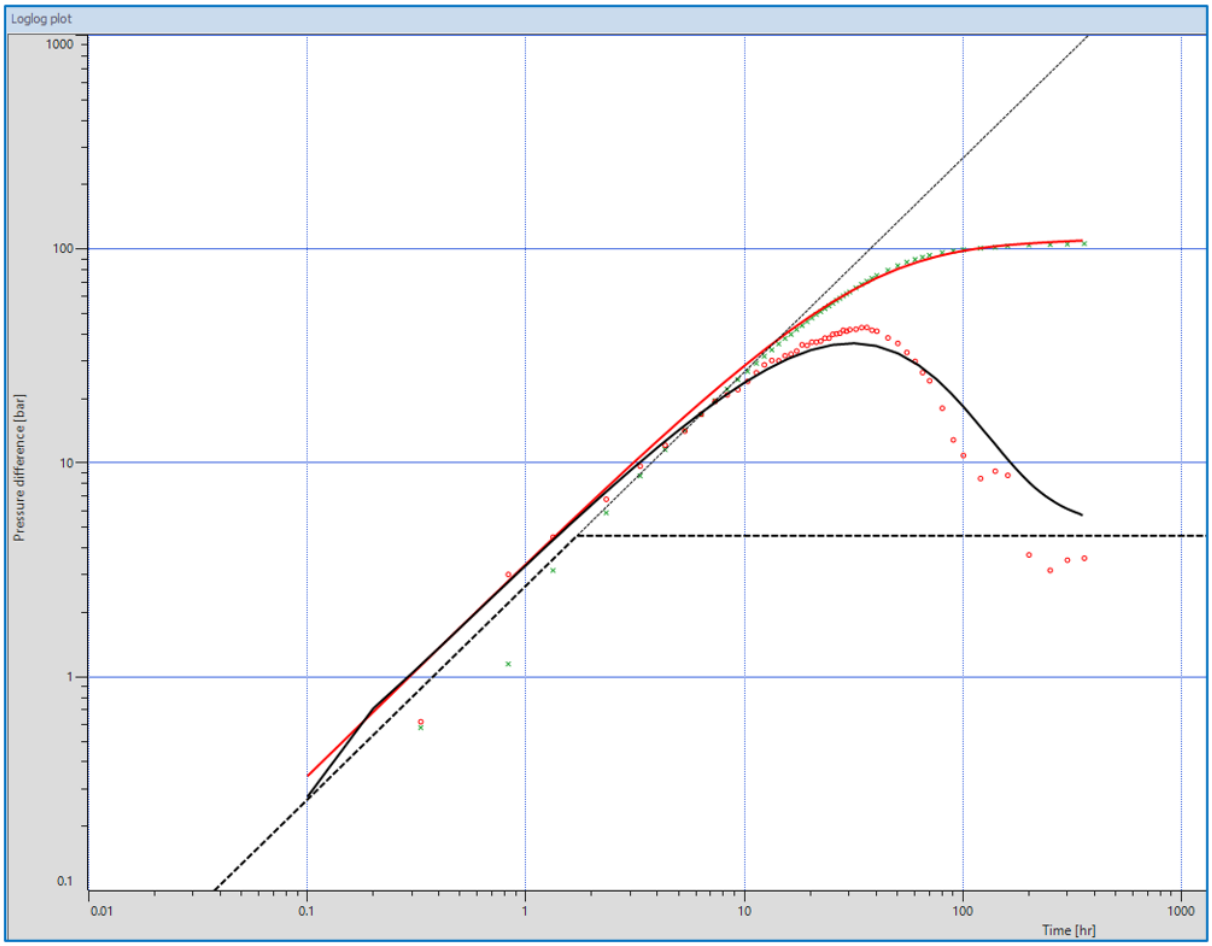

Figure 5: The second analysis for a two-phase fluid

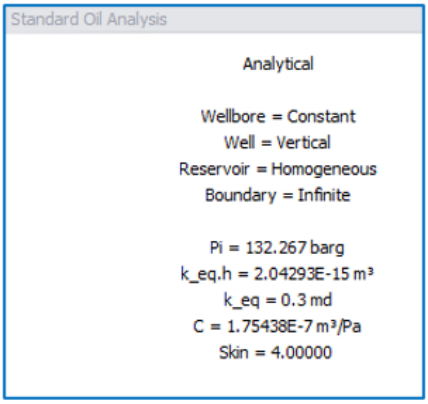

Figure 6: Results of the second analysis

4.3. Pressure analysis for a case of a multiphase fluid

Analogous to the second analysis, **Figure 7** shows the log-log diagram for the third analysis of the pressure build-up test, in which the input data for the PVT properties also had to be supplemented with additional laboratory parameters for the multiphase fluid (**Kamal and Pan, 2011; Koščak Kolin, et al., 2018; Perrine, 1956**), not all of which were available. For this reason, some of them were also corellated to provide a first insight into the evaluation of the results of the third analysis (**Figure 8**). As it can be seen again, the overlap of the measured and modelled data in the log-log diagram did not improve compared to either the first or the second analysis, i.e. it remained almost identical to the single-phase fluid. For this reason, the further option of the Saphir programme to improve the analytical model into a numerical one was not implemented, as there

would again be a lack of input parameters. This is a common case in practise, considering that the relatively expensive process of their determination in the laboratory is an additional cost factor in relation to the high price of the measurements and the price of their high-quality interpretation.

However, in the case of well X, the available production parameters indicate that the water and gas content in the production was not significant and therefore the single-phase assumption is optimal and sufficient. This ultimately means that the first analysis shows a smaller deviation in the results than the others, which assumed more parameters in the definition of the model.

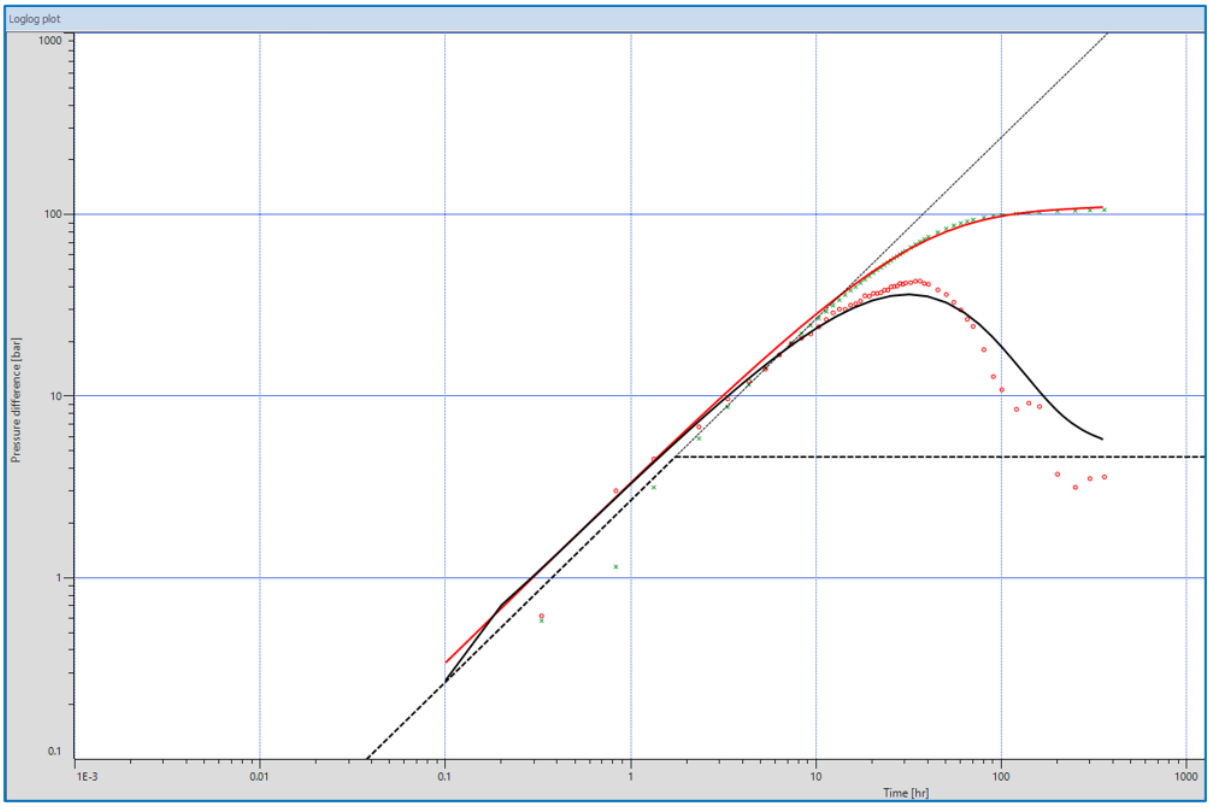

Figure 7: The third analysis for a multiphase fluid

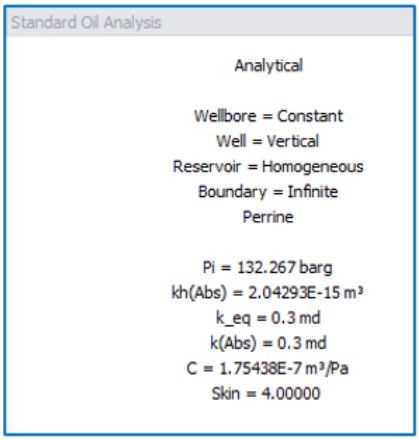

Figure 8: Results of the third analysis

5. Discussion

Table 1 shows the results of all three analyses of the pressure build-up test in the vertical oil well X, which lasted 360 hours (**Jukić, 2022**). From all the interpreted log-log diagrams in **Figures 3**, **5** and **7**, it can be concluded that the necessary pressure stabilisation at the end of the test is not completely fulfilled, as the second asymptote of 0.5 shows an incomplete overlap with the

derivatives of the last measured pressures. According to the theoretical assumptions of the PTA analysis described above, achieving the IARF is a condition for the applied model to provide reliable results. Another possibility of incomplete overlap could be the proximity of the fault, which could have an influence on the pressure response where the derivatives do not match the second asymptote even after a longer measurement period. However, it should be noted that although the modelled line does not overlap with the second asymptote, it still satisfactorily describes the derived data throughout the test. The same applies to the modelled line, which describes the entire pressure curve very well, meaning that the results can still be taken with approximate accuracy.

In this regard, the investigation of the influence of fault is omitted, as the dispersion of the results in each analysis is not too large, especially in relation to the values obtained for permeability. The main conclusion is therefore that the most reliable result was obtained in the first analysis, i.e. that the permeability of the reservoir rock is 0.18 mD (1.78E-16 m^2), regardless of the fact that a value of 0.3 mD (2.96E-16m^2) is obtained in the other two analyses. Although this is not a big difference compared to the first result, in the second and third analyses a larger number of assumptions are entered for the PVT parameters based on the built corelations, which increases the deviation of their results.

Taking the above explanations into account, the result for the skin factor is also selected from the first analysis because it depends on the permeability and is 3.7. Furthermore, it can be concluded that well X is a good candidate for hydraulic fracturing as its production rate has decreased from the initial production in 1989, when it produced about 10 m^3/day, to about 0.8 m^3/day in 2007, when the analysed build-up test was performed. According to INA's documentation (**INA, 2014**), well X is currently produces only 0.3 m^3/day of oil, and the water cut has also increased slightly compared to 2007.

Table 1: Results of the pressure build-up test analyses

Cases	PVT condition	**Results**	
		Permeability	Skin factor
		mD	-
1. analysis	Single-phase fluid	0.18	3.7
2. analysis	Two-phase fluid	0.3	4.0
3. analysis	Multiphase fluid	0.3	4.0

6. Conclusions

The main objective of the analysed well test is to determine the permeability of the rock and the skin factor after the well has been producing for a long period of time, so that the production possibilities of the reservoir and the well have changed and decreased compared to the initial period. In order to determine the most reliable results and compare them, three cases are analysed depending on the PVT properties of the fluid. In the first case, the fluid is assumed to be single-phase, in the second two-phase, and in the third case multiphase.

According to the interpretation of the associated log-log diagrams, all three analyses of the pressure build-up test indicate that the necessary stabilisation of the pressure at the end of the test is not completely fulfilled, which, according to the condition of the PTA, means that the IARF, i.e. the applied solutions of the specified analytical model, could give deviations in the accuracy of the results. It can be concluded from the diagram that the complete overlap of the measured and modelled curves most likely did not occur due to the proximity of the fault, but the modelled lines nevertheless describe the entire pressure curve and its derivative well, so that the results can be taken with sufficient accuracy.

The most reliable result is obtained in the first analysis and the permeability of the reservoir rock is determined to be 0.18 mD (1.78E-16 m^2), which is not very different from the results of

the second and third analyses, where, however, a larger number of assumptions are made for the input of the PVT parameters, which increased their deviation.

The result for the skin factor is selected from the first analysis, which means that the well is a good candidate for hydraulic fracturing, as its production capacities have drastically decreased from an initial flow of about 10 m^3/day to about 0.8 m^3/day in 2007, when the analysed build-up test was performed.

7. References

1. Azi, A. C., Gbo, A., Gringarten, A. C. (2008): Evaluation of Confidence Intervals in Well Test Interpretation Results. In Proceedings of the Europec/EAGE Conference and Exhibition, Rome, Italy, 9–12 June. https://doi.org/10.2118/113888-MS
2. Bourdarot, G. (1998): Well Testing: Interpretation Methods. Center for Petroleum Engineering and Project Development, Paris, 337 p.
3. Bourdet, D., Ayoub, J. A., Pirard, Y. M. (1989): Use of Pressure Derivative in Well-Test Interpretation. SPE Journal of Formation Evaluation, 4 (2), 293-302. https://doi.org/10.2118/12777-PA
4. Čikeš, M. (2015): Proizvodno inženjerstvo nafte i plina (*Oil and Gas Production Engineering*). Faculty of Mining, Geology and Petroleum Engineering University of Zagreb, Zagreb, 524 p.
5. Economides, M. J., Nolte, G. N. (2000): Reservoir Stimulation. John Wiley & Sons, 3rd edition, 20 chapters.
6. Gringarten, A. C. (2008): From Sraight Lines to Deconvolution: The Evolution of the State of the Art in Well Test Analysis. SPE Reservoir Evaluation & Engineering, 11 (1), 41-62. https://doi.org/10.2118/102079-PA
7. Houze, O. et al (2022): Dynamic Data Analysis v5.50, KAPPA, 778 p.
8. INA – Industrija nafte, d. d. (2014): Technical documentations.
9. Jirjis, A. Y., Abdulaziz, A. M. (2019): Influences of uncertainty in well log petrophysics and fluid properties on well test interpretation: An application in West Al Qurna Oil Field, South Iraq. Egypt. J. Pet., 28, 383–392. https://doi.org/10.1016/j.ejpe.2019.08.005
10. Jukić, N. (2022): Analiza testa porasta tlaka vertikalne bušotine primjenom programa Saphir (*Pressure build-up test of the vertical well in programme Saphir*). Graduate thesis, Rudarsko-geološko-naftni fakultet Sveučilišta u Zagrebu, Zagreb, 51 p. (*in Croatian – English abstract)*
11. Kamal, M. M., Pan Y. (2011): Pressure transient testing under multiphase conditions. Proceedings of the SPE Middle East Oil and Gas Show and Conference, Bahrain, 2528 September, Society of Petroleum Engineers, SPE 141752.
12. Kappa-Workstation (2024): Saphir (PTA) Tutorial. 18 p.
13. Koščak Kolin, S., Čikeš, M. and Babić, V. (2013): Analiza testa porasta tlaka horizontalne bušotine (*Pressure Build-up Test Analysis of the Horizontal Well*). Rudarsko-Geološko-Naftni Zbornik, 26 (1), 11-28. (*in Croatian – English abstract)*
14. Koščak Kolin, S., Kurevija, T., Grebenar, D. (2018): Pressure Build-up Test Analysis of the Reservoir System with the Multiphase Flow. Rudarsko-Geološko-Naftni Zbornik, 33 (3), 75-84. https://doi.org/10.17794/rgn.2018.3.8
15. Koščak Kolin, S. (2018): Pouzdanost određivanja propusnosti slabo propusnih plinskih ležišta optimiranjem trajanja testa porasta tlaka (*Reliability of the Permeability Determination of the Low Permeability Reservoirs by Optimizing the Pressure Build-up Test Duration*). Doctoral thesis, Faculty of Mining, Geology and Petroleum Engineering University of Zagreb, Zagreb, 244 p. (*in Croatian – English abstract)*
16. Liu, Q., Lu, H., Li, L., Mu, A. (2018): Study on characteristics of well-test type curves for composite reservoir with sealing faults. Petroleum, 4, 309–317. https://doi.org/10.1016/j.petlm.2018.03.011

17. Perrine, R. L. (1956): Analysis of Pressure Build-up Curves Theoretical Foundation of Multiphase Pressure Buildup Analyses. American Petroleum Institute, New York, API-56-482.
18. Sun, J., Schechter, D. (2015): Investigating the Effect of Improved Fracture Conductivity on Production Performance of Hydraulically Fractured Wells: Field-Case Studies and Numerical Simulations. Journal of Petroleum Technology, 54 (6), 442-449. http://dx.doi.org/10.2118/169866-PA
19. Valjak, A. (2021): Analiza testa porasta tlaka hidraulički frakturirane bušotine primjenom programa Saphir (*Pressure build-up test of the hydraulically fractured well in programme Saphir*). Graduate thesis, Faculty of Mining, Geology and Petroleum Engineering University of Zagreb, Zagreb,78 p. (*in Croatian – English abstract)*

Internet sources:
URL: https://www.kappaeng.com/software/saphir/overview (accessed 28th May 2024.)

SAŽETAK

Mogućnosti analize testa porasta tlaka u vertikalnoj naftnoj bušotini sa smanjenjem proizvodnje

U radu je opisana analiza testa porasta tlaka vertikalne naftne bušotine s pomoću programa Saphir. Glavni cilj je odrediti propusnost stijene i skin faktor, a u svrhu dobivanja što pouzdanijih rezultata, analizirana su tri slučaja, ovisno o PVT svojstvima fluida. U prvom slučaju je pretpostavljeno da je fluid jednofazan, u drugom da je dvofazan i u trećem da je višefazan. Iako metoda Bourdet log-log dijagrama nije dosegla prijelaznu fazu ni u jednom od tri slučaja, jer nije bilo potpunog preklapanja mjerenih podataka tlaka i njegove derivacije s modeliranim krivuljama, rezultati se mogu prihvatiti s dovoljnom točnošću prema obrazloženjima u diskusiji rezultata. Najpouzdaniji rezultat dobiva se u prvoj analizi. Propusnost stijene je određena u iznosu od 0,18 mD (1.78E-16 m^2), a pripadajući skin faktor je 3,7.

Ključne riječi: analiza testa porasta tlaka; propusnost; skin faktor

Author's contribution

Sonja Koščak Kolin (Assistant Professor, PhD) Formal analysis, Methodology, Interpretations and presentation of the results, Writing- Original draft preparation, Supervision, Writing – review & editing provided. **Vladislav Brkić** (Associate Professor, PhD) Investigation, Data validation, Interpretations and presentation of the results, Writing – review & editing provided. **Nikola Jukić** (Mag.ing.petrol., Petroleum engineer) Data curation, Methodology, Formal analysis, Interpretations and presentation of the results. **Sonja Buti Njie** (Mag.ing.petrol., Oil and gas production expert) Data validation, Writing – review & editing provided.

5th Croatian geomathematical congress
UDC: 622.1:550.8; category: original scientific paper

Compositional variability of minerals in outcrops and boreholes within the informal Bistra Formation, Medvednica Mt., Croatia

Danijel Ivanišević[1]; Anita Grizelj[2]
[1]Croatian geological survey, Sachsova 2, 10000 Zagreb, ORCID: https://orcid.org/0000-0001-7705-7230
[2]Croatian geological survey, Sachsova 2, 10000 Zagreb, ORCID: https://orcid.org/0000-0001-5230-4725
Corresponding author: divanisevic@hgi-cgs.hr

Abstract

This study investigates the compositional variability of minerals in the informal Bistra Formation at Medvednica Mountain, Croatia, focusing on Quaternary sediments from outcrops and boreholes. Employing modal analysis and compositional data (CoDa) statistical methodologies, the research aims to classify samples and establish associations of minerals to enhance the understanding of sediment differentiation. The analysis reveals significant variations in mineral compositions influenced by local depositional environments and weathering of specific geological formations. Key findings include the identification of two distinct depositional environments: high-energy riverine settings, which concentrate heavier minerals, and low-energy lakes or swamps, where lighter minerals accumulate. The utilization of principal component and cluster analysis further elucidates the relationships among minerals. This approach shows the usefulness of CoDa analysis in geosciences, providing deeper insights into the provenance and deposition dynamics of Quaternary sediments.

Keywords: Bistra Formation; Medvednica Mountain; modal analysis; compositional data analysis; classification

1. Introduction

The informal Bistra Formation is a lithostratigraphic unit encompassing Quaternary sediments around Medvednica Mountain. The Bistra Formation was deposited in an alluvial environment in the areas of sheet flows, breakthrough channels, longitudinal streams, and floodplains (**Avanić, 1997**; **Grizelj et al., 2017**). Similar Quaternary deposits, characterized by short transport and local provenance, can be found throughout the Pannonian Basin (**Grizelj et al., 2017**; **Nenadić et al., 2016**; **Mencin Gale et al., 2019**; **Zámolyi et al., 2017**).

These sediments were further subdivided chronologically using dating methods, and lithologically into clays, silts, sand, and gravel. However, they were not subdivided based on mineralogical composition. Although the provenance is local, the mineralogical composition can vary based on factors such as the type of source rocks and the intensity of weathering (**Peh et al., 1998**; **Novaković et al., 2018**). Different types of source rocks contribute distinct minerals to the sediments, while weathering processes can alter the original minerals and create new ones.
The aim of this study was to classify samples into groups and establish associations between minerals with minimal loss of information. The purpose of this study was to improve the differentiation of Quaternary sediments, which could be further complemented by dating, granulometric and chemical composition, and/or other methods.

2. Geographical and geological setting

The study area encompasses the south-southeastern foothills of Medvednica Mountain, extending into parts of the lower city of Zagreb (**Figure 1**). Medvednica Mountain, rising to an

elevation of 1,035 meters at its peak, is situated in northwestern Croatia, just north of the city of Zagreb.

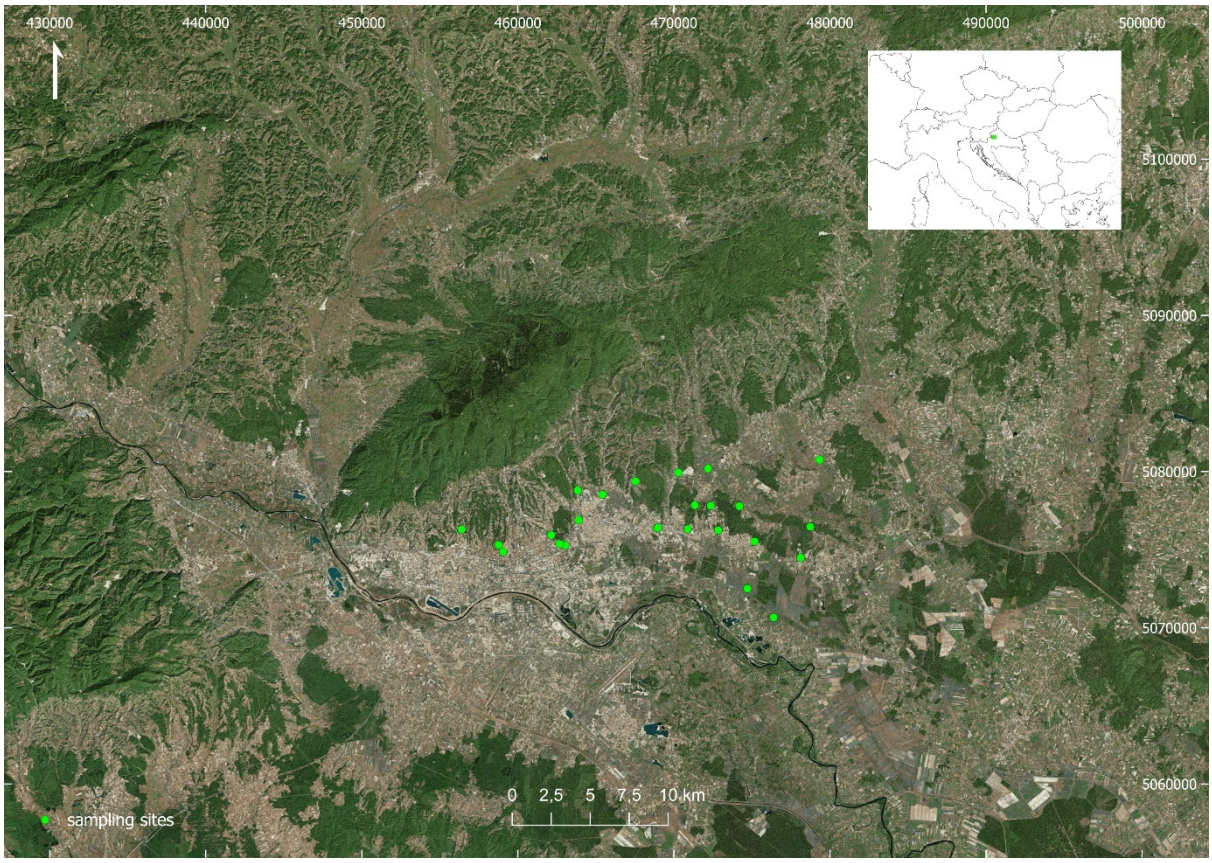

Figure 1: Study area (HTRS96 Projected coordinate system)

The geological characteristics of the study area, including sampling locations, are shown in **Figure 2**. The south-southeastern foothills of Medvednica Mountain are part of the southwestern Pannonian Basin System (**Pavelić and Kovačić, 2018**). The core of Medvednica Mountain consists mainly of metamorphic rocks, such as metapelites, metapsammites, slates, quartzites, marbles, and schists, originating from the Paleozoic and less frequently the Mesozoic eras (**Belak et al., 2022; Lugović et al., 2006**). Additionally, ophiolite mélange fragments (**Slovenec and Lugović, 2009**) and Mesozoic limestones and dolomites are present. Miocene sediments overlie the crystalline basement, consisting of various marine, brackish, and freshwater clastites. Pliocene and Quaternary sediments include clays, silts, sands, and gravels deposited in freshwater lakes, swamps, and rivers (**Basch, 1983a, 1983b**; **Vrsaljko et al., 2006**; **Kovačić and Grizelj, 2006**; **Ćorić et al., 2009**; **Brlek et al., 2016**; **Grizelj, 2017**).

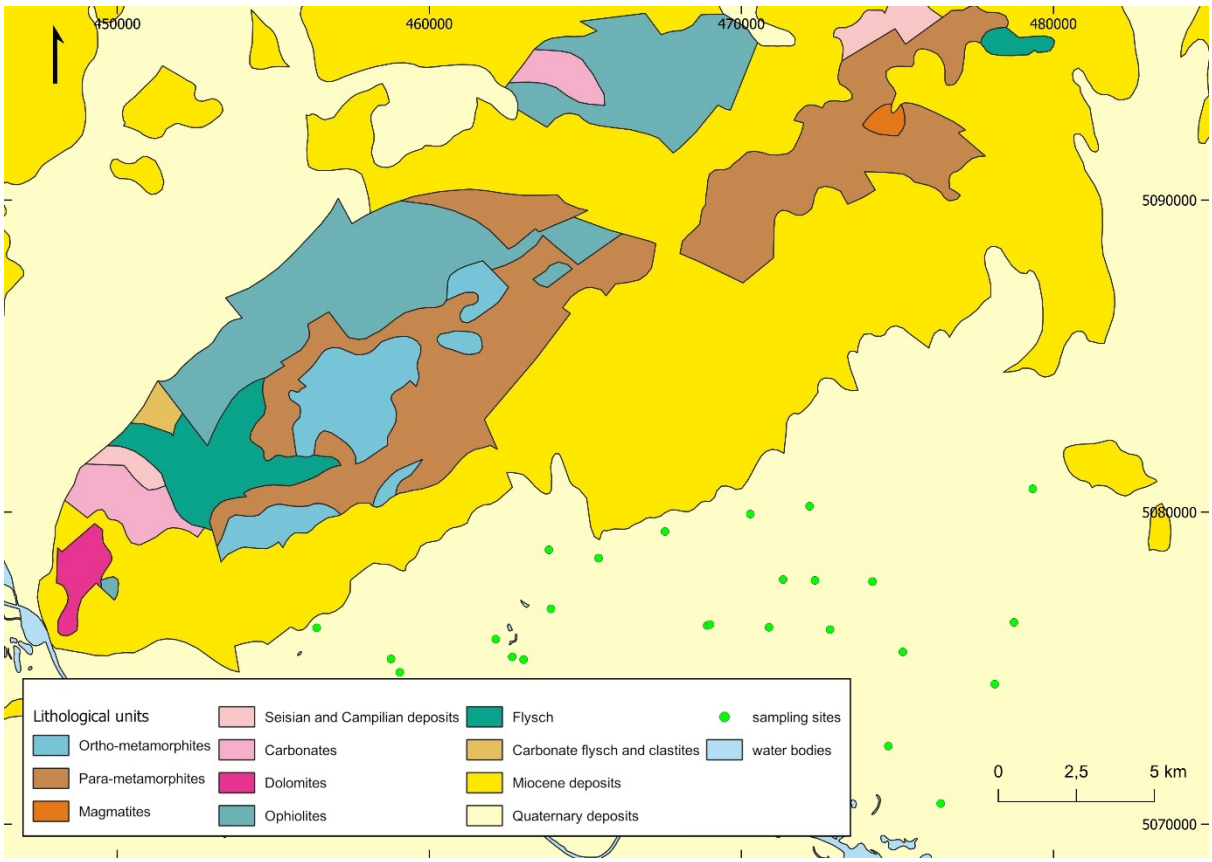

Figure 2: Geological map of the study area at a scale of 1:300,000 (simplified after **the Croatian geological survey** (**2009**); HTRS96 Projected coordinate system)

3. Materials and Methods

Data set consists of 45 samples collected from boreholes and outcrops analysed for the purpose of various projects including Geological map of the Republic of Croatia. The mineral composition of the samples at different depths was determined through modal analysis of fractions between 0.09 and 0.045mm. Calcite in the samples was dissolved using cold hydrochloric acid, and the remainder was separated into heavy and light mineral fractions using bromoform liquid. Mineral counting was performed on 300-400 grains using a microscope. The complete data set consisted of 14 variables in terms of minerals and 45 samples (**Table 1**). However, modal analysis resulted with 68 non-detects (10%). Thus, the data set represents compositional count data, consisting of non-negative integer values representing counts of different minerals.

Table 1: Counts of mineral grains (ZC – zero counts)

Sample	Opaque minerals	Chlorite	Tourmaline	Zircon	Rutile	Amphibole	Epidote-Zoisite-Clinozoisite	Garnet	Kyanite	Staurolite	Quartz	K-feldspar	Rock fragments	Muscovite
1	6	ZC	1	ZC	1	7	290	ZC	1	ZC	192	61	23	ZC
2	12	ZC	2	1	1	13	264	7	2	1	110	29	176	1
3	4	1	1	1	1	5	301	1	ZC	1	117	147	23	ZC
4	4	ZC	ZC	ZC	ZC	7	284	ZC	ZC	2	142	117	50	1
5	3	1	1	ZC	ZC	6	290	ZC	ZC	ZC	88	176	35	ZC
6	5	ZC	1	ZC	2	2	298	1	3	ZC	198	84	23	1
7	88	1	3	9	2	1	188	6	1	3	218	30	53	2
8	69	1	1	4	6	15	192	12	1	3	182	13	98	3
9	80	4	7	2	12	6	140	25	5	24	254	17	25	12
10	22	ZC	13	5	4	1	228	19	1	7	263	13	29	1
11	23	3	2	1	3	ZC	259	10	1	3	219	7	73	1
12	25	ZC	2	ZC	2	1	278	1	ZC	ZC	211	20	72	1
13	19	1	3	1	1	4	257	8	1	10	228	22	57	1
14	76	2	7	3	2	14	155	37	1	13	202	18	84	1
15	39	1	3	1	2	5	241	17	2	5	188	33	84	ZC
16	17	12	ZC	3	2	8	270	3	ZC	1	119	17	163	1
17	28	ZC	2	1	ZC	4	259	13	1	3	233	22	53	1
18	11	ZC	1	1	ZC	7	284	2	1	3	235	38	42	1
19	102	7	25	3	14	8	100	3	7	20	263	35	13	1
20	77	1	28	1	21	2	132	3	8	23	240	37	16	9
21	202	3	5	4	4	6	84	5	ZC	1	181	18	104	ZC
22	210	2	22	3	11	9	103	5	1	7	219	27	51	1
23	83	5	21	1	4	5	147	31	4	10	244	32	39	5
24	163	1	14	15	19	ZC	86	10	2	3	229	44	26	1
25	89	3	13	7	33	4	123	11	10	16	226	60	19	2
26	58	3	31	3	19	4	175	2	7	9	239	36	14	15
27	41	5	5	2	4	22	212	5	3	12	166	36	107	1
28	97	ZC	2	ZC	5	10	194	ZC	ZC	1	172	62	75	ZC
29	80	ZC	4	2	4	ZC	204	1	1	5	167	33	101	2
30	20	2	2	ZC	ZC	24	252	2	ZC	2	165	64	73	4
31	13	ZC	1	1	3	2	282	1	ZC	1	207	88	13	1
32	71	4	15	12	12	1	129	ZC	100	18	180	32	31	52
33	48	ZC	23	ZC	13	1	167	ZC	24	25	202	41	39	1
34	87	ZC	13	4	11	2	130	5	13	39	256	30	14	2
35	70	1	24	2	16	2	111	3	6	69	241	32	18	2
36	115	7	37	3	25	3	67	2	6	39	275	15	14	3
37	43	11	23	7	8	10	139	26	2	28	239	37	9	12
38	137	ZC	6	2	15	7	101	31	1	5	220	22	65	1
39	23	9	1	3	1	54	215	4	1	1	247	25	17	15
40	151	16	2	3	20	14	65	21	1	6	203	9	85	3

41	8	ZC	2	ZC	2	32	249	6	ZC	1	183	79	40	1
42	15	2	1	ZC	1	15	271	ZC	1	1	156	65	81	1
43	77	51	15	ZC	21	3	91	13	6	26	230	45	9	10
44	56	ZC	25	4	10	12	135	7	2	12	232	31	13	19
45	6	ZC	1	ZC	1	2	301	ZC	1	3	138	163	1	ZC

Traditional statistical methods may not be appropriate due to the data's constrained nature (**Pearson, 1987**; **Pawlowsky-Glahn and Egozcue, 2006**). Therefore, compositional data (CoDa) methodology was applied (**Aitchison, 1982**). CoDa methodology deals with positive values where multiple parts contribute to a whole. However, zeros in CoDa pose a significant challenge, either samples or variables containing zeros need to be removed which results with information loss, either they need to be addressed in some way. Zeros can occurr due to rounding, they can represent essential non-occurrence, or they can be a result of a counting process itself (**Martín-Fernández et al., 2003**).

One effective approach for handling zeros in compositional count data is the Bayesian-multiplicative method, specifically designed to handle count zeros, which often result from an insufficient number of trials rather than the absence of a category (**Martín-Fernández et al., 2015**). This method minimizes distortion in the covariance structure and transforms the data using log-ratio transformations to stabilize variances and make the distribution more symmetric, helping to meet the normality assumptions required for the parametric Bayesian approach.

Following replacement of count zeros, data set was described with normalized (**Egozcue et al., 2013**) variation matrix (**Aitchison, 1986**) containing the variances of all pairwise logratios, and a compositional (e.g. **Filzmoser et al., 2018**) biplot (**Gabriel, 1971**). Finally, groups of components and samples were determined according to the principal component analysis (PCA) loadings and scores, respectively, but also by the means of cluster analysis for compositional data (e.g. **Filzmoser et al., 2018**).

Statistical analysis, including production of diagrams was done in R 4.2.1 (**R Core Team, 2022**). Packages used in analysis were *compositions* (**van den Boogaart et al., 2024**), *robCompositions* (**Templ et al., 2023**) and *zCompositions* (**Palarea-Albaladejo and Martín-Fernández, 2024**). Maps were produced in QGIS 3.34.1 (**QGIS Development Team, 2023**).

4. Results and discussion

Figure 3 illustrates the patterns of zero counts across samples and minerals. Chlorite, zircon, and kyanite showed the highest occurrences of zero counts. Chlorite was frequently absent across the samples, often missing in conjunction with rutile. Since the rutile is indicative of high-grade metamorphism, the absence of both minerals in these samples could suggest a lack of material contribution from retrograde altered high-grade metamorphic rocks present at the Medvednica Mountain (**Belak et al., 2022**). Kyanite and muscovite were typically absent together, while amphibole was commonly found to be missing on its own. Kyanite and muscovite could be associated with metapelitic rocks where kyanite forms by metamorphose of clay sediments (e.g. **Slovenec and Bermanec, 2003**), thus, their absence in samples could indicate low input of weathered material from areas containing such rocks.

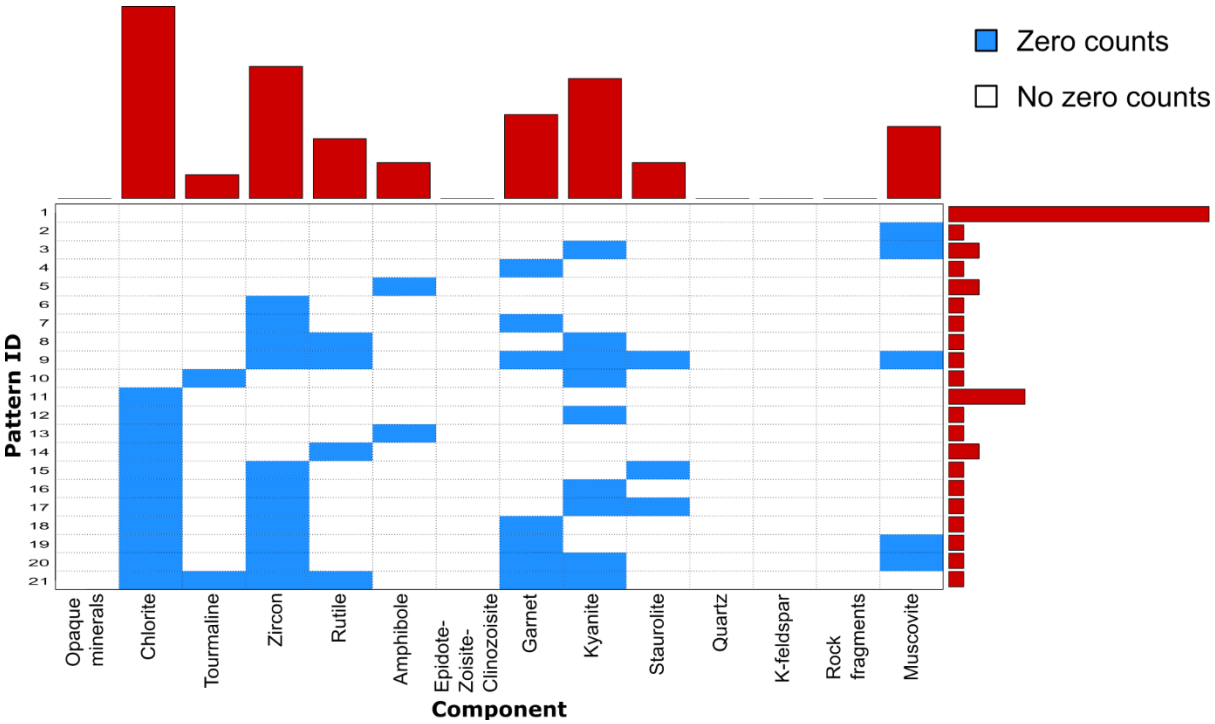

Figure 3: Distribution of zero counts for mineral grains across samples. Zero counts are displayed at the top of each column, and the counts of patterns are indicated on the right side of the table.

The variation matrix (**Table 2**) shows normalized values that indicate the degree of proportionality between pairs of minerals (values closer to zero indicate better proportionality). Low values among rutile, tourmaline, kyanite, staurolite, zircon, and muscovite suggest good proportionality among these minerals, likely indicating a similar source of metamorphic origin. Similarly, low values among epidote-zoisite-clinozoisite, quartz, and K-feldspar indicate their common source. Amphibole shows the highest values in the variation matrix, possibly pointing to its unique source or multiple sources, which affects its variance with other components. Relatively high values of chlorite with all minerals in the variation matrix could indicate its hydrothermal origin, which is widespread and not specifically tied to any single rock type.

Table 2: Variation matrix showing log-ratio variances of the corresponding two parts of the composition (variable in column stands for numerator, while variable in row stands for denominator)

	Chlorite	Tourmaline	Zircon	Rutile	Amphibole	Ep-Zo-Czo	Garnet	Kyanite	Staurolite	Quartz	K-feldspar	Rock fragments	Muscovite
Opaque minerals	0.93	0.48	0.51	0.32	1.48	1.24	0.80	0.83	0.67	0.54	1.45	1.04	0.88
Chlorite		1.20	1.01	0.96	1.07	1.17	1.10	1.11	1.15	0.77	1.35	1.32	0.79
Tourmaline			0.81	0.32	1.89	1.41	1.15	0.49	0.31	0.69	1.40	1.73	0.81
Zircon				0.68	1.48	1.07	0.81	0.94	0.93	0.59	1.36	1.15	0.82
Rutile					1.69	1.27	1.11	0.49	0.48	0.57	1.26	1.48	0.75
Amphibole						0.71	1.24	1.75	1.90	0.73	0.84	0.88	1.25
Ep-Zo-Czo							1.22	1.03	1.44	0.20	0.23	0.51	0.99
Garnet								1.55	1.11	0.75	1.71	1.14	1.23
Kyanite									0.47	0.61	1.02	1.53	0.62
Staurolite										0.77	1.53	1.87	0.83
Quartz											0.39	0.58	0.59
K-feldspar												1.02	1.15
Rock fragments													1.48

Figure 4 shows the form and covariance compositional biplot, respectively. Representation of samples is better in form, while variables in covariance biplot. The first two principal components (PC1 and PC2) explain 55% of the variability (37% and 18% respectively). Tourmaline, rutile, and staurolite show strong association and significant positive loadings on the first principal component (PC1+). Kyanite, zircon, and opaque minerals also exhibit positive loadings on PC1. Since all these minerals represent the heavy fraction and are relatively resistant mineral phases, it is likely that PC1+ represents a placer-like depositional environments, where heavier and more durable minerals are concentrated due to high-energy conditions such as those found in riverine settings. Conversely, epidote-zoisite-clinozoisite, K-feldspar, and quartz show strong association and significant negative loadings on PC1 (PC1-). All these components, except for amphibole and epidote-zoisite-clinozoisite, represent the light mineral fraction. Including rock fragments which were mostly made of greenschists (**Grizelj, 2017**), indicating they were composed of mostly light mineral fractions. Some amphiboles have densities closer to the boundary between what is typically considered heavy and light which could explain why are amphiboles grouped with other minerals of lighter fraction. Epidote-zoisite-clinozoisite has a similar density to tourmaline and is lighter than all other minerals significantly associated with PC1+. Accordingly, PC1- could represent depositional environments of low energy, such as lakes and swamps, where lighter mineral fraction could accumulate away from high-energy erosive processes.

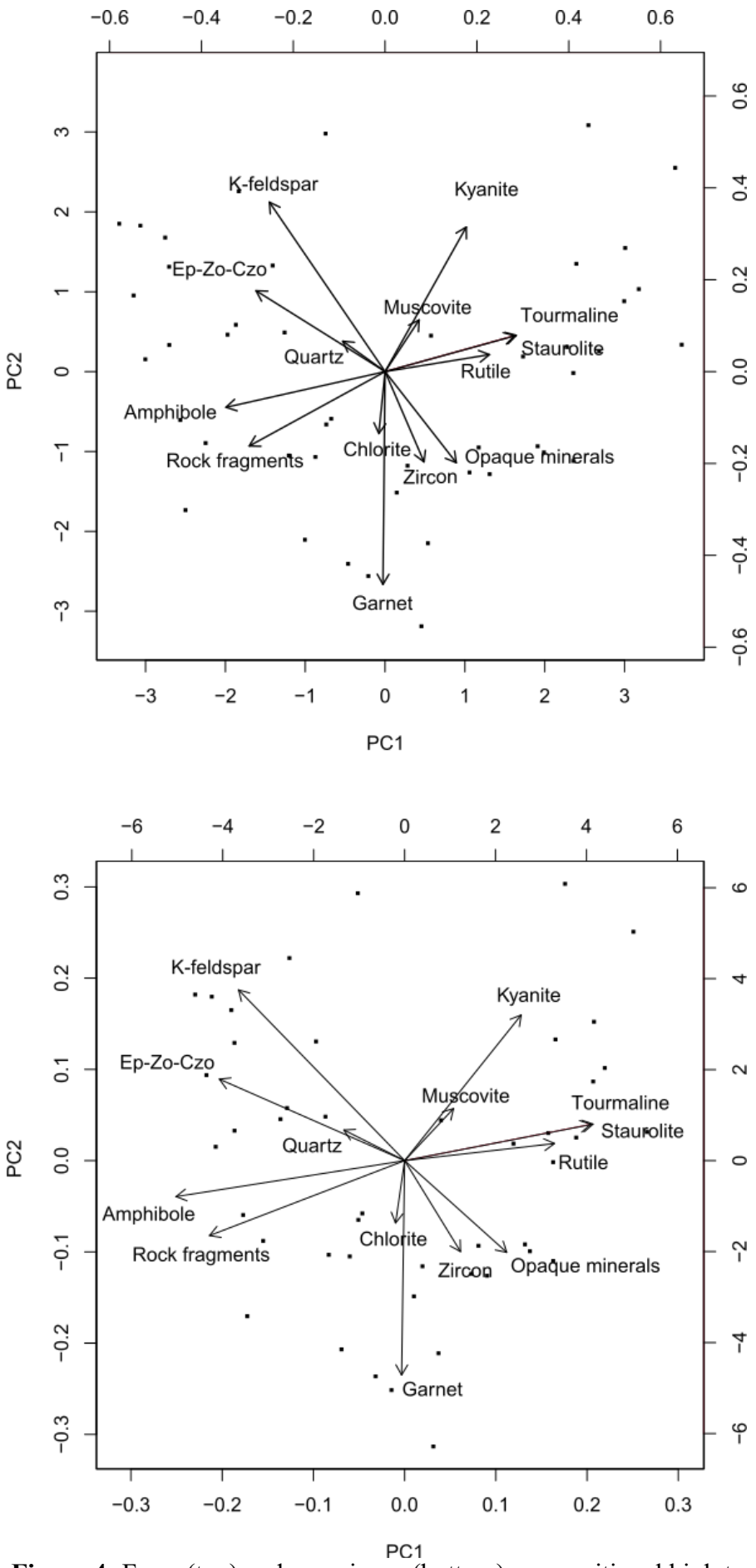

Figure 4: Form (top) and covariance (bottom) compositional biplots

The distribution of loadings on PC1 suggests it captures local variations in depositional environments, correlating high loadings with high-energy environments (e.g., rivers) and low loadings with low-energy environments (e.g., lakes and swamps). PC2, explaining only 18% of the variability in the dataset, indicates a need for more detailed investigation. However, garnet, chlorite, zircon, and opaque minerals show the lowest negative loadings on PC2 (PC2-), while kyanite, muscovite, and K-feldspar show positive loadings on PC2 (PC2+). Possibly, PC2 differentiates between weathering processes of different rock types present on Medvednica Mountain. For example, PC2+ could represent the weathering process of metamorphic rocks, while PC2- could represent a redepositional process of the Miocene clastites surrounding the crystalline core of Medvednica Mountain.

Cluster analysis yielded results similar to those of PCA (**Figure 5**). Two main groups of samples are visible. The second group (represented by pluses and triangles in **Figure 5** on the right), which consists of heavy minerals (except for muscovite and chlorite), can be divided into two subgroups. This division likely points to two different sources of weathering: metamorphic rocks and the Miocene clastites, which are predominantly present in the southeastern part of Medvednica Mountain. The first group (circles in **Figure 5** on the right) likely contains minerals found in the majority of rocks on Medvednica Mountain but are deposited in locally calmer environments, as they represent mostly the light mineral fraction.

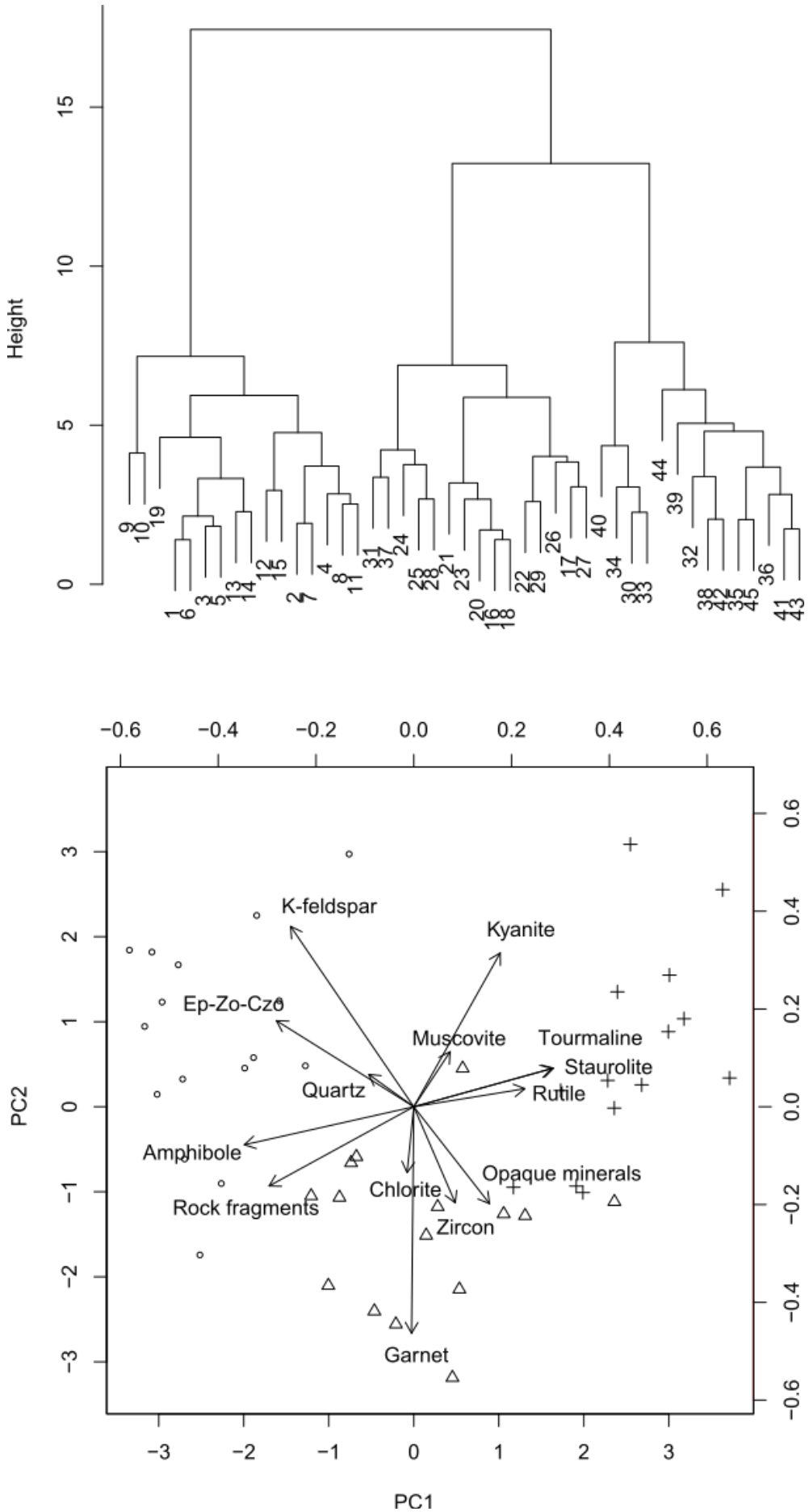

Figure 5: Cluster dendogram for samples (top) and compositional biplot with groups according to cluster analysis (bottom)

The cluster analysis of variables (**Figure 6**) yielded results similar to those of the PCA, yet with kyanite grouped with tourmaline and staurolite. This supports the assumption that the group marked with pluses represents the weathering process of metamorphic rocks. Garnet is grouped with chlorite and muscovite, which could all be products of the weathering of the Miocene clastites.

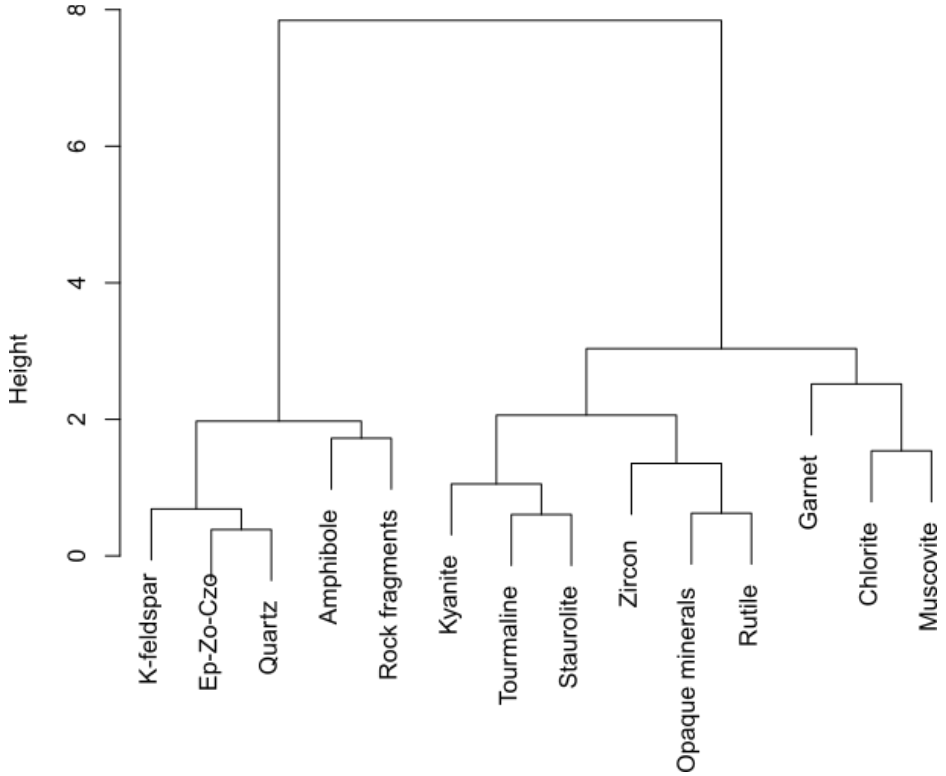

Figure 6: Cluster dendogram for variables

5. Conclusion

This study presents a detailed analysis of Quaternary sediments from the foothills of Medvednica Mountain, aimed at understanding their differences based on mineral associations and depositional environments. Through the use of compositional data analysis, including techniques such as cluster analysis and principal component analysis, the research has identified patterns in mineral distributions and associations, revealing significant geological complexities of the region. The findings indicate two main depositional environments: high-energy settings like rivers where heavier minerals are concentrated, and low-energy settings such as lakes and swamps where lighter minerals accumulate. These environments are reflective of a complex geological history that significantly influenced the observed mineralogical composition.

The study has confirmed findings of previos research that local rock weathering processes are the main driver in shaping the composition of Quaternary sediments in the region. This approach not only enhances our understanding of the geological framework of Medvednica Mountain but also demonstrates the application of compositional data analysis in geosciences, highlighting its value in addressing complex geological questions. However, there are limitations to this study, such as the limited number of samples and the constraints of the analytical methods used, which could affect the generalization of the findings. Future research should focus on expanding the sample size and incorporating advanced analytical techniques and dating to further refine our understanding of the depositional processes and mineral associations in this region.

6. References

1. Aitchison, J. (1982): The statistical analysis of compositional data (with discussion). Journal of the Royal Statistical Society, Series B (Statistical Methodology), 44, 2, 139–177. https://doi.org/10.1111/j.2517-6161.1982.tb01195.x
2. Aitchison, J., (1986): The Statistical Analysis of Compositional Data. Monographs on Statistics and Applied Probability. Chapman & Hall, London, 416 p.
3. Avanić, R. (1997): Analiza facijesa srednjeg miocena jugoistočnog dijela Medvednice (*Facies analysis of the Middle Miocene of the south-eastern part of the Mt. Medvednica*). Prirodoslovno-matematički fakultet, Zagreb, 54 p. (*in Croatian, English abstract*)
4. Basch, O. (1983a): Osnovna geološka karta SFRJ 1:100000, list Ivanić Grad L33-81 (*Basic Geologic Map of SFRY 1:100000, Ivanić-Grad sheet*). Geološki zavod Zagreb, Savezni geološki zavod, Beograd. (*in Croatian*)
5. Basch, O. (1983b): Osnovna geološka karta SFRJ 1:100000, Tumač za list Ivanić Grad (*Basic Geological Map of SFRY, 1:100000, Geology of the Ivanić Grad sheet*). Geološki zavod Zagreb, Savezni geološki zavod, Beograd, 66 p. (*in Croatian*)
6. Belak, M., et al. (2022): Low-grade metamorphic rocks of the Tethys subduction–collision zone in the Medvednica Mt. (NW Croatia). Geologica Carpathica, 73, no. 3, 207-229. https://doi.org/10.31577/GeolCarp.73.3.3
7. Brlek, M., Špišić, M., Brčić, V., Mišur, I. Kurečić, T., Miknić, M., Avanić, R., Vrsaljko, D., Slovenec, D. (2016): Mid-Miocene (Badenian) transgression on Mesozoic basement rocks in the Mt. Medvednica area of northern Croatia. Facies, 62/3, 1–21. https://doi.org/10.1007/s10347-016-0470-z.
8. Ćorić, S., Pavelić, D., Rögl, F., Mandić, O., Vrabac, S., Avanić, R., Vranković, A. (2009): Revised Middle Miocene datum for initial marine flooding of North Croatian Basins (Pannonian Basin System, Central Paratethys). Geologia Croatica, 62, 31–43. https://doi.org/10.4154/GC.2009.03
9. Croatian Geological Survey (2009): Geološka karta Republike Hrvatske M 1:300.000 (Geological Map of the Republic of Croatia at the scale of 1:300000). Hrvatski geološki institut, Zavod za geologiju, Zagreb.
10. Egozcue, J. J., Lovell, D. and Pawlowsky-Glahn, V. (2013): Testing compositional association. In: Hron, K., Filzmoser, P., Templ, M. (eds.): Proceedings of the 5th international workshop on compositional data analysis. University of Technology, Viena. - 28–36, 196 p.
11. Filzmoser, P., Hron, K. and Templ, M. (2018): Applied Compositional Data Analysis With Worked Examples in R. Springer. Cham, 280 p.
12. Gabriel, K. R. (1971): The biplot graphic display of matrices with application to principal component analysis. Biometrika, 58 (3), 453–467. https://doi.org/10.1093/biomet/58.3.453
13. Grizelj, A. et al. (2017): Occurrence of vivianite in alluvial Quaternary sediments in the area of Sesvete (Zagreb, Croatia). Geologia Croatica, 70, 41-52. https://doi.org/10.4154/gc.2017.01
14. Kovačić, M. and Grizelj, A. (2006): Provenance of the Upper Miocene clastic material in the southwestern part of the Pannonian Basin. Geologica Carpathica, 57/6, 495–510.
15. Lugović, B., Šegvić, B., Altherr, R. (2006): Petrology, geochemistry and tectonic significance of the orthogreenschists from the SW Zagorje-Mid-Transdanubian Zone (Medvednica Mts, Croatia). Ofioliti, 39/1, 31–50.
16. Martín-Fernández, J.A., Barceló-Vidal, C., Pawlowsky-Glahn, V. (2003): Dealing with zeros and missing values in compositional data sets using nonparametric imputation. Mathematical Geology, 35(3), 253-278. https://doi.org/10.1023/A:1023866030544
17. Martín-Fernández, J.A., Hron, K., Templ, M., Filzmoser, P., Palarea-Albaladejo, J. (2015): Bayesian multiplicative treatment of count zeros in compositional data sets. Statistical Modelling, 15, 134-158. https://doi.org/10.1177/1471082X145355
18. Mencin Gale, E., Jamšek Rupnik, P., Trajanova, M., Gale, L., Bavec, M., Anselmetti, F. S., Šmuc, A. (2019): Provenance and morphostratigraphy of the Pliocene-Quaternary sediments

in the Celje and Drava-Ptuj Basins (eastern Slovenia). Geologija, 62/2, 189-218. https://doi.org/10.5474/geologija.2019.009
19. Nenadić, D., Gaudenyi, T., Bogićević, K. et al. (2016): Stratigraphic and lithologic characteristics of Pleistocene fluvial deposits in the Danube and Sava riparian area near Belgrade (Serbia). Stratigraphy and Geological Correlation, 24, 427–437. https://doi.org/10.1134/S0869593816040055
20. Novaković, T., Lužar-Oberiter, B., Matoš, B., Wacha, L., Banak, A. (2018): The provenance of Quaternary sediments from Bilogora Mt. (Croatia). In: Novak, M. and Rman, N. (eds.): 5. slovenski geološki kongres: Book of abstracts. - Geološki zavod Slovenije, Ljubljana, 123-123, 143 p.
21. Palarea-Albaladejo, J., and Martín-Fernández, J. A. (2024): Package zCompositions. R package version 4.2.1. https://cran.r-project.org/web/packages/zCompositions
22. Pavelić, D., Kovačić, M. (2018): Sedimentology and stratigraphy of the Neogene rift-type North Croatian Basin (Pannonian Basin System, Croatia): A review. Marine and Petroleum Geology, 91, 455-469. https://doi.org/10.1016/j.marpetgeo.2018.01.026
23. Pawlowsky-Glahn, V. and Egozcue, J. J. (2006): Compositional data and their analysis: an introduction. In: Buccianti, A., Mateu-Figueras, G., Pawlowsky-Glahn, V. (eds.): Compositional data analysis in the geosciences. From theory to practice. - The Geological Society, London, 1–10, 212 p.
24. Pearson, K. (1897): Mathematical contributions to the theory of evolution. On a form of spurious correlation which may arise when indices are used in the measurement of organs. Proceedings of the Royal Society of London, 60, 489–502. https://doi.org/10.1098/rspl.1896.0076
25. Peh, Z., Novosel-Škorić, S., Kruk, Lj. (1998): Discriminant Analysis as a Tool for the Distinction of Quaternary Sediments in the Region of Djurdjevac. Geologia Croatica, 51 (1), 47-58. https://doi.org/10.4154/GC.1998.07
26. QGIS Development Team (2022): QGIS Geographic Information System. Open Source Geospatial Foundation. http://qgis.org
27. R Core Team (2022): R: A Language and Environment for Statistical Computing. R Foundation for Statistical Computing, Vienna, Austria. https://www.R-project.org/
28. Slovenec, D. and Bermanec, V. (2003): Sistematska mineralogija – mineralogija silikata (*Systematic mineralogy – mineralogy of silicates*). Denona, Zagreb, 359 p. (*in Croatian*)
29. Slovenec, D., Lugović, B. (2009): Geochemistry and tectono-magmatic affinity of mafic extrusive and dyke rocks from the ophiolite melange in the SW Zagorje- Mid-Transdanubian Zone (Mt. Medvednica, Croatia). Ofioliti, 34/1, 63–80.
30. Templ, M., Hron, K., Filzmoser, P., Fecevicova, K., Kynclova, P., Walach, J., Pintar, V., Chen, J., Miksova, D., Meindl, B., Menafoglio, A., Di Blasi, A., Pavone, F., Stefelova, N., Zeni, G. and Wiederkehr, R. (2023): robCompositions: Methods for analysis of compositional data including robust methods. R package version 2.0-4. https://cran.r-project.org/web/packages/robCompositions/index.html
31. van den Boogaart, K. G., Tolosana-Delgado, R., Bren, M. (2024): Compositions: Compositional Data Analysis. R package version 2.0-4. https://cran.r-project.org/web/packages/compositions/compositions.pdf
32. Vrsaljko, D., Pavelić, D., Miknić, M., Brkić, M., Kovačić, M., Hećimović, I., Hajek-Tadesse, V., Avanić, R., Kurtanjek, N. (2006): Middle Miocene (Upper Badenian/Sarmatian) Palaeoecology and Evolution of the Environments in the Area of Medvednica Mt. (North Croatia). Geologia Croatica, 59, no. 1, 51-63. https://doi.org/10.4154/GC.2006.04
33. Zámolyi, A., Salcher, B., Draganits, E. et al. (2017): Latest Pannonian and Quaternary evolution at the transition between Eastern Alps and Pannonian Basin: new insights from geophysical, sedimentological and geochronological data. International Journal of Earth Sciences (Geologische Rundschau), 106, 1695–1721. https://doi.org/10.1007/s00531-016-1383-3

SAŽETAK

Kompozitna varijabilnost minerala na izdancima i u bušotinama neformalne jedinice formacije Bistra, Medvednica, Hrvatska

Ovo istraživanje bavi se varijabilnošću mineralnog sastava uzoraka neslužbene Bistra formacije na Medvednici u Hrvatskoj. Proučavani su kvartarni sedimenti iz izdanaka i bušotina. Koristeći modalnu analizu i statističke metode obrade kompozicijskih podataka (CoDa), cilj istraživanja bio je klasificirati uzorke i definirati povezanost varijabli kako bi se poboljšalo razumijevanje različitosti sedimenta. Analiza je otkrila značajne varijacije u sastavu minerala kao rezultat lokalnih uvjeta taloženja i trošenja specifičnih geoloških formacija. Ključni rezultati podrazumijevaju odredbu dvije različite sredine taloženja: visokoenergetska riječna, u kojoj se koncentriraju teži minerali, i niskoenergetska jezerska ili močvarna, u kojoj se akumuliraju lakši minerali. Korištenje analize glavnih komponenata i klaster analize dodatno je pojasnilo odnose među mineralima. Ovaj pristup pokazuje korisnost CoDa analize u geoznanostima, pružajući dublje uvide u podrijetlo i dinamiku taloženja kvartarnih sedimenata.

Ključne riječi: Bistra formacija; Medvednica; modalna analiza; obrada kompozicijskih podataka; klasifikacija

Acknowledgments

Presented research was conducted in the scope of the internal research project „PAPER CLICHE“ at the Croatian Geological Survey, funded by the National Recovery and Resilience Plan 2021–2026 of the European Union – NextGenerationEU, and monitored by the Ministry of Science and Education of the Republic of Croatia.

Author's contribution

Anita Grizelj performed the fieldwork and provided the modal analysis. **Danijel Ivanišević** provided the statistical analysis and interpretation of the results.

5th Croatian geomathematical congress
UDC: 553.4; category: original scientific paper

Analyses of soil, rock and water samples from the location of "French Mines" in the Medvednica Mountain

Borna-Ivan Balaž[1] ; Tomislav Brenko [2] ; Stanko Ružičić[3] ; Zoran Kovač[4]
[1] University of Zagreb Faculty of Mining, Geology and Petroleum Engineering, Pierottijeva 6, Zagreb, Croatia, https://orcid.org/0000-0002-2642-3576
[2] University of Zagreb Faculty of Mining, Geology and Petroleum Engineering, Pierottijeva 6, Zagreb, Croatia, https://orcid.org/0000-0002-8935-1813
[3] University of Zagreb Faculty of Mining, Geology and Petroleum Engineering, Pierottijeva 6, Zagreb, Croatia, https://orcid.org/0000-0002-6000-085X
[4] University of Zagreb Faculty of Mining, Geology and Petroleum Engineering, Pierottijeva 6, Zagreb, Croatia, https://orcid.org/0000-0001-8091-7975
Corresponding author: borna-ivan.balaz@rgn.unizg.hr

Abstract

Historical mining site of the "French Mines" has great potential for promoting geodiversity and educating people about its significance and effects on the environment. In order to get more information about this location, combined preliminary geochemical and hydrogeological explorations were conducted following previous research in this area. Soil, stream sediments, rock and water samples were collected in two occasions and analyses were carried out. In this study, results of these preliminary geochemical and hydrogeological explorations, precisely pXRF (portable X-Ray Fluorescence) spectrometer analyses of soil, stream sediments and rocks, as well as results of in situ measurements and isotopic composition of groundwater and surface water samples are presented. Results suggest that previous mining activities did have significant impact on the overall chemical composition of soil due to elevated Pb, Zn and As contents that are significantly higher than the median value in this part of Croatia. In situ parameters and stable isotopes of water suggest existence of meteoric water.

Keywords: French Mines, Medvednica Mountain, hydrogeology, geochemistry

1. Introduction

According to the Nature Protection Law (OG 80/2013, OG 15/2018, OG 14/2019 and OG 127/2019), geodiversity is the diversity of non-living nature, and it consists of soil, rocks, minerals, fossils, landforms, underground objects, structures, natural phenomena and processes that created them through geological periods and are still creating them today. Considering the above mentioned, geological and related cultural heritage is one of the recognizable elements of the Medvednica Nature Park promoting geodiversity and educating people about its significance.
In this area combined geochemical and hydrogeological explorations were not performed. Considering the previous research, various authors explored different aspects associated with mining in this locality, precisely occurrences of lead and iron ore (**Šinkovec et al. 1988; Jurković, 2005**), geochemical characteristics of stream sediments (**Tomašić, 1997**), trace elements and heavy metal contents in the soil (**Pernar et al. 2008, Perković et al. 2017, Herceg, 2023**). Additionally, detailed speleological explorations were described by Bombardelli (**2003**). The newest research in the wider research area was related to the examination of soil water origin (**Kovač et al., 2022; Kovač et al., 2023**) as well to the usage of portable XRF to measure the influence of salt used during winter periods on the mobility of heavy metals in soil.

With that in mind, preliminary geochemical and hydrogeological explorations were conducted in the location of the "French Mines" on the northern side of Medvednica Mountain. Location was selected for having great potential in educational purposes and as good example of geodiversity and rich mining heritage in Croatia. According to Horvat (**1958**), French count Henri Carion opened these mines and mined galena for some period of time. Since the low amount of

ore containing silver could be mined (**Poljak, 1976**), the venture in the end failed and mines were closed. Historically, lenticular and vein ores were mined from Devonian-Carboniferous dolomites. The veins, which align with a southeast-northwest fault system, are mainly composed of galena and quartz, along with smaller quantities of sphalerite, Cu-Fe-As sulphides, carbonates, and secondary weathering products (**Šinkovec et al., 1988**).

The purpose of this research was to get new insight into the geochemical characteristics of soil and sediment, as well to determine water origin. For that purpose, samples of soil, stream sediments, rocks and water were collected, and analyses were carried out.

2. Field and laboratory work

Field work was carried out in two occasions in February 2024. In the first occasion, four mines were located. Although a fifth mine is mentioned in the literature (**Božičević, 1994**), it has not been found. Soil samples were taken at three locations (Figure 1 – locations marked with 1, 2 and 4) and sampling was done with a manual auger in front of each entrance to the mine from a depth of 25 cm. On location marked with 3 (Figure 1) stream sediments were collected in front of the mine because it was located in the stream bed of the Bistra stream. Additionally, in the location marked with 4 (Figure 1) rock samples were collected since it was the only mine which could be entered.

In addition to soil, stream sediments and rock samples, water samples were collected at two locations. First sample was taken from the spring zone of the Bistra stream and second sample from the Third Mine (marked 5 and 6 in Figure 1) that was completely flooded. In both locations in situ parameters were measured, precisely, temperature, pH, dissolved oxygen, electrical conductivity, and turbidity. On the second occasion only water samples were collected. Groundwater was sampled on locations 7, 8 and 9, as well as sample from retention on location 10 (Figure 1). In-situ parameters of water samples were measured with the portable multi-parameter Multi 3630 IDS.

Stable isotopes of water (δ^2H and $\delta^{18}O$) were determined at the Laboratory for Spectroscopy of the Faculty of Mining, Geology, and Petroleum Engineering, University of Zagreb, using a Liquid Water Isotope Analyzer (LWIA-45-EP, Los Gatos Research). Data interpretation was done using the Laboratory Information Management System (LIMS for lasers 2015; **Coplen and Wassenaar, 2015**), while the measurement precision of duplicate samples was ±0.19 ‰ for $\delta^{18}O$ and ±0.9 ‰ for δ^2H. All results are presented with respect to VSMOW (Vienna Standard Mean Ocean Water). For the interpretation purposes Local Meteoric Water Line (LMWL) for Zagreb, based on the long-term time series was used (**Krajcar-Bronić et al., 2020**), as well as the newest data from the Velika Gorica site (Figure 2), located in the vicinity of the City of Zagreb. For precipitation sampling, Palmex RS-1 precipitation sampler was used. RS-1 can protect water sample from evaporation and can be used in most hydrology studies (**Gröning et al., 2012; Michelsen et al., 2018**).

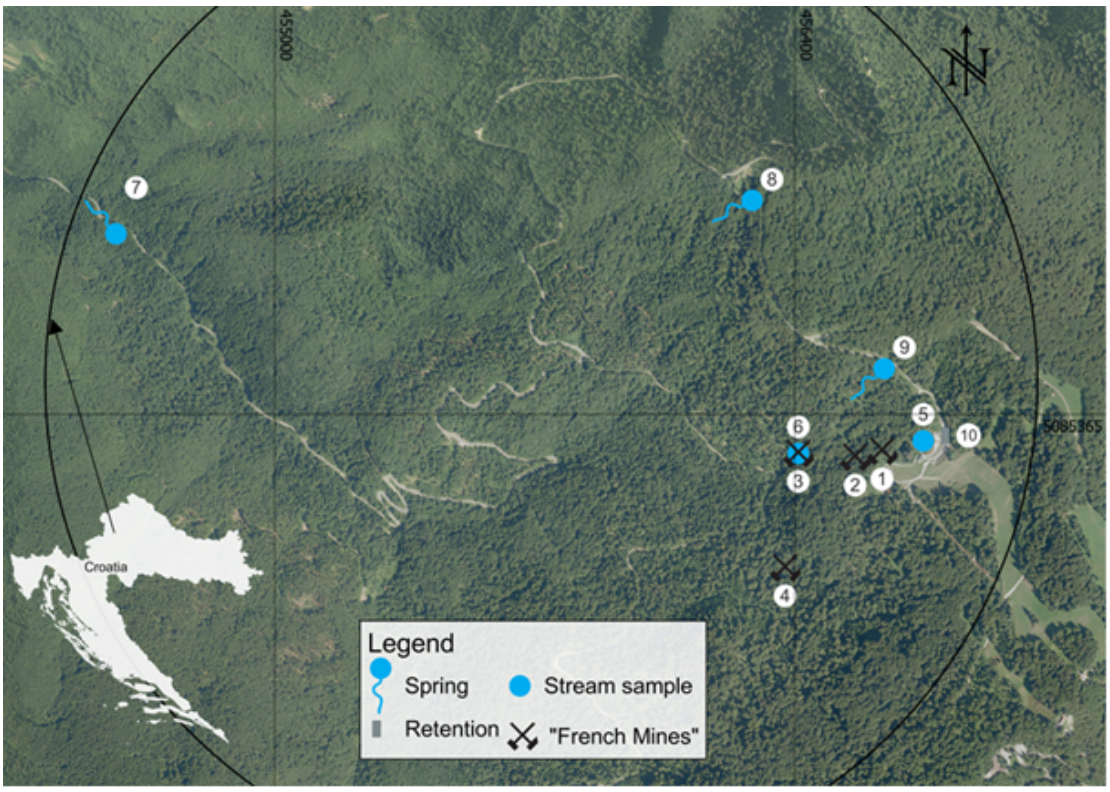

Figure 1: Overview map of the wider research area (northern slopes of Mt. Medvednica with sampling locations marked with numbers 1 to 10)

Figure 2: Location of "French Mines" compared to Velika Gorica site

3. Results and discussion

3.1. Preliminary soil and rock analyses

Considering the geological basemap of the research area (Sheet Zagreb) according to **Šikić et al. (1978)** and **Šikić et al. (1979)**, four major geological units can be differentiated (Figure 3). Devonian-Carboniferous? (D, C?) is represented with orthometamorphites (green schists) and parametamorphites i.e. methamorphosed volcanic-sedimentary complex. Following this, the Aptian-Turonian is represented with volcanic-sedimentary complex ($K_{1,2}$) and diabases and spilites ($\beta K_{1,2}$). The basic characteristic of this complex is the tectogenetic connection of sedimentation and magmatism. Sedimentary rocks are represented with sandstones, shales, marls, cherts and limestones. Palaeocene (Pc) is represented with clastites and limestones. Their occurrence is preserved along the NW slopes of Medvednica Mountain and represented with gray and brownish-gray clayey and sandy marls and sandstones which spatially coincide with the volcanic-sedimentary complex of the older Cretaceous.

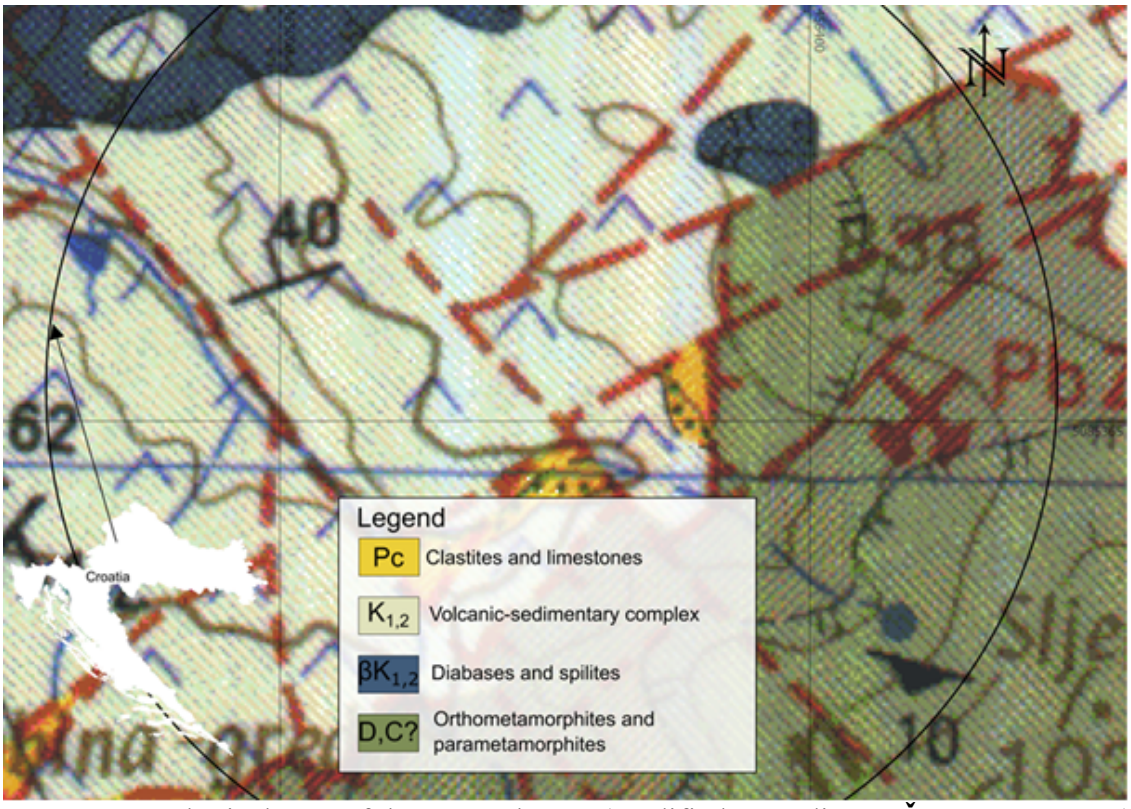

Figure 3: Geological map of the research area (modified according to **Šikić et al., 1978**)

Results of portable XRF analysis on four soil samples and two different types of mineralization in fourth mine, in the form of major and selected trace elements, aree given in Table 1. Four soil samples were taken in front of entrances to the mines, while the two additional samples represent two types of mineralisation in fourth mine (oxidative malachite mineralization and reductive galena mineralization). Typical elevated Ca and Mg contents are in line with carbonate rocks surrounding the mines. Silicon values are in line with occurrences of quartz which is hosting the mineralisation. Lead and zinc values are elevated in almost all cases, with values for Pb ranging from 160.00 up to 10976.40 ppm, and for Zn from 34.0 up to 278.20 ppm. Malachite and galena samples from fourth mine exhibit different chemistry than the rest of the samples. Malachite sample shows elevated Cu (81222.80 mg/kg = 8.12 %) and Fe (14.60 %), with also extreme enrichment of As (5586.20 mg/kg). Galena sample exhibits significantly elevated Pb (10976.60 kg/kg = 1.09 %) and S (1.56 %).

Measured contents of Pb (160.00– 10976.40 mg/kg, average 2863.40 mg/kg) and Zn (34.00 – 278.20 mg/kg, average 157.03 mg/kg) are significantly over the medium values for Pb and Zn in soil. The global average content of Pb in soils and sediments of Central Croatia is 25 mg/kg (**Halamić and Miko, 2009**). Same authors discovered that Pb in the central part of Croatia ranges from 13 to 198 mg/kg, with a median value of 25 mg/kg. In the central part of Croatia values of Zn are within the range of 27 – 362 mg/kg, with median value of 61 mg/kg. These values are significantly lower than the values obtained in this study. Elevated values are well in line with previous mining activity that was occurring in the study area during the 18th and 19th century as a part of quest for silver ore discovery.

Interestingly, arsenic values are also extremely elevated (42.00 – 5586.20 mg/kg), well above the range established by Halamić and Miko (**2009**) in Geochemical Atlas of Croatia (1.8 – 59 mg/kg). Possible reason is that arsenic mineralisation, such as arsenopyrite (FeAsS) can sometimes occur simultaneously with galena, or rather that up to 0.7% of As can be replacing Pb in galena (**George, 2013**).

Two samples from the fourth French mine, representing primary (galena) and secondary (malachite) mineralisation differ with regard to Pb, S, Cu and As. Arsenic content in malachite is most interesting. All studies analysing occurrence of malachite report very little, or no arsenic within malachite. Therefore, this could indicate that another mineralisation is present. It is proposed, that based on elevated Fe contents, occurrence of arsenopyrite is present here. As previously mentioned, arsenopyrite can sometimes occur alongside galena mineralisation, which might be the case here.

Table 1: Results of pXRF analyses. Bolded values for Cu, Pb, Zn, As and Ag represent values above maximum detected values in Central Croatia according to **Halamić and Miko** (**2009**)

Elemental Composition	**Concentration**	**Location number**					
		1	2	3	4	4 - galena	4 - malachite
Si	%	19.9	20.92	22.95	19.76	40.92	7.14
Ti	%	0.56	0.76	0.56	0.43	b.d.l.	b.d.l.
Al	%	8.71	7.89	7.13	8.06	0.2	1.7
Fe	%	6.9	9.21	5.76	5.27	0.59	14.6
Ca	%	9.46	7.4	8.61	12.15	0.85	21.31
Mg	%	4.14	3.94	4.76	3.62	b.d.l.	8.19
Mn	%	0.63	0.61	0.17	0.42	0.02	0.64
K	%	2.94	2.25	2.38	3.81	0.18	0.44
P	%	0.13	0.14	0.08	0.13	b.d.l.	0.08
S	%	b.d.l.	b.d.l.	b.d.l.	b.d.l.	1.56	b.d.l.
Cu	ppm	86.2	**1213**	70.2	271.6	**1233.8**	**81222.8**
Ba	ppm	284.33	217	209	229	210	375.25
Pb	ppm	**991.8**	**1060.4**	**160**	**3111**	**10976.4**	**880.8**
Zn	ppm	**154.8**	**239.8**	**107.4**	**128**	34	**278.2**
As	ppm	**190.2**	**304.8**	**42**	**199.4**	**256**	**5586.2**
Ag	ppm	b.d.l.	b.d.l.	b.d.l.	b.d.l.	b.d.l.	**119.5**

Abbreviation: b.d.l. – below detection limit

3.2. Preliminary water analyses

Temperature, pH, dissolved oxygen, electrical conductivity, and turbidity were measured on six locations and are given in the Table 2 and shown in the Figure 1. In general, sampling locations can be divided into surface water sampling point (location 10), groundwater sampling points (locations 5, 7, 8 and 9) and sample form Third Mine (location 6). Values of pH vary from

6.779 in the surface water from the retention to 7.945 in the Third Mine. Electrical conductivity was highest in the Volarski Spring closest to the "French Mines" with value of 921 µS/cm and lowest again in the Retention, 203 µS/cm. Highest value of dissolved oxygen was measured in surface water, at location 10 (10.60 mgO_2/l) and lowest in the spring on location 7 (4.21 mgO_2/l). Water temperature varied from 6.5 °C to 10.6 °C, and turbidity from 0.35 to 9.15.

During the first sampling, in situ parameters were measured in the spring zone of the Bistra stream (location 5) and in the Third Mine (location 6). Although, at the time the Bistra stream was not in direct contact with the mine shaft, it is clear that during high water levels the stream submerges the mine. As shown in Table 2 (locations 5 and 6) main difference is observed in pH, electrical conductivity, and turbidity. Water from the Third Mine had higher values of electrical conductivity (533 µS/cm compared to 368 µS/cm) as well as higher pH values (7.945 compared to 7.496). It was expected for the pH values to be lower than the ones measured, since water flow through mineralised rock zones where mining exposes rocks to oxidation usually causes lower pH values (**Fetter, 2018**). Water from the mine shaft also had higher turbidity than a flowing stream (4.84 compared to 0.99).

During the second sampling, in situ parameters were measured on retention (location 10) as well as on the three springs (locations 7, 8 and 9). Spring on location 7 is in literature (**Šikić, 1979**) determined as a mineral water spring and it is called Sulphuric Spring. It has pH value of 7.583 which is higher compared to Oštrica Spring and Volarski Spring with values 6.848 and 7.412. Electrical conductivity varies from 560 µS/cm for Sulphuric spring to 921 µS/cm for Volarski Spring and 896 µS/cm for Oštrica Spring. Dissolved oxygen had similar values on Oštrica Spring and Volarski Spring (10.47 and 10.51 mgO_2/l) and significantly lower for Sulphuric Spring (4.21 mgO_2/l). This could be an indication of O_2-consuming reactions such as decay of organic matter or oxidation of sulphide minerals (**Weight, 2008**). Temperature and turbidity are similarly grouped. For Oštrica Spring and Volarski Spring temperature was measured 8.7 °C and 8.9 °C and turbidity 0.35 and 0.68. Water temperature on location of Sulphuric Spring was 10.6 °C and turbidity was 4.46 which is again higher than two previously mentioned locations.

Table 2: Results of in-situ measurements of water samples

Location number	Location name	Date	pH	Electrical conductivity (µS/cm)	Dissolved oxygen (mgO_2/l)	Temperature (°C)	Turbidity (NTU)
5	Spring zone Bistra	8.2.2024	7.496	368	10.38	8.5	0.99
6	Third Mine	8.2.2024	7.945	533	9.96	8.6	4.84
7	Sulphuric Spring	19.2.2024	7.583	560	4.21	10.6	4.46
8	Oštrica Spring	19.2.2024	6.846	896	10.47	8.7	0.35
9	Volarski Spring	19.2.2024	7.412	921	10.51	8.9	0.68
10	Retention	19.2.2024	6.779	203	10.60	6.5	9.15
Average			7.344	580	9.36	8.6	3.41
Minimum			6.779	203	4.21	6.5	0.35
Maximum			7.945	921	10.60	10.6	9.15

Stable isotope composition of all water is very similar (Figure 4). However, these preliminary results show grouping of spring zone Bistra and Sulphuric Spring, Oštrica Spring with Third Mine and Volarski Spring with Retention. Spring zone Bistra and Sulphuric Spring isotope

composition suggest existence of the slightly different water with possible influence of Bistra stream on Sulphuric Spring. Grouping of Oštrica Spring and Third Mine suggests that water from the mine is not only from the Bistra stream, while grouping of Volarski spring and Retention is expected due to their morphology location and water which is probably coming from higher altitudes and flowing from northeast to southwest. However, in order to get more reliable results at least one year of isotope research is necessary, where sampling must be done in at least monthly sampling period. Additionally, these results should give relevant information for designing future sampling network. In general, all samples present meteoric water and are located slightly above the LMWL Zagreb, and between isotopic composition of precipitation which fell in December 2023 and January 2024 in the area of the Velika Gorica City. Results suggest that precipitation from February didn`t have a lot of influence on surface and groundwater samples taken within this research.

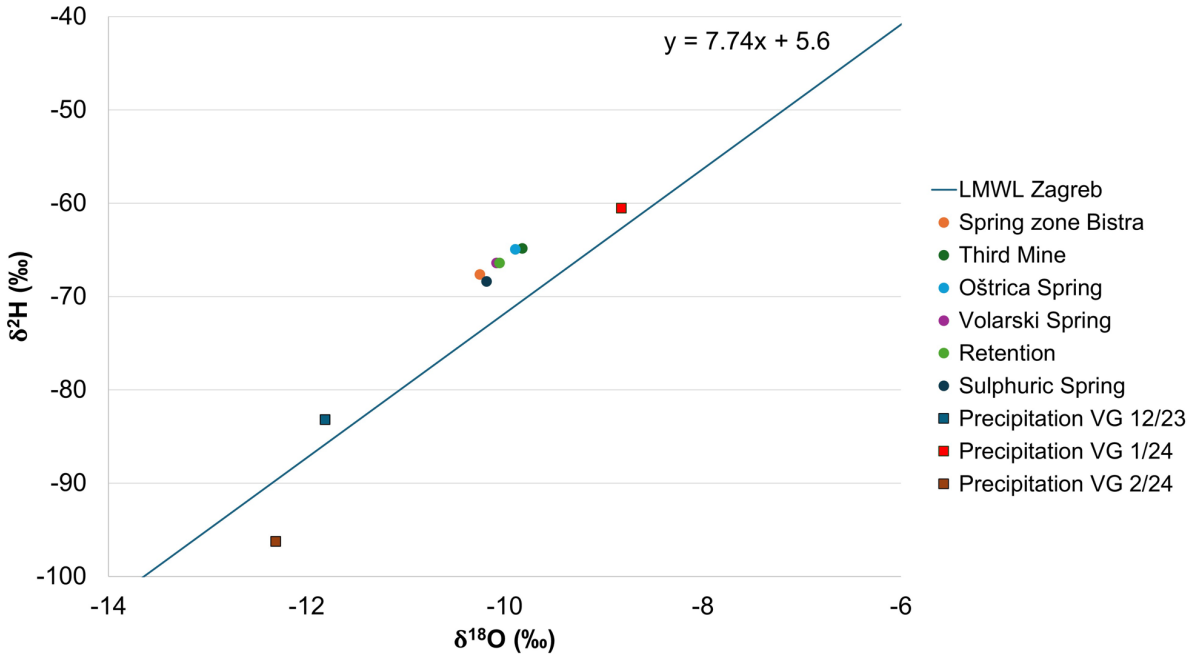

Figure 4. Isotopic composition of sampled water with respect to LMWL Zagreb and precipitation from Velika Gorica site in the period from December 2023 till February 2024

5. Conclusions

Combined geochemical and hydrogeological analyses were conducted in Medvednica Nature Park, mostly targeting zones in close vicinity of previously recognized French Mines. Based on the results obtained within this study, it can be concluded that previous mining activities did have significant impact on the overall chemical composition of soil.

Elevated Pb, Zn and As contents, significantly higher than the median valued in this part of Croatia, were discovered in all analysed sampled, suggesting intensive mining activities took place in this area. Furthermore, preliminary water stable isotope composition analyses suggest that water present in the Third Mine is the consequence of mixing between Bistra stream and groundwater. Also, variations in electrical conductivity, pH values and dissolved oxygen indicate that morphological and geological properties condition the diversification of the physio-chemical properties of the collected water samples which is also indicated with their preliminary grouping according to their stable isotope composition.

It is proposed that future studies include sequential extraction analysis to determine in what soil phases are heavy metals accumulating, as well as water chemistry in order to determine hydrogeochemical facies and ability for heavy metals to mobilize further in the environment, especially in groundwater. To conclude, all the above represents a significant insight into the

consequences of historical mining and, in general, anthropogenic impact on the environment. Therefore, the location of the French Mines can be an excellent example of an insight into Croatia's rich mining heritage and geodiversity of the Medvednica Nature Park, which should be investigated in much more detail within the future research.

6. References

1. Bombardelli, M. (2003): Francuski rudnici na Medvednici. Speleolog, 50, 1, 73-78.
2. Božičević, S. (1994): Zaboravljene zanimljivosti Medvednice. Hrvatski planinar, 86, 9-10, 198-201.
3. Coplen, T. B. and Wassenaar, L. I. (2015): LIMS for Lasers 2015 for achieving long-term accuracy and precision of δ^2H, $\delta^{17}O$, and $\delta^{18}O$ of waters using laser absorption spectrometry. Rapid Communications in Mass Spectrometry, 29, 22, 2122–2130. https://doi.org/10.1002/rcm.7372 .
4. Fetter, C. W. (2018). Applied hydrogeology. Waveland Press, 598 p.
5. George, L. (2013): Trace elements in Galena. Master thesis, University of Adelaide, 133 p.
6. Gröning, M., Lutz, H. O., Roller-Lutz, Z., Kralik, M., Gourcy, L. and Pöltenstein, L. (2012): A simple rain collector preventing water re-evaporation dedicated for $\delta^{18}O$ and δ^2H analysis of cumulative precipitation samples. Journal of Hydrology, 448–449, 195–200. https://doi.org/10.1016/j.jhydrol.2012.04.041 .
7. Halamić, J. and Miko S. (2009): Geochemical Atlas of the Republic of Croatia. Croatian Geological Survey, Zagreb, Croatia, pp 87.
8. Herceg, K. (2023): Poredbena analiza elemenata u tragovima različitim ekstrakcijskim sredstvima na primjeru tla s područja" Francuskih rudnika" na Medvednici. University of Zagreb. Faculty of Forestry and Wood Technology. Institute of Forest Ecology and Silviculture.
9. Horvat, V. (1958): 500 stuba i njihova okolina. Naše planine, 4., 210-219.
10. Jurković, I. (2005): Magnetite-hematite iron ore occurrences in the Triassic-Paleozoic metamorphic complex of Medvednica Mountain, Croatia. Rudarsko-geološko-naftni zbornik, 17, 1, 1-14.
11. Kovač, Z.; Krevh, V.; Filipović, L.; Defterdarović, J.; Buškulić, P.; Han, L. and Filipović, V. (2022): Utilizing Stable Water Isotopes (δ2H and δ18O) To Study Soil-Water Origin in Sloped Vineyard: First Results. Rudarsko-geološko-naftni zbornik, 37, 1–14. https://doi.org/10.17794/rgn.2022.3.1.
12. Kovač, Z.; Krevh, V.; Filipović, L.; Defterdarović, J.; Balaž, B.-I.; Filipović, V. (2023): Estimation of Precipitation Fraction in the Soil Water of the Hillslope Vineyard Using Stable Isotopes of Water. Water, 15, 988. https://doi.org/10.3390/w15050988.
13. Krajcar-Bronić, I.; Barešić, J.; Borković, D.; Sironić, A.; Lovrenčić Mikelić, I.; Vreča, P. (2022): Long-Term Isotope Records of Precipitation in Zagreb, Croatia. Water 2020, 12, 226.
14. Michelsen, N.; van Geldern, R.; Rossmann, Y.; Bauer, I.; Schulz, S.; Barth, J.A.C.; Schüth, C. (2018): Comparison of precipitation collectors used in isotope hydrology. Chemical Geology, 488, 171–179.
15. Perković, I., Lazić, A., Pernar, N., Roje, V., & Bakšić, D. (2017): Forest soil pollution with heavy metals (Pb, Zn, Cd, and Cu) in the area of the “French Mines” on the Medvednica Mountain, Republic of Croatia. South-east European forestry: SEEFOR, 8, 1, 31-40.
16. Pernar, N., Bakšić, D., Miko, S., Vrbek, B., Galović, L., Bukovec, D., & Perković, I. (2008): Trace elements in the soil of some specific localities on Mt. Medvednica. In EUROSOIL 2008 (pp. 107-107).
17. Poljak, Ž. (1976): Medvednica, tourist-mountaineering guide. Hrvastki planinarski savez, 4th edition, 35 p.

18. Šikić, K., Basch, O. & Šimunić, A. (1978): Osnovna geološka karta SFRJ 1:100.000. List Zagreb: l 38-80 [Basic geological map of SFRY 1:100 000, Zagreb sheet - in Croatian] – Institut za geološka istraživanja, Zagreb (1972), Savezni geolološki zavod, Beograd.
19. Šikić, K., Basch, O., & Šimunić, A. (1979): Tumač osnovne geološke karte 1: 100000, list Zagreb. Institut za geološka istraživanja Zagreb.
20. Šinkovec, B., Palinkaš, L., & Durn, G. (1988): Rudne pojave Medvednice. Geološki vjesnik, 1, 41, 395-405.
21. Tomašić, N. (1997): Geokemijske osobitosti potočnih sedimenata slivnog područja Zrinskog i Francuskih rudnika na Medvednici. Master's thesis, Faculty of Science University of Zagreb, 68 p.
22. Weight, W. D. (2008): Hydrogeology field manual. McGraw-Hill. Second Edition. Montana Tech of The University of Montana. Butte, Montana, 751 p.

Sažetak

Analiza uzoraka tla, stijena i vode s lokacije Francuskih rudnika na Medvednici

"Francuski rudnici" na Medvednici imaju veliki potencijal za promicanje georaznolikosti i edukaciju ljudi o njezinom značaju i učincima na okoliš. Kako bi se dobilo više informacija o ovome lokalitetu, provedena su preliminarna geokemijska i hidrogeološka istraživanja. U dva navrata prikupljeni su uzorci tla, potočnog sedimenta, stijena i vode te su provedene analize. U ovome radu prikazani su rezultati ovih preliminarnih geokemijskih i hidrogeoloških istraživanja, točnije pXRF (portable X-Ray Fluorescence) spektrometrijske analize tla, potočnih sedimenata i stijena, kao i rezultati in situ mjerenja i izotopnog sastava uzoraka podzemne i površinske vode. Rezultati pokazuju da su prethodne rudarske aktivnosti imale značajan utjecaj na ukupni kemijski sastav tla zbog povišenog sadržaja Pb, Zn i As koji su značajno viši od srednjih vrijednosti u ovom dijelu Hrvatske. In situ parametri i stabilni izotopi vode upućuju na postojanje atmosferske vode.

Ključne riječi: Francuski rudnici, Medvednica, hidrogeologija, geokemija

Author`s contribution

Borna-Ivan Balaž (1) (expert associate) participated in field sampling, laboratory analyses and wrote most of the manuscript. **Tomislav Brenko** (2) (assistant) participated in field sampling, laboratory analyses and wrote most of the manuscript. **Zoran Kovač** (3) (associate professor) participated in data processing and laboratory analyses, results interpretation and editing of the manuscript **Stanko Ružičić** (4) (associate professor) participated in data processing and editing of the manuscript.

5th Croatian geomathematical congress
UDC: 556.3:556.5; category: original scientific paper

Groundwater and surface water interaction in the City of Slavonski Brod, Croatia

Zoran Kovač[1]; Borna-Ivan Balaž[2]; Ferid Skopljak[3]; Lucijan Perić[4]
[1] University of Zagreb Faculty of Mining, Geology and Petroleum Engineering, Pierottijeva 6, Zagreb, Croatia; https://orcid.org/0000-0001-8091-7975
[2] University of Zagreb Faculty of Mining, Geology and Petroleum Engineering, Pierottijeva 6, Zagreb, Croatia; https://orcid.org/0000-0002-2642-3576
[3] Federal Institute for Geology; Ustanička 11, 71210 Sarajevo, Bosnia & Herzegovina; https://orcid.org/0000-0003-4114-0539
[4] University of Zagreb Faculty of Mining, Geology and Petroleum Engineering, Pierottijeva 6, Zagreb, Croatia
Corresponding author: zoran.kovac@rgn.unizg.hr

Abstract

Alluvial aquifers, mostly related to the Sava and Drava rivers, are protected by the Republic of Croatia which has designated them as strategic water reserves. In the Pannonian part of Croatia, they present main source of potable water for their inhabitants. Their relationship can be very dynamic, which is especially pronounced in the shallow unconfined aquifers. This research has been focused to the examination of groundwater and surface water interaction in the area of the City of Slavonski Brod using hydrological and hydrogeological analyses, cross-correlation analysis, and stable isotopes of water (δ^2H and $\delta^{18}O$). Results showed that aquifer response is faster in high water levels with respect to low water levels, while isotopic composition of all observed water showed that Sava River presents main source of recharge for the investigated aquifer. Additionally, it has been shown that within the long duration of low water levels Sava River influence is not that dominant. Furthermore, results also showed that more hydrological and hydrogeological investigations are necessary in the wider study area, in order to get more detailed and precise results. This is also important due to existence of transboundary water resources in the great part of the Sava River basin and if sustainable management of water resources wants to be achieved.

Keywords: Sava River; groundwater; cross-correlation analysis; stable isotopes of water; City of Slavonski Brod

1. Introduction

Alluvial aquifers in the Republic of Croatia are designated as strategic water reserves and are protected by Crotian state. They present main source of potable water in the Pannonian part of the Republic of Croatia. Their relationship can be very dynamic which is especially pronounced in the shallow unconfined aquifers. Most of the scientific research has been focused to the Zagreb (**Posavec et al., 2017; Parlov et al., 2019; Kovač et al., 2022a**) and Varaždin (**Marković et al., 2022**; **Karlović et al., 2022**) aquifers, while in the eastern Pannonian part of Croatia, in the Sava basin area, hydrogeological and hydrogeochemical research was mainly focused to Sikirevci well field (**Briški et al., 2013; Kopić et al., 2016; Filipović et al., 2022**). Regarding the research in the area of the City of Slavonski Brod, hydrogeological research has been done in recent time which suggested fast change of groundwater levels after the rise of Sava River water levels (**Perić, 2023**). The goal of this research is to evaluate groundwater and surface water interaction in the area of the City of Slavonski Brod using hydrological, hydrogeological, statistical analyses, mainly cross-correlation analysis, and stable isotopes of water (δ^2H and $\delta^{18}O$). Cross-correlation analysis presents the method which is used for the definition of similarity of two series, i.e. it defines the degree to which two series are correlated with respect to lag of one relative to the other (**Davis, 2002**). It has been shown in many cases that cross-correlation analysis can be used in different hydrogeology and meteorology research (**Crosbie et al. 2005, Ford & Williams, 2007; Lee et al. 2013, Welch et al. 2013, Kovač et al., 2023**). On the other hand, stable isotopes of water are often

used in the examination of groundwater and surface water interaction (**Parlov et al., 2019; Petersen et al., 2023**), but can also be used in different hydrology research, for example soil hydrology (**Kovač et al., 2022b; Kovač et al., 2023**). Although hydrogeological research in this area is not often performed, it must be emphasized that in this area well field Jelas exists, which pumps groundwater for the public water supply of the City of Slavonski Brod and surrounding settlements. This research was done within the regional IAEA (International Atomic Energy Agency) project RER 7013 (*„Evaluating Groundwater Resources and Groundwater-Surface-Water Interactions in the Context of Adapting to Climate Change"*).

2. Data and methods

Sava River water levels were assigned by Croatian Meteorological and Hydrological Service as daily data (hydrological station Slavonski Brod), while groundwater levels were measured at observation well P-9 which is located approximately 1000 m north of the Sava River (**Figure 1**). Groundwater levels were measured using logger which was set to measure in hourly interval. To get daily data, which were compared to the Sava River water levels, hourly data was averaged. For the calculation purposes, data from hydrological year 2021/2022 (1/10/2021 – 30/9/2022) were used. Groundwater and surface water interaction was evaluated using cross-correlation analyses in different time periods. Firstly, all data from whole hydrological year were used, while other statistical analyses were focused to the evaluation of the relationship between groundwater and surface water in periods with high and low water levels. For the high water level (hwl) periods 15 days before and after the peak were considered, while for the testing of the mentioned relationship in the low water level (lwl) periods 30 days before the low Sava River water level were taken into account. In some cases, less data was used (hwl 1 and hwl 6) because peaks were observed at the beginning and the end of the investigated period. In total, 11 cross-correlation analyses were done, one for all data, six for high water levels (hwl 1 to hwl 6) and four for low water levels (lwl 1 to lwl 4), based on the water level variation (**Figure 2**). Cross-correlation analyses was done using Visual Basic for Applications (VBA) code (**Posavec et al., 2017**), where the strength of the relationship between time series is determined by the correlation coefficient.

Stable isotopes of water (δ^2H and $\delta^{18}O$) were determined for surface water, groundwater and precipitation using a Liquid Water Isotope Analyzer (LWIA-45-EP, Los Gatos Research) at the Laboratory for Spectroscopy of the Faculty of Mining, Geology, and Petroleum Engineering, University of Zagreb. Before measurement, samples were stored in fridge and filtrated with 0.2 μm nylon filters. Data was prepared and interpreted using the Laboratory Information Management System (LIMS for lasers 2015; **Coplen & Wassenaar, 2015**), while the measurement precision of duplicate samples using nine injections was ±0.19 ‰ for $\delta^{18}O$ and ±0.9 ‰ for δ^2H. All results are presented with respect to VSMOW (Vienna Standard Mean Ocean Water). For the interpretation purposes Local Meteoric Water Line (LMWL) for the City of Slavonski Brod was constructed, and compared to LMWL Zagreb, which is made based on the long-term data series (**Krajcar-Bronic et al., 2020**). All water was sampled in a monthly interval. Groundwater was sampled from the observation well P-9, while precipitation was sampled with Palmex RS-1 precipitation sampler. Previous research showed that RS-1 can protect water sample from evaporation and can be used in most hydrology studies (**Grönnigen et al., 2012; Michelsen et al., 2018**).

For the quantitative evaluation, i.e., quantification of recharge sources, two or three-end mass balance equations can be used (**Peng et al., 2010; Vrzel et al., 2018; Parlov et al., 2019**). In these equations sum of the end member contributions are expressed as fractions (f) equal to 1. In this research two-component mixing model was used which assumes that aquifer recharge comes from two main sources, Sava River and precipitation. For the quantification of recharge, average values from the hydrological year 2021/2022 were used, for both δ^2H and $\delta^{18}O$, based on the following **Equations 1** and **2**:

$$f_{river} + f_{precipitation} = 1 \quad (1)$$

$$f_{river} \times \delta^{18}O_{river} + f_{precipitation} \times \delta^{18}O_{precipitation} = \delta^{18}O_{groundwater} \quad (2)$$

where are:

f_{river} and $f_{precipitation}$ - present Sava River and precipitation fractions respectively,
$\delta^{18}O_{groundwater}$ - presents isotopic composition of oxygen in the observation well P-9, while
$\delta^{18}O_{river}$ and $\delta^{18}O_{precipitation}$ - present isotopic compositions of oxygen in Sava River and precipitation respectively.

Calculations and figures creations were done using Microsoft© Office tools, except for **Figure 1** which was produced using ArcMap 10.8.1 with the georeferenced orthophoto image which was obtained from the geoportal of the Croatian Geodetic Administration. Map is presented using the official coordinate system of the Republic of Croatia (HTRS96/TM).

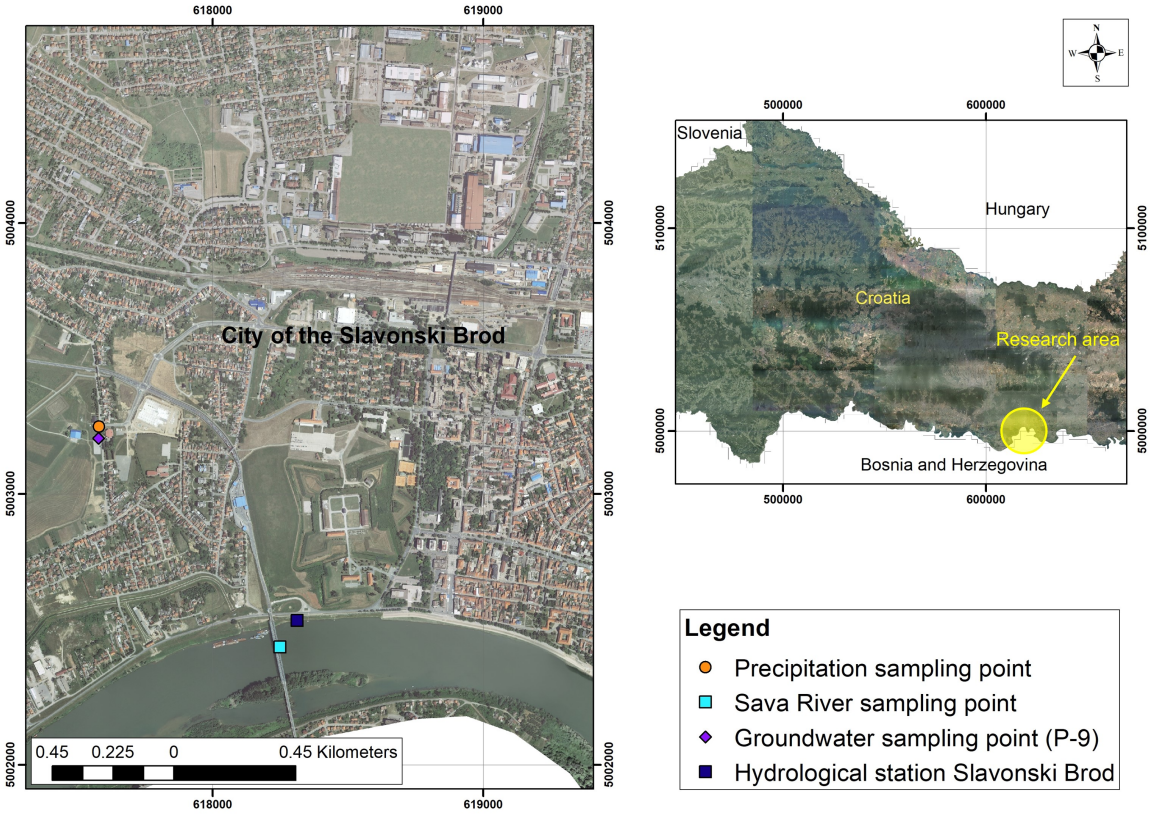

Figure 1: Location of the research area and sampling points

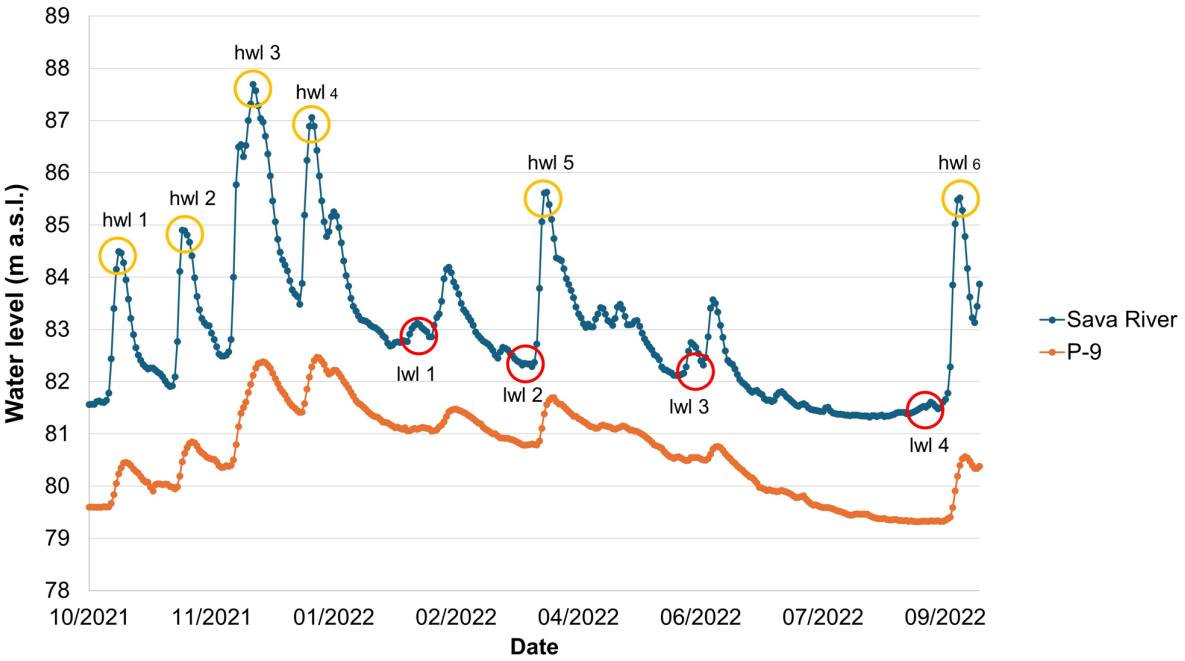

Figure 2: Variation of the Sava River and groundwater levels at observation well P-9 in hydrologic year 2021/2022

3. Results and discussion

In **Table 1** results of all cross-correlation analyses can be seen, while in **Figure 3** example of cross-correlation analysis for hwl 2 is presented. In general, all results show very high correlation coefficients, above 0.8. If all data is examined together, results suggest very fast reaction of the aquifer, where groundwater levels change with the delay of the 3 days, which corresponds to the results of the previous research (**Perić, 2023**). It can be clearly seen that in the high water levels transfer of pressure is much faster (2-3 days) than in the low water levels (2 to 8 days). Additionally, when very long duration of low water levels is present (lwl 4, **Table 1**), results showed negative correlation, which indicates that groundwater flow direction can be also to the Sava River. However, groundwater flow directions can be defined only if data from multiple observation wells exists that can enable construction of the equipotential maps in different hydrological conditions, which could not be used in this research due to lack of these type of data. In **Figure 4** LMWL Slavonski Brod for the hydrological year 2021/2022 is present as well as average values for all observed types of water. Slope of the LMWL Slavonski Brod (6.25) is lower than LMWL Zagreb (7.74) and corresponds to the warm (year 2021) and extremely warm (year 2022) period based on the average yearly air temperature as stated on the website of the Croatian Meteorological and Hydrological Service (**URL 1**).

Table 1: Summary results of cross-correlation analyses

Name	Date of the peak	Lag (day)	r_{lag} max.
All period	-	3	0.850
hwl 1	13/10/2021	3	0.942
hwl 2	8/11/2021	2	0.939
hwl 3	7/12/2021	3	0.947
hwl 4	31/12/2021	2	0.910
hwl 5	6/4/2022	2	0.972
hwl 6	22/9/2022	2	0.945
lwl 1	18/2/2022	8	0.920
lwl 2	31/3/2022	2	0.981
lwl 3	9/6/2022	7	0.924
lwl 4	13/9/2022	-8	-0.820

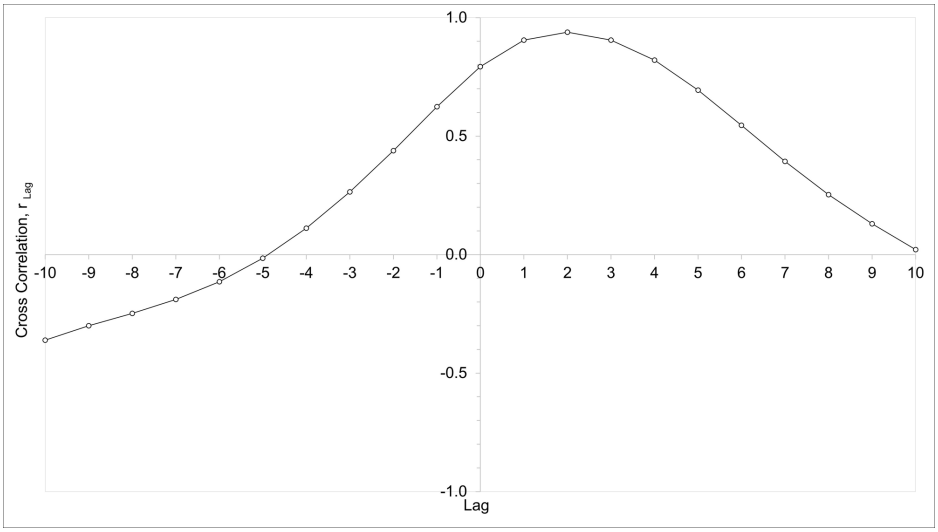

Figure 3: Cross-correlogram for hwl 2

Furthermore, results suggest that isotopic composition of groundwater is more similar to Sava River with respect to the precipitation. Average value of δ^2H in groundwater, Sava River and precipitation is -58.83 ‰, -61.11 ‰ and -48.06 ‰ respectively. Average value of $\delta^{18}O$ in groundwater, Sava River and precipitation is -8.32 ‰, -9.22 ‰ and -6.77 ‰ respectively. This corresponds to the results of two-component mixing models (**Table 2**) which suggest that Sava River presents the main source of recharge for the investigated aquifer, with percentage of recharge which varies from 63 % to 90 % for $\delta^{18}O$ and δ^2H respectively. This corresponds to the results of the cross-correlation analyses which in general showed very fast change in groundwater levels after the rise of Sava River water levels. This is not that pronounced in the low water levels, especially when low water levels last for a longer period. Here it must be noted that this research has been done only in one hydrological year, in which extremely warm meteorological conditions prevailed. More observation wells and more detailed hydrogeological research should be adopted in the study area, as well as continued monitoring, in order to get more detailed insight into the groundwater and surface water interaction. Additionally, as recognized in the previous research, vertical stratification is possible in the wider study area (**Kopić et al., 2016; Nakić et al., 2016; Filipović et al., 2022**), which provides necessity for the evaluation of water from the deeper parts of the aquifer and identification of aquifer layers of different origin. Furthermore, future research should include identification of depth till which infiltration from the Sava River is dominant, as well as cooperation with neighbouring Federation of Bosnia and Herzegovina due to existence of transboundary water resources.

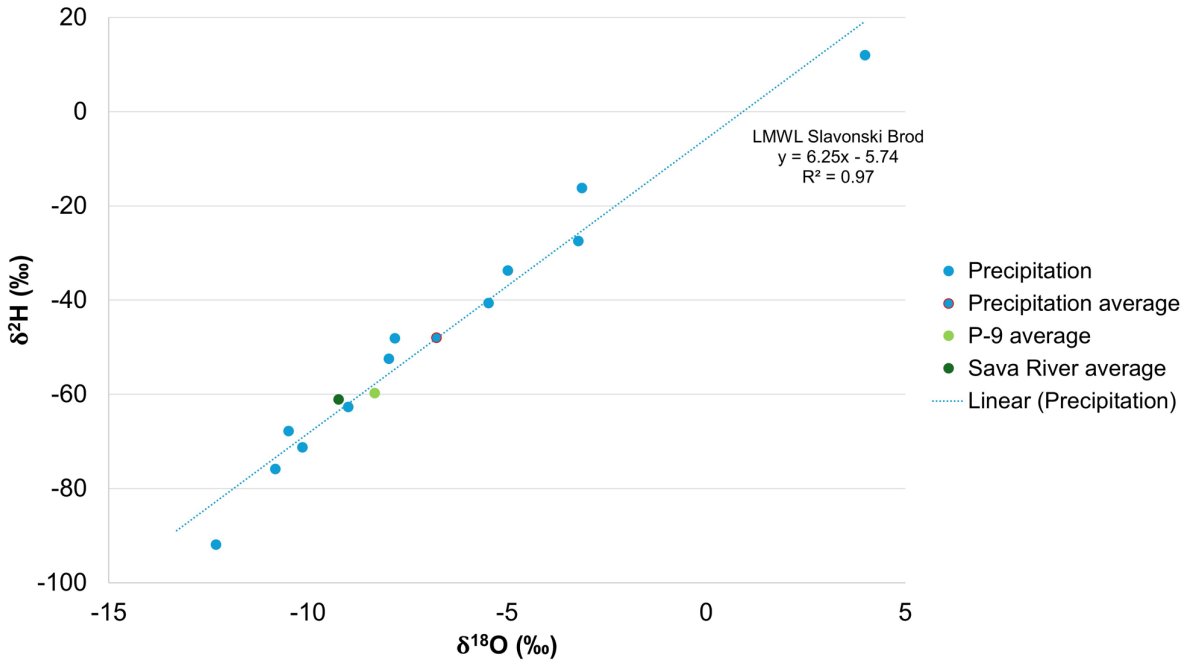

Figure 4: Isotopic composition of precipitation, Sava River, groundwater from the observation well P-9 and LMWL Slavonski Brod

Table 2: Results of two-component mixing models

Location	**δ^2H (‰)**	**$\delta^{18}O$ (‰)**
Observation well P-9	-59.83	-8.32
Sava River	-61.11	-9.22
Precipitation	-48.06	-6.77
	Recharge (%)	
Sava River (%)	90	63
Precipitation (%)	10	37

4. Conclusions

Evaluation of relationship between alluvial aquifers and surface waters present very important theme in Croatia, as well as in other countries. In the Pannonian part of Croatia alluvial aquifers, mostly related to the Sava and Drava rivers, present strategic water reserves. Research about this subject is neglected in some parts of Croatia except in the areas of big cities, mostly City of Zagreb and City of Varaždin. This research is located in the area of the City of Slavonski brod where Sava River water levels and groundwater levels, as well as their isotopic composition, were compared in order to define their relationship. Results showed different aquifer response in high water levels with respect to low water levels. As expected, response was faster in high water levels, resulting in lag times of 2 to 3 days. Isotopic composition of all observed water showed that Sava River presents main source of the recharge for the investigated aquifer, while long duration of low water levels suggest that Sava River is not that dominant in all hydrologic conditions. Although preliminary, these results provide new insight into the groundwater and surface water interaction in the study area which also showed that more detailed hydrogeological inspection of selected relationship, as well as inspection of the existing aquifer and its vertical stratification, is necessary. This is also extremely important due to transboundary water resources and in order to provide basis for sustainable management of water resources in the whole Sava River basin. In the future research continuation of monitoring is necessary to get data from more years and from different hydrological and meteorological conditions. Additionally, all available data from whole Sava River basin should be compared to identify areas of main sources of recharge of alluvial aquifers, especially those which are used for the public water supply.

5. References

1. Briški, M., Brkić, Ž. & Urumović, K. (2013): The conceptual model of groundwater system in a wider area Sikirevci. Proceedings V. Geological Consulting in Bosnia and Herzegovina, 77-78, Pale (in Croatian).
2. Coplen, T.B. & Wassenaar, L.I. (2015): LIMS for Lasers for achieving long-term accuracy and precision of δ^2H, $\delta^{17}O$, and $\delta^{18}O$ of waters using laser absorption spectrometry. Rapid Communications in Mass Spectrometry, 29, 2122–2130, https://doi.org/10.1002/rcm.7372.
3. Crosbie, R.S., Binning, P. & and Kalma, J.D. (2005): A time series approach to inferring groundwater recharge using the water table fluctuation method. Water Resources Research, 41 (1), https://doi.org/10.1029/2004WR003077.
4. Davis, J.C. (2002): Statistics and Data Analysis in Geology, Third Edition. John Wiley & Sons, Inc., New York, 638 p.
5. Filipović, V., Kovač, Z., Kopić, J., Nakić, Z., Parlov, J. & Skopljak, F. (2022): Isotopic signature of the Sikirevci well field and its connection with the Sava River. Mathematical Methods and Terminology in Geology 2022, Zagreb, Croatia.
6. Ford, D. & Williams, P. (2007): Karst Hydrogeology and Geomorphology. John Wiley & Sons, Chichester.
7. Gröning, M., Lutz, H. O., Roller-Lutz, Z., Kralik, M., Gourcy, L. & Pöltenstein, L. (2012): A simple rain collector preventing water re-evaporation dedicated for $\delta^{18}O$ and δ^2H analysis of cumulative precipitation samples. Journal of Hydrology, 448–449, 195–200, https://doi.org/10.1016/j.jhydrol.2012.04.041.
8. Karlović, I., Marković, T. & Vujnović, T. (2022): Groundwater Recharge Assessment Using Multi Component Analysis: Case Study at the NW Edge of the Varaždin Alluvial Aquifer, Croatia. Water 2022, 14 (1), 42, https://doi.org/10.3390/w14010042.
9. Kopić, J., Loborec, J. & Nakić, Z. (2016): Hydrogeological and hydrogeochemical characteristics of a wider area of the regional well field Eastern Slavonia – Sikirevci. Rudarsko-geološko-naftni zbornik 31 (3), 47-66, https://doi.org/10.17794/rgn.2016.3.4.
10. Kovač, Z., Barešić, J., Parlov, J. & Sironić, A. (2022a): Impact of Hydrological Conditions on the Isotopic Composition of the Sava River in the Area of the Zagreb Aquifer. Water 2022, 14, 2263, https://doi.org/10.3390/w14142263.
11. Kovač, Z., Krevh, V., Filipović, L., Defterdarović, J., Buškulić, P., Han, L. & Filipović, V. (2022b): Utilizing stable water isotopes (δ^2H and $\delta^{18}O$) to study soil-water origin in sloped vineyard: first results. Rudarsko-geološko-naftni zbornik 37 (3), https://doi.org/10.17794/rgn.2022.3.1.
12. Kovač, Z., Bačani, L., Ružičić, S., Parlov, J., Posavec, K. & Buškulić, P. (2023): Using Water Stable Isotopes and Cross-Correlation Analysis to Characterize Infiltration of Precipitation through Unsaturated Zone at the Velika Gorica Site of Zagreb Aquifer. Journal of Hydrologic Engineering, 28 (4), https://doi.org/10.1061/JHYEFF.HEENG-5806.
13. Krajcar-Bronić, I., Barešić, J., Borković, D., Sironić, A., Lovrenčić Mikelić, I. & Vreča, P. (2020): Long-Term Isotope Records of Precipitation in Zagreb, Croatia. Water 2020, 12 (1), 226, https://doi.org/10.3390/w12010226.
14. Lee, J.Y., H.S. Lim, H. I. Yoon & Park, Y. (2013): Stream Water and Groundwater Interaction Revealed by Temperature Monitoring in Agricultural Areas. Water, 5 (4), 1677–1698, https://doi.org/10.3390/w5041677.
15. Marković, T., Karlović, I., Orlić, S., Kajan, K. & Smith, A.C. (2022): Tracking the nitrogen cycle in a vulnerable alluvial system using a multi proxy approach: Case study Varaždin alluvial aquifer, Croatia. Science of the Total Environment, 853, 158632, https://doi.org/10.1016/j.scitotenv.2022.158632.
16. Michelsen, N., van Geldern, R., Rossmann, Y., Bauer, I., Schulz, S., Barth, J.A.C. & Schüth, C. (2018): Comparison of precipitation collectors used in isotope hydrology. Chemical Geology, 488, 171–179, https://doi.org/10.1016/j.chemgeo.2018.04.032.

17. Nakić, Z., Bačani, A., Parlov, J., Duić, Ž., Perković, D., Kovač, Z., Tumara, D. & Mijatović, I. (2016): Trends definition and groundwater status assessment in the Pannonian part of Croatia. Professional study. University of Zagreb, Faculty of Mining, Geology and Petroleum Engineering (in Croatian).
18. Parlov, J., Kovač, Z., Nakić, Z. & Barešić, J. (2019): Using water stable isotopes for identifying groundwater recharge sources of the unconfined alluvial Zagreb aquifer (Croatia). Water 2019, 11(10), 2177, https://doi.org/10.3390/w11102177.
19. Peng, T.R., Wang, C.H., Hsu, S.M., Wang, G.S., Su, T.W. & Lee, J.F. (2010): Identification of groundwater sources of a local-scale creep slope: Using environmental stable isotopes as tracers. Journal of Hydrology, 381 (1-2), 151–157, https://doi.org/10.1016/j.jhydrol.2009.11.037.
20. Perić, L. (2023): Relationship between the Sava River and groundwater in the area of the City of Slavonski Brod. Undergraduate thesis, Faculty of Mining, Geology and Petroleum Engineering, University of Zagreb, Croatia (in Croatian).
21. Petersen, R.M., Nel, J.M., Strydom, T., Riddell, E., Coetsee, C. & February, E. (2023): The use of stable isotopes to identify surface water–groundwater interaction in the Kruger National Park, South Africa. Water SA 49(2) 96–102, https://doi.org/10.17159/wsa/2023.v49.i2.3992.
22. Posavec, K., Vukojević, P., Ratkaj, M. & Bedeniković, T. (2017): Cross-correlation Modelling of Surface Water – Groundwater Interaction Using the Excel Spreadsheet Application. Rudarsko-geološko-naftni zbornik 673 32 (1), 25–32, https://doi.org/10.17794/rgn.2017.1.4.
23. Vrzel, J., Kip Solomon, D., Blaženka, Ž. & Ogrinc, N. (2018): The study of the interactions between groundwater and Sava River water in the Ljubljansko polje aquifer system (Slovenia). Journal of Hydrology, 556, 384–396, https://doi.org/10.1016/j.jhydrol.2017.11.022.
24. Welch, C., Cook, P.G., Harrington, G.A. & Robinson, N.I. (2013): Propagation of solutes and pressure into aquifers following river stage rise. Water Resources Research, 49, 5246–5259, https://doi.org/10.1002/wrcr.20408.

Internet sources:

URL 1 - Croatian Meteorological and Hydrological Service (CHMS, 2024). Available online: https://meteo.hr/klima.php?section=klima_pracenje&param=ocjena&el=msg_ocjena&MjesecSezona=godina&Godina=2022 (accessed on May 25th 2024).

SAŽETAK

Odnos podzemne i površinske vode na području grada Slavonskog Broda, Hrvatska

Aluvijalni vodonosnici, većinom vezani uz rijeke Savu i Dravu, zaštićeni su od strane Republike Hrvatske koja ih je proglasila strateškim vodnim rezervama. U panonskom dijelu Hrvatske one predstavljaju glavni izvor pitke vode za svoje stanovnike. Njihov odnos može biti vrlo dinamičan, što je posebno izraženo u plitkim otvorenim vodonosnicima. Ovo istraživanje je usmjereno na istraživanje odnosa podzemne i površinske vode na području grada Slavonskog Broda korištenjem hidroloških i hidrogeoloških analiza, kros-korelacijske analize te stabilnih izotopa vode (δ^2H i $\delta^{18}O$). Rezultati su pokazali da je reakcija vodonosnika brža pri visokim vodostajima u odnosu na niske vodostaje, dok je izotopni sastav svih promatranih voda pokazao da rijeka Sava predstavlja glavni izvor napajanje promatranog vodonosnika. Dodatno, pokazalo se da kod dugog trajanja niskih vodostaja utjecaj rijeke Save nije toliko dominantan. Nadalje, rezultati su također pokazali da je potrebno više hidroloških i hidrogeoloških istraživanja na širem području istraživanja, kako bi se dobili što detaljniji i precizniji rezultati. Ovo je također važno zbog postojanja prekograničnih vodnih resursa u velikom dijelu sliva rijeke Save te ako se želi postići održivo upravljanje vodnim resursima.

Ključne riječi: rijeka Sava; podzemna voda; kros-korelacijska analiza; stabilni izotopi vode; grad Slavonski Brod

Author`s contribution

Zoran Kovač (1) (associate professor) participated in data processing and laboratory analyses, results interpretation and wrote most of the manuscript. **Borna-Ivan Balaž (2)** (univ. spec. oecoing., mag. ing. geol.) participated in field sampling, laboratory analyses and editing of the manuscript. **Ferid Skopljak (3)** (full professor) participated in data interpretation and editing of the manuscript. **Lucijan Perić (4)** (univ. bacc. ing. geol.) participated in data processing and editing of the manuscript.

5th Croatian geomathematical congress
UDC: 622.1; category: preliminary communication

Circular Economy Approaches to Produced Formation Water: Opportunities and Challenges

Karolina Novak Mavar[1a]; Ivan Zelenika[2]; Katarina Simon[1b]
[1a,b] University of Zagreb, Faculty of Mining, Geology and Petroleum Engineering, Pierottijeva 6, 10000 Zagreb Croatia
[2] Gas Storage System Operator (PSP L.T.D.), Veslačka 2-4, 10000 Zagreb, Croatia
ORCID: [1a] 0000-0002-3526-6496; [2] 0000-0003-0632-5511; [1b] 0000-0001-7527-6173
Corresponding author: karolina.novak-mavar@rgn.unizg.hr

Abstract

As exploitation fields mature, oil and gas production generates huge quantities of formation water-brine, the handling of which is becoming an increasing problem in the petroleum industry. In line with the concepts of the circular economy, alternative uses for formation water (brine) are therefore being considered in order to reduce freshwater consumption. One of these is the production of "green" hydrogen in electrolysers. In electrolysis, high-purity water is crucial for the efficiency and longevity of the systems, which is why water treatment processes are required. The direct use of brine in electrolysis systems is associated with problems such as corrosion and contamination of equipment. In the paper, brine produced during oil and gas exploitation in the eastern part of the Drava Depression is analysed. The required power of the electrolysis system of 418 MW to convert all the produced water that is now returned to the fields is a challenge, but a model that utilises some of the water and uses the excess electricity to convert the produced water into hydrogen could be a viable option.

Keywords: formation water; Drava Depression; hydrocarbon exploitation; hydrogen; electrolysis; circular economy.

1. Introduction

The volatility of energy prices, the dependence of most countries on energy imports and increasing climate change have placed renewable energy at the centre of national energy strategies. In this context, the use of sustainable energy sources based on the circular economy is the right way forward for a clean energy transition.

According to the International Renewable Energy Agency (IRENA), a scenario in which the average global temperature increase is limited to 1.5 °C considers the climate-friendly production of 614 million tonnes of hydrogen (H_2) by 2050, which means that hydrogen would cover 12% of total energy demand (**IRENA, 2022; IRENA & Bluerisk 2023**). Hydrogen can be used as a raw material to produce steel, ammonia, methanol, fertilisers and synthetic fuels, but also to power vehicles or store seasonally limited renewable energy.

The production of "brown" or "grey" hydrogen, considering that hydrogen is produced from coal by gasification or from methane by methane steam reforming (SMR), causes significant greenhouse gas emissions, which is not in line with climate-neutral targets. "Blue" hydrogen refers to "brown" and "grey" hydrogen combined with carbon capture, utilisation and storage (CCUS), which limits greenhouse gas emissions. There are other hydrogen production technologies, but only SMR with biogas and nuclear electrolysis have reached a certain level of commercialisation (**IRENA & Bluerisk 2023**).

"Green" hydrogen is considered an acceptable alternative to fossil resources as it can be produced by water electrolysis, in in which water is split into O_2 and H_2 using renewable electricity. The main advantages of this technology are that no greenhouse gases (GHG) are released into the atmosphere, while the required electricity can be generated from renewable energy sources such as wind, solar, hydrothermal sources or biomass (**Kabir et al., 2023).**

According to **Marouani et al. (2023),** many challenges arise when it comes to production costs, ensuring adequate infrastructure for storage, distribution and use in various applications, and the development of innovative technologies. Specialised techniques are needed to prevent hydrogen leakage and improve safety measures in the storage, transport and use of hydrogen. In addition, many aspects of "green" hydrogen production are still questionable, such as land utilisation or actual greenhouse gas emissions considering carbon lifecycle analysis (**IRENA & Bluerisk 2023**). Currently, the production costs for 1 kg of H_2 from fossil fuels are $1.2, while the costs for 1 kg of green H_2 are $4 (**Blay-Roger et al., 2024**).

One of the most important prerequisites for water electrolysis is the need for high-purity water. According to the American Society for Testing and Materials (ASTM), the minimum requirement is Type II deionised water (DI water) (resistance >1 MΩ cm), while ASTM Type I DI water (>10 MΩ cm) is preferred for high purity (99.99%) hydrogen. According to one estimate, 21 billion m^3 of fresh, pure water will be needed by 2030 to achieve the desired hydrogen economy. Since clean water is needed to produce green hydrogen and clean water is fast becoming a scarce resource, the question arises as to whether it can be called "green". It is important to realise that accessible freshwater only accounts for <1% of the water on our planet. About 99% is almost exclusively salt water or water trapped in ice in the polar regions (**Abdel-Aal et al., 2010**). Such available salt water appears to be more convenient for use as an electrolysis feedstock for hydrogen production. As a 10 MW electrolyser requires 50-60 m^3/day of clean water, salt water treatment would be crucial for the production of sustainable green hydrogen (**Farràs et al., 2021; *https://www.alfalaval.com/***). Therefore, using salt water with the right desalination technology seems to be an optimal option to preserve scarce freshwater supplies. Another option is the direct utilisation of salt water as electrolyser feed.

The paper analysed the possibility of utilising the formation water (brine) produced in the exploitation of hydrocarbons in electrolysers to produce hydrogen. An overview of the available technologies was given, and an example of the water produced from seven (7) hydrocarbon fields in the Eastern Part of the Drava Depression was used as a case study.

2. Formation water (brine) production

Highly mineralized water, produced during hydrogen production, also known as "formation water" or "brine", is the main waste produced in oil and gas exploitation activities. This can be water that is naturally present in the reservoir and flood water that is injected into the oil field. The increase in oil and gas production has raised a global environmental issue related to the disposal of produced brine–water (**Nasiri & Jafari, 2017**). Produced water, which generally increases in volume as the field matures, can be 98% contained in the produced fluid (**Neff et al., 2011; Al-Ghouti et al., 2019**). The global average of this ratio is around 3 (barrels of water):1 (barrels of oil). As a result, the management of produced water is becoming an increasingly important part of oil and gas operations (**Wenzlick & Siefert, 2020**). Worldwide, daily brine production has reached 250 million barrels and is expected to reach 600 million barrels in the next ten years (**McCabe, 2020; Amakiri et al., 2022**).

After being produced within the formation fluid, the water is separated and treated (de-oiled) before being discharged. The limits for the discharge of produced water are often regulated and the oil content is specified in the oil content limits. According to the report by the International Association of Oil and Gas Producers (IOGP), which collected and published environmental data from its 40 operations, 46% of produced water is discharged, while 54% of produced water is reinjected underground. Even 79% of the water produced from onshore activities in 2021 was injected underground to maintain reservoir pressure or for disposal. Around 22% of the water discharged comes from offshore operations and 78% from onshore operations. The overall average oil content of produced water discharges in 2021 totalled 14.4 mg/l, with an average value of 17.1 mg/l for offshore activities and 5.7 mg/l for onshore activities (**Figure 1**; **IOGP, 2022**).

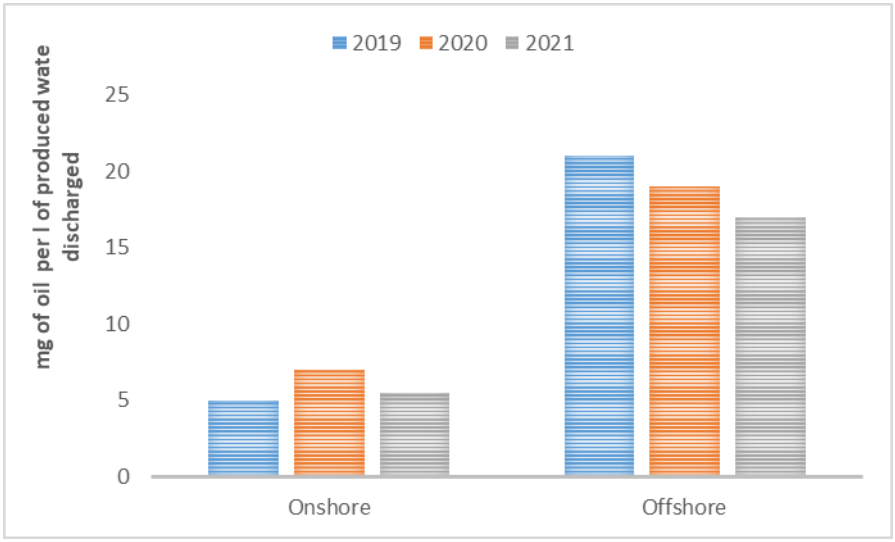

Figure 1: Oil content of produced water discharges (according to **IOGP, 2022**)

Although in general almost two-thirds of the de-oiled water extracted offshore is discharged into the sea, this is handled differently in different regions, i.e. companies operating in the Russia and Central Asia region reported reinjection of all water quantities produced offshore, while in Africa only one-fifth was reinjected (**Figure 2**).

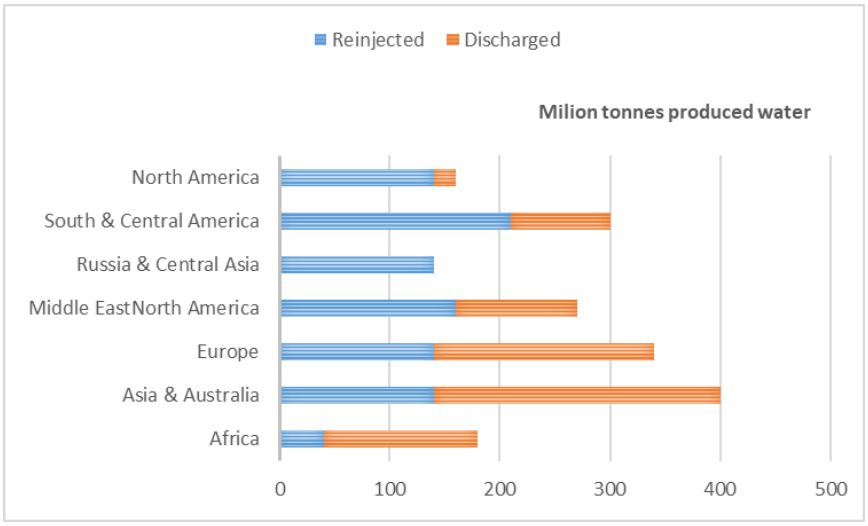

Figure 2: Quantities of formation water reinjected and discharged by region (according to **IOGP, 2022**)

The composition and properties of the produced water vary depending on reservoir (**Alley et al., 2011**). The properties of produced saline water change and its volume increases over the life of the field. The main constituents of produced water generally include dissolved and dispersed oil, dissolved minerals, solids, treatment chemicals and dissolved gases. **Tables 1 and 2** show the main components of oil field brine and its average content.

Table 1: Main constituents in oil field brine (**Fakhru'l-Razi et al., 2009; Amakiri et al, 2022**)

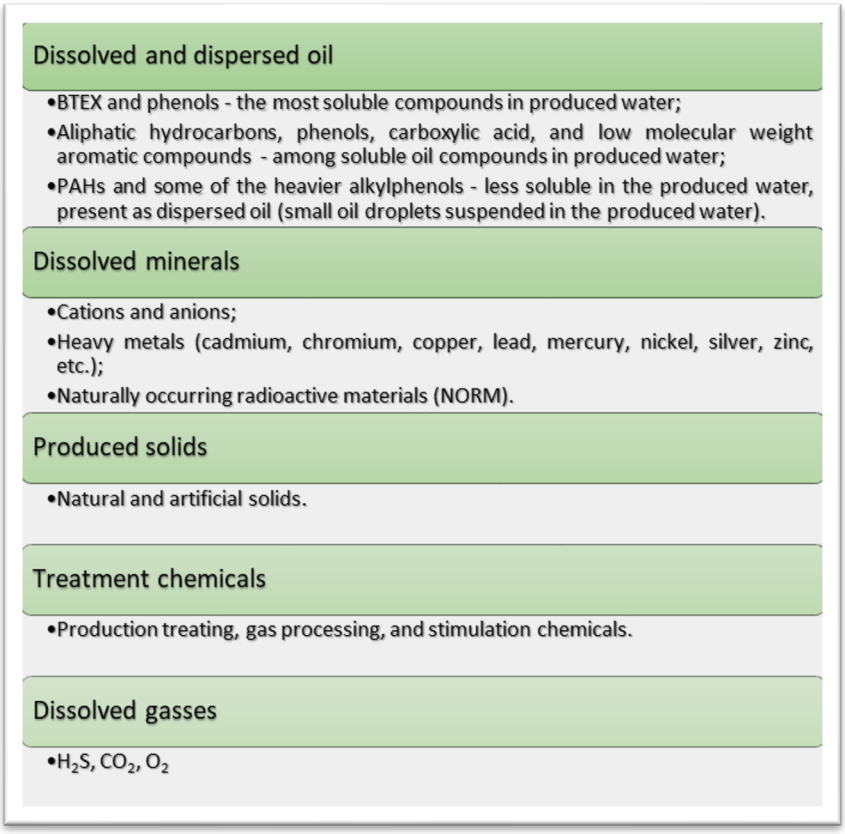

Table 2: Average oilfield brine content (**Ahmadun et al, 2009; Nasiri & Jafari, 2017**)

PARAMETER	VALUE (mg/l)
Total organic carbon, TOC	0-1500
Chemical Oxygen Demand, COD	1220
Total Suspended Solids, TSS	1.2-1000
Total oil (mg/l)	2-565
Benzene, Toluene, Ethylbenzene and Xylen, BTEX	0.39-35
Chloride	80-200000
Bicarbonate	77-3990
Sulphate	2-1650
Sulphide	10
Total polar compounds	9.7-600
Higher acids	1-63
Phenols	0.009-23
Calcium	13-25800
Sodium	132-97000
Potassium	24-4300
Magnesium	8-6000
Iron	<0.1-100
Aluminium	310-410
Boron	5-95
Barium	1.3-650
Cadmium	<0.005-0.2
Chromium	0.02-1.1
Copper	<0.002-1.5
Lithium	3-50
Manganese	<0.004-175
Lead	0.002-8.8
Strontium	0.002-1000
Titanium	<0.01-0.7
Zinc	0.01-35
Arsenic	0.005-0.3
Mercury	<0.001-0.002
Silver	<0.001-0.15
Beryllium	<0.001-0.004

3. Produced brine treatment technologies

The treatment of wastewater includes physical, chemical and biological methods. Physical methods include gravity separation, adsorption, the use of hydrocyclone separators and techniques based on membrane filtration. Methods such as coagulation, flocculation and advanced oxidation processes, ion exchange and electrochemical processes belong to the chemical methods, while conventional activated sludge processes, solids reactors, membrane bioreactors and constructed wetlands belong to the biological methods (**Figure 3; Al Ghouti et al., 2019; Sahu, 2021**).

The selection of a suitable method is usually a challenge that is orientated towards costs and the goals of technical efficiency. To achieve these goals, a combination of different technologies is used to remove different components (**Figure 3**). The specific combination of these treatment methods depends on the characteristics of the produced water, regulatory requirements and the intended use. The impurities removed are categorised as Total Suspended Solids (TSS),

organic compounds (such as phenols, Benzene, Toluene, Ethylbenzene and Xylen (BTEX), Polycyclic aromatic Hydrocarbons (PAHs)) and dissolved inorganic compounds, including heavy metals (**Arthur et al., 2005; Amakiri et al., 2022**).

METHOD	1	2	3	4	5	6	
API separator	■	■					
Deep bed filter	■	■					
Hydro cyclone	■	■					
Aeration and sedimentation		■					
Precipitation		■	■	■			1. De-oiling
Ion exchange			■				2. Suspended particles removal
Biological treatment					■		3. Iron removal
Thermal desalinisation		■		■		■	4. Softening
Activated carbon	■		■	■	■		5. Soluble trace/organics removal
Chemical treatment	■				■		6. Desalting
Ultrafiltration	■	■			■		
Nanofiltration	■	■	■	■	■	■	
Reverse osmosis	■	■	■	■	■	■	
Electrodialysis			■	■		■	

Figure 3: Technologies for specific components removal (according to **Nasiri & Jafari, 2017**)

All technologies can be categorised into primary, secondary and tertiary treatment (**Arthur et al., 2005; Amakiri et al., 2022**). By primary treatment oil droplets and suspended particles in the range of 5 to 15 μm are removed (hydrocyclone, API (American Petroleum Institute) separator, coagulation and flocculation). Adsorption, biodegradation, stripping and membrane separation are used to remove dissolved aromatic hydrocarbons such as BTEX. About 90 % of the oil droplets and soluble organic substances that have left the first treatment stage are removed in the second treatment stage (adsorption, activated sludge process, flotation). If required, the secondary effluent can be further treated by several tertiary processes (e.g. Advance Oxidation Process (AOP), electrodialysis). Tertiary treatment, known as final polishing, is used to remove dissolved solids, gases and dispersed hydrocarbons and focuses on the removal of salts from the treated production water. The tertiary treatment stages are used to remove other ultra-small oil droplets and other contaminants such as aromatic hydrocarbons (PAHs) (**Amakiri et al., 2022; Salem & Thiemann, 2022**).

Most of the methods-analysed in detail in the literature (adsorption, membrane filtration, activated sludge) have removal efficiency of over 90%. Reverse Osmosis (RO) globally appears to be the most commonly used desalination technology (**Randy & Inambao, 2019**). There are some new technologies that enable high water recovery of 90–98, e.g. Forward Osmosis (FO), Membrane Distillation (MD), Membrane Crystallisation (MCr), Electrodialysis (ED), Electrodialysis Reversal (EDR), Capacitive Deionisation (CDI), Eutectic Freeze Crystallisation (EFC) and Advanced Oxidation Processes (AOP). The extraction of organic pollutants from saline wastewater has already been analysed (**Lefebvre & Moletta 2006; Xiang et al. 2019**). Anaerobic/aerobic biological treatment and AOP have been shown to be viable for removing carbonaceous, nitrogenous and phosphorus contaminants at high salinity concentrations (**Sahu, 2021**). Theoretically, desalination of 1 m^3 of salt water requires around 0.86 kWh of energy, but the practical figures are 5 to 26 times higher than the theoretical minimum (**https://www.desware.net/**).

Several treatment systems are generally used in series. Which technology is most suitable depends on various conditions, e.g. the composition of the wastewater, the legal requirements, the overall costs, the by-products produced, etc.

4. Water electrolysis

In electrolysis, H_2O is converted to H_2 and O_2 using an external power supply to drive the oxidation of water at the anode and the reduction of water at the cathode, as in the following half-reactions (**Eq. 1-2**) (**Marouani et al., 2023**):

- Anode: $H_2O(l) \rightarrow ½\ O_2(g) + 2H^+(aq) + 2e^-$ (1)

- Cathode: $2H_2(l) + 2e^- \rightarrow H_2(g)$ (2)

Eq. 1 refers to the Hydrogen Evolution Reaction (HER), and **Eq. 2.** to the Oxygen Evolution Reaction (OER).The amount of energy (nFE) required at equilibrium for splitting water molecules (1 mole of water) corresponds to the Gibbs free energy change (ΔGd) of the water dissociation reaction (**Eq. 3; Millet, 2015**):

- $\Delta Gd - n *x\ F\ x\ *E = 0;\ \Delta Gd > 0$ (3)

Where are:
ΔGd - free energy change (J/mol);
n - number of electrons exchanged during the electrochemical splitting of 1 water molecule (2);
F - Faraday constant (electric charge of 1 mole of electrons, approx. 96485 C/mol);
E - free energy electrolysis voltage (volts).

There are several organisations that have defined quality standards for the electrolysis inlet water, e.g. American Society for Testing and Materials (ASTM D1193 2011) or International Organisation for Standardisation (ISO 3696). The American Society for Testing and Materials classifies four different categories of water by quality (**Table 3**), with the Type 1 (of the highest quality) being used for electrolysers. A water treatment plant (WTP) is therefore required, the treatment process of which depends on the quality of the supply water (***https://jhuesa.com/***).

Table 3: ASTM water quality chategories (***https://jhuesa.com/***)

PARAMETER	Type I	Type II	Type III	Type IV
Max el. conductivity (μS/cm at 25 °C)	0.056	1	4	5
Max el. resistivity (MΩ m at 25 °C)	18.2	1	0.25	0.2
pH (at 25 °C)	--	-	-	5.0-8.0
TOC max (μg/l)	10	50	200	Unlimited
Sodium max (μg/l)	1	5	10	50
Silica max (μg/l)	33	3	500	Unlimited
Chlorine max (μg/l)	1	5	10	50

Theoretically the use of 9 m^3 of ultrapure water can lead to 1 kg of H_2, and in practice over 11 m^3 is required (**Simoes et al., 2021**).

5. Case study: potential of produced formation water from the hydrocarbon fields of the Drava Depression for H_2 production by electroliysis

In the case study, the formation water from seven (7) hydrocarbon fields located in Eastern part of the Drava Depression in the Croatian part of the Pannonian Basin System was analysed. After separation during the treatment and processing of formation fluid, the water is now disposed of by reinjection into deep wells. Instead of disposal, this paper analyses the potential of utilising this water for the production of green hydrogen.

The geotectonic position of the Drava Depression (red) within the Pannonian Basin System and area that approximately covers the Drava Depression are shown in **Figures 4** and **5**.

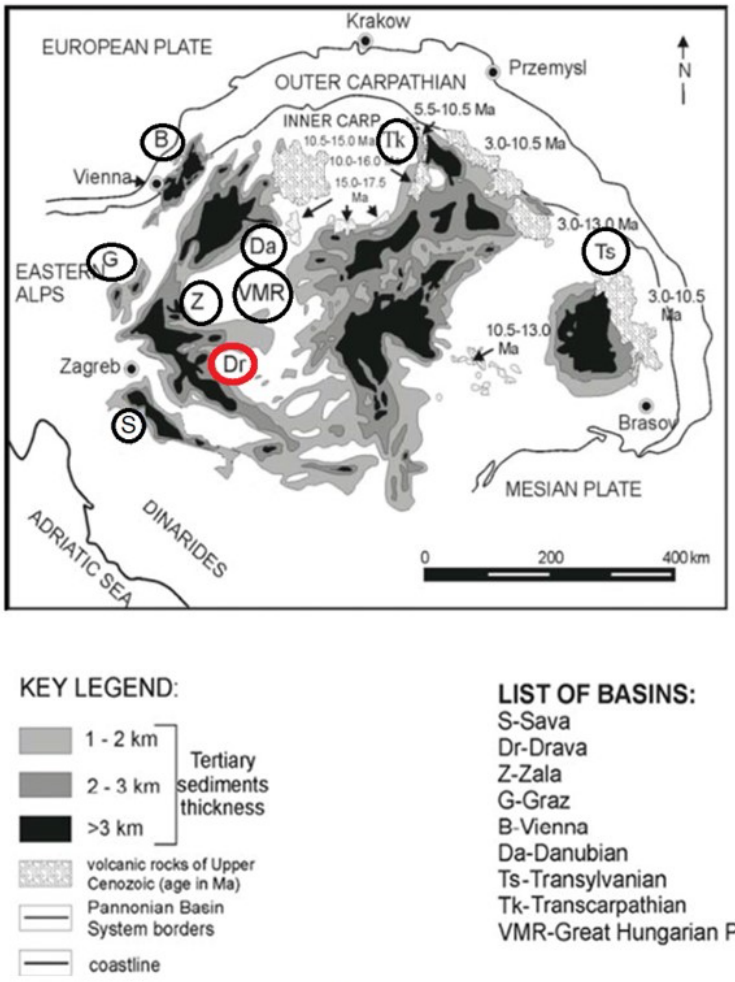

Figure 4: The geotectonic position of the Drava Depression within the Pannonian Basin System (**Malvić & Rusan, 2009**; **Ivšinović, 2017**)

Figure 5: Area that approximately covers the Drava Depression (**Malvić & Cvetković, 2013**)

The stratigraphic relationships in the subsurface of the eastern part of the Drava Depression are defined by lithostratigraphic units. The formations are defined by EK markers, which are characterised by clear recognisability and correlative properties due to their low thickness and large lateral extent, or by EK benchmarks, which in this case represents a discordance between younger Neogene-Quaternary and older magmatic-metamorphic-sedimentary rocks. **Figure 6** shows a schematic stratigraphic column of the Drava Depression (Croatian Western, Eastern and Hungarian parts).

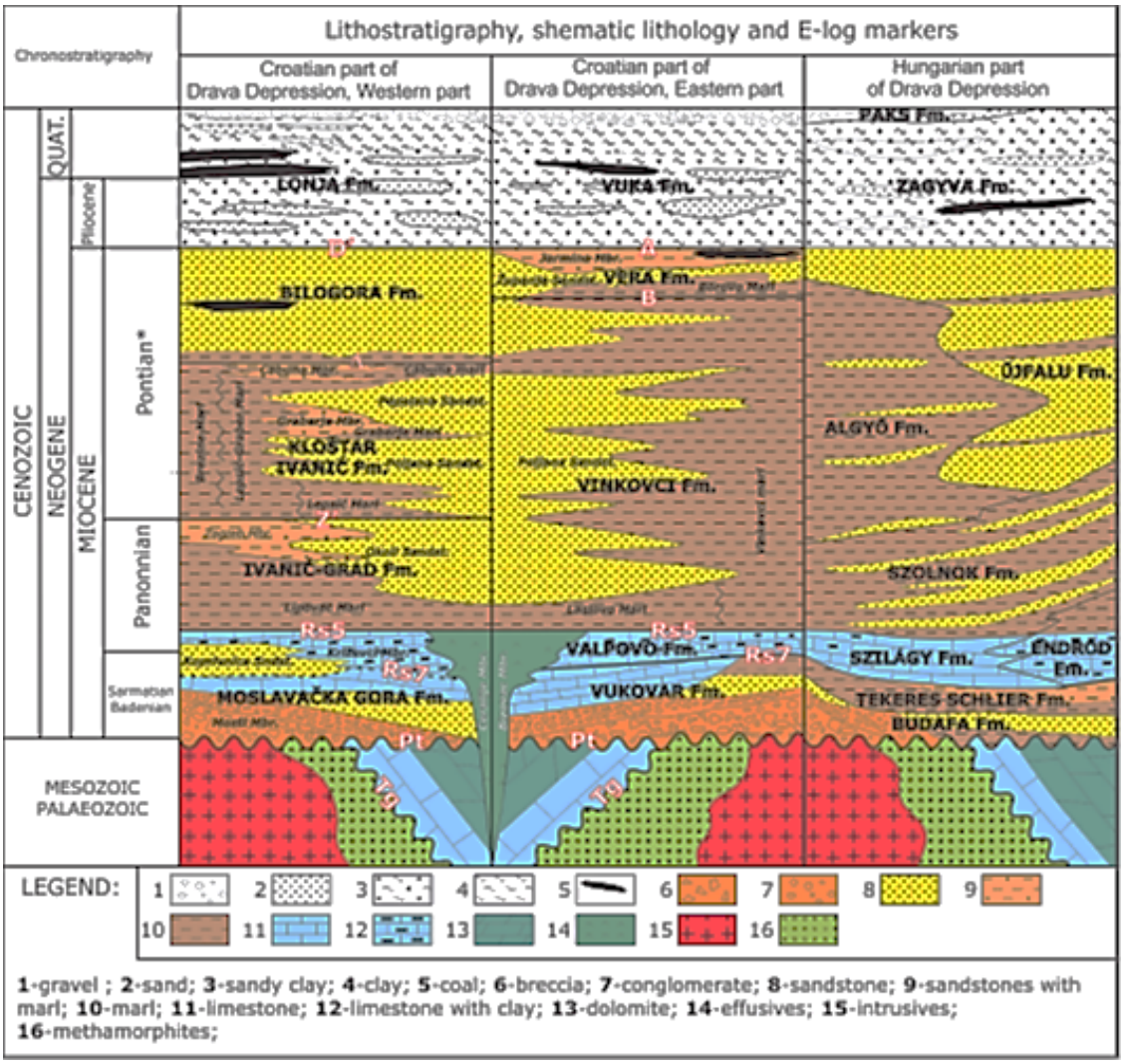

Figure 6: Lithostratigrphic column of the Drava Depression (**Malvić & Cvetković, 2013**)

A brief description of the existing gathering system of the oil fields under consideration is given further in the text. Fluid produced from the oil field "A" by flowing production or by gas lift, is trasported through flowlines to one of the three existing measuring stations (MS-1, MS-2, MS-3). The fluid produced from the field "B" by gas lift is transported through flowlines to the collector and further by the gathering pipeline to the collecting separator at the Oil Processing Plant (OPP). From the oil production fields "C" and "D" and "E", fluid is produced by using sucker road pumps and transported via flowlines to the collector and further via gathering lines to the collecting separator in the OPP. Well-production fluid from the hydrocarbon fields "E", "F" and "G" is carried by flowlines to the MS 4 and further to OPP (**INA d.d., 2017**).

At the measuring stations, the liquid is separated from the gas, the liquid and gas volumes are measured and then the fluids are transported separately to OPP site. The gas collected from the measuring stations is transported from the OPP through the gas pipeline to the consumer, while the liquid (mixture of oil and water) is transported to the heat exchangers in the OPP. From the

heat exchanger, the liquid is channelled into the gun-barrel. The separated water is extracted and passes into the decanter and then through the waste water separator into brine tank. The brine is then pumped from the tank to the injection wells.

The oil is transported from the dehydrator to the dry oil tank. The dehydrated (dry) oil from the process tanks is then transferred to the 5 000 m^3 dry oil tanks (R-5000). Gravity separation is used to separate an additional quantity of water in the R-5000, which is pumped into the injection wells together with the remaining water separated during oil processing. The water injection is only used for disposal, not for pressure maintenance (**INA d.d., 2017**).

Annually almost 500 000 m^3 of formation water is produced and reinjected (**INA Group, 2020**). The average content of produced formation water is given in **Table 4**. The quantities of water produced and re-injected underground are shown in **Figure 7.**

Table 4: The average content of formation water processed at OPP

PARAMETER	VALUE	PARAMETER	VALUE
pH	6.8	Fe^{2-}(mg/l)	-
Max el. conductivity (µS/cm at 25 °C)	1803	Fe (mg/l)	0.632
Max el. resistivity (MΩ m at 25 °C)	0.555	Cl^- (mg/l)	5424.3
Density (kg/dm^3)	10086	CO_3^{2-}(mg/l)	-
Suspended solids (mg/l)	43	HCO_3^- (mg/l)	1792
NH_4^- (mg/l)	26.3	SO_4^{2-} (mg/l)	51
Na (mg/l)	3860	Salinity (gNaCL/l)	8.94
K (mg/l)	86.4	H_2S (mg/l)	8.7
Mg (mg/l)	69	CO_2 (mg/l)	440.5
Ca (mg/l)	177.3	Br- (mg/l)	28
Sr (mg/l)	17.2	TOC (No/ml)	48.3

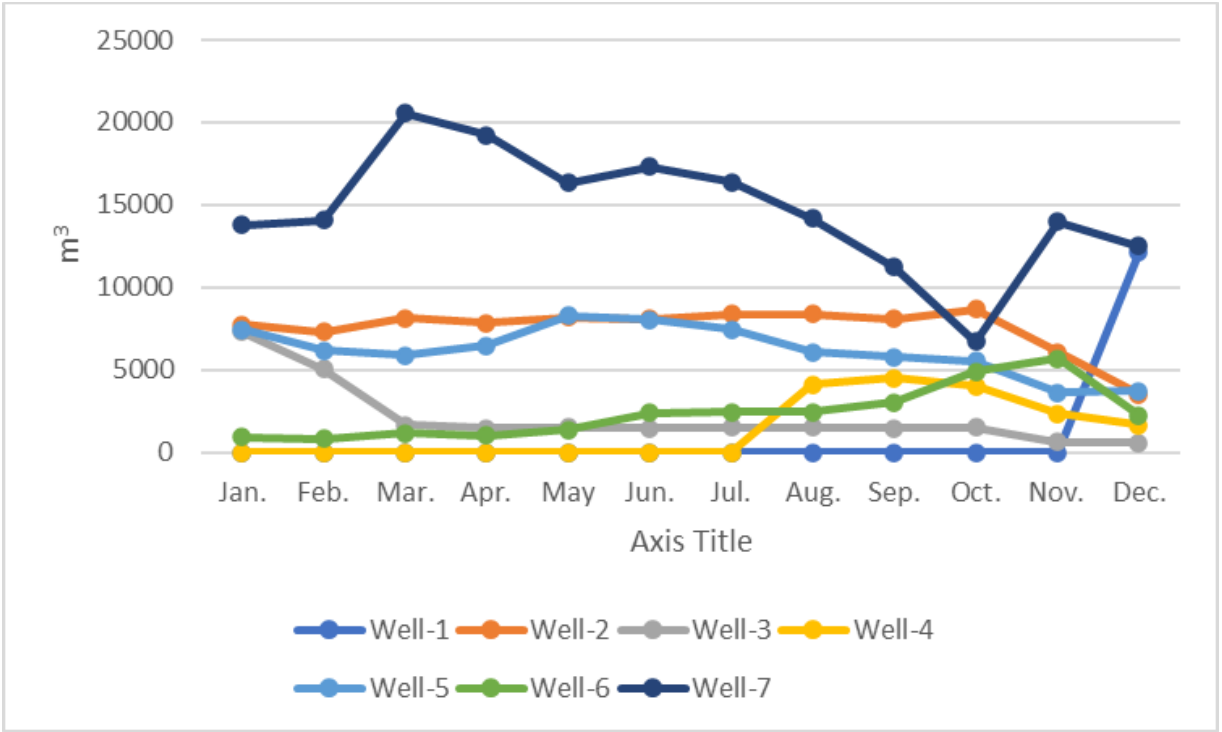

Figure 7: Quantities of brine reinjected

5.1. Calculation of the hydrogen production potential from brine and required energy

The total volume of production water to be disposed of within a year can be estimated at approx. 500 000 m^3. If the entire water production to hydrogen takes place by means of electrolysis plants, the amount of electrical energy that would have to be available to the electrolysis plants

must be calculated. The amount of produced H_2 can be calculated using the following equations, which are based on Faraday's laws of electrolysis:

1. Total electric charge (Q):

- $Q = I \times t$ (4)

Where are:
Q - total electric charge (C)
I - electric current (A)
T - time of electrolysis (s)

2. Mass of produced H_2:

- $m = (M \times Q) / (n \times F)$ (5)

Where are:
m - mass (g)
M - molar mass (approx. 2 g/mol for H_2)
n - number of electrons required (2 for H_2)
F - Faraday's constant (approx. 96485 C/mol)

3. Volume of hydrogen (V) produced at standard conditions:

$V = (Q \times V_m) / (n \times F)$ (6)

Where are:
V - volume of hydrogen (l)
V_m - molar volume of gas at standard conditions (approx. 22.4 l/mol)

For calculation of the required energy for electrolysis **(Eq. 9)**, total number of moles of hydrogen **(Eq. 7-8)** is required, as follows:

- **Calculation of the number of moles of water**
  Water mass = 500 000 000 kg (water density = approx. 1 kg/l)
  Moles of water = $\frac{500\,000\,000\ kg}{0{,}018\ kg/mol} \approx 27\,777\,777\,778$ mol (7)

- **Calculation of moles of hydrogen:**
  Each mole of water (H_2O) yields 1 mole of O_2 and 2 moles of H_2.
  Total number of moles of hydrogen = 2 x 27 777 777 778= (8)
  = 55 555 555 556 mol

- **Calculation of the required energy for electrolysis:**
  According to Faraday's law of electrolysis, producing 1 mole of hydrogen requires approximately 237 kJ of electrical energy. Total required energy is calculated according to **Eq. 9-10:**

Total required energy = 55 555 555 556 * 237 =13166666666772 kJ (9)
≈13 167 000 000 MJ

Expressed in MWh (1 kWh = 3600 kJ):

$$\text{Total Energy} = \frac{13166666666772\ \text{kJ}}{3600\ kj/kWh} \approx 3\ 657\ 407,407\ \text{MWh} \quad (10)$$

Using the basic expression for calculating power, the required power of the electrolyser system amounts to **(Eq. 11)**:

- $P = \frac{3,657,407,407\ \text{kWh}}{8760h} = 417\ 661\ \text{kWh} \approx 418\ \text{MW}$ (11)

The PEM (Proton Exchange Membrane) electrolysers from Siemens, in particular the Silyzer 300 model, are known for their high efficiency and performance in hydrogen production. The efficiency of these systems is between 75 % and 80 %, which is quite high for electrolysis technology. In terms of the specific energy required to produce hydrogen, Siemens electrolysers generally require around 60 kWh of electricity to produce one kilogramme of hydrogen. With an electrolyser output of 418 MW and continuous operation over a period of one year, around 61 000 t of H_2 could be produced. **Figure 8** shows the calculated H_2 volumes, and the electrical energy required per volume of water quantities injected underground, expressed by each well.

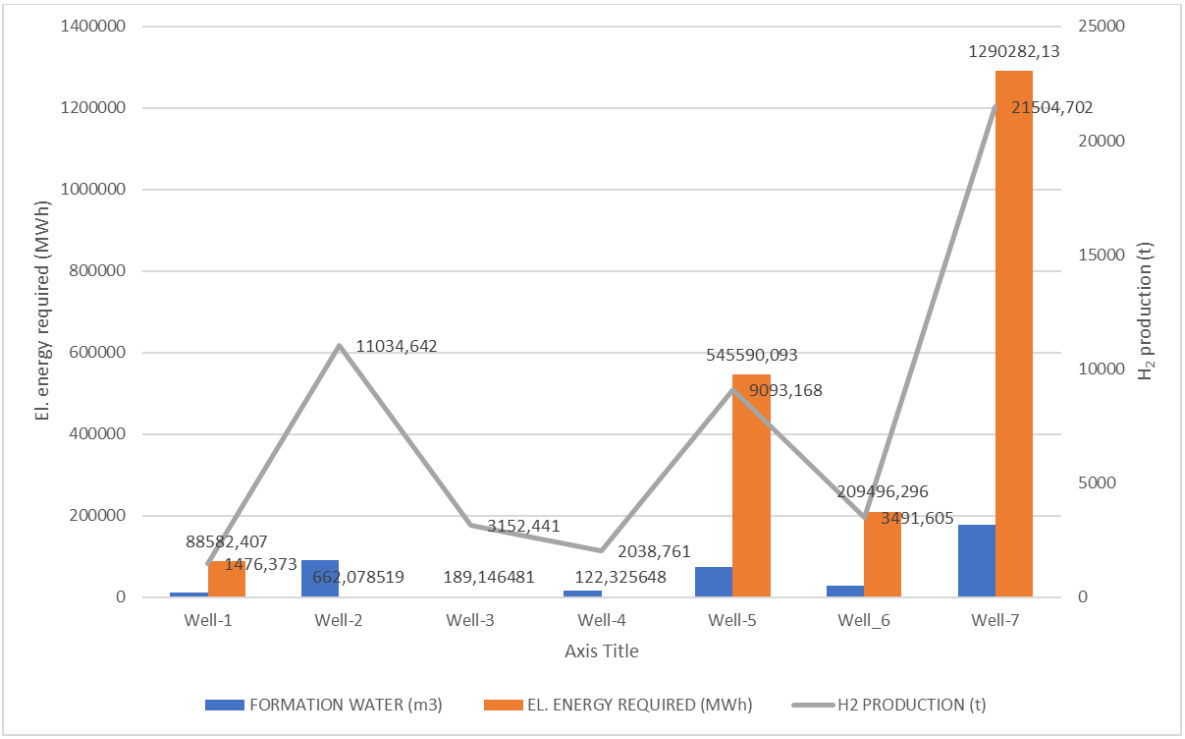

Figure 8: H_2 production and electrical energy required for the quantities of water currently injected by the well

6. Discussion

The EU climate target of decarbonisation by 2050 envisages a share of at least 13% hydrogen in the energy mix by 2050, which is feasible with the installation of 40 GW of renewable hydrogen electrolysers by 2050 (**EC, 2020).** Technological improvements being developed in various scientific fields with the aim of cost efficiency are crucial. The production of hydrogen from formation water by electrolysis using green electrical energy would be a good example of the circular economy concept. To achieve commercialisation, many obstacles to existing technologies need to be overcome.

Alkaline water electrolysis is the current technology for large-scale electrolytic hydrogen production. It is characterised by low efficiency, low current density and the lack of suitable scale-up practise. Since high-quality water is used for electrolysis, additional purification pre-treatment

is required, which increases the cost of such a project (**Abdel-Aal et al., 2010**). **Nasiri & Jafari (2017)** analysed different methods of produced water treatment along with challenges and opportunities of each of them. When saline water is used as an inlet, the required ASTM Type I water quality can be achieved using commercially available reverse osmosis and deionisation systems. Nevertheless, the question of the energy consumption of WTP is often raised, especially when it comes to water desalination. However, it must be emphasised that the attractive forces between water molecules and ions must be overcome during water treatment, while at the same time the strong covalent bonds between the atoms in the water molecules must be overcome during electrolysis (***https://hydrogentechworld.com/***).

While the treatment of fresh groundwater involves pre-treatment by sand filtration and aeration, saltwater must be desalinated. Softening, degassing, demineralisation and polishing are required to obtain pure water. In electrolysis systems such as Proton Exchange Membrane (PEM) and Anion Exchange Membrane (AEM), which work with ultrapure water, the water entering the electrolysis system is continuously contaminated with metal ions from the pipes and process equipment as well as with ions and organic substances from the electrolyser stack. Due to extension of the electrolyser lifetime, such components are being removed with the aid of side stream polishers (**Farràs et al., 2021; https://www.eurowater.com/).**

Theoretically, 39.4 kWh, but taking into account various inefficiencies, water electrolysis requires an average of 50 – 55 kWh/kg. The most commonly used reverse osmosis systems consume an average of 0.0012 kWh/l of brackish water or 0.0046 kWh/l of seawater as feedstock. If a system for treating demineralised water is also used to meet the required quality standards, the energy consumption increases by around 0.0016 kWh/l. The total energy consumption for treatment is about 0.055 to 0.077 kWh/kg of H_2, which is less than 0.2% of the total energy consumption for hydrogen production. Innovative reverse osmosis and demineralisation plants are cost-efficient, so that the total costs for water desalination can be reduced to around 0.85 USD/m^3 (***https://www.weforum.org/***).

As presented in previous chapter, to convert 500 000 m^3 of produced water (treated up to the level of pure water) into chemical energy of hydrogen by electrolysis, a total of 3.7 TWh of electrical energy is required over the course of one year.– With a 418 MW electrolyser in continuous operation over a period of one year, around 61 000 t of H_2 could be produced. Considering that the current hydrogen demand in Europe is 8.7 million tonnes (Mt) per year (grey hydrogen), as well as the EU's ambitious target of producing 10 Mt of renewable hydrogen and importing 10 Mt of renewable hydrogen by 2030 (**EC, 2020**), it is obvious that only a small proportion of the produced formation water from the fields considered in this work could be realised in hydrogen production.

As already mentioned, another way to utilize brine for electrolysis is to develop an electrolysis system that can utilise seawater for direct electrolysis. It is likely that these systems would operate at a low power density and would only electrolyse a small proportion of the water in contact with the electrodes.

In addition to the potential advantages in terms of reusing of the produced water, which is actually waste, there are many disadvantages resulting from the lack of technology to overcome corrosion and contamination problems and the development of undesirable electrochemical products such as chlorine. Due to the low conductivity of brine, the sluggish HER kinetics require a high conductivity electrolysis catalyst to enable rapid charge transfer, which represents the first problem. The second problem is the presence of bacteria and microbes in the seawater and the resulting formation of insoluble deposits on the catalyst surface, and the third issue is the corrosiveness of brine, which negatively affects most metal-containing catalysts. Since the same current surge that is responsible for O_2 generation at the anode also converts the chloride ions in the brine into highly corrosive chlorine gas that corrodes the electrodes and catalysts, this causes the electrolysers to fail immediately within a few hours (normally they can function for years). Such major obstacles have resulted with small progress made so far (**Alasali et al., 2024; Huang**

et al., 2024; Kasani et al., 2024; Shi et al., 2024; Sun et al., 2024; Wang et al., 2024; ***https://www.science.org/***).

The cell for freshwater electrolysis is known as an H_2/O_2 cell, while the cell for saturated brine behaves more like an H_2/Cl_2, which is responsible for caustic soda production. In the H_2/O_2 cell, hydrogen/oxygen is produced in a ratio of 2:1, while in the H_2/Cl_2 cell hydrogen/chlorine is produced in a molar ratio of 1:1, which means that the hydroxide ions migrate to the anode (positive electrode) where oxidation takes place, but there is competition between the hydroxide ions and the chloride ions to be oxidised. In the electrolysis of a sodium chloride solution, four products therefore appear to be possible (sodium, chlorine, hydrogen and oxygen). It is worth to note that the sodium is extremely reactive and therefore reacts immediately with water, producing sodium hydroxide (NaOH)(aq) (***https://www.nagwa.com/***). However, the overall process is given by the **Eq. 12 – 14**.

$$2NaCl+2e^- = 2Na + Cl_2 \quad (12)$$

$$2Na+2HOH = 2NaOH + H_2 \quad (13)$$

$$2Cl = Cl_2 + 2e^- \quad (14)$$

The use of oxygen-selective electrodes seems to be the most promising way for the electrolysis of brine. The oxygen reaction is more dependent on the electrode material than the chlorine reaction, and at low overpotential with different electrode materials (manganese or MnO_2), at a pH value of 0-3, the reaction potential of O_2 is higher than that of Cl_2 (**Abdel-Aal et al., 2010**).

Furthermore, in terms of its contents, seawater is much less complex than average oil-fields produced water (**Shaddel & Tabatabae-Nejad, 2014**). It is therefore obvious that one line of further research and technology development would lead to improving the efficiency and cost of both water treatment methods, while another line of research would cover the issue of direct utilisation of produced formation water in electrolysis.

7. Conclusion

While reinjecting produced water into wells for reservoir pressure maintenance or permanent disposal remains the predominant commercial method for brine management, modern circular economy models emphasis using resources for as long as possible. This approach opens up alternative uses for produced water, aligning with environmental goals by reducing freshwater consumption.

However, the suitability of formation water for electrolysis depends on factors such as its composition and the required purity. The purity of Type 1 water is crucial for achieving high hydrogen production efficiency and preventing the degradation of electrolysis components. Depending on the specific composition of formation water, treatments such as reverse osmosis and deionization are necessary.

The various electrolysis technologies have varying tolerance levels for impurities in the water feedstock. Electrolysers for direct usage of formation water are under development, but significant issues like corrosion, contamination, and the development of undesirable electrochemical products such as chlorine need to be addressed.

Both the hydrogen economy and water electrolysis are well-established concepts, but currently, green hydrogen is generally not cost-effective compared to hydrogen produced from fossil fuels (grey hydrogen), due to the high cost of electrolysis and expensive renewable energy. However, there is significant potential for cost reductions in the future. Technological advancements, economies of scale, and supportive government policies could all contribute to lowering the cost of green hydrogen.

Although the total power of the electrolysis system of 418 MW calculated in this study seems technically very demanding, the continuous increase in the share of renewable energy sources (wind farms and solar systems) in Croatia, the limitations of the electrical energy infrastructure, and the increasingly problematic ability to balance the electrical energy system necessitate the construction of infrastructure capable of performing energy balancing with larger capacities. The conversion of part of the produced water into hydrogen by utilizing excess electricity from the grid, rather than its disposal, might prove economically viable upon further techno-economic analyses, especially when considering the permanence of the constructed infrastructure and the possibility of expanding the electrolyser capacities depending on the availability of electrical energy.

8. References

1. Abdel-Aal, H.K., Zohdy, K.M., Abdel Kareem, M. (2010): Hydrogen production using sea water electrolysis. The Open Fuel Cells Journal, 3, 1-7.
2. Ahmadun F. R., Pendashteh, A., Abdullah, L. C., Awang Biak, D. R., Madaeni, S. S., Abidin, Z. Z. (2009): Review of technologies for oil and gas produced water treatment. Journal of Hazardous Materials, 170, 2/3, 530-551. 2009.
3. Alasali, F., Abuashour, M.I., Hammad, W., Almomani, D., Obeidat, A.M., Holderbaum, W. (2024): A review of hydrogen production and storage materials for efficient integrated hydrogen energy systems. Energy Science & Engineering, 12, 1934–1968.
4. Al-Ghouti, M.A., Al-Kaabi, M.A., Ashfaq, M.Y., Da'na, D.A. (2019): Produced water characteristics, treatment and reuse: A review. Journal of Water Process Engineering, 28, 222-239.
5. Alley, B., Beebe, A., Rodgers, J., Castle W.J. (2011): Chemical and physical characterization of produced waters from conventional and unconventional fossil fuel resources. Chemosphere, 85/1, 74-82.
6. Amakiri, K.T., Ramirez Canon, A., Molinari, M., Angelis-Dimakis A. (2022): Review of oilfield produced water treatment technologies. Chemosphere, 298, 134064, 20 p.
7. Arthur, J.D., Langhus, B.G., Patel, C. (2005): Technical Summary of Oil & Gas Produced Water Treatment Technologies. All Consulting, LLC, Tulsa, OK, http://www.all-llc.com/publicdownloads/ALLConsulting-WaterTreatmentOptionsReport.pdf, 53 p.
8. Blay-Roger, R., Bach, W., Bobadilla, L.F., Reina, T.R., Odriozola, J.A., Amils, R., Blay, V. (2024): Natural hydrogen in the energy transition: Fundamentals, promise, and enigmas. Renewable and Sustainable Energy Reviews, 189, A, 113888, 9 p.
9. EC (2020): Communication from the Commission to the European Parliament, the Council, the European Economic and Social Committee and the Committee of the Regions A Hydrogen Strategy for a Climate-Neutral Europe. European Comission COM(2020) 301 final, https://eur-lex.europa.eu/legal-content/EN/TXT/?uri=CELEX%3A52020DC0301, 24 p.
10. Fakhru'l-Razi, A., Pendashteh, A., Abdullah,L.C., Biak, D.R.A., Madaeni, S.S., Abidin, Z.Z. (2009): Review of technologies for oil and gas produced water treatment. Journal of Hazardous Materials, 170/ 2–3, 530-551.
11. Farràs, P., Strasser, P., Cowan, A.J. (2021): Water electrolysis: Direct from the sea or not to be? Joule, 5/8, 2021, 1921-1923.
12. Huang, H., Xu, T., Chen, J., Zhao, Y., Lv, Y, Liu, B., Zhang, B., Yuan, J., Wu, Y. (2024): Efficient nanocatalysis of Ni/Sc2O3@FLG for magnesium hydrolysis of hydrogen generation. Journal of Materials Science & Technology, 175, 235-243.
13. INA Industrija nafte d.d. (2017): Izvješće o sigurnosti: Otpremna stanica Beničanci (*Safety Report: Dispatching Station Beničanci*). DLS d.o.o., 132 p. (in Croatian)
14. INA Group (2021). Godišnje izvješće, 2020 (*Annual Report 2020*), 296 p. (in Croatian)
15. IOGP (2022): International Environmental performance indicators – 2021 data. International Association of Oil & Gas Producers, London, UK, https://www.iogp.org/, 78 p.

16. IRENA (2022): Global hydrogen trade to meet the 1.5°C climate goal: Part I – Trade outlook for 2050 and way forward. International Renewable Energy Agency, Abu Dhabi, United Arab Emirates, https://www.irena.org, 114 p.
17. IRENA and Bluerisk (2023): Water for hydrogen production. International Renewable Energy Agency, Bluerisk, Abu Dhabi, United Arab Emirates, https://www.irena.org, 66 p.
18. Ivšinović, J. (2017): The cost analysis of the separation of produced formation water from the hydrocarbon reservoir using the example of the Upper Miocene sandstone deposits of the Sava Depression. Rudarsko-Geološko-Naftni Zbornik, 33/1, 35–43.
19. Kabir, M.M., Akter M.M., Huang, Z., Tijing, L., Shon, H.K. (2023): Hydrogen production from water industries for a circular economy. Desalination, 554, 116448.
20. Kasani, A., Maric, R., Bonville, L., Stoyan Blizankov, S. (2024): Catalysts for Direct Seawater Electrolysis: Current Status and Future Prospectives. ChemElectroChem, 11, e202300743, 21 p.
21. Lefebvre, O., Moletta R. (2006): Treatment of organic pollution in industrial saline wastewater: A literature review. Water Research 40, 3671–3682.
22. Malvić, T., Cvetković, M. (2013): Lithostratigraphic units in the Drava Depression (Croatian and Hungarian parts) – a correlation**.** Nafta, 64/1, 27-33.
23. Malvić, T., Rusan, I. (2009): Investment risk assessment of potential hydrocarbon discoveries in a mature basin. Case study from the Bjelovar Sub-Basin, Croatia, Oil, gas - European Magazine (Hamburg), 35, 67-72.
24. Marouani, I., Guesmi, T., Alshammari, B.M., Alqunun, K., Alzamil, A., Alturki, M., Abdallah, H.H. Integration of renewable-energy-based green hydrogen into the energy future. Processes 2023, 11/9, 2685, 29 p. https://doi.org/10.3390/pr11092685
25. McCabe, P. (2020): Oil and Natural Gas: Global Resources.. In: Malhotra, R. (ed.): Fossil Energy. -Springer, 7-23, 631 p.
26. Millet, P. (2015): Fundamentals of Water Electrolysis. In Godula-Jopek, A. (ed.): Hydrogen Production: by Electrolysis, First Edition. - Wiley-VCH Verlag GmbH & Co. KGaA, Weinheim, 33-62.
27. Nasiri, M., Jafari, I. (2017): Produced water from oil-gas plants: A short review on challenges and opportunities. Periodica Polytechnica Chemical Engineering, 61/2, 73–81.
28. Neff, J., Lee, K., DeBlois E.M. (2011): Produced water: overview of composition, fates, and effects. In: Lee, K., Neff, J. (eds.): Produced Water. -Springer, New York, NY, 3-54, 608 p.
29. Ncube, Randy, N., Inambao, F. (2019). Sea water reverse osmosis desalination: energy and economic analysis. International Journal of Mechanical Engineering and Technology (IJMET), 10, 12, 716-731.
30. Sahu, P. (2021): A comprehensive review of saline effluent disposal and treatment: conventional practices, emerging technologies, and future potential. Water Reuse, 11/1, 33–65.
31. Salem, F., Thiemann, T. (2022): Produced water from oil and gas exploration—Problems, solutions and opportunities. Journal of Water Resource and Protection, 14, 142-185.
32. Shaddel, S., Tabatabae-Nejad S.A.R. (2014): Wettability response to low salinity water flooding with insight to oil/water relative permeability and oil recovery. The 8th International Chemical Engineering Congress & Exhibition (IChEC 2014) Kish, Iran, 24-27 February, 7 p.
33. Shi, K., Wan, H., Wang, K., Fang, F., Li, S., Wang, Y., Lei, L., Zhuang, L, Xu, Z. (2024): Self-sustaining Alkaline Seawater Electrolysis via Forward Osmosis Membranes. Green Energy & Environment, 369. In press.
34. Simoes, S.G., Catarino, J., Picado, A, Lopes, T.F., di Berardino, S., Amorim, F., Gírio, F., Rangel, C.M. de Leão, T.P. (2021): Water availability and water usage solutions for electrolysis in hydrogen production, Journal of Cleaner Production, 315, 128124.
35. Sun, B., Li, C., Yang, J., Bai, H., Meng, X. (2024): An interface-engineered Co 2 P/CoMoP 2 heterojunction with greatly improved electrocatalytic activity in water/seawater splitting. Inorganic Chemistry Frontiers, 11/7, 1978-1992.

36. Wang, Y, Wang, Y., Fu, W., Gao, G., Liu, Y., Wang, L. (2024): Self-templated synthesis of Ni3S2@NiCoN with core-shell structure for effective hydrogen evolution reaction. International Journal of Hydrogen Energy, 59, 1419-1426.
37. Wenzlick, M., Siefert, N. (2020): Techno-economic analysis of converting oil & gas produced water into valuable resources. Desalination, 481, 114381, 27 p.
38. Xiang Q., Nomura Y., Fukahori S., Mizuno T., Tanaka H., Fujiwara T. (2019): Innovative treatment of organic contaminants in reverse osmosis concentrate from water reuse: A mini review. Current Pollution Reports 5, 294–307.

Internet Sources

URL no. 1: https://www.alfalaval.com/industries/energy-andutilities/sustainablesolutions/sustainable-solutions/clean-energy/clean-hydrogen/water-purification-for-green-hydrogen/
URL no. 2: https://www.desware.net/Energy-Requirements-Desalination-Processes.aspx
URL no. 3: https://www.eurowater.com/en/hydrogen-production
URL no. 4: https://hydrogentechworld.com/water-treatment-for-green-hydrogen-what-you-need-to-know
URL no 5: https://jhuesa.com/en/water-needs-associated-with-hydrogen-production
URL no. 6: https://www.nagwa.com/en/explainers/206121679847/
URL no. 7: https://www.science.org/content/article/splitting-seawater-provide-endless-source-green-hydrogen
URL no. 8: https://www.weforum.org/agenda/2023/09/seawater-electrolysis-a-hydrogen-revolution-or-technological-dead-end-here-are-the-numbers/

SAŽETAK

Pristup kružnog gospodarstva kod proizvedene slojne vodi: mogućnosti i izazovi

Procesi eksploatacije nafte i plina generiraju i slojnu vodu čija se količina povećava s vremenom, pa postupanje s istom postaje sve veći problem. U skladu s konceptom kružnog gospodarstva, a s ciljem smanjenja potrošnja svježe vode, razmatraju se alternativne mogućnosti upotrebe slojne vode. Jednu od takvih mogućnosti predstavlja iskorištavanje slojne vode za proizvodnju zelenog vodika u elektrolizatorima. Za elektrolizu potrebna je voda visoke čistoće kojom se osigurava učinkovitost i dugovječnost sustava, zbog čega su potrebni procesi obrade. Izravna uporaba slojne vode povezana je s problemima, kao što su korozija i onečišćenje opreme. U radu su analizirane količine slojne vode proizvedene u sastavu ležišnog fluida, tijekom eksploatacije nafte i plina u istočnom dijelu Dravske depresije, a koje se trenutno utiskuju u ležišta radi deponiranja. Iako model koji uključuje snagu sustava za elektrolizu od 418 MW, a kojim bi se iskorištavala sva proizvedena slojna voda, predstavlja izazov, model kojim bi se iskorištavao dio slojne vode i koristio višak električne energije za pretvaranje iste u vodik, mogao bi biti održiva opcija.

Ključne riječi: slojna voda; Dravska depresija; eksploatacija ugljikovodika; vodik; elektroliza, kružna ekonomija.

Authors contribution

Karolina Novak Mavar: provided the methodology and elaboration of the initial design; provided final concept, discussion and conclusion; **Ivan Zelenika:** provided the calculations for the case study; reviewed and supervised the work; **Katarina Simon**: provided the brine treatment technologies and gave a brief description of the existing gathering system of the considered oil fields; reviewed and supervised the work.

5th Croatian geomathematical congress
UDC: 551.44, 552.5; category: original scientific paper

Magnetic Susceptibility in Slovačka Cave and Crnopac Cave System: KM-7 vs. Bartington MS2B

Ana Kamenski[1]; Uroš Barudžija [2]
[1] Croatian Geological Survey, Sachsova 2, 10 000 Zagreb, Croatia, ORCID: 0000-0002-1237-1007
[2] University of Zagreb, Faculty of Mining, Geology and Petroleum Engineering, Pierottijeva 6, 10 000 Zagreb, Croatia, ORCID: 0000-0002-1617-9362
Corresponding author: akamenski@hgi-cgs.hr

Abstract

This study focuses on two key locations: the deep Slovačka Cave and the extensive Crnopac Cave System (Kita Gaćešina entrance). Magnetic susceptibility in soft sediments was measured at all sites using the Kappameter KM-7 for in situ measurements and the Bartington MS2B System for laboratory analysis. Sampling locations were selected based on accessibility, and the results were subjected to statistical analysis. Significant discrepancies were observed between the measurements obtained from the two devices. The Bartington MS2B System exhibited greater precision, suggesting possible calibration or suitability issues with the Kappameter KM-7 for cave environments. For future magnetic susceptibility measurements, the Bartington MS2B is recommended, with portable devices used initially to assess relative variations in magnetism along the sedimentary profile.

Keywords: Croatian cave sediments; magnetic susceptibility; correlation coefficients, Normal distribution

1. Introduction

Cave sediments are excellent archives of geological, paleoenvironmental, and speleogenetic processes due to the stable climate conditions within caves (**Sasowsky, 2007; White, 2007**). These environments provide valuable insights into geological (**Stroj et al., 2024; Lacković et al., 2011**), physical (**Stroj and Paar, 2018**), and paleontological perspectives (**Kurečić et al., 2022**). The Dinaric Karst is notable for its well-developed profiles of allogenic cave sediments (**Zupan Hajna et al., 2020**), but the Croatian part remains underresearched, with most studies focusing on paleontological excavations (**Malez et al., 1980**). Recently, there has been a shift towards sedimentological and mineralogical research to establish a chronostratigraphic framework for depositional processes (**Kurečić et al., 2021**).

In the northwestern Dinaric Karst, magnetostratigraphy of cave deposits is well-developed (**Zupan Hajna et al., 2010**). However, research on magnetism and magnetic susceptibility in Croatian caves is significantly lacking. Magnetic susceptibility is a valuable metric for analyzing material magnetism, identifying magnetically rich minerals, and understanding rock formation or transport processes (**Dearing, 1994**). It is straightforward, non-destructive, and can be conducted on various rock types both in the laboratory and in the field. These measurements are quick, cost-effective, and support a wide range of studies, making them especially useful for remote areas lacking laboratory access (**da Silva et al., 2015**). Croatian allogenic cave sediments originate from diverse areas, resulting in varied mineral compositions and magnetic properties. Near the Kita Gaćešina entrance of the Crnopac Cave System in Velebit Mountain, occurrences of opaque minerals, pyroxene, chromite, and biotite have been documented (**Kurečić et al., 2021**). Additionally, the speleogenesis of this area is primarily linked to Mesozoic carbonate host rock (**Vlahović et al., 2005; Korbar, 2009**), suggesting the presence of calcium carbonate. The presence of both carbonate clasts and heavier minerals indicates that paramagnetic and diamagnetic materials are likely present in these caves. This study aimed to measure magnetic susceptibility in speleological sites on Velebit Mountain (**Figure 1 and Figure 2**).

Figure 1: Map of the research area, highlighted with black rectangle, with locations of investigated speleological sites – Slovačka Cave and Crnopac Cave System

Study focuses on determining the measurability of magnetic susceptibility subsurface and assessing changes in values across different depth profiles. It also aimed to establish whether significant correlation exhibits within measured values. A comparative analysis was conducted between in situ measurements and laboratory results to evaluate device compatibility. In situ measurements were performed using the Kappameter KM-7 from SatisGeo s.r.o., while laboratory measurements employed the Bartington MS2B System. Sampling targeted soft sediments, with locations selected based on accessibility.

Figure 2: Speleological maps of Kita Gaćešina-Draženova puhaljka, part of the Crnopac Cave System (left, adopted and modified from **Barišić, 2010**), highlighting the sampling area for profiles KG1 and KG2 within yellow rectangle, and Slovačka Cave (right, adopted and modified from **Bakšić 2016**), showing the enlarged area of the investigated SL1 profile within the blue rectangle

2. Methods

Magnetic susceptibility was initially measured with the Kappameter KM-7 on one profile in Slovačka Cave and two profiles in the Crnopac Cave System (**Figure 2**). Following this, the same samples underwent a second round of magnetic susceptibility measurements in the laboratory using the Bartington MS2B System. The results were analyzed using two types of correlation coefficients and tested for normal distribution. The research methods are outlined in the chronological order in which they were employed throughout this study.

2.1. Magnetic Susceptibility Measurement

The in situ magnetic susceptibility values were measured using the handheld Kappameter KM-7 device, manufactured by SatisGeo s.r.o. This device is widely utilized in mineral deposit research, borehole core analysis, and archaeology due to its high resolution, precision, and extensive measurement range. The Kappameter KM-7 features durable, non-erasable memory, individual and scanning measurement modes, a measuring needle, and Bluetooth-enabled GPS connectivity. Its specifications include a sensitivity of $1x10^{-6}$ SI units (or $1x10^{-5}$ SI units in scanning mode), a measurement range of +/- $999x10^{-3}$ SI units with automatic precision, and an operating frequency of 10 kHz. The device can store up to 999 readings without GPS data and has a power consumption of 8 mA (excluding Bluetooth and backlight). It is powered by two AAA batteries and operates in temperatures ranging from -20 °C to +60 °C, with dimensions of 165x68x28 mm and a weight of 250 g (including batteries), making it a versatile tool for field measurements. The Kappameter KM-7 offers three modes for measuring magnetic susceptibility: individual, scanning, and remote. For this field research, the individual measurement mode was used to capture readings. The measuring process involves three steps: first, positioning the device at least 30 cm away from the rock (AIR1); second, aligning the measuring needle parallel to the rock surface to obtain the SAMPLE value; and third, taking another measurement at least 30 cm away from the rock (AIR2). The SAMPLE value recorded between AIR1 and AIR2 is the measured magnetic susceptibility. One profile was measured in Slovačka Cave, and two profiles were assessed in the Crnopac Cave System. The locations and lengths of these profiles were selected based on the accessibility of the sampling sites within these speleological environments.

In the laboratory environment when measuring magnetic susceptibility, the Bartington sensor generates a subtle magnetic field through alternating electric current and detects the material's magnetization. The resulting magnetic susceptibility value is displayed on the digital screen. Bartington sensors measure magnetic susceptibility relative to air, which serves as a calibration standard for the device. In this study, the MS2B sensor was employed for laboratory research, providing magnetic susceptibility values in SI units. Samples were prepared following specific protocols: plastic utensils and bags were used to avoid metallic contamination, samples were dried for three days, crushed, and then placed into 10 cm^3 plastic vials. The MS2B sensor, a portable laboratory device, conducts measurements at two different frequencies, essential for detecting superparamagnetic minerals, crucial in soil and rock analysis.

The procedure with the MS2B sensor is more intricate than with the KM-7 device. It is configured to display magnetic susceptibility in dimensionless SI units (10^{-5}). Before measuring samples, a calibration plastic vial provided by the manufacturer is used to verify the device's calibration. Samples are first measured at a low frequency (LF) of 0.46 kHz with a 0.1 range multiplier, with air and sample measurements taken sequentially. Ideally, there is no difference between the first and third readings; otherwise, measurements are repeated. The device calculates volume susceptibility, denoted by κ, indicating the ratio of sample magnetization to the magnetic field (80 Am^{-1}) in the SI system. Values of κ on the MS2B device are typically in the order of 10^{-5}. After low-frequency measurements, samples are measured at a high frequency (HF) of 4.65 kHz. Plastic vials are consistently oriented to minimize measurement errors (**Dearing, 1994**).

After measurement, key parameters are calculated. Specific mass susceptibility χ is obtained by dividing the κ value by the total sample density ρ. Density is calculated by dividing mass by volume, and specific mass susceptibility (χ) has units in m^3/kg. Alternatively, the specific mass susceptibility of dual frequency, χ_fd, can be obtained from the **Equation 1** (**Dearing, 1994**):

$$\chi_{fd} = \frac{(\kappa_{lf} - \kappa_{hf})}{\rho} \quad (1)$$

Where are:
χ_{fd} – specific mass susceptibility of dual frequency (m^3/kg),
κ_{lf} – volume susceptibility at low frequency,
κ_{hf} - volume susceptibility at high frequency,
ρ - density (kg/m^3).

The difference in magnetic susceptibility of dual frequency is expressed as a percentage calculated using the **Equation 2** (**Dearing, 1994**):

$$\chi_{fd} = \kappa_{lf} - \frac{(\kappa_{hf})}{\kappa_{lf}} x100 \quad (2)$$

Where are:
χ_{fd} – specific mass susceptibility of dual frequency (m^3/kg),
κ_{lf} – volume susceptibility at low frequency,
κ_{hf} - volume susceptibility at high frequency.

These parameters are computed using Bartington Multisus software, providing comprehensive data analysis and storage capabilities. The MS2B sensor is widely used across various fields. In geology and soil analysis, it is crucial for individual sample assessments. In archaeology, it aids in locating former settlements, stratigraphic analysis, and identifying magnetic materials. It supports environmental pollution research by analyzing rock, soil, and vegetation samples. Additionally, it

is used in construction material testing, facilitating geological origin determination and material permeability assessment (**Dearing, 1997**).

2.2. Statistical Analysis

The measured values of magnetic susceptibility were evaluated through cross-correlation of the values. Two correlation coefficients were calculated: Pearson's and Spearman's. The correlation coefficient, ranging from -1 to +1, indicates both the strength and direction of the linear relationship between two variables. A coefficient closer to +1 or -1 signifies a strong positive or negative correlation, respectively, where increasing values in one array correspond to increasing or decreasing values in the other. Conversely, a coefficient closer to 0 suggests a weak or no correlation between the arrays. Widely utilized in science and finance, this statistical measure assists in assessing associations between variables. The Pearson correlation coefficient, a commonly employed, precisely quantifies the strength and direction of a linear relationship. Spearman correlation, a nonparametric alternative to Pearson's, evaluates association based on ranked values rather than raw data. Unlike Pearson, which focuses on linear changes, Spearman assesses monotonic relationships where variables change together but not necessarily at a constant rate. It is preferred in scenarios involving non-linear relationships, non-normal distributions, ordinal variables, or significant outliers.

The correlation coefficient is a statistical metric that gauges the strength of the relationship between the relative movements of two variables. It quantifies how closely the predicted trend aligns with the actual trend. In this study, the variables under consideration are magnetic susceptibility values. Both correlation coefficients were calculated for all three frequencies used (10 kHz, 0.46 kHz, 4.64 kHz) and for all three analysed profiles (SL1, KG1, KG2).

To examine the measured values using the F and T tests, the values were first tested for normal distribution using the Shapiro-Wilk normality test. For cases where a normal distribution was established, F and T tests were conducted.

3. Results and discussion

In Slovačka Cave, magnetic susceptibility *in situ* was measured using the Kappameter KM-7 device along the profiles near the speleologist's rest stop ("bivak" in Croatian), located 360 meters from the cave entrance (**Figure 2**). The profile was recorded vertically, from top to bottom. Profile SL1 was selected due to its intriguing morphology, extensive vertical spread, and the feasibility of safely anchoring a researcher above it, making sampling both safe and practical.

Magnetic susceptibility values were obtained at 27 locations along the 2.85-meter length of the profile and are shown in **Figure 3** (green line). Samples from these points were later analyzed in the laboratory using the Bartington device. From 0 to 0.45 meters, 10 locations were measured and sampled at 0.05-meter intervals, with magnetic susceptibility ranging from 65.00 x 10^{-5} SI to 120.00 x 10^{-5} SI. Between 0.45 meters and 1.45 meters, another 10 measurement points were determined, showing a range of 7.00 to 88.00 x 10^{-5} SI. From 1.45 meters to the end of the profile, seven measurement points were placed at 20-centimeter intervals, with values ranging from -45.00 x 10^{-5} SI to 21.00 x 10^{-5} SI, resulting in a range of up to 66 x 10^{-5} SI. Notably, measurement points SL1-21, SL1-23, and SL1-26 recorded negative values (see **Figure 3**).

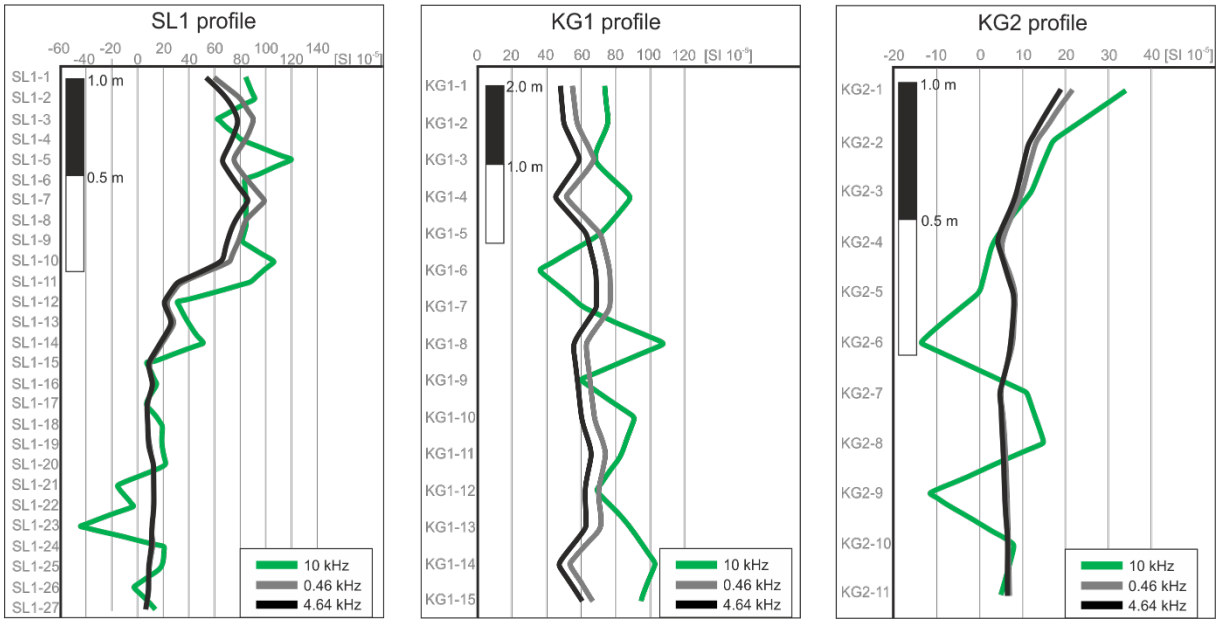

Figure 3: Magnetic Susceptibility values recorded on the investigated profiles. Green lines represent values obtained with the portable Kappameter KM-7 device (10 kHz frequency), and grey and black lines represent values acquired in the laboratory environment with the Bartington MS2B device at two frequencies respectively (0.46 and 4.64 kHz).

In the Crnopac Cave System (Kita Gaćešina entrance), *in situ* magnetic susceptibility measurements were conducted on two profiles, recorded from top to bottom. Both profiles are situated on the first level of the Crnopac Cave System, relative to the Kita Gaćešina entrance (**Figure 2**).

Profile KG1, which is seven meters long, is located at the end of the "Perzijska ljubav" channel (**Figure 2**). Measurement points on the KG1 profile are spaced half a meter apart. The magnetic susceptibility values range between 36.00 x 10^{-5} SI and 95.00 x 10^{-5} SI (**Figure 3**). The lowest value, 36.00 x 10^{-5} SI, is at measurement point KG1-6, located at 2.50 meters on the profile. The highest value, 95.00 x 10^{-5} SI, is at the last measurement point, KG1-15, which is also the lowest in the spatial profile. Profile KG2 is located directly adjacent to the "Ašov" resting point (**Figure 2**). This profile is two meters long, with measurement points spaced 20 centimeters apart. The highest magnetic susceptibility recorded is 34.00 x 10^{-5} SI, and the lowest is -14.00 x 10^{-5} SI (**Figure 3**). Measurement points KG2-6 and KG2-9 exhibit negative values.

In the laboratory, magnetic susceptibility measurements were performed using the Bartington MS2B System on the same samples previously measured in the cave systems with the KM-7 device at a frequency of 10 kHz. After recording magnetic susceptibility values at all measurement points on profiles SL1, KG1, and KG2 with the KM-7, soft sediment samples were collected. These samples were then analyzed for magnetic susceptibility at two frequencies: lower (0.465 kHz) and higher (4.65 kHz).

For profile SL1 from Slovačka Cave, no negative magnetic susceptibility values were observed (**Figure 3**, grey and black lines). At the lower frequency, values ranged from 6.60 to 99.40 x 10^{-5} SI. The lowest value was recorded in sample SL1-27, the lowest point on the profile, while the highest value corresponded to sample SL1-7. At the higher frequency, values ranged from 6.50 x 10^{-5} SI in sample SL1-27 to 86.40 x 10^{-5} SI in sample SL1-7.

In the Crnopac Cave System, magnetic susceptibility values for profile KG1 at a frequency of 0.465 kHz ranged from 51.00 to 77.20 x 10^{-5} SI. The lowest value was recorded in sample KG1-4, while the highest values were found in samples KG1-6 and KG1-7. At the higher frequency, values varied from 44.80 x 10^{-5} SI to 69.30 x 10^{-5} SI, with the lowest susceptibility in sample KG1-4 and the highest in sample KG1-7. For profile KG2, magnetic susceptibility values at the lower frequency ranged from 4.50 to 21.40 x 10^{-5} SI, and at the higher frequency from 4.00 to 19.00 x

10^{-5} SI. The lowest value at both frequencies was recorded in sample KG2-4, while the highest value was in sample KG2-1 (**Figure 3**).

Correlation coefficients were calculated for the obtained results, as detailed in **Table 1**. Subsequently, Shapiro-Wilk normality tests were conducted on the measured values depicted in **Figure 3**. The results indicated significant correlation coefficients (coefficients values in bold in **Table 1**), as well as enabled the application of t-tests and f-tests.

Table 1: Pearson and Spearman correlation coefficients for three analysed profiles

Profile	Correlation type	10 kHz/0.46 kHz	10 kHz / 4.64 kHz	0.46 kHz/4.64 kHz
SL1	Pearson	0.841517	0.846089	0.999713
	Spearman	**0.762668**	**0.765873**	**0.996947**
KG1	Pearson	**-0.495143**	**-0.482872**	**0.997293**
	Spearman	-0.503571	-0.456250	0.984821
KG2	Pearson	0.672635	0.652831	0.998824
	Spearman	**0.379545**	**0.381818**	**0.997727**

Values in bold represent significant correlations for the respective comparison. The results of magnetic susceptibility were also assessed for normal distribution. The corresponding P-values are displayed in **Table 2**.

Table 2: present the p-values from the normality tests. Values in italic indicate non-normal distributions

Profile	Frequency	P-value
SL1	10 kHz	0.1363
	0.46 kHz	*0.00006731*
	4.64 kHz	*0.000072*
KG1	10 kHz	0.8641
	0.46 kHz	0.3188
	4.64 kHz	0.2845
KG2	10 kHz	0.7872
	0.46 kHz	*0.006219*
	4.64 kHz	*0.0109*

Given that only the magnetic susceptibility values measured at the KG1 profile passed the normality test for all three frequencies, t-test and f-test were conducted specifically for this profile. Detailed results are presented in **Table 3**.

Table 3: displays the results of t-test and f-test on magnetic susceptibility values obtained from the KG2 profile

Profile	Tests	10 kHz/0.46 kHz	10 kHz / 4.64 kHz	0.46 kHz/4.64 kHz
KG1	t	0.017369	0.000683	0.008258
	f	0.005584	0.002586	0.780149

The investigation of magnetic properties in Croatian cave systems is significantly underrepresented in research, despite the excellent preservation of cave sediments. Given the presence of heavier mineral compositions in allogenic cave sediments within the Dinaric Karst (**Kurečić et al., 2021**), this study aimed to assess the feasibility of measuring magnetism in cave environments and to compare a portable measuring device with a commonly used laboratory instrument.

Magnetic susceptibility values measured in Slovačka Cave and the Crnopac Cave System using the Kappameter KM-7 (KM-7) device showed significant differences compared to laboratory measurements with the Bartington MS2B device (see **Figure 3**). This disparity is supported by statistical analyses (see **Tables 1-3**). Across all profiles investigated, KM-7 device readings were notably lower than laboratory measurements at both low and high frequencies. The correlation coefficient between values obtained at different frequencies in the laboratory was significantly higher (see **Figure 3**). KM-7 measurements consistently passed normality tests, suggesting suitability for such measurements, albeit with occasional anomalies attributable to the device's small sampling area on irregular outcrop surfaces compared to the lab's larger sample volume of 10 cm^3. Furthermore, negative readings recorded by the KM-7 device on the SL1 and KG 2 profiles (Figure 3 and Table 2) highlight the challenges posed by subsurface karst environments for studies such the one described in this paper. Readings that did not pass the normality test should be examined for non-normal distributions in further research.

Temperature fluctuations at the measurement needle's contact point and lateral mineral variations within the outcrop, spanning just a few millimeters, could influence measurement accuracy with the KM-7 device. Additionally, sparse measurement points may negatively impact precision. These factors collectively affect magnetic susceptibility recordings in speleological settings. Notably, the repeatability of results and measurement point density are crucial considerations influencing measurement accuracy and the interpretation of profile data.

4. Conclusions

Initial measurements of magnetic susceptibility were conducted using the Kappameter KM-7 on one profile within Slovačka Cave and two profiles in the Crnopac Cave System (Figure 2). Subsequently, these samples underwent additional magnetic susceptibility measurements in the laboratory using the Bartington MS2B System. The results were then subjected to analysis using two types of correlation coefficients and tested for normal distribution.

Magnetic susceptibility measurements in Croatian cave sediments have revealed significant variations along specific profiles. In Slovačka Cave on northern Velebit Mountain, and in the Crnopac Cave System (specifically at Kita Gaćešina entrance), magnetic susceptibility measurements identified changes presumably linked to variations in sediment mineral composition.

Considering higher correlation coefficient values, the Bartington MS2B device provided precise and reliable results suitable for detailed interpretation. In contrast, measurements using the Kappameter KM-7 device yielded preliminary field results that partially aligned with MS2B measurements. However, the accuracy of KM-7 results depended heavily on the measurement protocol and the design of measurement points along the profiles.

5. References

1. Bakšić, D., Petričević, J., Rakovac, M. (2016): Slovačka jama: Mali Kuk, Sjeverni Velebit. Speleološki nacrt. Zagreb: Speleološki odsjek Velebit.
2. Barišić, T., Branica, B. (2010): Jamski sustav Kita Gaćešina – Draženova puhaljka: Crnopac, južni Velebit. Speleološki nacrt. Zagreb: Speleološki odsjek Velebit.
3. Dearing, J. A. (1994): Environmental Magnetic Susceptibility: Using the Bartington MS2 System. Chi Pub.
4. Lacković, D., Glumac, B., Asmerom, Y. and Stroj, A. (2011): Evolution of the Veternica Cave (Medvednica Mountain, Croatia) drainage system: insights from the distribution and dating of cave deposits. Geologia Croatica. 64/3, 213-221. DOI: 104154/gc.2011.18
5. Korbar, T. (2009): Orogenic evolution of the External Dinarides in the NE Adriatic region: a model constrained by tectonostratig-raphy of Upper Cretaceous to Paleogene carbonates. Earth-Science Reviews. 96, 4:296-312. DOI: 10.1016/j.earscirev.2009.07.004

6. Kurečić, T., Hajek Tadesse, V., Wacha, L., Horvat, M., Trinajstić, N. and Mišur, I. (2022): Sub-recent microfauna within allogenic sediments at the bottom of a deep cave, Njemica (Biokovo Mt., Croatia). International Journal of Speleology. 51(3), 223-233. https://doi.org/10.5038/1827-806X.51.3.2428
7. Kurečić, T., Bočić, N., Wacha, L., Bakrač, K., Grizelj, A., Tresić Pavičić, D., Lüthgens, C., Sironić, A., Radović, S., Redovniković, L. and Fiebig, M. (2021): Changes in Cave Sedimentation Mechanisms During the Late Quaternary: An Example From the Lower Cerovačka Cave, Croatia. Frontiers in Earth Science. 9, 672229. DOI: 10.3389/feart.2021.672229
8. Malez, M., Smith F.H., Radovčić, J. and Rukavina, D. (1980): Upper Pleistocene Hominids from Vindija, Croatia, Yugoslavia. Current Anthropology. 21 (3). DOI: 10.1086/202463
9. Sasowsky, I.D. (2007): Clastic Sediments in Caves – Imperfect Recorders of Processes in Karst. Acta Carsologica. 36(1), 143-149. https://doi.org/10.3986/ac.v36i1.216
10. da Silva, A. C., Whalen, M. T., Hladil., J., Chadimova, L., Chen, D., Spassov., S., Boulvain, F. and Devleeschouwer, X. (2015): Magnetic Susceptibility Application: A window onto Ancient Environments and Climatic Variations. Geological Society London, Special Publications. 414, 1-13. https://doi.org/10.1144/SP414.12
11. Stroj, A., Lacković, D., Sasowsky, I. D., Bajo, P. and Glumac, B. (2024): The application of cave morphological and sedimentary deposit investigations to unravel tectonic history and landscape evolution: Insights from Veternica Cave, Medvednica Mountain, Croatia. Geomorphology. 446. https://doi.org/10.1016/j.geomorph.2023.109000
12. Stroj, A. and Paar, D. (2018): Water and air dynamics within a deep vadose zone of a karst massif: Observations from the Lukina jama – Trojama cave system (1.431 m) in Dinaric karst (Croatia). Hydrological Processes. 1-11. DOI: 10.1002/hyp.13342
13. Vlahović, I., Tišljar, J., Velić, I. and Matičec, D. (2005): Evolution of the Adriatic Carbonate Platform: Paleogeography, main events and depositional dynamics. Palaeogeography, Palaeoclimatology, Palaeoecology. 220, 3-4, 333–360.
14. White, W. B. (2007): Cave sediments and paleoclimate. Journal of Cave and Karst Studies. 69(1), 76-93.
15. Zupan Hajna, N., Bosák, P., Pruner, P., Mihevc, A., Hercman, H. and Horáček, I. (2020): Karst sediments in Slovenia: Plio-Quaternary multi-proxy records. Quaternary International. 546, 4-19. https://doi.org/10.1016/j.quaint.2019.11.010
16. Zupan Hajna, N., Mihevc, A., Pruner, P. and Bosák, P. (2010): Paleomagnetic research on karst sediments in Slovenia. International Jour-nal of Speleology. 39 (2), 47-60. DOI: 10.5038/1827-806X.39.2.1

SAŽETAK

Magnetski susceptibilitet u Slovačkoj jami i Jamskom sustavu Crnopac: KM-7 nasuprot Bartington MS2B

Istraživanje magnetizma u hrvatskim speleološkim sustavima znatno je nedovoljno istraženo, unatoč izvrsnoj očuvanosti sedimenata špilja. Ova studija fokusira se na dva lokaliteta: Slovačku Jamu i Jamski Sustav Crnopac (ulaz Kita Gaćešina). Magnetna susceptibilnost u mekim sedimentima mjerena je na svim lokacijama korištenjem uređaja Kappameter KM-7 za terenska mjerenja i Bartington MS2B sustava za potrebe laboratorijske analiza. Lokacije uzorkovanja odabrane su prema dostupnosti, a rezultati su podvrgnuti statističkoj analizi. Uočene su značajne razlike između mjerenja dobivenih s oba uređaja. Bartington MS2B sustav pokazao je veću preciznost, sugerirajući moguće probleme s kalibracijom ili prikladnošću KM-7 Kappametera za špiljski okoliš. Za buduća mjerenja magnetske susceptibilnosti preporučuje se Bartington MS2B, s početnom uporabom prijenosnih uređaja za procjenu relativnih varijacija magnetizma duž sedimentnog profila na terenu.

Ključne riječi: hrvatski špiljski sedimenti; magnetski susceptibilitet; korelacijski koeficijenti; normalna distribucija

Author's contribution

Ana Kamenski (1) performed the field work, laboratory and statistical analyses, interpretation and presentation of the results, wrote the first draft of manuscript. **Uroš Barudžija (2)** supervised analytics and reviewed the manuscript.

5th Croatian geomathematical congress
UDC: 551.3, 552.5; category: original scientific paper / invited lecture

Granulometry and morphometry of river sediments – sand and gravel studies in the Sava River (Zagreb, Croatia)

Uroš Barudžija[1]**; Matteo Blatančić** [1]
[1] University of Zagreb, Faculty of Mining, Geology and Petroleum Engineering, Pierottijeva 6, HR10000 Zagreb, Croatia, https://orcid.org./0000-0002-1617-9362
Corresponding author: uros.barudzija@rgn.unizg.hr

Abstract

Morphometry of pebbles from the Sava River gravel sampled in the Zagreb City area revealed shape distributions along the observed waterway. Predominant carbonate pebbles have disc and sphere shapes implying mainly distant sources. Distributions of pebble shapes in sandstones and other minor lithologies indicate local and distant sources. Granulometry of the Sava River sand sampled in the same area and obtained by dry sieving and laser granulometry showed a predominately fine and medium sand deposition. Medium sand increased downstream, probably due to artificially channelized riverbed in the urban area. Fine sand prevails further downstream in a more meandering river area.

Keywords: river sediments; granulometry; morphometry, Sava River, Zagreb

1. Introduction

Morphometric analysis of the gravels often aims to describe weathering, transporting and depositional processes (**Müller, 1967; Tucker, 1988**). Holocene alluvial sediments deposited in the Sava River alluvial terraces near the City of Zagreb (Croatia), are especially suitable for this purpose. These sediments were used for a case study that analyses morphometric characteristics of gravel pebbles, aiming to describe transport and depositional mechanisms. Contribution of eroded material from the local sources, brought from the nearby hills and Medvednica Mountain, was compared to the contribution of material from the upstream sources. The research was performed at selected sites along the Sava River watercourse.

Granulometric analysis of the sand bodies deposited at riverbanks of the Sava River was also undertaken. Sava River flows partly through the Zagreb city area, and its natural grain size distribution consequently has been changed. Zagreb City arose between Medvednica Mt. and the Sava River, channelized and embanked after the 1964. flood. Natural grain size distribution in sand bodies is now restricted to several sites at the riverbanks. Further downstream Sava River re-establishes its natural meanders.

The Sava River follow transition in the underlying geomorphology and riverbed changes accordingly. In the high-relief area upstream, riverbed is shallower and mainly gravels are deposited. West of Zagreb as well as downstream towards the east, river morphology transitions to a predominantly meandering form. Recently, watercourse in the urban city area has been highly regulated and embanked after the major flooding of the City of Zagreb in 1964. Deposits of the meandering Sava River system are nowadays mainly exploited in gravel pits. For the Middle Pleistocene gravels in the area west of Zagreb it was determined that predominant sandstone pebbles originated from a nearby source area (Medvednica Mt. and surrounding hills), and for the overlying Holocene gravels predominantly carbonate lithology of the Alpine provenance is determined **(Barudžija et al., 2020)**.

2. Methods

Several field and laboratory procedures were performed to obtain morphometric characteristics of the gravel pebbles. Representative sites for sampling gravel were chosen at nearby gravel pits, Sava riverbanks and riverbed gravel bars (red dots in **Figure 1**).

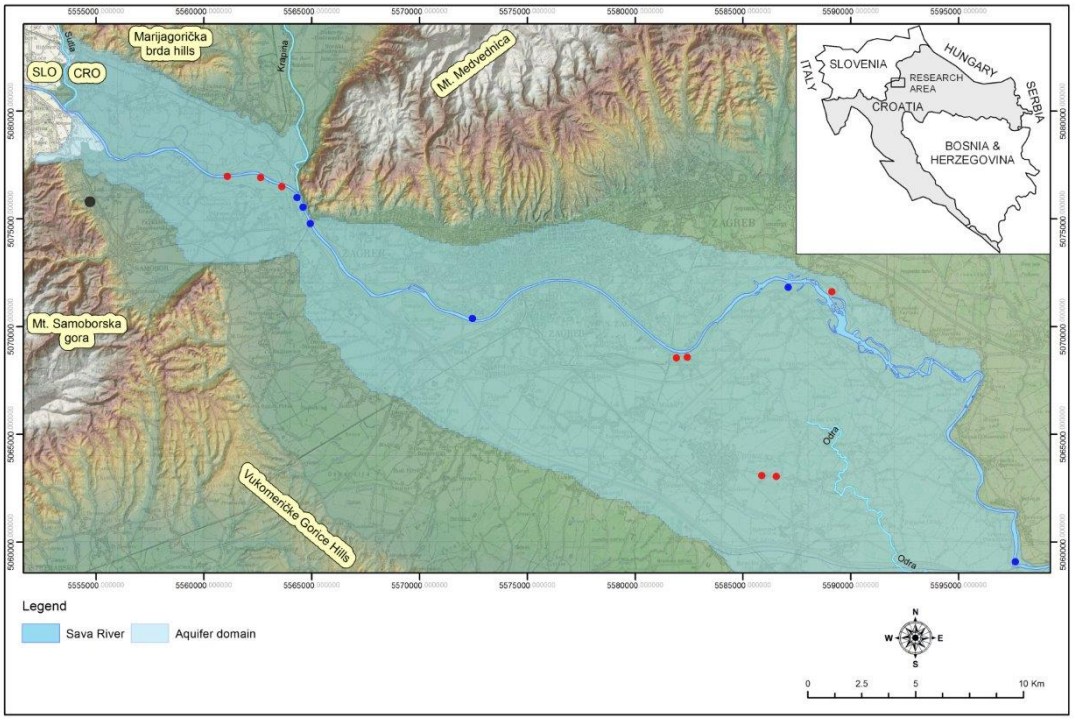

Figure 1: Sampling sites: gravel pebbles for morphometry (red dots); and sand samples for granulometry (blue dots)

Statistically representative sets of 300 pebbles of various sizes were taken from the >6 mm separated fractions of each sample. Pebbles were also determined by their lithology as lithotypes. Direct measurements of three perpendicular geometrical axes on the pebbles were made with Vernier calliper on all selected pebbles, according to well-established procedure **(Zingg, 1935; Krumbein, 1941; Muller, 1967**). According to their b/a and c/b ratios, basic grain shape names were attributed: disc, sphere, blade or rod (**Table 1**). Measurements and notations are reliable with less than 1% of outliers, which are excluded as measurement errors. The original method (**Zingg, 1935**) upgraded by (**Muller, 1967**) to characterize and classify pebble shapes has been applied. Flatness ratios, defined by **Equation 1**:

$$F = (a + b) / 2c \quad (1)$$

Where are:

a - the longest diameter/length,
b - the middle diameter/width,
c- the shortest diameter/height.

were further calculated for each selected pebble. They usually vary for gravel pebbles between 1.2 and 5.

Table 1: Basic types of pebble shapes (**Zingg, 1935**)

	b/a	**c/b**	**Shape**
I.	>2/3	<2/3	disc
II.	>2/3	>2/3	sphere
III.	<2/3	<2/3	blade
IV.	<2/3	>2/3	rod

Riverbed sand sampling sites for granulometric analysis (blue dots in **Figure 1**) were chosen at riverbanks, in sandy point bar sedimentary bodies. The following analytical procedures were performed on the collected samples: granulometric analysis by dry sieving and granulometric analysis by laser granulometry in the Laboratory for Geological Materials (LaGeMa) at the RGN Faculty, University of Zagreb, according to procedures from **Müller, 1967** and **Tucker, 1988**. Samples were air-dried, quartered to cca 100 g, and sieved manually through the set of sieves. Each fraction is weighed, with the accuracy of > 99%. Laser granulometric analysis is performed with a Malvern Panalytical Mastersizer 3000 device, operating on the laser diffraction principle (**URL 1**).

Standard granulometric parameters were read off directly from a cumulative granulometric curve, or calculated from standard equations (**Müller, 1967** and **Tucker, 1988**):

(1) Median (Md), grain size value on a cumulative granulometric curve at the 50th percentile (at 50%).

(2) Mean (M), average grain size value, calculated from grain size values at the 16th (Φ16), 50th (Φ50) and 84th (Φ84) percentile (**Equation 2**):

$$M = \frac{\Phi_{16}+\Phi_{50}+\Phi_{84}}{3} \quad (2)$$

Where are:

Φn – grain size at the nth percentile,
M – mean grain size.

(3) Mode is the value in the middle of the most represented class (class with the largest number of grains).

(4) Sorting (So) is the measure of standard deviation - width of the grain size distribution (**Equation 3**). It shows efficiency of the transporting media (river water) to separate various grain sizes.

$$So = \frac{\Phi_{84}-\Phi_{16}}{4} + \frac{\Phi_{95}-\Phi_{5}}{6.6} \quad (3)$$

Where are:

So –sorting coefficient,
Φn – grain size at the nth percentile.

(5) The asymmetry coefficient – Skewness (Sk) shows prevailing fractions in the sample (larger or smaller grains than the median value). It changes the cumulative granulometric curve toward the larger grains (Sk < 1) or toward the smaller grains (Sk > 1). It is calculated from **Equation 4**.

$$Sk = \frac{\Phi_{16}+\Phi_{84}-2\Phi_{50}}{2(\Phi_{84}-\Phi_{16})} + \frac{\Phi_{5}+\Phi_{95}-2\Phi_{50}}{2(\Phi_{95}-\Phi_{5})} \quad (4)$$

Where are:

Sk – coefficient of asymmetry,
Φn – grain size at the nth percentile.

3. Results

Pebble shapes (disc, sphere, blade or rod) were quantitatively defined for all main lithotypes in each sample by comparing their measured axes (according to **Table 1**). The results are presented in the Zingg diagrams with the Wadell sphericity values curves and in histograms (see **Figures 2** and **3**), from the west downstream to the east. Measured diameters and calculated flatness ratios, depend also on different lithologies and hydrodynamic conditions during the transport of the pebbles, and these attributions are further critically evaluated.

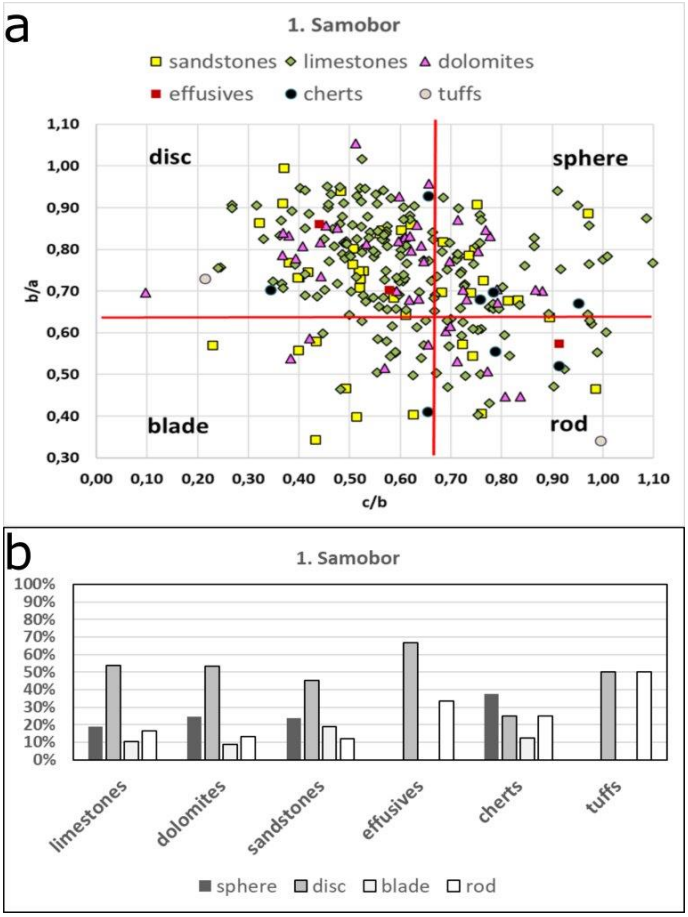

Figure 2: Pebble shapes of main lithotypes plotted in Zingg diagram with the overlapping curves for the same Wadell sphericity values (a) and presented in histograms (b). The far west sampling site (red dot) in **Figure 1**. Adapted after **Barudžija et al., 2020**.

In the far west location predominant limestone and dolomite pebbles have mainly disc to mildly sphere shapes (see **Figure 2**). Subordinate lithotypes show more scattered distributions of pebble shapes, with sandstones being the most diverse.

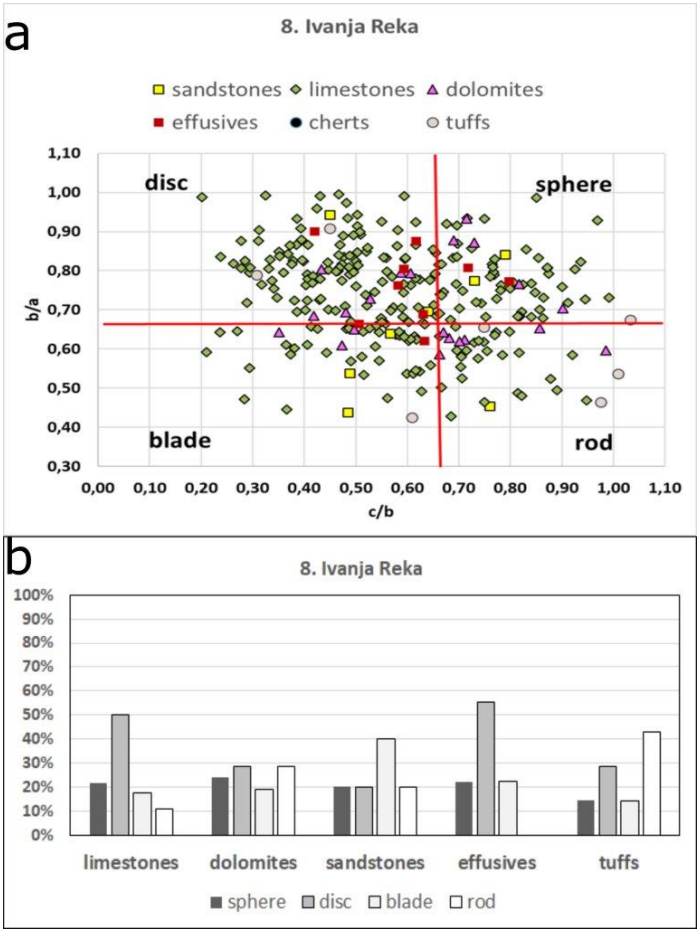

Figure 3: Pebble shapes of main lithotypes plotted in Zingg diagram with the overlapping curves for the same Wadell sphericity values (a) and presented in histograms (b). The far east sampling site (red dot) in **Figure 1**. Adapted after **Barudžija et al., 2020**.

In the far east site, all major lithotypes are significantly present (see **Figure 3**). Limestones slightly increase, having mainly disc to sphere pebble shapes. Sandstone pebbles with mainly blade shapes prevail.

The results of granulometric analysis are presented downstream the Sava River by a histograms of grain size distribution, cumulative frequency curves of grain size and a cumulative granulometric curves (see examples in **Figures 4** and **5**).

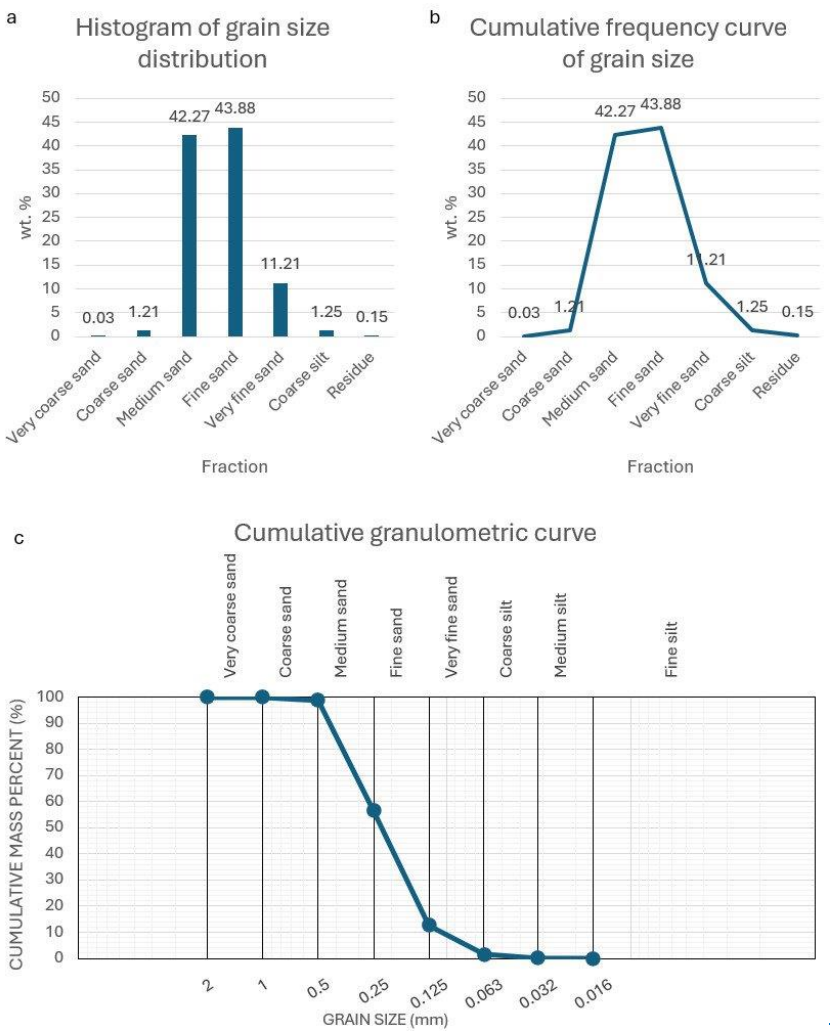

Figure 4: Histograms of grain size distribution, cumulative frequency curve of grain size and a cumulative granulometric curve. The far west sampling site (blue dot in **Figure 1**).

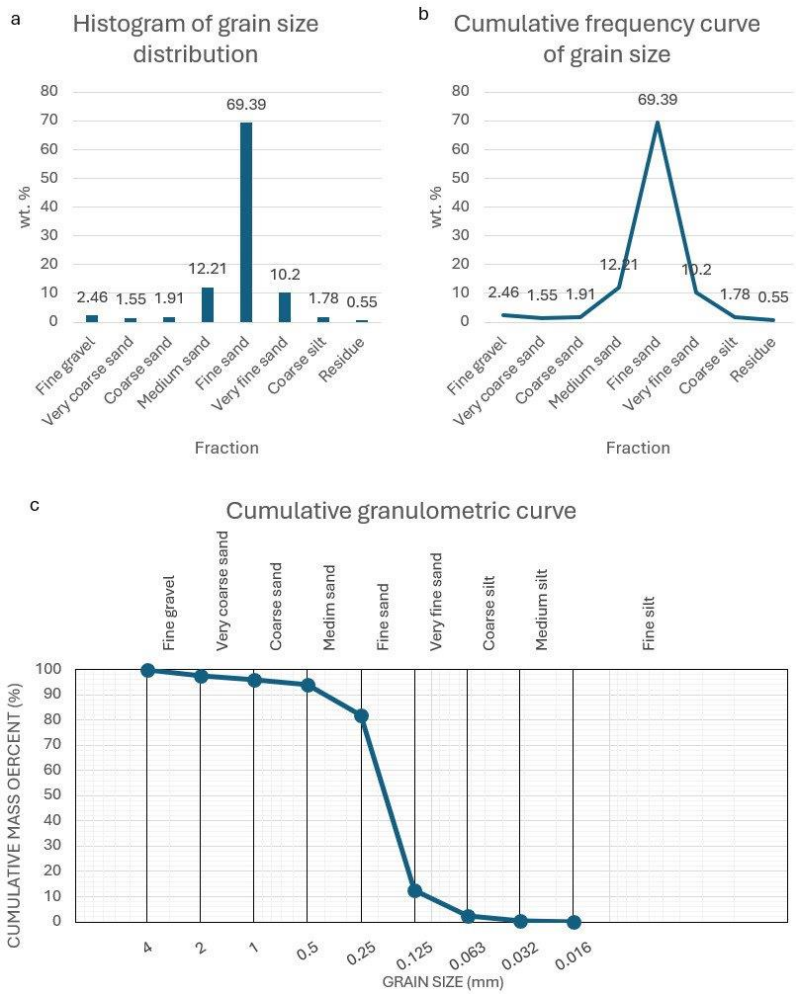

Figure 5: Histograms of grain size distribution, cumulative frequency curve of grain size and a cumulative granulometric curve. The far east sampling site (blue dot in **Figure 1**).

Grain size distribution in all samples is presented on a jointed graph showing cumulative granulometric curves (see **Figure 6**). Shapes of the curves, steepened at fine and medium sand sections, indicate grain size distribution with prevailing medium sand fraction at western sites, as well as the predominance of fine sand at the far east site.

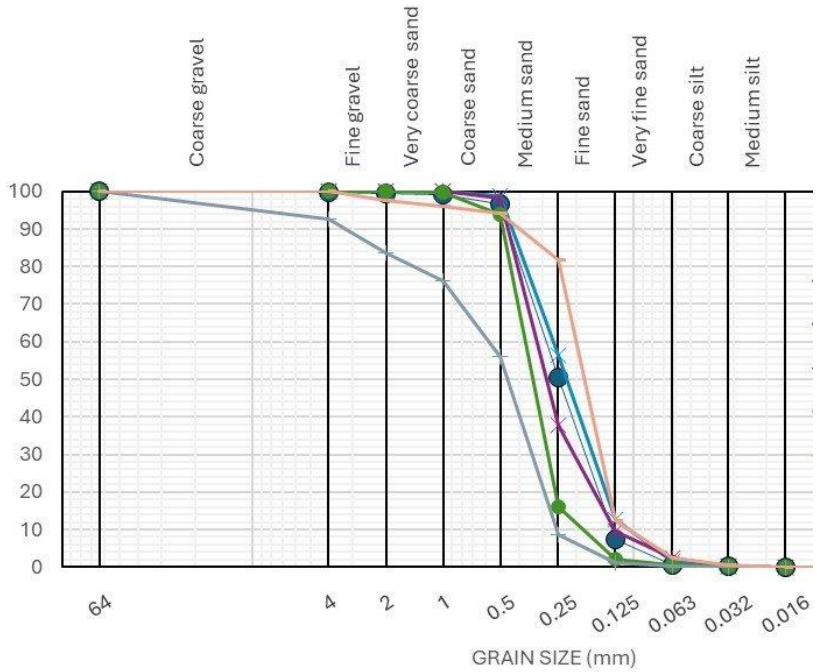

Figure 6: Cumulative granulometric curves for all sampling sites (blue dots in **Figure 1**)

4. Discussion

In the west, significant narrowing of Sava River watercourse is visible: between Medvednica and Samoborska gora, it enters the Zagreb alluvial plain and flows further eastwards as a reduced flow meandering river. This change reflects the distribution of gravel pebbles and its morphometric characteristics, which are mainly related to their lithology. Carbonate pebbles predominantly accumulate at western sites. Incision and deep erosion of the riverbed strongly influenced distribution of other lithotypes downstream.

Pebble shapes in alluvial sediments are primarily influenced by lithology and fabric, and then by hydrodynamic conditions during transport (**Collinson, 1986**). Approaching to ideal sphere pebble shape correlates also well with the increasing hydrodynamic conditions or with relatively long transport. Predominant limestone pebbles at all sites, are of intermediate to moderately high sphericity and have mainly disc to sphere shapes, implying relatively long transport.

Disc and sphere pebble shapes distributions correlate well with main lithologies -limestones and dolomites. Contribution of limestone and dolomite pebbles with predominantly disc and sphere shapes implies similar sources (predominantly distant, with possible local influence) as well as similar transport conditions.

Sandy gravel lake deposits are often recorded in the underlying Middle Pleistocene deposits **(Velić and Durn, 1993; Velić et al, 1999)**, and predominance of the pebbles from such environments indicate redeposition further downstream during the Holocene. However, the potential for reworking of gravel fraction from these older deposits is limited to those parts of the watercourse in which water energy suddenly increase, such as in channelized and embanked parts of the river, like in the urban Zagreb City area.

Predominant carbonate pebbles in the Sava River and their morphometric characteristics can be easily compared with the physical and mechanical properties of local carbonates from the Samoborska gora and Medvednica, described by **(Pavičić et al., 2017; Maričić et al., 2018)**, as well with some world examples, i.e. with one described by **Oluwajana et al., 2021**.

Granulometric research focused on the grain size distribution of Sava River sand in the urban area of the City of Zagreb, as well as downstream. Grain size distribution shows that upstream of the Sava River cumulative medium sand/fine sand fractions are predominant at the western sampling sites, and very fine sand fraction is subordinately present. Hydrodynamic properties of the Sava riverbed in this area allows the deposition of medium and fine sand particles. Further

downstream, away from the channelized and embanked riverbed in the urban city area, fine sand fraction increase, due to low hydrodynamic conditions in the low relief area. Granulometric research can be as well compared some world examples, i.e. with one described by **Etobro et al., 2024**.

Prevailing carbonate sands in the western and more siliciclastic content downstream in the eastern part of the investigated area, showed a similar pattern as the distribution of gravel pebbles in the study **(Barudžija et al., 2020)**.

5. Conclusions

- Predominantly disc and sphere shapes of limestone and dolomite pebbles imply similar sources (mainly distant and some local), as well as similar transport conditions.
- Scattered distributions of sandstones pebble shapes indicate possible multiple sources, some of them highly probable as local, from the SW Medvednica and Samoborska gora in the west, and from the SE Medvednica in the east.
- Scattered distributions of pebble shapes for minor lithotypes show no significantly recognized provenance.
- Grain size distribution of the Sava River sands near the city of Zagreb show predominately medium and fine sand deposition with prevailing medium sand downstream, due to a more artificially channelized riverbed.
- Further downstream fine sand deposition significantly prevails, influenced by the lower hydrodynamic conditions.

6. References

1. Barudžija, U., Velić, J., Malvić, T., Trenc, N. and Matovinović, N. (2020): Morphometric Characteristics, Shapes and Provenance of Holocene Pebbles from the Sava River Gravels (Zagreb, Croatia), Geosciences, 10, 92. https://doi.org/10.3390/geosciences10030092
2. Collinson, J.D. (1986): Alluvial Sediments. In: Reading, H.G. Sedimentary Environments and Facies, 2nd ed., Blackwell Scientific Publications, Oxford, 20-62, 615 pp.
3. Etobro, I. A. A., Ejeh, O. I., & Ovwamuedo, G. O. (2024). Fluvial sedimentology of the river Ethiope sediments, Niger Delta, Southern Nigeria. Rudarsko-geološko-naftni zbornik, 39(2), 45-61.
4. Maričić, A., Starčević, K. and Barudžija, U. (2018): Physical and mechanical properties of dolomites related to sedimentary and diagenetic features - case study of the Upper Triassic dolomites from Medvednica and Samobor Mts., NW Croatia. Rudarsko-Geološko-Naftni Zbornik, 33(3), 33-44. https://hrcak.srce.hr/ojs/index.php/rgn/article/view/6147
5. Krumbein, W.C. (1941): Measurement and geologic significance of shape and roundness of sedimentary particles. Journal of Sedimentary Petrology, 11, 64–72.
6. Müller, G. (1967): Methods in Sedimentary Petrology Sedimentary Petrology-Part1, Schweizerbart, Stuttgart, pp. 283.
7. Tucker, M.E. (1988): Techniques in Sedimentology, Blackwell Scientific Publications, Oxford, 394 pp.
8. Oluwajana, O. A., Ugwueze, C., Ogbe, O., & Egunjobi, K. (2021). Pebble morphogenesis of the Cretaceous conglomerates from the Abeokuta Formation near the Oluwa River, Eastern Dahomey Basin, Southwestern Nigeria. Rudarsko-geološko-naftni zbornik, 36(5).
9. Pavičić, I., Dragičević, I., Vlahović, T. and Grgasović, T. (2017): Fractal analysis of fracture systems in Upper Triassic Dolomites in Žumberak Mountain, Croatia. Rudarsko-Geološko-Naftni Zbornik, 32(3), 1-13. https://doi.org/10.17794/rgn zbornik.v32i3.4894
10. Velić, J. and Durn, G. (1993): Alternating Lacustrine-Marsh Sedimentation and Subaerial Exposure Phases During Quaternary: Prečko, Zagreb, Croatia. Geologia Croatica, 46/1, 71–90. doi: 10.4154/GC.1993.06

11. Velić, J., Saftić, B. and Malvić, T. (1999): Lithological Composition and Stratigraphy of Quaternary Sediments in the Area of the „Jakuševec“ Waste Depository (Zagreb, Northern Croatia). Geologia Croatica, 52/2, 119–130. doi: 10.4154/GC.1999.10
12. Zingg, T. (1935): Beiträge zur Schotteranalyse. Min. Petrog. Mitt. Schweiz., 15, 39–140.

URL1: https://www.atascientific.com.au/principles-laser-diffraction/

SAŽETAK

Granulometrija i morfometrija riječnih sedimenata – studije pijesaka i šljunaka rijeke Sava (Zagreb, Hrvatska)

Morfometrijom valutica uzorkovanih iz korita rijeke Save na području Zagreba definirana je distribucija oblika na promatranom dijelu vodotoka. Prevladavajuće karbonatne valutice su diskoidalnih i sfernih oblika, što može ukazivati na udaljene izvore materijala. Distribucije oblika valutica u pješčenjacima i ostalim manje zastupljenim litologijama ukazuju na lokalne i udaljene izvore materijala. Granulometrija pijeska uzorkovanih iz korita rijeke Save dobivena suhim sijanjem i laserskom granulometrijskom analizom ukazuje na taloženje prevladavajuće sitnog i srednje krupnog pijeska. Udio srednje krupnog pijeska raste nizvodno, vjerojatno zbog umjetno kanaliziranog riječnog korita u urbanom području. Sitni pijesak prevladava dalje nizvodno u meandrirajućem riječnom području.

Ključne riječi: riječni sedimenti; morfometrija; granulometrija; Sava; Zagreb

Author's contributions

Uroš Barudžija - conceptualisation, methodology, validation, investigation, writing - original draft, writing - review and editing. **Matteo Blatančić** - conceptualisation, methodology, investigation, writing - original draft, visualisation.

5th Croatian geomathematical congress
UDC: 56; category: original scientific paper

Application of biometrical analyses in the determination of the coralline algal genus *Sporolithon* – examples from the Eocene deposits of Omiš (SE Croatia)

Jasenka Sremac[1*]; Filip Huić [2]; Marija Bošnjak [3]
[1] Department of Geology, Faculty of Science, University of Zagreb, Horvatovac 102 b, 10000 Zagreb, Croatia, https//orcid.org/0000-0002-4736-7497
[2] FH Centre for English and Anthropology, Oboj 9D, https//orcid.org/0000-0002-0888-9882
[3] Croatian Natural History Museum, Demetrova 1, 10000 Zagreb, Croatia, https//orcid.org/0000-0002-1851-1031
Corresponding author: jsremac@geol.pmf.hr

Abstract

Middle Eocene "Nummulitic limestones" in the area of Omiš (Central Dalmatia), besides the large benthic foraminifera, comprise a rather variable and complex association of bioconstructors, including the warm-water non-geniculate coralline alga *Sporolithon*. We visually distinguished two main types of *Sporolithon* thalii. This study aims to determine *Sporolithon* to the species level and to compare the results with biometrical studies of the size and form of sporangial compartments (diameter-d, height-h, and their ratio-d/h). We found one taxon similar to the Middle-Upper Eocene Tethyan species *S. lugeonii* (Pfender) Ghosh and Maithy, 1996, considering the shape and number of sporangial compartments, although having some differences in size. Another species, *Sporolithon* sp., has wider compartments, arranged in smaller numbers. The collected specimens of the second species had too few visible compartments for a reliable biostatistical analysis. Biometrical characteristics of reproductive structures of the previously known Eocene *Sporolithon* species helped narrow the choice of similar taxa but were not characteristic enough to determine the species.

Keywords: Rhodophyta, *Sporolithon*, biometry, sporangial compartments, Dalmatia

1. Introduction

Coralline red algae (Rhodophyta: Corallinophycidae) are generally known for depositing calcium carbonate polymorphs on their cell walls (calcite, dolomite, magnesite, aragonite, low-magnesium calcite), which makes them highly suitable for preservation in the fossil record. They can be divided into 2 morpho-functional groups: geniculate (G) (with non-calcified joints linking calcified segments) and non-geniculate (NG) corallines (lacking such articulations) (**Basso, 2012**). The group of non-geniculate corallines, with orders Corallinales, Hapalidiales, and Sporolithales is particularly complex in morphological features and therefore complicated for taxonomic studies. Their identification to species level requires the analysis of their reproductive structures (conceptacles or calcified compartments) from the tetra/bisporophytic phases combined with the study of their vegetative characteristics (e.g. the shape of epithelial cells, type of cell connections) (**Leão et al., 2020** and references therein). Biometrical methods (e.g. measuring the diameter *d* and height *h* of compartments and counting their number in a tetrasporangium) are useful in the studies of reproductive structures.

Red algae described in this study occur within olistolites of the Middle Eocene "Nummulitic limestones" (or "Nummulitic breccias") dispersed along the beaches in the Omiš area (Central Dalmatia, SE Croatia), which mark the collapse of the platform edge during the Eocene in the wider region (**Sremac et al., 2020, 2024** and references therein). This study aimed to cross-check the taxonomical determinations based on visual characteristics with biometrical studies.

Furthermore, a comparison with other Sporolithales taxa from the wider region was presented, in order to evaluate the importance of biometrical studies for the Eocene genera.

2. Methods

The study of red algae, whether existing or fossil, includes the field collecting of algal samples and the preparation of thin sections. It is easier to perform such a study on the biological material, while in sedimentary rocks, it is important to prepare a well-oriented cross-section, to get realistic measures, e.g. of the compartment diameter and height.

2.1. Field collecting and preparing the *Sporolithon* samples

Sporolithon samples (**Figure 1 A-D**) were collected in the area between Omiš and Vruja, at the Stanići beach, with the coordinates: Latitude 43.4152 N, Longitude 16.7239 E. Thin sections from rhodolith samples were prepared at the Department of Geology, Faculty of Science in Zagreb. Cross sections were studied and photographed using the Olympus−SZX10 stereo-microscope. Four samples with *Sporolithon* bioconstructions were recognized, three of them with longitudinally cut sporangial compartments, suitable for measuring.

2.2. Biometrical methods

Measurements of compartments were performed by the program Quick Photo Camera connected with the Olympus−SZX10 stereo-microscope, and double-checked by measuring the diameter and height on the printed photomicrographs. The choice of the comparative *Sporolithon* taxa depended on the availability of the compartment size values. The measured dimensions (**Figure 1 D**) are:

d – compartment diameter
h – compartment height
No.comp.- number of compartments *per* tetrasporangium.

Results obtained by biometrical methods, including the calculated diameter/height ratio, were compared with the classic paleontological determinations and presented graphically.

3. Results

Sporolithon samples were analysed using the available palaeontological literature, highlighting the Tethyan region. Representatives of this genus were sometimes originally described under the generic name *Archaeolithothamnium* (e.g. **Studencki, 1988**; **Moussavian and Kuss, 1990**; **Aguirre and Braga, 1998**; **Braga and Bassi, 2007**; **Bassi et al., 2007** and references therein).

Sporolithon bioconstructions occur in two main forms: producing regularly shaped, monospecific, or not very complex rhodoliths (**Figure 1 A**), or, less commonly, irregularly shaped macroids, in combination with acervulinid foraminifera and other red algae (**Figure 1 B**) (**Sremac et al., 2024**). Calcified compartment shapes and their number are also different in these two main types of bioconstructions.

Phylum Rhodophyta Wettstein, 1901
Class Florideophyceae Cronquist, 1960

Subclass Corallinophycidae Le Gall and Saunders, 2007
Order Sporolithales Le Gall, Payri, Bittner and Saunders, 2010
Family Sporolithaceae Verheij, 1993
Genus *Sporolithon* Heydrich, 1897

Sporolithon lugeonii (Pfender) Ghosh and Maithy, 1996
Figures 1 A, B

1926 *Archaeolithothamnium Lugeoni* - Pfender, p. 324, pls. 9, 12.
1996 *Sporolithon lugeonii* – Ghosh and Maithy, p. 68, pl. 1, figs. 1-4.
2011 *Sporolithon lugeonii* - Aguirre et al., p. 274-276.
2022 *Sporolithon lugeonii* - Aguirre et al., fig. 9 D.
2022 *Sporolithon lugeonii* – Hrabovský and Starek, fig. 2.

Two thin sections comprise ca. 4-5 mm wide spherical rhodoliths. One sample comprises only transversal sections, while the other is suitable for measuring the compartment height (**Table 1**). Sporangial compartments, 25 in a row, range from 30-50 µm in diameter, and 60-80 µm in height, the average values are 39.7 µm in diameter and 76.8 µm in height. Specimens from Omiš have a d/h ratio ranging from 0.38-0-71, the average value is 0.52.

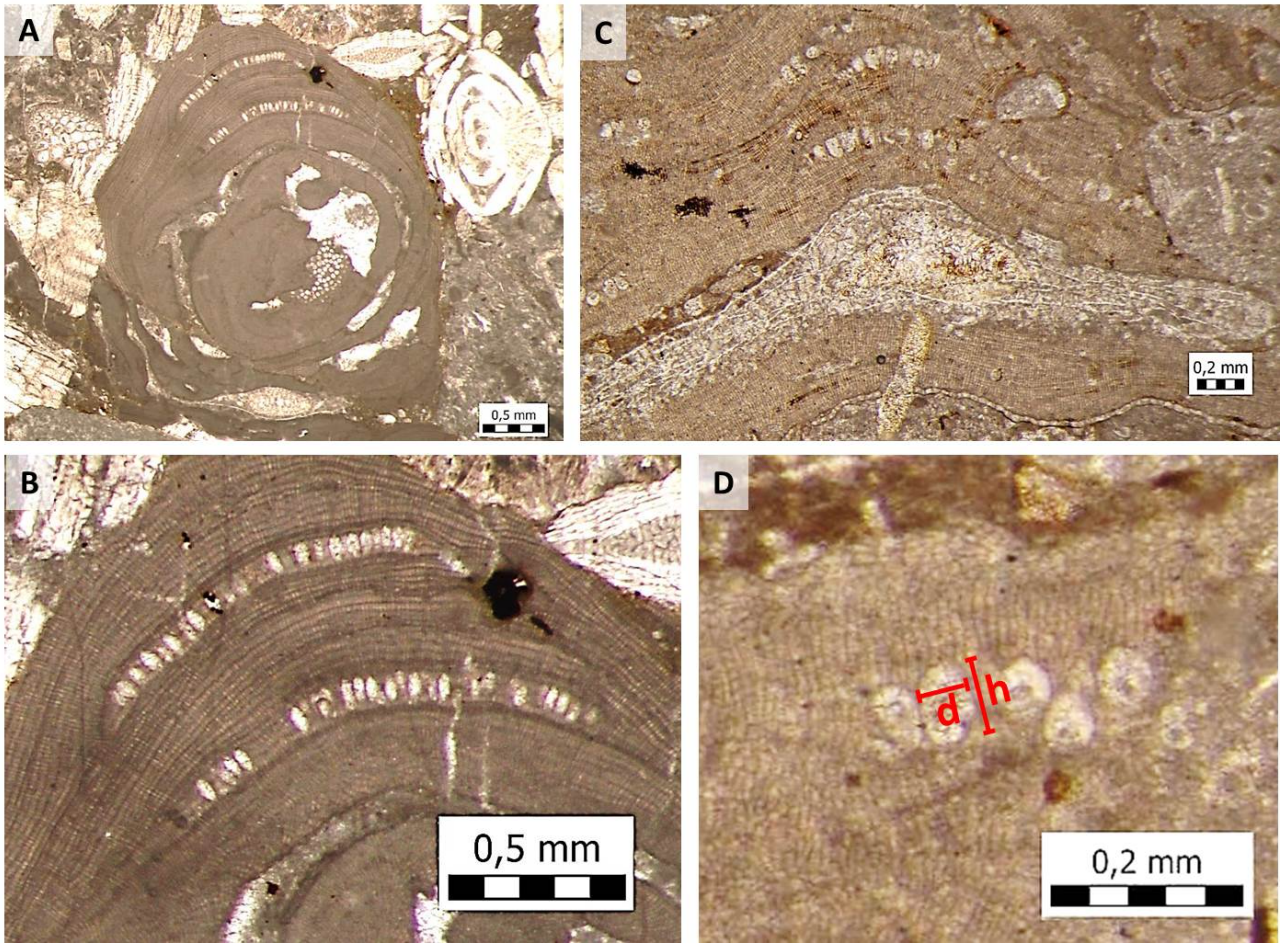

Figure 1: Cross sections of the genus *Sporolithon* from the Eocene deposits of Omiš, collected during the study **Sremac et al. (2020, 2024)**: A) *Sporolithon lugeonii* rhodolith within the

"Nummulitic limestone", measured sample 1; B) a detail of the *Sporolithon lugeonii,* Sample 1, with sporangial compartments; C) a crustose *Sporolithon* sp. form overgrowing the foraminifera *Acervulina linearis* and red alga *Lithoporella*, sample 2; D) a crustose *Sporolithon* sp., sample 3, with the position of the measured dimensions: *d* = compartment diameter; *h* = compartment height.

The species was previously known from the Middle and Upper Eocene deposits of Spain (**Pfender, 1926; Aguirre et al., 2011, 2022**), the Cretaceous and the Paleogene of India (**Rao and Pia 1936; Chaurpagar et al., 2010**), and from the Slovak Carpathians (**Hrabovský and Starek, 2022**) (**Figure 2**).

The shape of compartments, elongated in the longitudinal section (**Figures 1 A, B**) and round in oblique-transverse sections (central part of the rhodolith in **Figure 1 A**) also correspond to the description of *S. lugeonii* offered by **Aguirre et al.** (**2011, 2012**).

Sporolithon sp. indet.
Figures 1, C, D

Two *Sporolithon* specimens have less elongated, oval-shaped compartments, with a smaller number in a sporangium (6 in one specimen and 12-13 in another specimen) in a tetrasporangium (**Table 1**). They occur in complex bioconstructions, composed of several taxa of red algae, together with acervulinid foraminifera.

The specimen with 10-13 sporangial compartments (**Figure 1 C**) shows some similarities in compartment shape with the Pacific species *S. kobamazimense* (Ishijima, 1942) from the Eocene of SW Japan (**Iryu et al., 2009**).

Table 1: The dimensions, diameter/height ratio and number of sporangial compartments in three *Sporolithon* bioconstructions from Omiš (**Figure 1**)

Sample/Photo No.	Compartment No.	Compartment diameter d (µm)	Compartment height h (µm)	d/h	No. comp. *per* tetraspor.
1 /P00033 (Figure 1 A, B) *Sporolithon lugeonii*	1a1	50	80	0.63	25
	1a2	50	70	0.71	
	1a3	50	80	0.63	
	1a4	30	80	0.38	
	1a5	50	80	0.63	
	1a6	40	80	0.5	
	1a7	40	80	0.5	
	1a8	30	70	0.43	
	1a9	40	70	0.57	
	1a10	40	80	0.5	
	1a11	40	80	0.5	
	1a12	40	70	0.57	
	1a13	30	80	0.38	
	1a14	30	80	0.38	
	1a15	40	80	0.5	
	1b1	50	80	0.63	
	1b2	40	80	0.5	
	1b3	40	80	0.5	
	1b4	40	80	0.67	
	1b5	40	80	0.5	
	1b6	40	80	0.5	
	1b7	40	80	0.5	
	1b8	40	80	0.67	
	1b9	40	80	0.5	
	1b10	40	80	0.5	
	1b11	30	80	0.38	
	1b12	40	80	0.5	
	1b13	40	80	0.5	
	1b14	40	80	0.5	
	1b15	30	80	0.43	
2 /P00121 (Figure 1 C) *Sporolithon* sp.	2a	50	90	0.56	10-13
	2b	50	90	0.56	
	2c	50	90	0.56	
	2d	50	90	0.56	
	2e	50	90	0.56	
	2f	50	90	0.56	
	2g	50	80	0.63	
	2h	50	80	0.63	
3/P00093 (Figure 1 D) *Sporolithon* sp.	3a	50	60	0.83	>6
	3b	60	60	1	
	3c	60	90	0.67	
	3d	50	80	0.63	

The specimen presented in **Figure 1 D** slightly resembles the *S. afonense* species (Maslov, 1956) from the Early Eocene of Abhasia (**Bassi et al., 2007**). The number of sporangial compartments available for measuring is too small for a reliable biostatistical study. While the genus *Sporolithon* is rather widespread, the occurrences of *Sporolithon lugeonii* were up to now known from four localities in the Tethyan realm (**Figure 2**).

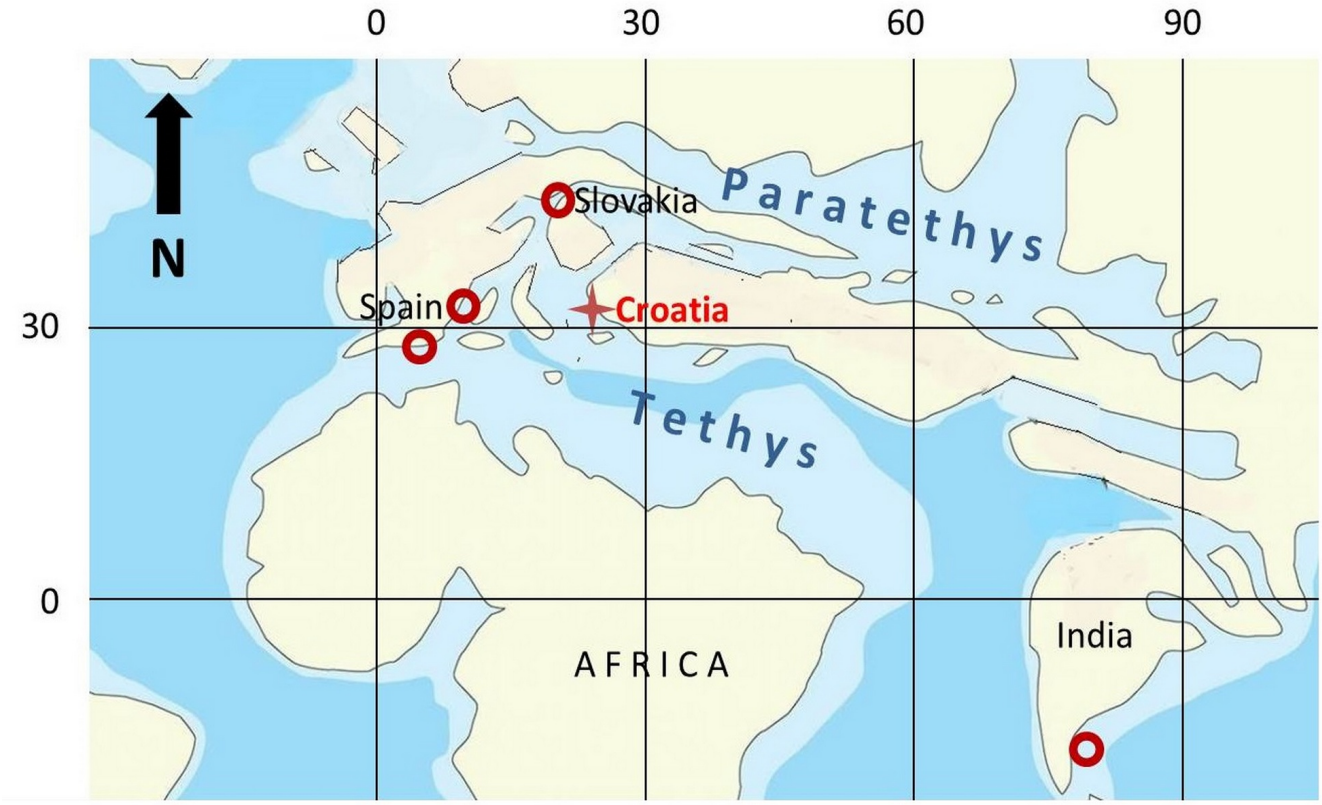

Figure 2: Findings of the species *Sporolithon lugeonii* (red circles) on the palaeogeographic map (after **Sremac et al., 2024**), according to the available literature (**Pfender, 1926; Aguirre et al., 2011, 2022; Rao and Pia 1936; Chaurpagar et al., 2010; Misra et al., 2011; Hrabovský and Starek, 2022**). The location of Omiš (Croatia) is marked with an asterisk.

4. Discussion

The micropalaeontological study revealed that the four studied samples of *Sporolithon* from the Eocene "Nummulitic limestones" of the Omiš area belong to two (maybe even three) species (**Figures 1 A-D, 3; Table 1**).

The number of sporangial compartments and their size and shape are different for all three measured specimens (**Table 1**). The species *Sporolithon lugeonii* (**Figures 1 A, B**) built irregularly spherical rhodoliths, having up to 25 regularly distributed, elongated calcified compartments.

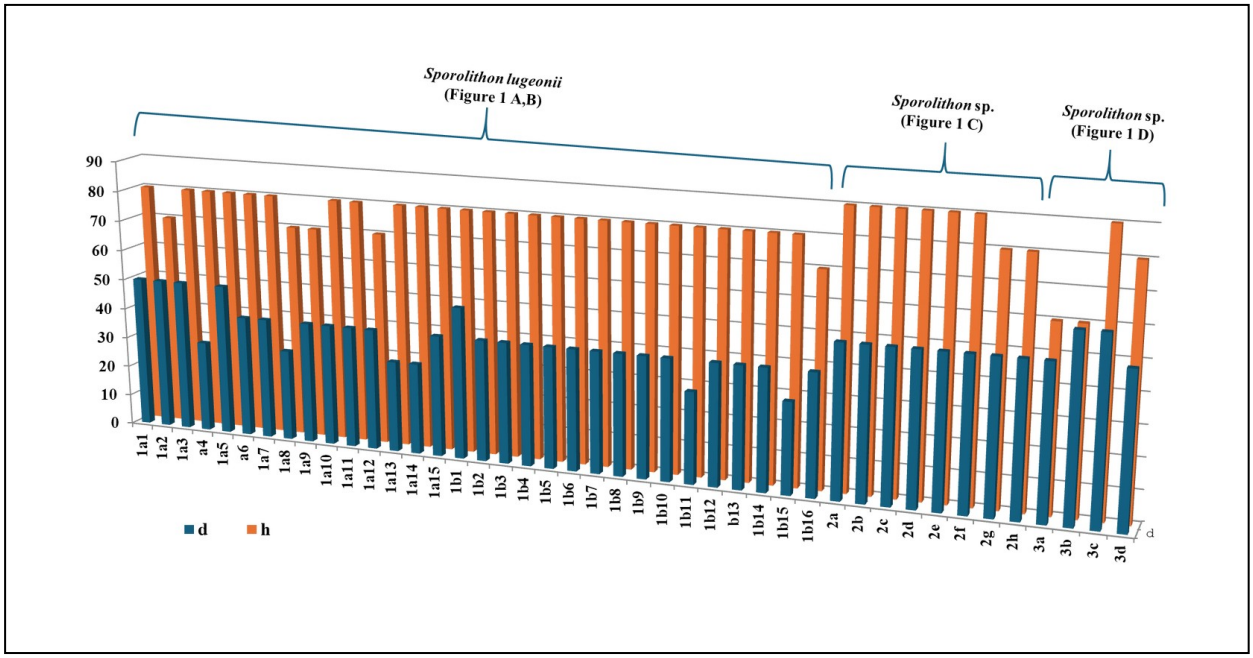

Figure 3: The compartment diameter (d) and height (h) values measured for the three *Sporolithon* samples (**Table 1**). Specimen 1 (**Figure 1 A, B**), determined as *Sporolithon lugeonii*, has rather uniformly large sporangial compartments. The differences between the second and third measured specimen (**Figures 1 C and D**) may be the consequence of the position of the cross sections.

Another two specimens (**Figures 1 C, D**), determined to the generic level, are characterized by a smaller number of compartments *per* tetrasporangium, the shape of the compartments is less elongated. They compose encrusting forms in combination with *Lithoporella* and acervulinid foraminifera. The d/h ratio is highly variable, even in the same cross-section, which points to unequal positions of the compartment axes. It is also possible that specimens 2 and 3 belong to two different species, but for a more detailed taxonomical study, it would be necessary to have more available fertile *Sporolithon* samples.

The comparison with the *Sporolithon* taxa from the wider region included the study of their sporangial compartments and their shape, in order to confirm the visually done determinations (**Table 2, Figures 4 and 5**).

The measurements of the compartment diameters and heights of the Eocene species (**Table 2**) show a variety of values, sometimes with no clear differences between the taxa.

Comparing the d/h ratio itself also did not contribute enough to the species determination. Specimens 1 and 2 from Omiš have a similar pattern of d/h values, but their sporangial compartments are morphologically clearly different. The variation of d/h values within the sporangial compartments of a single specimen (**Figure 3**, specimen 3) may be the consequence of the variable position of the compartment axes and therefore is not significant enough for the species determination.

Table 2. The list of *Sporolithon* species from the wider region (**Verheij, 1993; Townsed et al., 1995; Ghosh and Maithy, 1996; Bassi, 1998; Vannucci et al., 2000; Misra et al., 2011; Chaurpagar et al., 2010; Aguirre et al., 2011, 2022; Basso et al., 2019; Hrabovský and Starek, 2022**) with the dimensions of the sporangial compartments.

***Sporolithon* species**		**Dimensions (µm) and d/h ratio**					
		d min	**d max**	**h min**	**h max**	**d/h min**	**d/h max**
From published papers	*S. afonense* (Maslov, 1956)	65	80	95	115	0.68	0.7
	S. airoldii (Fravega, 1984) **Quaranta & Basso, 2010**	25	45	60	80	0.42	0.56
	S. aschersoni (Schwager,1883)	44	46	56	56	0.79	0.82
	S. cf. *aschersoni* (Schwager,1883) 1883)	30	40	60	70	0.5	0.57
	S. bericum (Mastrorillii, 1973)	35	45	70	90	0.5	0.5
	S. ferganense (Maslov, 1956)	40	55	65	85	0.62	0.65
	S. keenanni Howe, 1934	40	60	90	130	0.44	0.46
	S. kobamazimense (Ishijima, 1942)	50	60	70	80	0.7	0.75
	S. lugeonii (Pfender, 1926)	24	44	55	95	0.42	0.67
	S. nummuliticum (Gümbel) Rothpletz, 1891	50	55	80	85	0.59	0.69
	S. oulianovi (Pfender, 1956)	35	45	50	55	0.7	0.82
	S. praeerythraeum (Airoldi, 1932)	45	78	88	118	0.5	0.66
From this study	***Sporolithon lugeonii* (Pfender, 1926)**	**30**	**50**	**60**	**80**	**0.5**	**0.62**
	***Sporolithon* sp.**	**50**	**60**	**60**	**90**	**0.67**	**0.83**

Comparing all measured values (minimal and maximal values of diameter and height, together with the minimal and maximal values of the d/h ratio) (**Figure 5**) can be useful in combination with previous visual determinations. These values point to some similarities among the species, *S. lugeonii* (**Figure 4**)*, S. afonense*, *S. keenanni,* and *S. praeerythraeum* (**Figure 5**). Biometrical data could be reliably applied to the specimen determined visually as *S. lugeonii*, due to the sufficient number of measurable compartments. The number of compartments for the other two specimens is too small for more precise determinations, and they are determined only at the generic level.

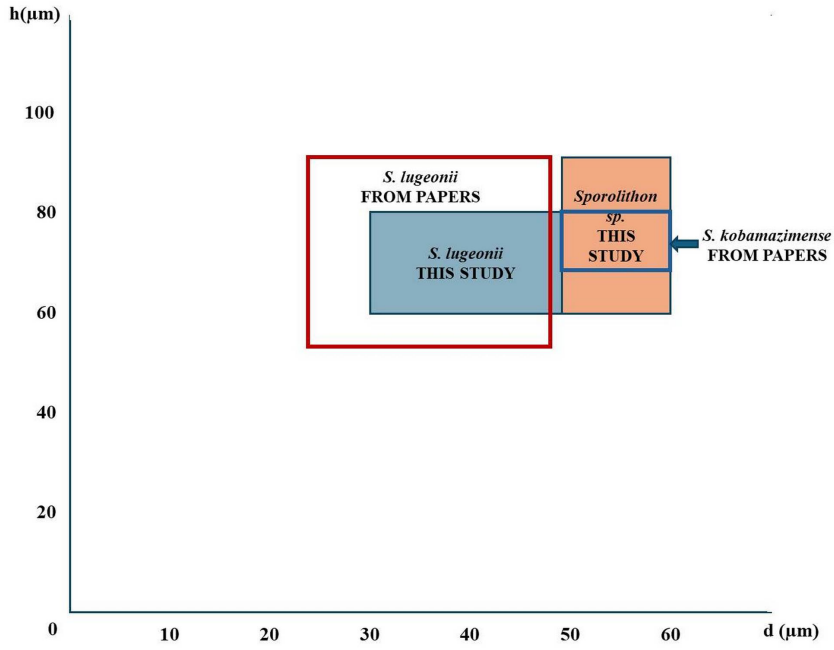

Figure 4: The comparison of diameter (d) and height (h) values measured for sporangial compartments of three *Sporolithon* samples (**Table 1**): The specimen determined as *Sporolithon lugeonii* (Figure 1 A, B) fits well within the biometrical borders of this species. Another two specimens, visually resembling the Pacific species *S. kobamazimense*, have a wider range of compartment heights, but have similarities with this species in compartment diameter and shape.

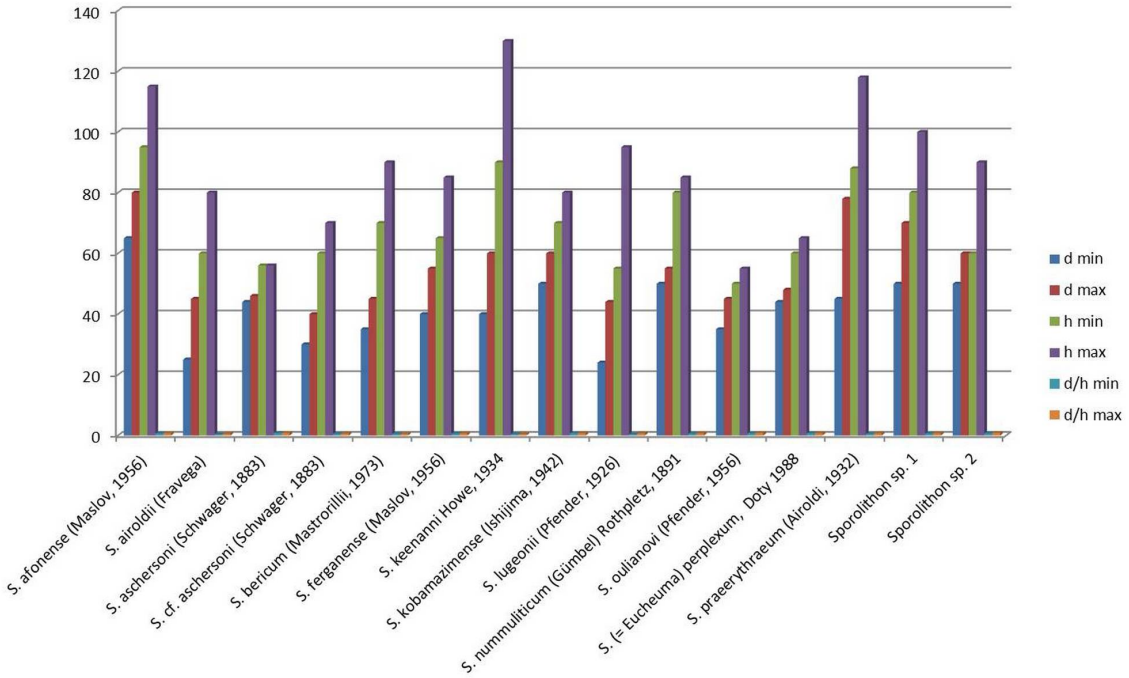

Figure 5: The distribution of maximal and minimal values of the diameter and height, and the diameter/height ratio for the Eocene *Sporolithon* species available in the published papers. *Sporolithon* sp.1 (= *Sporolithon lugeonii*) and *Sporolithon* sp. 2 are the two species from Omiš.

5. Conclusions

- The Genus *Sporolithon* (Rhodophyta: Sporolithales) is one of the bioconstructors found in the Eocene "Nummulitic limestones" in Omiš vicinity.
- Fertile specimens have sporangial compartments of different shapes and sizes, pointing to the existence of two (maybe even three) species.
- Some specimens of *Sporolithon* have up to 25 narrow sporangial compartments, ranging in diameter from 30 to 50 μm, and with a height of 60 to 80 μm. They are determined as the species *S. lugeonii*, which has previously been found in the Middle-Upper Eocene deposits.
- The two specimens determined as *Sporolithon* sp. have less than 13 oval compartments in a cluster, ranging in diameter from 50 to 60 μm, and with a height of 60 to 90 μm. They remain determined at the generic level.
- Measured values can be an additional tool in taxonomical studies of *Sporolithon* species, but only in combination with visual determinations.
- More *Sporolithon* samples should be measured, including the additional study of their fertile and vegetative parts, in order to obtain more precise taxonomical conclusions for the Sporolithales from Omiš.

6. References

1. Aguirre, J., Braga, J.C. and Bassi, D. (2011): Taxonomic assessment of coralline algal species (Rhodophyta: Corallinales and Sporolithales) described by Pfender, Lemoine, and Miranda from northern Spain type localities. Annalen des Naturhistorischen Museums in Wien, Serie A, 113, 267-289.
2. Aguirre, J., Braga, J.C., De Reviers, B. and Woelkerling, W.J. (2012): Reassessment of Lemoine´s newly discovered types of fossil corallines (Corallinales, Rhodophyta) preserved at the Muséum national d'histoire naturelle, Paris. Cryptogamie, Algologie, 33, 289-326.
3. Aguirre, J. and Braga, J.C. (1998): Redescription of Lemoine's (1939) types of coralline algal species from Algeria. Palaeontology 41, 489-507.
4. Aguirre, J., Baceta, J.I. and Braga, J.C. (2022): Coralline Algae at the Paleocene/Eocene Thermal Maximum in the Southern Pyrenees (N Spain). Front. Mar. Sci., Sec. Marine Ecosystem Ecology, 9. https://doi.org/10.3389/fmars.2022.899877
5. Bassi, D. (1998): Coralline red algae (Corallinales, Rhodophyta) from the Upper Eocene Calcare di Nago (Lake Garda, Northern Italy). Ann. Univ. Ferrara Sci. Terra 7, 1-51.
6. Bassi, D., Braga, J. C., Zakrevskaya, E. and Petrovna Radionova, E. (2007): Redescription of the type collections of Maslov's species of Corallinales (Rhodophyta). II. Species included by Maslov in *Archaeolithothamnium* Rothpletz, 1891. Revista Española de Paleontología, 22 (2), 115-125. ISSN 0213-6937.
7. Basso, D. (2012): Carbonate production by calcareous red algae and global change. Geodiversitas 34, 13-33
8. Basso, D., Coletti, G., Bracchi, V.A. and Yazdi-Moghadam, M. (2019): Lower Oligocene coralline algae of the Uromieh section (Qom Formation, NW Iran) and the oldest record of *Titanoderma pustulatum* (Corallinophycidae, Rhodophyta). Rivista Italiana di Paleontologia e Stratigrafia, 125, 197-218.
9. Braga J.C. and Bassi D. (2007): Neogene history of *Sporolithon* Heydrich (Corallinales, Rhodophyta) in the Mediterranean region. Palaeogeography, palaeoclimatology, palaeoecology 243, 189-203.

10. Chaurpagar, S.N., Humane, S.K., Kundal, P. and Humane, S.S. (2010): Nongeniculate Coralline algae and their Palaeoenvironments in the Middle Eocene Sylhet Limestone Formation, Bengal Basin, India. XXII Spec. Vol. of ICMS.
11. Ghosh, A.I. and Maithy, P.K. (1996): On the present status of coralline red alga *Archaeolithothamnium* Roth. from India. Palaeobotanist, 45, 64-70.
12. Hrabovský, J. and Starek, D. (2022): Priabonian non-geniculate coralline algae from the Central Carpathian Paleogene Basin. Carnets Geol. 22,12. DOI 10.2110/carnets.2022.2212
13. Iryu, Y., Bassi, D. and Woelkerling, W.J. (2009): Reassesment of the type collections of fourteen corallinalean species (Corallinales, Rhodophyta) described by W. Ishijima (1942–1960). Palaeontology, 52, 401-427. https://doi.org/10.1111/j.1475-4983.2009.00850.x
14. Leão, L.A.S.; Bahia, R.G.; Jesionek, M.B.; Adey, W.H.; Johnson, G.; Salgado, L.T. and Pereira, R.C. (2020): *Sporolithon franciscanum* sp. nov. (Sporolithales, Rhodophyta), a New Rhodolith-Forming Species from Northeast Brazil. Diversity, 12, 199. https://doi.org/10.3390/d12050199
15. Misra, P.K., Jauhri, A.K., Tiwari, R.P.; Kishore, S.; Singh, A.P and Singh, S.K. (2011): Coralline algae from the Prang Formation (middle-late Eocene) of the Lumshnong area, Jaintia Hills, Meghalaya. Journal Geological Society of India, 78**,** 355-364.
16. Moussavian, E. and Kuss, J. (1990): Typification and status of *Lithothamnium aschersoni* Schwager, 1883 (Corallinaceae, Rhodophyta) from Paleocene limestone of Egypt. A contribution to synonymy and priority of genera *Archaeolithothamnium* Rothpletz and *Sporolithon* Heydrich. Berliner Geowissenshaftliche Abhandlungen Reihe A, Geologie und Paläontologie, 120, 929-942.
17. Pfender, J. (1926): Sur les organismes du Nummulitique de la colline de San Salvador près Camarasa. Boletín de la Real Academia Española de Historia Natural, 26, 321-330.
18. Rao, L.R. and Pia, J. (1936): Fossil algae from the Uppermost Cretaceous beds (The Niniyur group). of the Trichinopoly District, south India. Mem. Geol. Surv. Ind. Pal. Indica, n. ser. 21 (4), 1-49.
19. Sremac, J.; Huić, F.; Bošnjak, M. and Drempetić, R. (2020): Morphometric characteristics and origin of Palaeogene macroids from beach gravels in Stanići (vicinity of Omiš, Southern Croatia). In: Malvić, T.; Barudžija, U.; Bošnjak, M. et al. (eds.). Mathematical methods and terminology in geology 2020, Zagreb, Rudarsko-geološko-naftni fakultet Sveučilišta u Zagrebu, Hrvatsko geološko društvo, 49-61.
20. Sremac, J.; Huić, F.; Bošnjak, M. and Marjanac, T. (2024): The Composition of Acervulinid – Red Algal Macroids from the Paleogene of Croatia and Their Distribution in the Wider Mediterranean Region. In: Recent Research on Sedimentology, Stratigraphy, Paleontology, Geochemistry, Volcanology, Tectonics, and Petroleum Geology Proceedings of the 2nd MedGU, Marrakesh 2022 (Volume 2). Cham, Switzerland: Springer Nature, 59-62. doi: 10.1007/978-3-031-48758-3
21. Studencki, W. (1988): Red algae from the Pińczów Limestones (Middle Miocene; Świętokrzyskie Mountains, Central Poland). Acta Palaeontologica Polonica, 33, 1.
22. Vannucci, G., Piazza, M., Fravega, P. and Basso, D. (2000): Revision and re-documentation of M. Airoldi's species of *Archaeolithothamnium* from the Tertiary Piedmont Basin (NW Italy). Rivista Italiana di Paleontologia e Stratigrafia, 106, 2, 191-202.
23. Verheij, E. (1993): The genus *Sporolithon* (Sporolithaceae fam. nov., Corallinales, Rhodophyta) from the Spermonde Archipelago, Indonesia. Phycologia, 32, 3, 184-196. https://doi.org/10.2216/i0031-8884-32-3-184.1

SAŽETAK

Značenje biometrijskih analiza za taksonomsku odredbu vrsta roda *Sporolithon*: primjeri iz eocenskih naslaga Omiša

U numulitnim vapnencima eocenske starosti na području Omiša nađeni su raznoliki ostatci crvenih algi, među kojima i predstavnici toplovodne skupine Sporolithales. Ove alge imaju složenu građu kalcificiranih segmenata, pa ih je teško determinirati na razini vrste. Fertilni primjerci koje smo pronašli tijekom ovog istraživanja razlikuju se prema izgledu, broju i veličini sporangijskih odjeljaka, pa su radno bili determinirani kao dvije vrste roda *Sporolithon*. Prva vrsta ima niz karakteristika bliskih vrsti *Sporolithon lugeonii* (Pfender, 1926), s kojom dijeli broj odjeljaka u tetrasporangiju. Sama je vrsta varijabilne veličine, no ima uske kopljaste odjeljke, koji su gusto i dosta ravnomjerno raspoređeni. Preostala dva pronađena primjerka determinirana su samo na razini roda (*Sporolithon* sp.), imaju manji broj širih odjeljaka, pa im je omjer dijametra i visine odjeljaka (d/h) veći. Mjerenja odjeljaka dala su dosta varijabilne rezultate, koji otvaraju mogućnost da *Sporolithon* sp. zapravo sadrži dvije različite vrste, no sačuvan je premali broj odjeljaka za validnu biometrijsku analizu. Za detaljnije taksonomsko istraživanje roda *Sporolithon* potrebno je dodatno uzorkovanje, a ova preliminarna studija je pokazala da samo biometrijsko istraživanje nije dostatno, već je potreban kombinirani pristup, koji će uz veličinu uzeti u obzir i njihove druge reproduktivne i vegetativne karakteristike.

Ključne riječi: Rhodophyta, *Sporolithon*, biometrija, sporangijski odjeljci, Dalmacija

Acknowledgment

During the fieldwork and laboratory preparations, authors were supported by the Croatian Science Foundation Project "Sedimentary paleobasins, water corridors, and biota migrations" led by Marijan Kovačić (Faculty of Science), and University of Zagreb Faculty of mining, Geology and Petroleum Engineering grant "Mathematical researching in geology IX" led by Tomislav Malvić and University of Zagreb Faculty of Sciences grant led by Alan Moro. Renato Drempetić was of great help during the fieldwork.

Author's contribution

Jasenka Sremac (1) (retired full professor, paleontologist) provided the fieldwork, micropalaeontological analyses, interpretations, and presentation of the results. **Filip Huić (2)** (anthropologist and linguist, highly involved in palaeontology) provided the fieldwork, measurements, and the database of contemporary taxa. **Marija Bošnjak (3)** (senior curator, palaeontologist) provided the biostatistical analyses and associated interpretations.

5th Croatian geomathematical congress
UDC: 622.1; category: review scientific paper

Advancements and Applications of the Discrete Element Method in Mining and Geotechnical Engineering

Dubravko Domitrović[1*]; Tomislav Korman[2]; Mario Klanfar[3]; Vjekoslav Herceg[4]
[1] University of Zagreb, Faculty of mining, geology and petroleum engineering, Pierottieva 6, Zagreb, https://orcid.org/0000-0001-9861-8471
[2] University of Zagreb, Faculty of mining, geology and petroleum engineering, Pierottieva 6, Zagreb, https://orcid.org/0000-0002-5252-299X
[3] University of Zagreb, Faculty of mining, geology and petroleum engineering, Pierottieva 6, Zagreb, https://orcid.org/0000-0003-1629-873X
[4] University of Zagreb, Faculty of mining, geology and petroleum engineering, Pierottieva 6, Zagreb, https://orcid.org/0000-0002-5706-9135
Corresponding author: dubravko.domitrovic@rgn.unizg.hr

Abstract

The application of numerical methods, particularly the Discrete Element Method (DEM), has significantly advanced the understanding of the complex mechanical behaviour of materials in mining and geotechnical engineering. DEM, which simulates systems of particles, enables detailed analysis of the interactions between individual particles, which are crucial for predicting the behaviour of granular materials such as soil, rock and other discrete element systems. This study explores the various applications of DEM in mining, including the modelling of crushing, transport and storage processes of ore materials, leading to process optimization, cost reduction and enhanced safety. In geotechnical engineering, DEM is used to analyse slope stability, foundations, supporting structures, and soil-structure interactions to enable accurate predictions of soil and rock responses to natural and anthropogenic impacts. The study also discusses the importance of selecting appropriate contact models and input parameters in DEM simulations and emphasises the need for calibration procedures to ensure accurate simulations. Examples of DEM simulations in mining and geotechnical applications demonstrate the method's ability to optimise designs, improve efficiency and enhance safety.

Keywords: Discrete Element Method (DEM) simulation; mining; geotechnical engineering

1. Introduction

The application of numerical methods such as the Discrete Element Method (DEM) in mining and geotechnical engineering represents a significant advance in the understanding of the complex mechanical behaviour of materials. DEM is a numerical technique used to simulate the behaviour of systems of particles, such as granular materials, powders, food, and even molecular systems. In DEM, the material is modelled as an assembly of discrete, interacting particles, each of which can have a different shape and move independently. The method calculates the motion and interactions of these particles over time, considering forces such as gravity, contact forces, and friction. DEM is particularly useful for studying complex behaviours like flow, mixing, and breakage in granular systems, where traditional continuum methods may fall short. This numerical method allows for a detailed analysis of interactions between individual particles, crucial for predicting the behaviour of granular materials such as soil, rock, and other materials composed of discrete elements. Discrete elements or granular materials can adopt different states such as solid, liquid or gaslike which can be simulated in DEM with many contact models. Processes in nature or industry that include that discrete elements can also involve static and dynamic behaviour.

In mining, DEM enables the precise modelling of crushing, grinding, transport and storage processes of ore materials, which leads to the optimization of these processes, cost reduction and increased safety. The discrete element method provides deeper insights into the mechanics of rock fractures, the stress distribution within mining structures and the prediction of potential landslides or collapses, which can significantly improve the planning of mining activities and risk management (**Aftabi et al, 2023; Munir et al., 2022; Salkynov et al., 2023; Chehreghani et al., 2022**).

In geotechnical engineering, the application of DEM extends to the analysing the stability of slopes, foundations, retaining structures such as walls and embankments, and the interaction of soil with geotechnical structures such as piles and anchors. Modelling soil and rock behaviour using DEM enables more accurate predictions of their responses to natural and anthropogenic impacts, including seismic actions, loads and changes in water content. This leads to better design, increased safety and cost reduction in geotechnical projects.

With the development of computer capabilities and the possibility of performing calculations in computer clusters, the numerical DEM method is now available to more and more engineers and researchers. The study shows how efficiency can be increased both in mining and in geotechnics through improved simulation possibilities with the DEM.

2. Contact models used in DEM

In the DEM simulation, the simulation takes place in time steps. Each time step deals with a finite number of discrete elements that interact with each other. The calculation is carried out in two phases. In the first phase, the contact forces between the discrete elements are generated. The force-displacement law plays a crucial role here, as the contact forces between neighbouring discrete elements lead to force changes. In the second phase, the discrete elements move or break due to the current state of the contact forces. The force-displacement law is defined by contact models. Therefore, the choice of a contact model plays a crucial role in the interactions between discrete elements. Nowadays, there are many contact models, from basic ones (e.g. elastic contact models) to advanced ones (e.g. elastoplastic adhesive contact models, adhesive rolling resistance contact models, fragmentation contact models). In the second phase, Newton's second law is applied to predict the movement based on the contact force calculated in the first phase. **Figure 1** shows an example of a DEM model for the simulation of the angle of repose due to hopper discharge and the calculation of stress at discrete element contact. The grey contours in **Figure 1b** represent the stress that is above the yield.

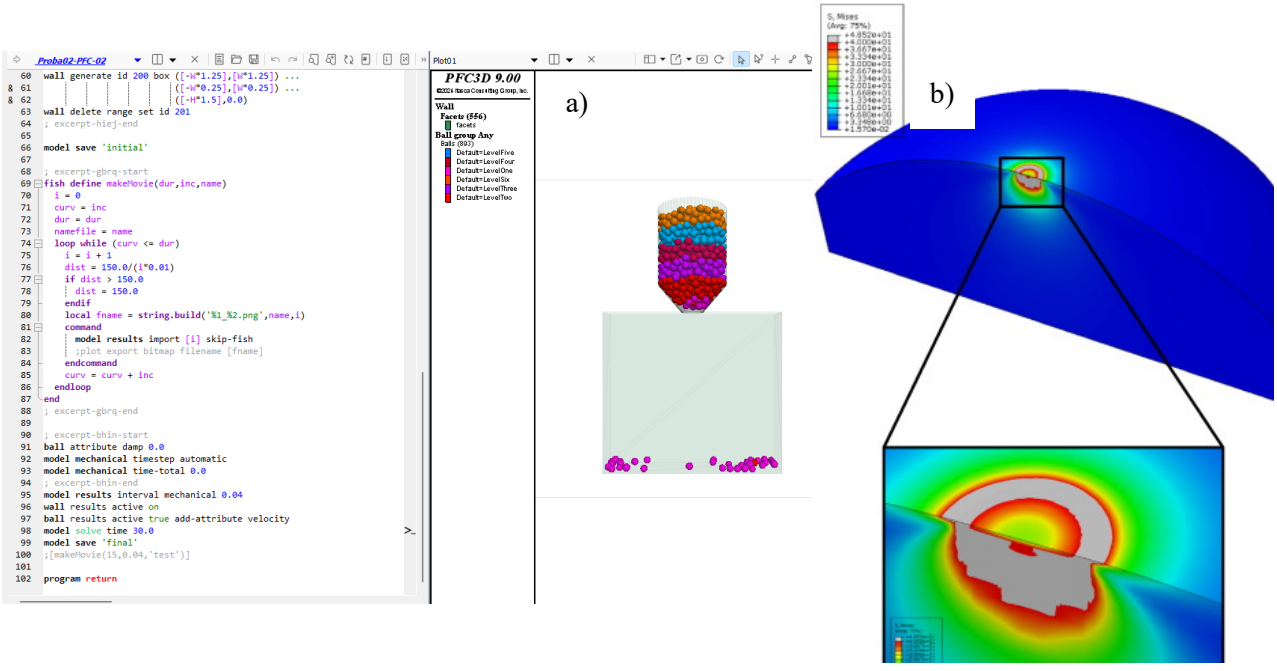

Figure 1: Simulation of the angle of repose due to hopper discharge, created in PFC3D: a) DEM model with input code, b) the contours show the stress on the sphere after the DEM calculation (modified from **Rathbone et al., 2015**).

In elastic contact models, it is assumed that discrete elements are behave elastically on contact. This behaviour can be achieved by a linear relationship, which is the simplest model. The most frequently used non-linear elastic model is the Hertz model (**Hertz, 1881**). Elastic models are suitable for the simulation of materials such as rubber. For other materials where attractive forces between discrete elements, yielding (plastic deformations) or fragmentation play a role, advanced models must be used to realistically represent the static or dynamic behaviour of the material.

3. DEM input parameters

Unlike e.g. finite element methods, where most input parameters can usually be obtained directly by in-situ or laboratory experiments (e.g. internal friction angle, cohesion, particle density) and some can be assumed based on experience (e.g. Poisson's ratio), DEM often requires calibration procedures to determine the input parameters. The reason for this is that material input parameters are needed at the microscale or particle level, e.g. contact properties, cohesion, damping between particles. The determination of these microparameters is a challenge as it is relatively difficult to measure them directly by laboratory experiments. In calibration, numerical tests are used to individually calibrate the parameters used at the particle level one by one through an iteration process until a bulk behaviour observed in the laboratory is satisfactorily predicted (**Coetzee and Nel, 2014**). In mining and geotechnical engineering, bulk material with fines plays an important role and a certain water content is often present. To simulate this type of material during conveyor belt transport, elastoplastic adhesion models (e.g. the Edinburgh Elastoplastic Adhesion Model - EEPA) can be considered (**Morrissey, 2013**). The following parameters would be required for this simulation (**Carr et al., 2023**). The loading spring stiffness defines the initial loading stiffness of the particles, while the unloading spring stiffness defines the unloading/reloading stiffness condition as a ratio to the loading stiffness. The adhesive force indicates the constant pull-off force acting between the particles. The adhesive surface energy quantifies the adhesion that holds the particles together. The adhesion branch exponent determines the strength of the adhesive force after the peak tensile force is reached. Additionally, the sliding friction and the rolling friction of the particles are also required for the model.

If we consider the example of the EEPA model, a unique set of parameters is needed. To calibrate it, a series of non-standard laboratory experiments are required. To meet the requirements of the model, the calibration procedure should include a series of laboratory experiments that cover various dynamic flow conditions in contact with handling equipment.

Apart from the required non-standard experiments, the number of particles or discrete elements in the model also plays a major role in the DEM simulation. With increasing complexity of the chosen contact model and a larger number of particles, the computational requirements and calculation time increase exponentially. In general, more fines mean more discrete elements for the calculation.

The range of particle size distribution used in DEM simulations is also very important. It is often impractical to simulate an industrial material handling system with the complete particle size distribution of the material. For example, an angle of repose which is frequently used as a laboratory test for model parameter input and DEM calibration, would require several million discrete elements for a 50 kg sample if the full particle size distribution of bulk material with fines is used. This issue becomes even more challenging when simulating a transfer system that handles several tonnes per hour. Therefore, it is more feasible to either scalp (remove smaller particles from the DEM model, as shown in **Figure 2**) or scale (increase the particle diameters for some ratio) the particle size distribution of the bulk material for calibration and simulations.

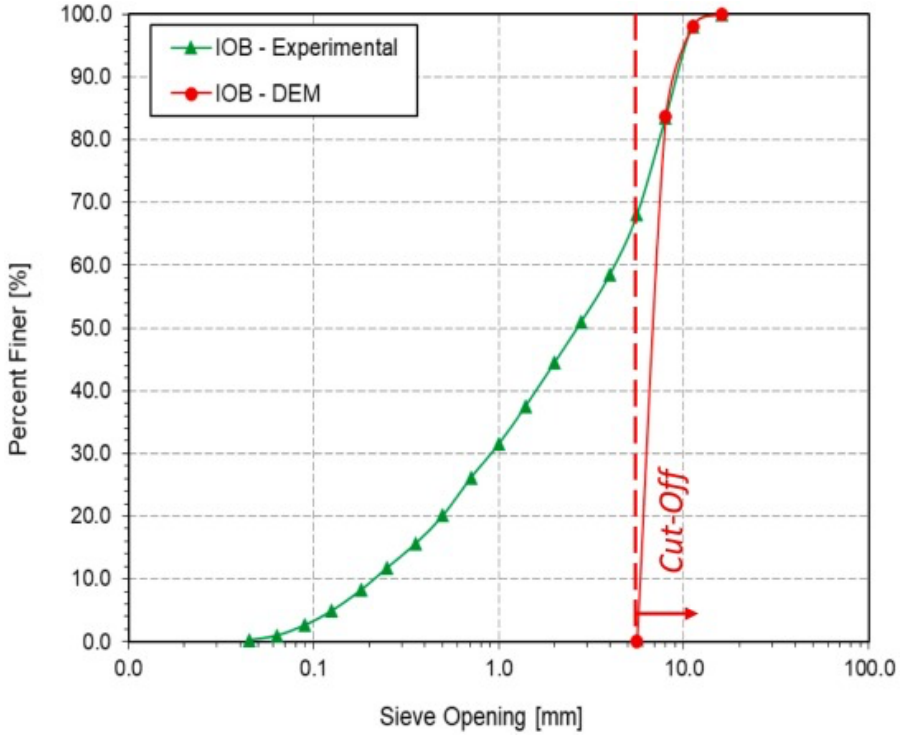

Figure 2: Example of scalping for DEM analysis (**Carr et al., 2023**)

Scaling technique is usually used when only small particles (e.g. powder) are simulated, as there are issues with very small discrete elements (e.g. calculation time). In both cases, it should be kept in mind that smaller particles have a larger contact area than particles with larger diameter, which influences the calculated attraction force (**Thakur et al., 2016**). It is therefore recommended to do sensitivity analysis for these two techniques when deciding on a particle cut-off value or increasing ratio.

If a dry, non-cohesive bulk material is simulated, some of the notable calibration experiments such as the angle of repose test (**Klanfar et al., 2021**), the shear box test (**Ilic, 2013**) and more recently the draw-down test (**Roessler et al., 2019**) can be used. The shear box test and the draw down test are more suitable for cohesive wet materials. A basic schematic of the tests mentioned is shown in **Figure 3**. The most important parameters obtained from these tests are the angle of repose (b_{cyl} and b_{DD}) and the shear angle (j_{SB} and j_{DD}).

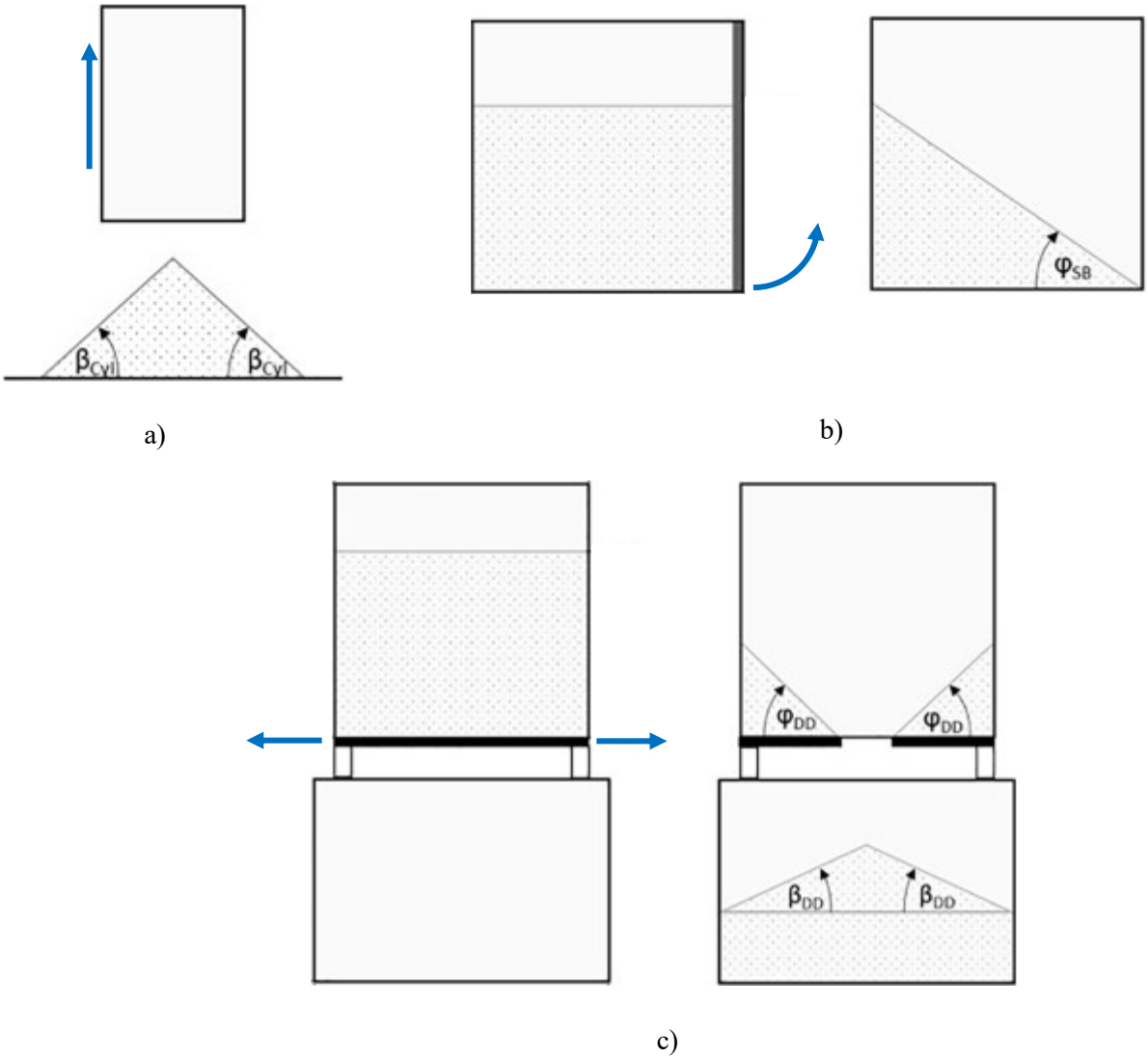

Figure 3: Basic schematic of calibration laboratory tests: a) the angle of repose, b) the shear box test and c) the draw down test (modified from **Roessler et al., 2019**)

4. Application of DEM simulation in mining

DEM is a powerful computational technique that is widely used in the mining industry today to simulate and analyse the behaviour of granular systems, rock and soil. It is able to provide valuable insights into various processes (e.g. griding, crushing, cyclones, rock and soil deformation, etc.) and helps to optimise operations, improve efficiency and enhance safety (e.g. conveyor systems, transfer chutes, etc.). Some of the key applications of DEM are outlined here. In the material handling and transfer, the simulation of conveyor systems and bulk material such as ore, coal and aggregates on conveyer belts leads to design optimization, spillage reduction and improved efficiency. Also, optimization of storage and retrieval operations can be done by analysis of stockpile formation, reclaiming processes, and flow patterns. The analysis of bulk material flow through transport chutes can be used to minimise wear, blockage and materials degradation. The modelling of crushers and crushing processes provides the particle size distribution after the crushing process, wear patterns and energy consumption. In addition to crushers, griding mills are also an integral part of the mineral processing and are used to separate and purify raw minerals. Simulation of ball mills and other types of mills analyses the impact of various operating conditions on grinding efficiency, throughput, and wear. Processes for particles screening and separation can also be successfully analysed. In this case, the screening efficiency and wear of

vibrating screens are obtained. The simulation of hydrocyclones helps to optimise separation efficiency and reduce energy consumption. The first step in mining is the extraction of ore. To get to the ore, the solid rock is usually blasted. The modelling of rock blasting describes the fragmentation process, predicts the particle size distribution and optimises the blasting. DEM is able to simulate even and a leaching process to study the flow of solutions through the ore heaps and optimise the efficiency of the leaching.

Before showing an example of simulations, it should be noted that the real advantage of DEM simulations is the possibility of coupling them with other types of numerical simulations, for example with CFD (Computational Fluid Dynamics) or FEM (Finite Element Method) method. An example of a DEM simulation and the coupling of DEM and FEM methods is the analysis of the dynamic deflection of conveyor belts (**Munir et al., 2022**), the results of which can be seen in **Figure 4**. The results show the deflection of the belt, the energy required to overcome the elastic deformation of the belt and the maximum stress in the belt for two cases, case one with the rollers gap of 1 m and case two with the rollers gap of 2 m.

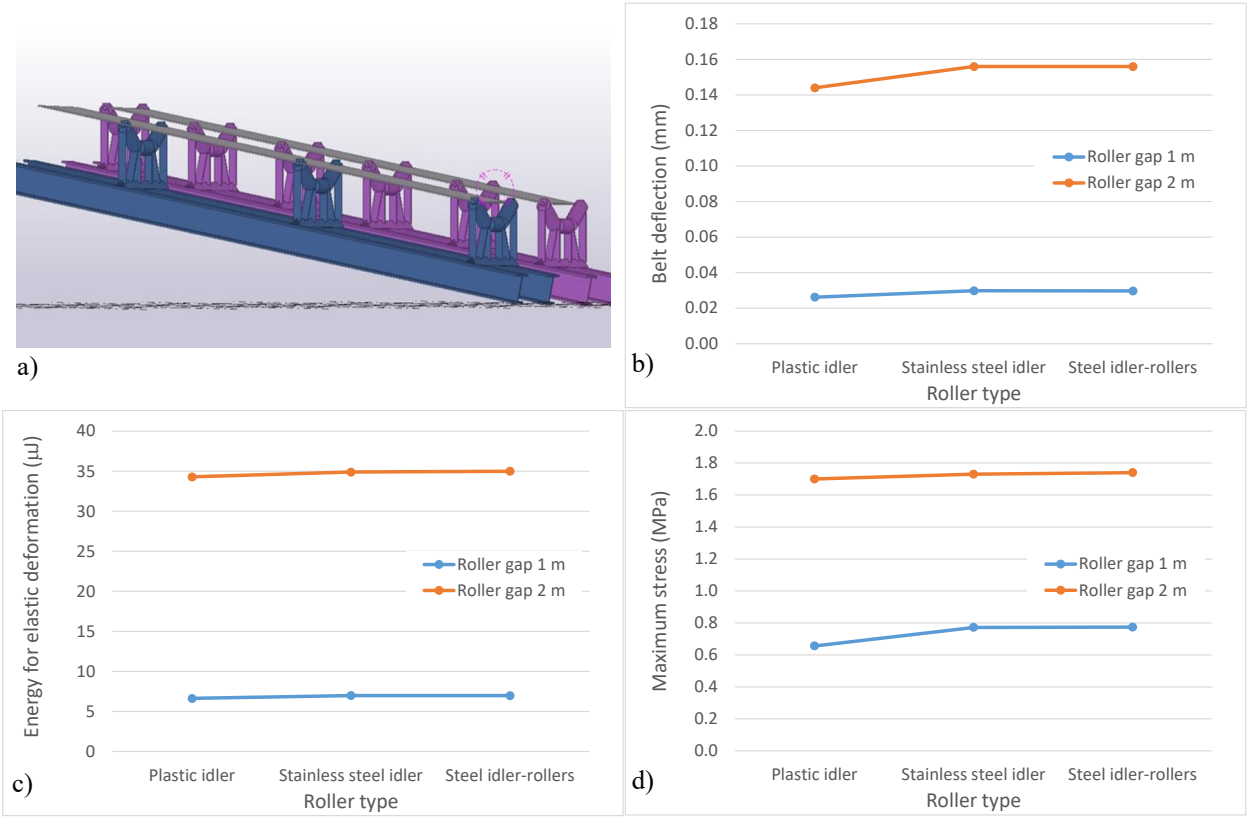

Figure 4: Simulation results of the dynamic deflection of a conveyor belt, a) conveyor belt model, b) deflection of the belt, c) energy required to overcome the elastic deformation during transport and d) maximum stress in the belt (modified from **Munir et al., 2022**)

Another example of DEM simulation shows the comparison of the results of an industrial-scale crusher for problematic material such as copper ore with a DEM simulation (**Doroszuk and Krol, 2022**). The aim was to optimise the design of the hammers in the crusher. The experiment in the jaw crusher was used for DEM model calibration. The simulation of the hammer crusher was then used to optimise the hammers (**Figure 5)**.

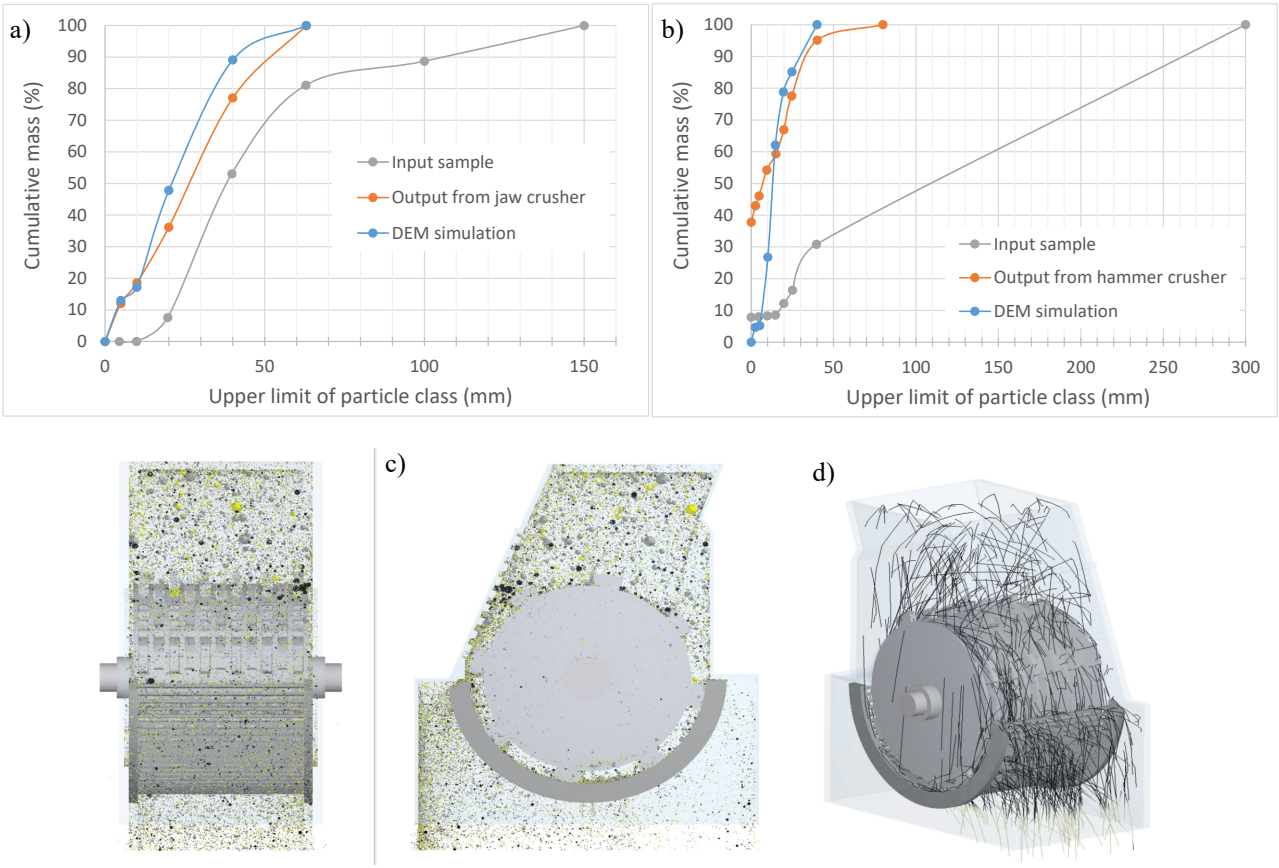

Figure 5: Results of the analysis of industrial-scale crusher work: a) particle size distribution from the jaw crusher, b) particle size distribution from hammer crusher, c) particles in hammer crusher and d) particle trajectories in hammer crusher (modified from **Doroszuk and Krol, 2022**)

5. Application of DEM simulation in geotechnical engineering

Complex geotechnical processes and the behaviour of granular materials, rock masses and soil deposits can also be simulated with DEM. The simulation of stress-strain responses in soils and rocks predicts their mechanical behaviour under different loading conditions. Analysing the shear strength and potential failure surfaces in soils and rock masses leads to stability assessments and the bearing capacity of shallow and deep foundations under various loading conditions. The effectiveness of slope reinforcement techniques such as soil nails, retaining walls and geosynthetics can be evaluated. The settlement behaviour of foundations on different soil types can be predicted, leading to an optimisation of structural design. The DEM can be useful for underground excavations. The modelling the underground excavations, tunnels and their support systems such as rock bolts and shotcrete ensures prevention of collapses and safety. The compaction process is one of the most important factors in geotechnical engineering, ensuring sufficient density of soil particles and thus suitable mechanical properties of the soil for foundations, embankments, dams and other earthworks. The simulation of soil compaction techniques helps to achieve the desired soil density and mechanical properties.

Man-made materials such as geosynthetics are nowadays commonly used in mining and geotechnical engineering (**Herceg et al., 2023**). Geotextiles and geogrids are commonly utilized in road embankments, retaining walls and slopes because of their superior properties and high economic efficiency compared to natural materials. The interaction between soil and reinforcement is widely acknowledged as a critical factor in the performance and design of geosynthetic-reinforced structures. As an example of the use of DEM, a pullout test with geogrids can be modelled. **Miao et al. (2017)** modelled the pullout behaviour of geogrid reinforcement with an emphasis on the influence of grain shapes on the pullout force. The peak pullout forces are

shown because they reflect the yielding properties of a geogrid-reinforced system (**Figure 6**). **Figure 6** also shows the final axial deformation of the geogrid at the end of the pullout test.

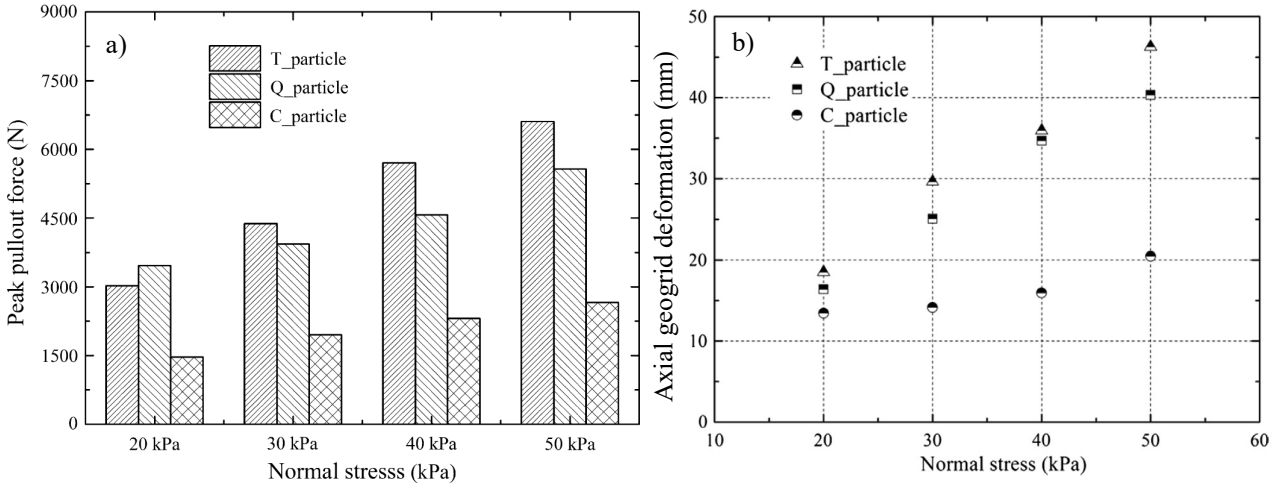

Figure 6: Results of DEM simulation of pullout test on geogrid (**Miao et al., 2017)**: a) peak pullout forces in respect to particle shape and normal stress during pullout test and b) final axial deformation of geogrid in respect to particle shape and normal stress during pullout test

Another example of DEM usage in geotechnical engineering is the simulation of the shear behaviour in the critical state at the soil-structure interface. **Gu et al. (2017)** showed results from a series of monotonic direct shear tests using a sand-structure interface in tests with constant normal stiffness tests. A comparison was made between the laboratory tests and the DEM simulation. **Figure 7** shows the simulation results of particle displacements in vicinity of soil-structure interface at a horizontal displacement of 12 mm. In laboratory experiments, particle movements during testing can be measured. However, these measurements are usually associated with various problems (e.g. measurements in certain points, the accuracy of the measurements is questionable, especially if you want to measure the rotation of the particles). Therefore, this type of simulation is often the only way to get a good picture of what happens in the soil during the critical state shear behaviour in the soil or at the soil-structure interface.

The advantage of the DEM method is the possibility of coupling simulations with other numerical methods (e.g. FEM, CFD), as already mentioned. The water and pore pressure can be simulated in DEM, but if you only use DEM simulation, this effect is modelled by microscale or particle-to-particle contact input parameters (e.g. contact properties, cohesion). On the other hand, if a real physical fluid needs to be modelled, a coupling of DEM and CFD can be performed. Dynamic loading conditions in soil can also be modelled by combining DEM and FEM. One of the examples where pore pressure and dynamic loading play a role is the study of **Flores-Johnson et al. (2016)**. In this case, the FEM is used to specify the dynamic loading in the model.

Modelling clay particles would be more challenging due to their non-spherical shape. In this case, a particle is considered as a group of connected discrete elements. The disadvantage of such a model is the enormous enlargement of the model and the computational effort. An example of such a modelling approach is the study of **Bono and McDowell (2016)**, in which the authors used the DEM method to model the compression of clay.

Another advantage of the DEM method is that we can theoretically define each particle or even each molecule separately. So it is relatively easy to define the particle size distribution of the input sample and the particle shapes. Then the sample can randomly fill a certain space and confinement can be defined. As a result of the DEM simulation, the rotation of the particles, their breakage and stress distribution can then be monitored during the numerical simulation.

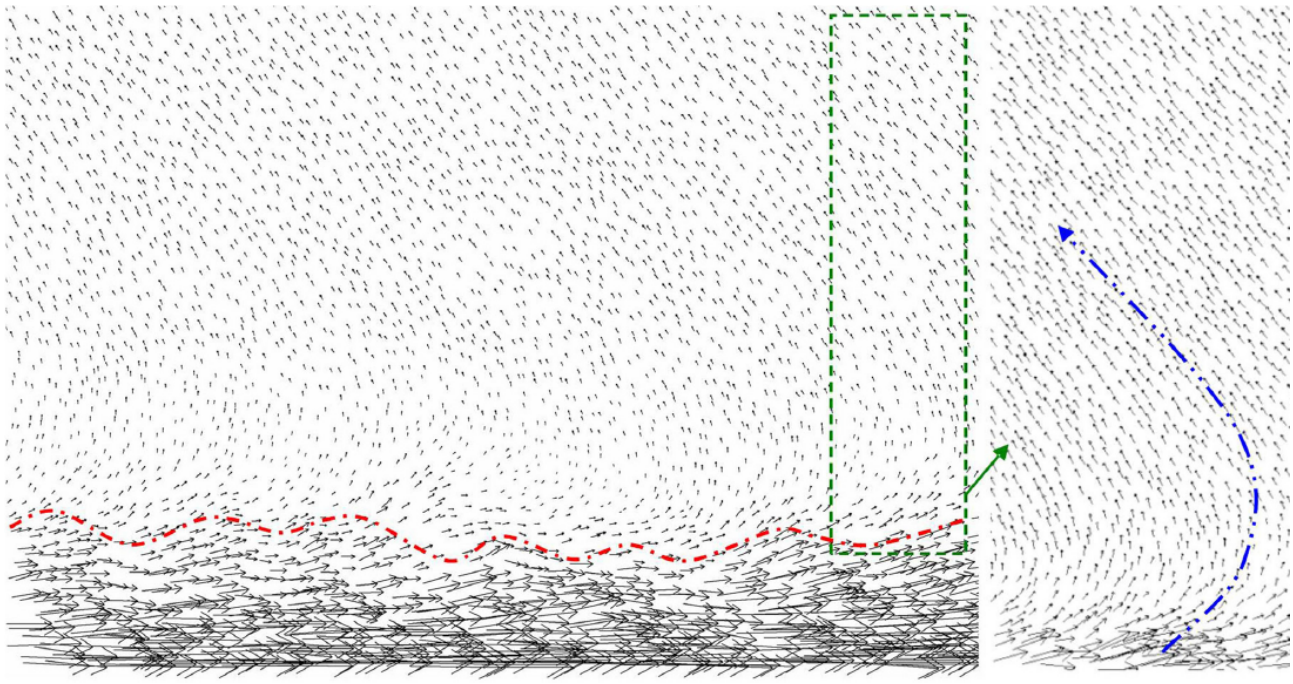

Figure 7: A simulation results of the particle displacement (as vectors) in vicinity of soil-structure interface at a horizontal displacement of 12 mm (**Gu et al., 2017**)

6. Conclusions

The Discrete Element Method (DEM) has proven to be an invaluable tool in both mining and geotechnical engineering, providing deep insights into the behaviour of granular materials and the complex interactions within particle systems. In mining, DEM has enabled accurate modelling of processes such as crushing, grinding and material handling, leading to significant improvements in process efficiency, cost reduction, and operational safety. The ability to simulate rock fracture mechanics and stress distribution within mining structures has enhanced planning and risk management.

In geotechnical engineering, DEM has contributed to a better understanding of soil and rock behaviour under various loading conditions, enabling more accurate predictions of slope stability, foundation performance and soil-structure interactions. The application of the method in the simulation of compaction processes and geosynthetic reinforcement has further optimised design and construction practices and ensures greater safety and reliability in geotechnical projects.

The study emphasises the critical importance of selecting appropriate contact models and accurately calibrating input parameters to achieve reliable simulation results. The examples given illustrate the practical benefits of DEM in optimising design plans and improving operational outcomes in both areas. It is expected that future research and advances in DEM technology will further improve its application and enable even greater accuracy and efficiency in mining and geotechnical projects.

7. References

1. Aftabi, M., Ahangari, K. & Dehghan, A. N. (2023): Investigating the effect of layering and schistosity on the mechanical behavior of rocks using the discrete element method. Rudarsko-geološko-naftni zbornik, 38 (5), 41-48. https://doi.org/10.17794/rgn.2023.5.4
2. Bono, J. P. de, & McDowell, G. R. (2022): Discrete element modelling of normal compression of clay. Journal of the Mechanics and Physics of Solids, 162, 104847. https://doi.org/10.1016/j.jmps.2022.104847
3. Carr, M. J., Roessler, T., Robinson, P. W., Otto, H., Richter, C., Katterfeld, A., & Wheeler, C. A. (2023): Calibration procedure of Discrete Element Method (DEM) parameters for wet and

sticky bulk materials. Powder Technology, 429, 118919. https://doi.org/10.1016/j.powtec.2023.118919
4. Chehreghani, S., Sola, H. A., Chakeri, H. (2022): Stability analysis and support system design of Angouran underground mine batching room. Mining of Mineral Deposits, 16(1), 92-100. https://doi.org/10.33271/mining16.01.092
5. Coetzee, C. J., Nel, R. G. (2014): Calibration of discrete element properties and the modelling of packed rock beds. Powder Technology, 264, 332–342. https://doi.org/10.1016/j.powtec.2014.05.063
6. Doroszuk, B., & Król, R. (2022): Industry Scale Optimization: Hammer Crusher and DEM Simulations, Minerals, 12(2). https://doi.org/10.3390/min12020244
7. Flores-Johnson, E. A., Wang, S., Maggi, F. et al. (2016): Discrete element simulation of dynamic behaviour of partially saturated sand. International Journal of Mechanics and Materials in Design, 12, 495–507. https://doi.org/10.1007/s10999-016-9350-5
8. Gu, X., Chen, Y., & Huang, M. (2017): Critical state shear behavior of the soil-structure interface determined by discrete element modeling. Particuology, 35, 68–77. https://doi.org/10.1016/j.partic.2017.02.002
9. Herceg, K., Minažek, K., Domitrović, D., & Horvat, I. (2023): Pullout Behavior of a Polymeric Strap in Compacted Dry Granular Material. Applied Sciences, 13(15). https://doi.org/10.3390/app13158606
10. Hertz, H. (1881): On the contact of elastic solids. Journal für die reine und angewandte Mathematik, 92 (156-171).
11. Ilic, D. (2013) Bulk solid interactions in belt conveying systems (Doctoral dissertation, The University of Newcastle).
12. Klanfar, M., Korman, T., Domitrović, D., & Herceg, V. (2021): Testing the novel method for angle of repose measurement based on area-weighted average slope of a triangular mesh. Powder Technology, 387, 396–405. https://doi.org/10.1016/j.powtec.2021.04.051
13. Miao, C., Zheng, J., Zhang, R., & Cui, L. (2017): DEM modeling of pullout behavior of geogrid reinforced ballast: The effect of particle shape. Computers and Geotechnics, 81, 249–261. https://doi.org/10.1016/j.compgeo.2016.08.028
14. Morrissey, J. P. (2013): Discrete Element Modelling of Iron Ore Pellets to Include the Effects of Moisture and Fines. PhD Thesis, The University of Edinburgh, Scotland, United Kingdom.
15. Munir, H. A., Zakaria, A., Ponniran, A., Rahman, M. T. A., & Marimuthu, T. (2022): Investigation of The Dynamic Deflection of Conveyor Belts Via Simulation Modelling Methods on Idler Factor. Journal of Physics: Conference Series, 2312(1), 012027. https://doi.org/10.1088/1742-6596/2312/1/012027
16. Rathbone, D., Marigo, M., Dini, D., & van Wachem, B. (2015): An accurate force–displacement law for the modelling of elastic–plastic contacts in discrete element simulations. Powder Technology, 282, 2–9. https://doi.org/10.1016/j.powtec.2014.12.055
17. Roessler, T., Richter, C., Katterfeld, A., & Will, F. (2019): Development of a standard calibration procedure for the DEM parameters of cohesionless bulk materials – part I: Solving the problem of ambiguous parameter combinations. Powder Technology, 343, 803–812. https://doi.org/10.1016/j.powtec.2018.11.034
18. Salkynov, A., Rymkulova, A., Suimbayeva, A., Zeitinova, S. (2023): Research into deformation processes in the rock mass surrounding the stoping face when mining sloping ore deposits. Mining of Mineral Deposits: 17(2), 82-90. https://doi.org/10.33271/mining17.02.082
19. Thakur, S. C., Ooi, J. Y., & Ahmadian, H. (2016): Scaling of discrete element model parameters for cohesionless and cohesive solid. Powder Technology, 293, 130–137. https://doi.org/10.1016/j.powtec.2015.05.051

SAŽETAK

Razvoj i primjena metode diskretnih elemenata u rudarstvu i geotehničkom inženjerstvu

Primjena numeričkih metoda, posebno metode diskretnih elemenata (DEM), značajno je unaprijedila razumijevanje složenog mehaničkog ponašanja materijala u rudarstvu i geotehničkom inženjerstvu. DEM, simulira sustave čestica i omogućava detaljnu analizu interakcija između

pojedinih čestica, što je ključno za predviđanje ponašanja granuliranih materijala poput tla, stijena i drugih sustava diskretnih elemenata. Ova rad daje pregled različitih primjena DEM-a u rudarstvu, uključujući modeliranje procesa drobljenja, transporta i skladištenja rudnih materijala, s ciljem optimizacije procesa, smanjenja troškova i povećane sigurnosti. U geotehničkom inženjerstvu, DEM se koristi za analizu stabilnosti kosina, temelja, potpornih struktura i interakcija tla i struktura, kako bi se omogućila točna predviđanja ponašanja tla i stijena na prirodne i antropogene utjecaje. U radu je posebno naglašena važnost odabira odgovarajućih kontaktnih modela i ulaznih parametara u DEM simulacijama te potreba za kalibracijskim postupcima kako bi se osigurale točne simulacije. Primjeri DEM simulacija u rudarskoj i geotehničkoj praksi ukazuje na uspješnu primjenu metode u optimizaciji dizajna, poboljšanju učinkovitosti i povećanoj sigurnosti.

Ključne riječi: simulacija metodom diskretnih elemenata (DEM); rudarstvo; geotehničko inženjerstvo

Author's contribution

Dubravko Domitrović (1) (Associate professor) preformed conceptualization, methodology, data collection writing - original draft. **Tomislav Korman (2) (**Associate professor) preformed visualization, data collection, writing - original draft. **Mario Klanfar (3) (**Associate professor) preformed data collection, writing - original draft. **Vjekoslav Herceg (4) (**Senior assistant) preformed data collection**,** writing - original draft.

5th Croatian geomathematical congress
UDC: 622.8; category: original scientific paper

Numerical model of MSW landfill stability after change in waste composition

Helena Vučenović[1]; Želimir Veinović [2]; Domitrović Dubravko[3], Karolina Herceg[4]
[1] University of Zagreb, Faculty of Mining, Geology and Petroleum Engineering, Pierottijeva 6, Zagreb, Croatia, orcid.org/0000-0001-6512-0669
[2] University of Zagreb, Faculty of Mining, Geology and Petroleum Engineering, Pierottijeva 6, Zagreb, Croatia, orcid.org/0000-0002-1572-2191
[3] University of Zagreb, Faculty of Mining, Geology and Petroleum Engineering, Pierottijeva 6, Zagreb, Croatia, orcid.org/0000-0001-9861-8471
[4] University of Zagreb, Faculty of Mining, Geology and Petroleum Engineering, Pierottijeva 6, Zagreb, Croatia, orcid.org/0000-0002-3450-4296
Corresponding author: helena.vucenovic@rgn.unizg.hr

Abstract

Municipal waste management in Europe has evolved over the last two decades. Today, more emphasis is placed on prevention and recycling than on disposal. Despite increasing awareness, progress and new methods in waste management, the total amount of waste continues to increase. For this reason, there will continue to be a need for landfilling. Landfills are designed, constructed, managed and monitored to ensure compliance with government regulations. They are also designed to protect the environment from contaminants that may be present during and years after disposal. For this reason, the waste is deposited in the landfill between the upper and lower protective layers, which fulfil the function of sealing, drainage, separation and protection. The stability of the landfill is influenced by many factors, but the shear strength parameters play the biggest role. Considering the fact that the waste is a heterogeneous material and occupies the largest volume of the landfill, the shear strength parameters of the waste are of utmost importance for the stability of the landfill. In order to develop a numerical model of the landfill, suitable strength parameters for the waste as well as parameters for other layers in the landfill must be selected in the first place. In recent years, the management policy in Croatia has been gradually adapted to the European directives, which changes the composition of the waste. The components paper, plastic, glass and biowaste are separated from the waste, which significantly affects the density, moisture and granulometric composition of the landfilled waste. All of this affects the stability and deformation of the landfill body itself and the stability of the protective layer system. In this paper, a numerical model of the landfill was developed and the changes in the stability of the landfill body due to changes in the composition of the municipal waste were analysed

Keywords: landfill, stability, shear strength parameters, waste composition

1. Introduction

No matter which principles, methods and technologies are, and will be, used for municipal solid waste (MSW) management, landfills will remain a necessary part. Though the current, modern waste management, requires minimization of the amount of mixed waste which is to be disposed at landfills (**Puntarić et al., 2023**), and no matter how intensive 3R principle (*reduce, reuse, recycle*) and incineration (e.g.) are used, there will always remain something to be disposed of in some kind of landfill. Intensive separate collection of MSW, done in order to facilitate recycling, will result in a reduction of amounts of MSW which is to be disposed of at landfill, however, separate collection will also affect geomechanical properties of MSW, thus affecting stability of landfill (**Gomes et al., 2013; Singh & Uchimura, 2023**).

One of specific problems related to landfills which were operating before and after a decision of separate collection was made, or intensified, is – how one object constructed with two significantly different materials will perform, and which consequences can be expected? Also, there is always an issue of technology – how will the transition from one material to another be organized in sense of material emplacement? One material is mixed MSW with minimal amount of recyclable components removed, and other is significantly different kind of material with less glass, plastics, metals, and biodegradables. Again, the question is: what will change considering geomechanical properties of the disposed material and the stability of the landfill? To give a proper answer to that question, the reduction of certain waste components must be quantified, and from that either calculated and assessed or measured real changes of geomechanical properties of MSW.

While working on the publication preceding this one (**Vučenović et al., 2024**), which was dealing with the parametric study of stability in landfills due to changes in waste composition, an accident happened at the Zagreb's (capital of the Republic of Croatia) landfill. Likely, but still unconfirmed and unproven, the reason is either change in geomechanical properties of waste material due to intensive separate collection, or unadjusted disposal technology, or high level of leachate. Whether the real reason for landslide occurrence is either one or combination of all above mentioned potential causes, change in the composition of waste related to amounts of certain materials, will definitely change properties of waste being disposed of, and hence the disposal technology is supposed to be adjusted (geometry and high of layers, number of compaction cycles, rate of disposal, etc.).

Prudinec, Zagreb's MSW landfill, was formed in 1965 as an illegal dumpsite, at the location of old gravel and sand exploitation. In 1995 started a remediation of the site which included the preparation of the new disposal surface and the construction of the bottom protective layer system (BPLS). Simultaneously both, the old waste from the original dumpsite and a fresh waste collected at the time in Zagreb, were disposed of at the newly prepared disposal surface (**Budiša et al., 2014**). In 2003 all the existing waste from the dumpsite was dealt with and the disposal of only fresh waste begun.

Separate waste collection in the city of Zagreb intensively begun in 2002 (**Fundurulja, 2009**) and in the period 2002-2018 there was a gradual increase of the separate waste collection of plastics, metals, glass, paper, and textile. According to the "Act on the method of providing the public service of collecting mixed municipal waste and biodegradable municipal waste and services related to public service in the City of Zagreb" (**City of Zagreb, 2018**), from the January 30th, 2018, separate collection of the mixed plastic and metal waste, in yellow bags provided by city, and the compostable materials, in also provided brown biodegradable bags, become mandatory. Paper and container glass were separately collected, but at a smaller intensity, since the 80's. On September 23rd, 2022, a decision was made by the *Zagreb Holding*, city owned company, according to which mixed MSW must be collected in "blue bags" whose purchase price is 2,6 €/10 pcs of 10 l bag; 5,3 €/10 pcs of 20 l bag and 10,6 €/10 pcs of 40 l bag (**Zagreb Holding, 2022**). The intensity of separate collection of paper also increased somewhat with the introduction of a larger number of bins and containers for wastepaper, while the separate collection of waste container glass, textiles and other components carried on in the same manner as previously. The quantities of separated container glass and textile certainly has increased, but in large part due to the increase in the total amount of produced waste in the city of Zagreb (**Puntarić et al., 2023**). Therefore, since the September of 2022 collected and landfilled mixed MSW has a reduced amount of paper, metal, plastics, and compostable (NOT all biodegradable) waste.

Variations in the composition of waste, due to removing compostable materials, plastic and metal, paper and cardboard, reflects in changes in cohesion, angle of the internal friction, density, water content and some other parameters (**Cho et al., 2011; Gomes et al., 2013; Singh & Uchimura, 2023**). For that reason, this paper gives different solutions of numerical models of

sliding a MSW landfill slopes due to a change in waste composition, and hence changes in geomechanical properties.

2. The MSW landfill site Prudinec

Landfills are constructions which are designed as to contain MSW and products of its decomposition, with an option of controlled release of landfill gases and leachate through the system for their treatment and management. In that way the environment is protected from the harmful effects of materials contained in landfill (Vucenovic et al., 2017). The engineered protective system of landfill include:

- surface protective layer system: SPLS (top cover);
- bottom protective layer system: BPLS (bottom screen);
- gas extraction and management system and
- leachate removal and management system.

The Prudinec landfill (colloquially known as the "Jakuševec landfill") is situated in the south-eastern part of the City of Zagreb, on the southern bank of the Sava river, not far from the ornithological reserve Savica, system of lakes artificially made as the as a result of gravel exploitation nearby the Sava River. In 1965 the dumpsite Jakuševec was also constructed in one of depressions made by gravel excavation. Therefore, not only that the dumpsite and later landfill is located nearby the river but in the river alluvium, with the direct contact of Zagreb's aquifer. From 1965 till 1995 waste was disposed of inadequately and without protective layer systems. Work on the reclamation of the dumpsite began in 1995 with the construction of "cell 1" (**Fig. 1**), prepared surface in the immediate vicinity of the dumpsite where old waste was disposed of. The remediation was completed in 2003 with the construction of cell 5 and the transfer of the remaining old waste to a new disposal surface. In all, 7 000 000 m^3 of old waste was relocated. The fresh waste was deposited in cells 4 and 5, and today the waste is being deposited in the cell 6. The average volumetric weight of the waste of 0.8 t/m^3 is assumed (**Vukelić et al. 2004; Budiša et al., 2014; Vujević et al., 2014**).

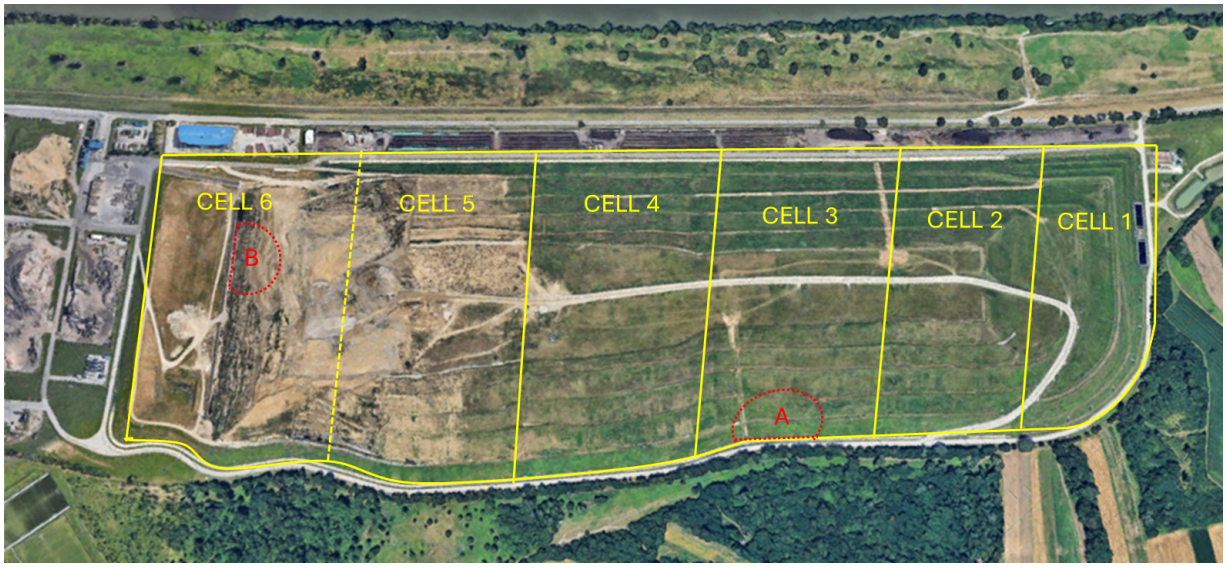

Figure 1: Satellite image of the Prudinec landfill with disposal cells (1-6), and failures (A & B) marked (Google maps, 2024).

Today, the cell No. 6 is being filled, and the size (area) of cells 1-6 vary between 6 and 9 ha. The footprint of the landfill is 1400 m and a width of approx. 450 m. The lower level of the landfill is on average 109.00 m above sea level, and the landfill body was designed for a final height of approx. 155.00 m above sea level, with the actual height of 46 m, and slopes with gradient 1:2.85.

Since the Prudinec landfill is located in the alluvium of the Sava River, the subsoil at the site of the landfill consists of gravel-sand mixtures with the gravel prevailing. When considering the profile of the site, with depth sand and sand-clay mixtures prevail. However, the very material in which the landfill is placed represents aquifer which extends from, practically, the surface to a depth up to 100 metres (**Nakić, 2003**). In the area of the Prudinec landfill, groundwater level is at 3 m. Apart from the mentioned issues, the fact that the landfill is within the city limits, nearest houses are located merely 400 m from the landfill, it is obvious that the location of the landfill is at least unfavourable.

2.1. Landfill protection layers

To form the landfill during the remediation, add to stability of the construction and help the installation of the protective layers, an 8 m high berm was constructed at the foot of the disposal cells. The BPL consists of 1 m compacted clay liner, 2,5 mm thick HDPE geomembrane (protected by geotextile), 0,5 m thick leachate drainage system and filter layer made of geotextile. Compacted clay liner is made with highly plastic clay with average values of w_L=55%, I_p=30% and w_{opt}=20% (**Vukelić et al., 2004**).

The SPLS consists of gas drain composite, geosynthetic clay liner (GCL), 2,5 mm HDPE geomembrane, water drainage composite for the drainage of precipitation water, 0.85 m thick protective soil layer (protection from the freezing of lower protective layers) and 0,15 m thick recultivating layer made of humus. The geomembrane is only used in the top part of the landfill's SPLS, on the slopes only GCL is used as a liner.

2.2. Historical instabilities

In August 2002, a localised slope failure on the south side of cell 3 occurred (Fig. 1). Failure happened on the contact between SPLS and the berm. The estimated affected area of the landfill was approx. 52 m long and 140 m wide, and the amount of the displaced waste was 100 000 m^3 (**Vukelić et al., 2004**)

Field investigation showed that the content of materials in waste that was affected did not differ from the waste deposited elsewhere in the landfill (**Vukelić et al., 2004**) it was a mixture of old municipal waste, soil and construction waste. It is important to point out that the leachate level was at the 0,7-11,5 m, measured from the top of the BPLS (**Vukelić et al., 2004**).

The second slope failure was observed in 2023 on the north side of cell 6, at the very place of current deposition of waste, after a brief but intense period of rain. This failure was more intensive than the first one, and hence received much intensive media coverage.

If "usual" reasons for slope failures at landfills are saturation of the waste material or protective layers materials with rainwater or leachate, next group of reasons is definitely related to geomechanical properties of waste and protective materials, e.g. poor compaction or composition related poor geomechanical properties or the geometry of landfill (the angle of the slope).

2.3. The impact of waste composition on landfill stability

The stability of a landfill slope depends on several factors, including geotechnical characteristics, slope geometry, hydrogeology, load distribution, sealing systems, monitoring and

maintenance. In addition to the main causes of instability, climate change also influences landfill stability of landfills through changes in precipitation patterns, soil behaviour, erosion and sea level rise. In addition to the aforementioned influences, it is important to point out that the stability of the slope is significantly influenced by the properties of the waste material itself, namely: the composition of the waste (Singh & Uchimura, 2023; Cho et al. 2011; Jahanfar et al., 2017; Ivšić et al., 2004).As it was mentioned in the Introduction, the change of MSW that is being disposed of at the Prudinec, occurred in recent years as a result of the introduction of a new waste separation and disposal policy conditioned by European Commission. Change in the composition of wase affected the unit weight of waste, and thusly shear strength parameters of waste (cohesion and internal friction angle). These changes certainly had impact on the stability of the landfill slope, which was proved by research and numerical model presented in this paper.

As it was mentioned previously, the changes in waste management system in Zagreb (separate waste collection) began with implementation in 2002 and gradually increased until 2018. For this reason, 2018 was considered a turning point when the composition of waste began to change significantly.

The quantity of individual components e.g. paper, glass, plastic and biowaste, previously made up a large proportion of mixed waste which was disposed of in the landfill, however, the composition gradually changed to finally become significantly different from the one at the beginning of the disposal. It is therefore logical that the majority of newly disposed waste consists of kitchen waste (non-compostable biodegradable materials), which is actually processed food waste. The term processed food waste refers to all waste that is produced during the preparation of food and should not be disposed of in organic waste. This includes the remains of thermally processed food, meat, fish, bones, skin, dairy products, oils and fats, etc. Due to this, one can assume that the geomechanical parameters of newly disposed of waste would change the stability of landfill, especially if the geometry, disposal technology and control did not change as the composition of waste changed.

For the numerical analysis of stability, it was necessary to acquire parameters of the BPLS layers and the waste. All parameters were taken from previous investigations (**Vukelić et al., 2004; Kovačević Zelić et al. 2002.; Petrović et al. 2015; Cho et al. 2011**). For the subsoil, liners and drainage material, parameters are known and used in various previous analyses, but the parameters for municipal waste are in a very wide range, especially since the composition changed with time. The fact that the materials in MSW are continuously degrading and their parameters are being changed with time due to various chemical and biological processes, while the properties of certain materials (smaller amount in the mixture) do not change (**Štefanák & Chalmovský 2022; Machado et al., 2002**). For this reason, it was necessary to use parameters corresponding to a specific composition of the waste. Therefore, from several studies acquire parameters of the BPLS layers and the waste. All parameters were taken from previous investigations of the change in strength parameters depending on the waste material composition (**Cho et al. 2011; Singh 2023; Machado et al. 2002**) the parameters corresponding to the composition of the waste in Prudinec landfill, over a certain period of time were deduced and applied to numerical model.

3. Numerical model

The numerical analysis of the landfill stability was carried out using the finite element method. Plane strain models were created with Plaxis 2D 2024. Fifteen-noded triangular finite elements were used. The slope is analysed as a plane strain model. Displacements and strains in the z direction are assumed to be zero. The mathematical model was created with dimensions of 306 m width and 77 m height. The geometry of the landfill is simplified and consists of a subsoil, a protective layer, a drainage layer, dyke on the edge of the waste layer and the waste layer (**Figure**

2). The standard fixings are used to define the boundary conditions or are considered as standard boundary conditions. A medium coarse grain size was selected for the mesh generation.

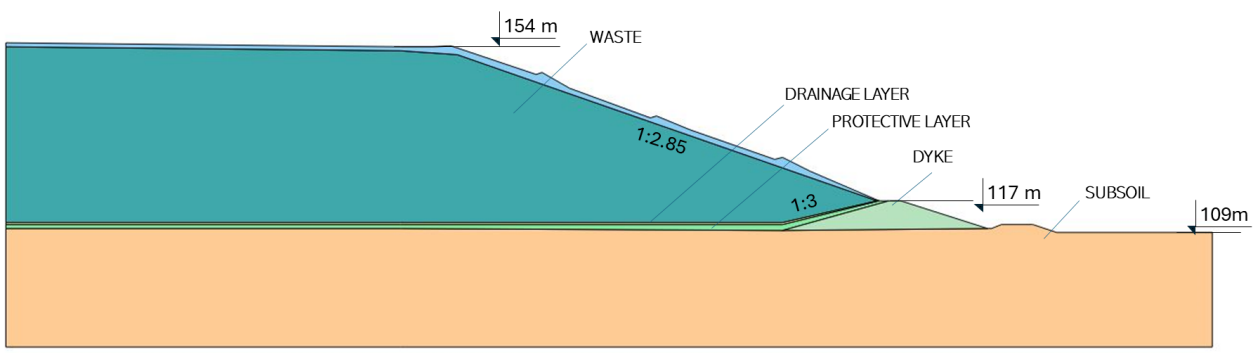

Figure 2: Prudinec landfill cross-section

The properties of the soil and the waste material were modelled using the Mohr-Coulomb model and stored in the material data set. In order to determine the influence of the proportion of processed food waste in the waste layer, the analysis was carried out for three proportions of processed food waste in the municipal waste: 10%, 30% and 60%.

The input parameters for the waste were obtained from previous experimental studies (**Cho et al. 2011; Ivšić et al. 2004**). The material properties of the municipal solid waste layers were selected based on the results of extensive statistical analyses of the strength parameters of MSW from studies describing the Prudinec landfill (**Petrović et al. 2015, Kovačević Zelić et al. 2002, Vukelić et al. 2004**). The geotechnical parameters are listed in **Table 1**.

Table 1: Geotechnical parameters

Parameter	Unit weight γ (kN/m^3)	Friction angle φ (°)	Cohesion c (kN/m^2)	Young's modulus E' (kN/m^2)	Poisson's ratio ν' -
Subsoil	18	32	10	40000	0.33
Drainage layer	18	30	0.3	30000	0.3
Sealing layer	19	21	24	10000	0.3
Dyke	19	24	15	12000	0.3
Processed food waste 10%	8	33	5	3000	0.33
Processed food waste 30%	9	26	6	2500	0.33
Processed food waste 60%	10	17	7	2500	0.33

The calculation was carried out in stages. In the initial phase all existing layers are defined, in the first phase plastic analysis is defined and in the second phase the safety analysis begins. In the Safety approach the shear strength parameters *tan φ* and *c* of the soil as well as the tensile strength are successively reduced until failure of the structure occurs. If that is the case, the factor of safety is given by **Eq. 1**:

$$SF = \frac{\tau_f}{\tau} \quad (1)$$

Where are:

SF - Safety factor

τ_f – available strength (kN/m^2),

τ – strength at failure (kN/m^2),

The principal results of a Safety calculation are the failure mechanism and the corresponding ΣM_{sf}, which is the safety factor (**Plaxis, 2020**).

4. Results of numerical analysis

In the stability analysis, the results are presented in graphical and numerical form. The graphical form is a slip surface, which is selected as the critical slip surface, and indicates the smallest safety factor, which is determined numerically from the previously mentioned expression.

The numerical analysis was performed three times The same model with the corresponding layers and parameters was used for each individual calculation, whereby the layer with the municipal waste was replaced by a different proportion of processed food waste. Three cases were modelled with 10%, 30% and 60% of processed food waste in the composition of municipal waste (**Figure 3**).

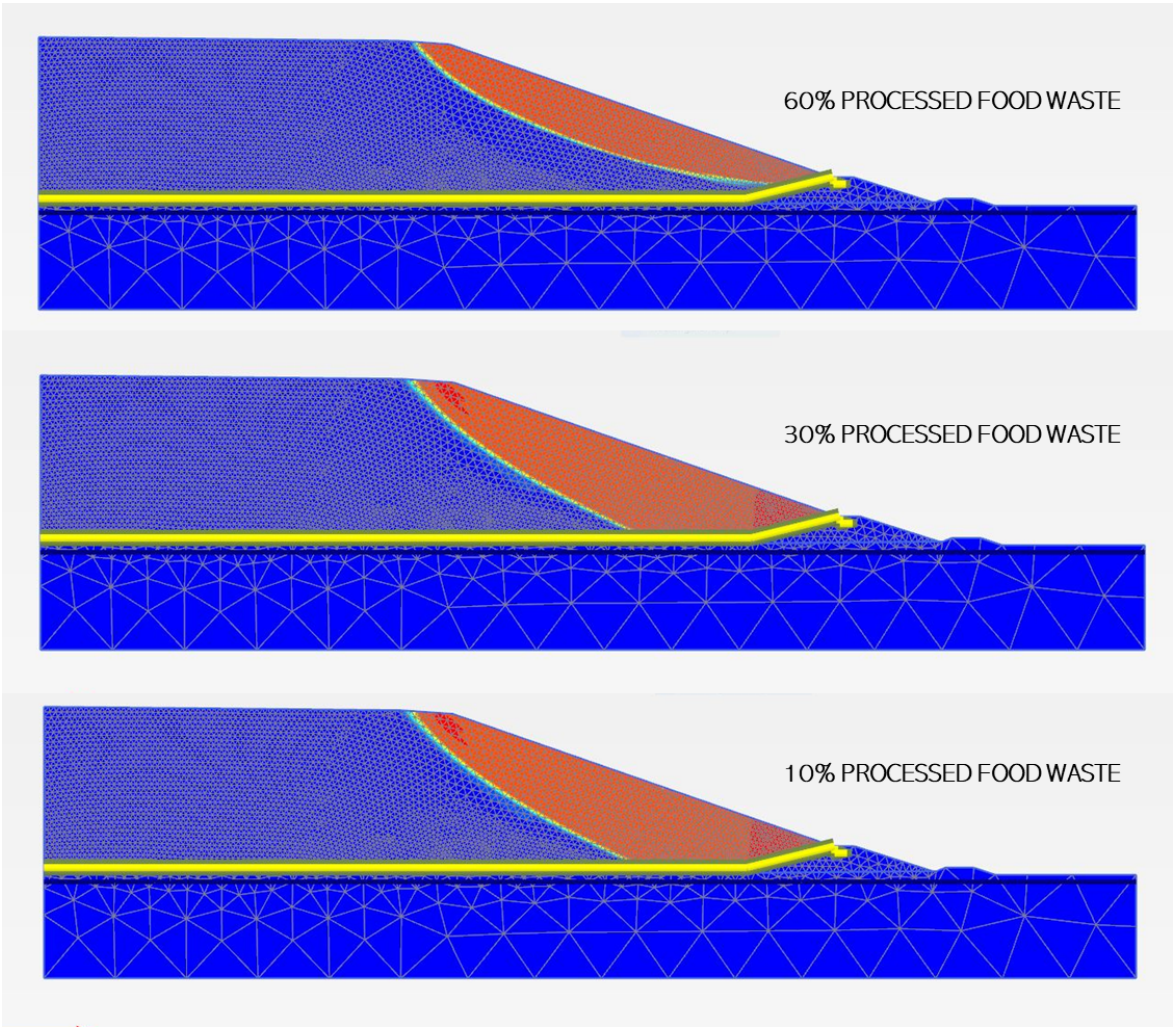

Figure 3: Failure planes for different amount of processed food– 10%, 30% and 60% (from PLAXIS software)

The results of the numerical analysis show that as the proportion of processed food waste increases, the safety factor decreases and the slip surface is shallower, as shown in **Figure 4**.

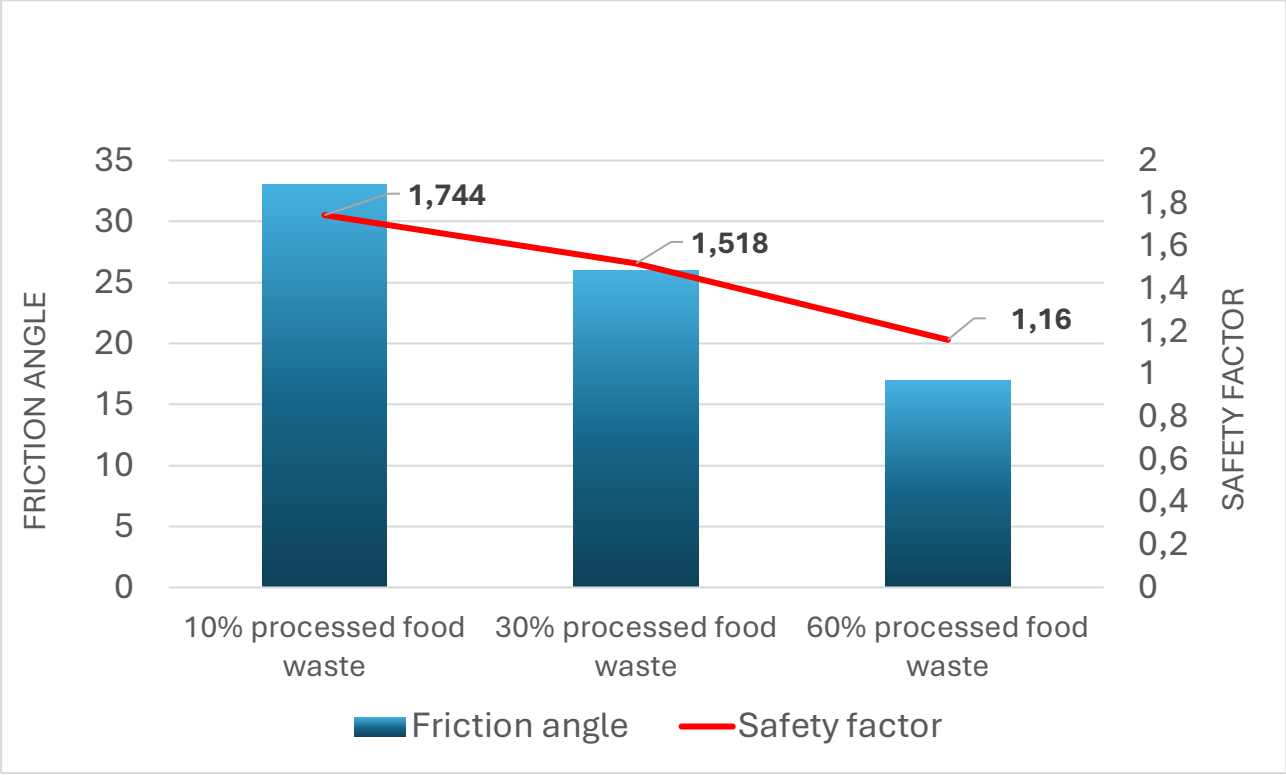

Figure 4: Change in the factor of safety due to the change in the proportion of the processed foodwaste and the friction angle of the waste

In the model in which the waste layer contains a low proportion of kitchen waste, the layers in the lower sealing layer have a greater influence and the sliding surface occurs mainly at the contact points of these layers. For waste with a higher proportion of processed food waste, the probability of a slip surface forming in the landfill body itself is higher.

5. Conclusions

The stability of municipal solid waste landfills depends largely on the mechanical parameters of the waste and the protective layers. The mechanical properties of the waste, in particular the internal friction angle and cohesion, depend on its composition. These parameters vary greatly and change over time as the waste ages. For this reason, the numerical analysis of the slope stability of the landfill requires a careful selection of parameters.

With the change in waste management policy over the last two decades, the composition of waste has also gradually changed. Waste with the largest proportion of plastic and paper has now been replaced by waste with the largest proportion of processed food waste. Since paper and plastic, due to their fibrous composition, fulfilled the function of reinforcement, the composition of today's waste has changed considerably.

The results of the numerical analysis carried out in Plaxis show that the change in the composition of the waste significantly affects the reduction of the safety factor and therefore the stability of the landfill slope. In order to select the parameters that define the model, it is important to continuously collect data on the composition of the waste as well as research results from

measurements of waste samples at landfills. It can be concluded that the selection of the relevant waste parameters and the protective layer system is very important when creating a mathematical model for assessing the overall safety of the landfill.

This paper also shows how a change in waste management policy can affect the change in strength parameters, which ultimately affects the stability of the landfill slope. For these reasons, it is particularly important to continuously collect and monitor direct data and take appropriate measurements at landfill sites in order to recognise changes that may result in undesirable consequences.

6. References

1. Budiša, M., Burela, S., Šeparović, M., Končurat, L. (2014): Technical – technological solution of the existing waste disposal facility Prudinec/Jakuševec ECOINA, Zagreb, Croatia, Rep. 1.
2. City of Zagreb (2018): Act on the method of providing the public service of collecting mixed municipal waste and biodegradable municipal waste and services related to public service in the City of Zagreb, 2/2018, Official Act by the City Assembly of the City of Zagreb, Croatia.
3. Cho, Y. M., Ko, J. H., Chi, L., and Townsend, T. G. (2011): "Food waste impact on municipal solid waste angle of internal friction." Waste Manage., 31(1), 26–32.
4. Fundurulja, D. (2009): A combination of tradition and interesting solutions (original title: Spoj tradicije i zanimljivih rješenja, in Croatian). FONDEKO svijet – Naučno popularna revija o prirodi, čovjeku i ekologiji, 29, pp. 23-25.
5. Gomes, C, Lurdes Lopes, M. Venda Oliveira, P. J. (2013): Municipal solid waste shear strength parameters defined through laboratorial and in situ tests, Journal of the Air & Waste Management Association, 63(11), 1352-1368, http://doi.org/10.1080/10962247.2013.813876.
6. Ivšić, T., Petrović, I. i Verić, F. (2004): Overview of parameters for stability analysis on waste disposal sites, Građevinar, 56 (11.).
7. Jahanfar, A.; Gharabaghi, B.; McBean, E.; Dubey, B. (2017): Municipal Solid Waste Slope Stability Modeling: A Probabilistic Approach. Journal of Geotechnical and Geoenvironmental Engineering. 143. http://doi.org/10.1061/(ASCE)GT.1943-5606.0001704.
8. Kovačević-Zelić, B.; Kvasnička, P.; Domitrović, D. (2002): Stability Analysis for the Landfill Jakusevec, Proceedings of the 12TH; Danube-European Conference, Passau, 27-28 May 2002., pp. 503-506
9. Machado S.L., Carvalho M.F., and Vilar O.M. (2002) Constitutive Model for Municipal Solid Waste, Journal of Geotechnical and Geoenvironmental Engineering, Volume 128, Issue 11, https://doi.org/10.1061/(ASCE)1090-0241(2002)128:11(940)
10. Petrović, I; Hip, I; Fredlund, M (2016): Application of continuous normal–lognormal bivariate density functions in a sensitivity analysis of municipal solid waste landfill // Waste management, 55, SI; 141-153 doi:10.1016/j.wasman.2015.11.021
11. PLAXIS (2020): PLAXIS 2D Reference Manual, Bentley Systems International Limited, Dublin.
12. Puntarić, E., Požgaj, Đ., Korica, Ž., Gumhalter Malić, L., Kušević-Vukšić, M., Bulat, V., Vešligaj, G., Krivanek, G. (2023): Report on municipal waste for 2022, Croatian Ministry of Economy and Sustainable Development, Zagreb, Croatia, Rep. 1.
13. Singh. V., Uchimura, T. (2023): Effect of Material Composition on Geotechnical Properties—Study on Synthetic Municipal Solid Waste, Geotechnics, 3, 397-415, https://doi.org/10.3390/geotechnics3020023.
14. Štefaňák, J.; Chalmovský, J. (2022): Assessment of the Landfill Barrier System through Numerical Analysis: Rehabilitation and Expansion of Belgrade Landfill Case Study. Sustainability 2022, 14, 7647. https://doi.org/10.3390/su14137647

15. Vučenović, H., Herceg, K., Domitrović, D., Veinović, Ž. (2024): Parametric study of stability in landfills due to changes in waste composition, Proceedings of the XVIII European Conference On Soil Mechanics and Geotechnical Engineering in Lisbon, Portugal, 26-30 August 2024.
16. Vučenović, H., Domitrović, D. i Kovačević-Zelić, B. (2017): Gas permeability of geosynthetic
17. clay liners. Rudarsko-geološko-naftni zbornik, 32 (1), 7-16. https://doi.org/10.17794/rgn.2017.1.2
18. Vujević, D., Čalopek, M., Novosel, M., Anić Vučinić, A., (2014): Sastav odlagališnog plina na odlagalištu Prudinec/Jakuševec // Environmental engineering = Inženjerstvo okoliša, 1; 33-41.
19. Vukelić, A, Kovačević Zelić, B. and Drnjević, B. (2004): "Landslide at the Jakusevec landfill." Geotechnical Engineering with Geosynthetics, eds. Floss, R., Brau, G., Nussbaumer, M. and Laackmann, K.. München, DGGT, 2004. 87-9
20. Zagreb Holding (2022): Decision on the collection of municipal waste in the center of the city of Zagreb Zagreb holding, Zagreb, Croatia.
21. Zagreb Holding (2014): Waste disposal plan on the cell 5d and 6 Zagreb holding, Zagreb, Croatia.

SAŽETAK

Numerička simulacija odlagališta komunalnog otpada uslijed promjene sastava otpada

Gospodarenje komunalnim otpadom u Europi znatno se razvilo u posljednja dva desetljeća. Međutim danas se veći naglasak stavlja na prevenciju i recikliranje nego na zbrinjavanje otpada. Unatoč sve većoj svijesti, napretku i novim metodama gospodarenja otpadom, ukupna količina otpada i dalje raste. Iz tog razloga će i dalje postojati potreba za odlaganjem otpada. Odlagališta otpada trebala bi biti projektirana, izgrađena, upravljana i nadzirana u skladu sa državnim propisima. Također bi se trebala projektirati kako bi se očuvao okoliš i kako bi se zaštitilo od štetnih utjecaja koja mogu biti prisutna tijekom odlaganja i godinama nakon zatvaranja odlagališta. Zbog toga se otpad na odlagalištu odlaže između gornjeg i donjeg zaštitnog sloja koji ispunjavaju funkciju brtvljenja, odvodnje, filtriranja i zaštite. Na stabilnost odlagališta utječu brojni čimbenici međutim najveću ulogu u tome imaju parametri čvrstoće. Obzirom da je otpad heterogen materijal i da zauzima najveći volumen odlagališta, parametri čvrstoće otpada su od primarne važnosti za stabilnost odlagališta. Za razvijanje numeričkog modela odlagališta primarno je odabrati odgovarajuće parametra čvrstoće za otpad kao i parametre za ostale slojeve na odlagalištu. U Republici Hrvatskoj se proteklih godina politika gospodarenja postupno prilagođava europskim smjernicama, a time se mijenja i sastav otpada. Iz otpada se odvajaju komponente papira, plastike, stakla i biootpada sto bitno utječe na gustoću, vlažnost i granulometrijska sastav odloženog otpada. To sve pak utječe na stabilnost i deformacije samog tijela odlagališta, kao i na stabilnost sustava zaštitnih slojeva. U ovom radu razrađen je numerički model odlagališta otpada te su analizirane promjene stabilnosti tijela odlagališta uslijed promjene sastava komunalnog otpada.

Ključne riječi: odlagalište, stabilnost kosina, parametri posmične čvrstoće, sastav otpada

Author's contribution

Helena Vučenović (1) (Asisstant professor) preformed conceptualization, methodology, numerical modelling, data collection, writing - original draft. **Želimir Veinović (2) (**Associate professor) preformed methodology, visualization, data collection, writing - original draft. **Dubravko Domitrović (3) (**Associate professor) preformed data collection, visualization, writing - original draft. **Karolina Herceg (4) (**Asisstant professor) preformed data collection**,** numerical modelling - original draft.

5th Croatian geomathematical congress
UDC: 622.3; category: original scientific paper / invited lecture

Modelling of kinetics of lithium sorption onto Mn-based adsorbents obtained via solid state reaction

Ewa Knapik[1*], Grzegorz Rotko[1], Marek Leszek Solecki[1], Katarzyna Chruszcz-Lipska[1]
[1] AGH University of Krakow, Faculty of Drilling, Oil and Gas, Al. Mickiewicza 30, 30-059 Krakow, Poland
Corresponding author: eknapik@agh.edu.pl

Abstract

Lithium recovery from brines (oilfield brines, geothermal waters, mine tailings) is reported as a sustainable method of lithium production. Mn-based adsorbents offer a high sorption capacity hence are often applied for lithium harvesting. In this study two Mn-based adsorbents were prepared via solid state reactions. The morphology of materials were evaluated with a scanning electron microscopy (SEM) confirming the high surface area. After activation the sorbents were contacted with a model brine to test sorption kinetics. Three different kinetic models including the pseudo-first order rate equation, the pseudo-second order rate equation and logistic model were fitted to the experimental data. The results indicate that experiments are well described by the pseudo-second order rate equation. Conditions for sorption to occur are favorable: sorbents reach a high sorption capacity of about 10-12 mg/g in a short time (less than 2 hour). Further research should focus on optimization of sorption conditions (pH, temperature, sorbent regeneration).

Keywords: oilfield brine; lithium recovery; sorption; kinetics; modelling

1. Introduction

The role of lithium is crucial to the development of electromobility, for one Tesla S model with a 70kWh battery about 63 kg of lithium carbonate is needed (**Goonan, 2012**). According to Bloomberg NEF, in 2030 global demand for lithium could reach 2 million tons of Li_2CO_3, or five times its sales in 2021 (**"BloombergNEF Ups Battery Demand Forecast", 2021**). Poland and the European Union are importers of lithium, there are no large and easily accessible deposits of lithium-bearing raw materials in Europe hence lithium was included in the list of critical elements (**Blengini et al., 2020**). Moreover, in Poland there is a significantly demand for lithium is growing due to the development of lithium-ion battery factories. In Lower Silesia two large lithium-ion battery factories are being built: the Korean LG Energy Solution in Kobierzyce and China's GTHR in Prusice. Similar factories are being built in neighboring countries. In view of the above, it is reasonable to start production of lithium from domestic resources. In Poland there are no recognized deposits of lithium-bearing minerals hence it can only be extracted from geothermal waters and formation brines (**Fijałkowska et al. 2008**). Thus, there is a need to develop a technology to recover lithium from brines. This issue strictly relates to another problem occurring in the mining industry - the increasing amount of waste water accompanying mineral extraction. In the final phase of exploitation of the hydrocarbons reservoir, mainly waste brine is extracted (as much as 15 m^3 of water per 1 m^3 of oil) (**Clark and Veil, 2009**). Similarly, in coal mining, about 3 m^3 of brine is extracted per 1 ton of coal mined (**Tsalidis et al., 2022**) and even after the mine is closed, dewatering of the pits is still required. In view of this, the method of brine treatment and management often determines the profitability of the entire project. Study of Miranda et al. (**2022)** estimates profits from recovering valuable resources from produced water in the Permian Basin, USA. Taking into account the composition and volume of produced water the metal revenue per

single well could reach up to 16 000 USD in the case of lithium recovery. Trends in consumption and nominal price of lithium encourages to start new exploitation activities (**Shojaeddini et al. 2024**).

Different approaches were tested for direct lithium recovery from brines including advanced lithium ion-sieves (**Chen et al., 2024**; **Zhang et al., 2024**; **Yu et al., 2022**), membranes **(Guo et al., 2024; Zavahir et al., 2024)**, extractants (**Li et al. 2024**). Among these techniques adsorption is considered as a cost-efficient and easy-to-operate method. Mn-based materials are one of the most tested groups of sorbents for lithium recovery. The selectivity of these sorbents relies on the small ionic radius of lithium ions comparing to other alkali and earth alkali metal cations. The first proposed mechanism of lithium sorption was ion exchange reaction between Li^+ and H^+ according to the reaction **(Shen and Clearfield, 1986)**:

$HMn_2O_4 + Li^+ \rightarrow LiMn_2O_4 + H^+$

Further research of Feng et al. **(1992)** postuled that lithium incorporation into the λ-MnO_2 structure is related to the reduction of Mn(IV) to Mn(III) and release of oxygen. For many Mn-based sorbents the sorption mechanism is mixed especially that during the sorbent synthesis some undesirable impurities such as $LiMn_2O_4$ or Li_2MnO_3 may be produced and complicate sorption course. Mn-based sorbent can be synthesized by a simple solid state reaction (mixing between lithium and manganese salts followed by calcination) and this approach was used in this study as more roboust and less expensive. The alternative way to produce Mn-based materials is a hydrothermal reaction between γ -MnOOH and Li salts. The sorption capacities towards lithium for so obtained materials are high, up to 73 mg/g, but the wet chemistry route requires more advanced equipment and is time-consuming **(Safari et al., 2020)**. The activation and regeneration of all adsorbents requires an acid treatment (H^+ ions replace Li^+ in the crystal structure of sorbent). Li desorption from sorbents is accompanied by Mn loss which reduces the lifetime of the sorbent and poses a challenge in its commercialization **(Gao et al., 2019)**. Our previous study shows that Mn-based sorbents exhibit high sorption capacity and selectivity even in brines of very complex composition **(Knapik et al. 2023).** All large-scale recovery processes are carried out continuously so the kinetics of the sorption plays an important role. The aim of this paper was to study kinetics of lithium sorption from a model brine using previously synthesized sorbents to extend our findings. A novel modified logistic equation was proposed to better describe the experimental data.

2. Method section

2.1. Materials

Manganese(II) acetate tetrahydrate, hydrochloric acid and lithium carbonate were purchased from Vitaya, Poland. NaCl, KCl, $CaCl_2*2H_2O$ and $MgCl_2*2H_2O$ were analytical-grade and delivered by Pol Aura (Morąg, Poland). Standard solutions for AAS were produced by PerkinElmer (Waltham, MA, USA). The tests were performed using an artificial (model) brine containing 220 mg/kg of Li^+, 7.21 wt% of Na^+, 3.0 wt% of Ca^{2+} and 1000 mg/kg of Mg^{2+}.

2.2. Sorbents synthesis via solid state reaction

180 g of $Mn(CH_3COO)_2*4H_2O$ was mixed with 20 g of Li_2CO_3. The resulting mixture was crushed in a mortar and divided into two parts. The first batch of sorbent was calcinated at 400 ^oC for 4 hours (material denoted as MnT1) and the second at 600 ^oC (denoted as MnT2), both of which were then cooled freely (to ambient temperature). Calcination was carried out in a muffle furnace in air in an alumina crucible. The obtained materials were activated which means that Li ions were washed out from the structure using 0.1 M HCl. Delithation procedure was as follows: 5 g of sorbent

was mixed with 500 mL of distilled water and 8 g of 38% HCl. The sorbent dispersion was shaken for 1 h and left to settled down for 24 hours. After this time the solution was decanted and new portion of water and HCl was added. Washing with HCl was repeated 3 times, then the sorbent was washed similarly using 1 L of water. The concentration of Li and Mn was determined in solutions after each washing step to obtain lithium removal ratio and manganese losses. The obtained materials were dried in oven at temperature of 40 °C for 8 hours and used in kinetic study.

2.3. Analytical methods

The concentration of Li and Mn in water solutions was determined by flow injection atomic absorption spectrometry (FI-AAS) using the AAnalyst 100 Atomic Absorption Spectrometer by PerkinElmer. The surface morphology of obtained sorbents was analyzed with a scanning electron microscope (SEM, FEI Quanta FEG 250).

2.4. Kinetics of adsorption

0.5 g of sorbent was contacted with 75 g of modeled brine (alkalized with NaOH to pH=8) in 100 ml plastic container at a given contact time (from 1 minute to 24 hours). The pH was continuously monitored throughout the process. Samples of the sorbent suspension in brine with a volume of about 0.5 ml were centrifuged for 30 s at 2500 rpm and diluted to determine lithium content. Sorption capacity towards lithium at time *t* was calculated according to Eq. (1):

$$q_t = V_s \frac{C_i - C_t}{m_s} \quad (1)$$

where C_i is the initial lithium concentration in brine (mg/L), C_t is the concentration of lithium in brine at given time *t* (mg/L), V_s is the volume of brine used in the experiment (L) and m_s is the mass of sorbent (g), respectively.

2.5. Modeling approach

To describe sorption kinetics three different models were used including the pseudo-first-order equation, logistic equation and the pseudo-second-order equation. The pseudo-first order (PFO) model can be described as follows (**Płaziński and Rudziński 2011**):

$$\frac{dq_t}{dt} = K_1(q_e - q_t) \quad (2)$$

where q_t and q_e are the amount of lithium adsorbed by the sorbent at time *t* and at equilibrium, respectively (mg/g) and K_1 is the rate constant (1/min). The linearized form of Eq. 2 is expressed as:

$$\ln(q_e - q_t) = \ln q_e - K_1 t \quad (3).$$

The PSO model well predicts the initial stage of the sorption before reaching the equilibrium stage (Tan and Hameed 2017).

The pseudo-second-order (PSO) kinetic model can be described as (**Płaziński and Rudziński 2011**):

$$\frac{dq_t}{dt} = K_2(q_e - q_t)^2 \quad (4)$$

where K_2 refers to the adsorption rate constant of PSO kinetic model. This equation can be integrated for initial condition $q_t = 0$ at $t = 0$ and described according to Eq. (5):

$$\frac{t}{q_t} = \frac{1}{K_2 q_e^2} + \frac{t}{q_e} \quad (5).$$

The applicability of PSO and PFO do not explain the mechanism of sorption process and other more realistic models are needed. In our previous study (**Knapik and Stopa 2021**) we developed an new

modified logistic equation that provides more information about interactions in studied systems in the form:

$$\frac{1}{q_t}\frac{dq_t}{dt} = F(t)(q_e - q_t) \quad (6)$$

where *F(t)* is a function of time and can be expressed as:

$$F(t) = \frac{k_{lg}}{t^{\alpha}} \quad (7)$$

where k_{lg} is an adsorption rate constant (-) and α is a constant describing sorbent-sorbate interactions. After the integration with the initial condition $q_{t\to\infty} = q_e$ we obtain:

$$q_t = \frac{q_e}{1+C\cdot exp\left(\frac{-q_e\cdot k_{lg}}{1-\alpha}t^{1-\alpha}\right)} \quad (8)$$

where *C* is the model constant.

All three models were fitted to experimental data using nonlinear regression (the least squares method in the Mathcad software). To assess the goodness of fit the RMSE (root mean square error) and chi^2 statistical criteria were applied. These parameters were calculated according to formulas:

$$RMSE = \sqrt{\frac{1}{N}\sum_{i=1}^{N}\left(q_{e,exp} - q_{e,calc}\right)^2} \quad (9),$$

$$chi^2 = \sum_{i=1}^{N}\frac{\left(q_{e,exp}-q_{e,calc}\right)^2}{q_{e,calc}} \quad (10)$$

where *n* is the data numbers, $q_{e,exp}$ and $q_{e,calc}$ are the empirical and calculated values, respectively.

3. Results and discussion

MnT1 and MnT2 materials differ in the calcination temperature during their synthesis which influences their structural properties. **Table 1** summarizes the process of sorbent synthesis and **Figure 1** shows the surface morphology of both materials.

Table 1: Differences during synthesis and activation of MnT1 and MnT2 sorbents

Material	MnT1	MnT2
Mass after calcination (as wt % of initial mass)	0.40	0.40
Bulk density, g/mL	0.77	0.86
Lithium removal during activation, %	96	91
Manganese losses, wt%	20	17

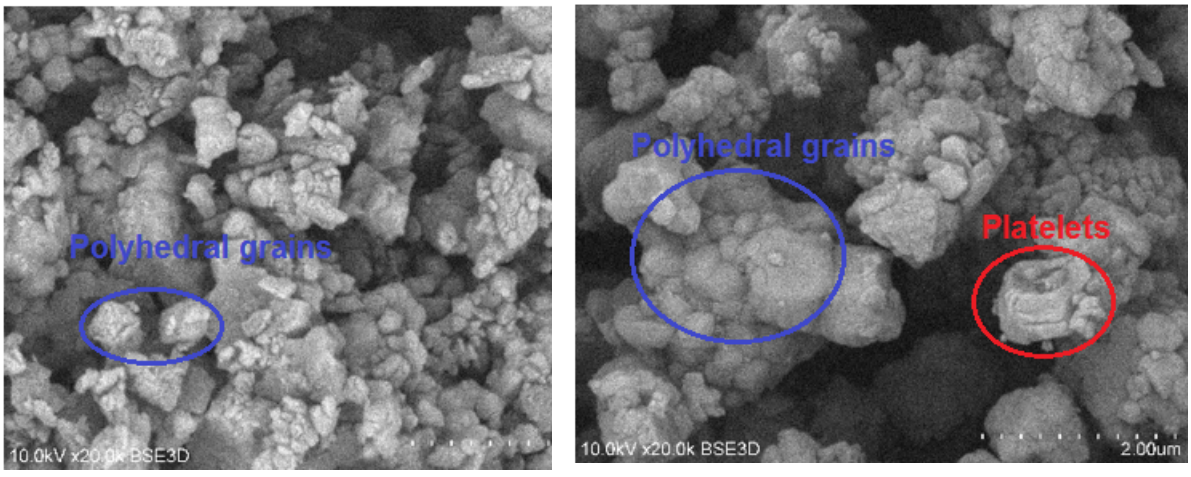

(a) **(b)**

Figure 1: SEM images of a) MnT1 and b) MnT2 materials

For both obtained materials the grain size is no larger than 5 µm, with most of the grains composed of smaller structures. There are both small grains in the form of platelets, strongly anisotropic as well as polyhedral grains typical for sintering process. Larger grains are covered by smaller ones. The surface area for MnT1 is larger than for MnT2, the surface of MnT2 is rougher (more fine grains). The morphology of the materials indicates that they are heterogeneous and may consist of several different crystalline structures. A higher surface area offers more active sites for sorption hence the MnT1 material has better sorption properties than the MnT2 (**Figure 2**).

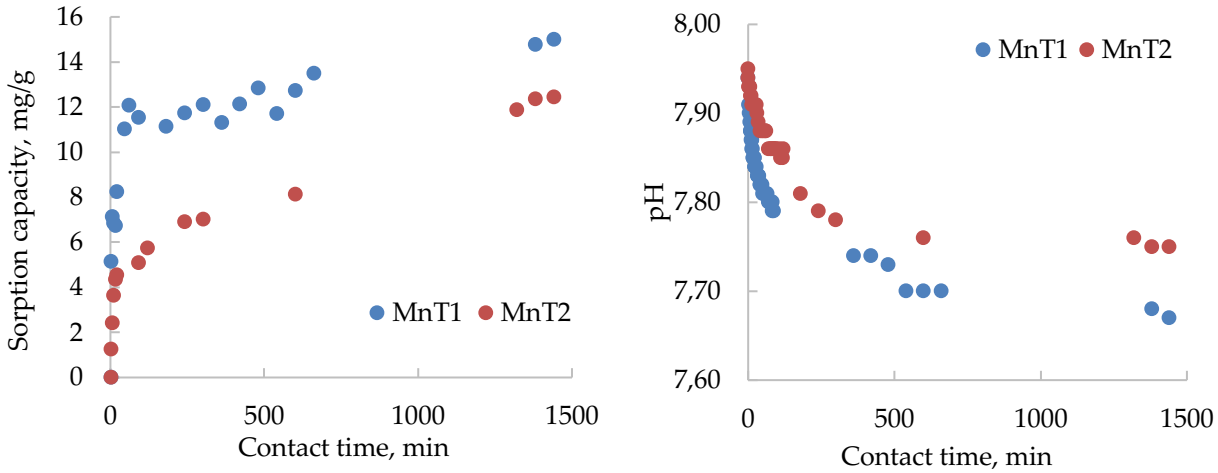

Figure 2: Changes in a) sorption capacity towards lithium and b) pH during lithium recovery from a model brine

The contact time significantly affects the sorption of lithium as shown in **Figure 2**. The MnT1 material is almost twice as effective as material MnT2 (at least during the initial sorption period). Changes in sorption capacity are strictly correlated with changes in pH value which is related to the mechanism of the process itself. Obtained results confirm that adsorbents work on the principle of ion exchange. Lithium, which incorporates into the structure of the sorbent, displaces H^+ ions from it, which causes a decrease in pH. It is an equilibrium exchange, 1 mole of Li^+ ions displaces 1 mole of H^+. The sorption occurs relatively fast, after 2 hours of contact both materials reach about 80% of available capacity. The sorption equilibrium is established after 24 hours of contacting. The maximum sorption loading for lithium is 15.004 and 12.435 mg/g for MnT1 and MnT2 materials, respectively. The obtained materials have better (or at least similar) sorption capacities to other Mn-based materials reported in the literature as shown in **Table 2**. The initial composition of brine and synthesis path of sorbent strongly influence sorption capacity. The direct comparison is difficult because test conditions differ greatly and for each raw material (seawater or brine) sorption needs to be tested individually.

Table 2: Comparison of sorption capacities of selected Mn-based sorbents

Sorbent (name or structure)	Synthesis	Brine	Sorption capacity, mg/g	Reference
MnT1	Solid-state reaction	Artificial brine (Li^+: 220 mg/L)	15.004	this study
MnT2	Solid-state reaction	Artificial brine (Li^+: 220 mg/L)	12.435	this study
λ-MnO_2	Hydrothermal synthesis	Salt lake at pH 8 (Li^+: 20 mg/L)	1	Marthi and Smith, 2019
λ-MnO_2	Solid-state reaction	Spiked seawater (Li^+: 3.5 mg/L)	1.7	Chitrakar et al., 1990
$H_{1.6}Mn_{1.6}O_4$	Hydrothermal synthesis/calcination	LiCl solution (Li^+: 150 mg/L)	6.22	Herrmann et al., 2022
$Li_{1.6}Mn_{1.6}O_4$	Sol–gel, hydrothermal and heat treatment	Seawater (Li^+: 6.08 mg/L)	10.05	Liu et al., 2015
$Li_{1.5}Mn_2O_4$	Hydrothermal reaction	Artificial seawater (Li^+: 10 mg/L)	15.3	Kitajou et al., 2003
$Li_{1.33}Fe_xMn_{1.67-x}O_4$	Solid-state reaction	Salt lake brine from the Salar de Uyuni, Bolivia (Li^+: 1630 mg/L) at pH 7.2	28	Chitrakar et al., 2014

Figure 3 and **Table 3** summarize the fitting of kinetic models to experimental data.

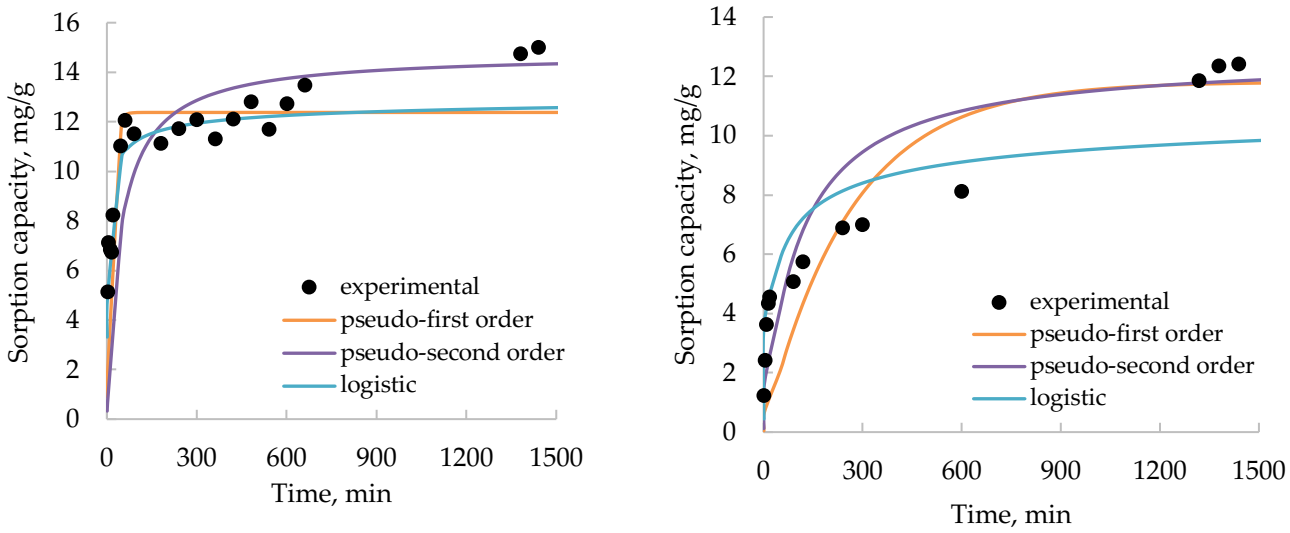

Figure 3: Fitting of kinetic models to experimental data for a) MnT1 and b) MnT2 materials

Table 3: Kinetic parameters for the recovery of Li from model brine

Model	Parameters	MnT1	MnT2
Pseudo-first order	K_1, 1/min	0.076	0.0038
	q_e, mg/g	12.38	11.811
	chi^2	24.381	114.636
	RSME	1.665	2.087
Pseudo-second order	K_2, g/(mg*min)	0.0015	0.0008
	q_e, mg/g	14.763	12.697
	chi^2	108.409	31.492
	RSME	2.669	1.848
Modified logistic	q_e, mg/g	18.607	13.392
	k_{lg}	0.023	0.086
	C	0.04	0.1
	α	1.098	1.203
	chi^2	1.628	4.866
	RSME	0.911	1.506
Maximum sorption capacity determined experimentally, q_{exp}, mg/g		15.004	12.435

Lower values of the RSME and chi^2 for the PSO model than for the PFO model confirm that the PSO model is more effective when describing the sorption of lithium on the tested sorbents. The maximum sorption capacities predicted by PSO model are consistent with experimental values. Despite the used model the constant rate for MnT1 material are higher than for MnT2 which suggest that sorption is more intense/privileged for the MnT1. The proposed logistic equation offers the best match to experiments based on the lowest chi^2 and RSME values but overestimates maximum sorption capacities. Kinetics favours lithium sorption and high lithium uptake may be achieved under relatively short time of contact which suggest that obtained materials could be applied in real-field lithium production facilities.

4. Conclusions

The mechanism of lithium incorporation into Mn-based sorbents is well-known and current research activities focus on cost-effective and reliable synthesis of these materials. The proposed solid state reaction was successful in obtaining cheap and effective sorbents. Synthesis conditions like calcination temperature influence the sorption properties - the MnT1 material obtained at 400 ^oC was more effective than the MnT2 calcinated at 600 ^oC. The adsorption process complies well with the pseudo-second-order model. The logistic model gives a better fit to the experimental results but it requires fitting of 4 parameters while PSO only 2 and for this reason the PSO model is more useful. Different parameters (like pH, sorption, mixing method) may influence sorption effectiveness and further research should focus on process optimization.

5. References

1. Blengini, G.A., El Latunussa, C., Eynard, U., Torres de Matos, C., Wittmer, D., Georgitzikis, K., Pavel, C., et al. (2020): "Study on the EU's List of Critical Raw Materials . Final Report." Brussels. https://rmis.jrc.ec.europa.eu/uploads/CRM_2020_Report_Final.pdf.
2. "BloombergNEF Ups Battery Demand Forecast." (2021):

https://www.canadianminingjournal.com/news/bloombergnef-ups-battery-demand-forecast/.
3. Chen, Q., Chen, Z., Li, H., and Ni, B.-J. (2024): "Advanced Lithium Ion-Sieves for Sustainable Lithium Recovery from Brines." Sustainable Horizons 9: 100093. https://doi.org/https://doi.org/10.1016/j.horiz.2024.100093.
4. Chitrakar, R., Makita, Y., Ooi, K., Sonoda, A. (2014): Synthesis of iron-doped manganese oxides with an ion-sieve property: lithium adsorption from Bolivian brine. Ind Eng Chem Res 53:3682–3688.
5. Chitrakar, R., Tsuji, M., Abe, M., Hayashi, K. (1990): A Comparative Study of Li+ Uptake by a Variety of Inorganic Ion Exchangers. Bull. Soc. Sea Water Sci. Jpn. Vol, 44 (4).
6. Clark, C.E., and Veil, J.A. (2009): "Produced Water Volumes and Management Practices in the United States. Argonne National Laboratory (ANL), Oak Ridge." https://doi.org/10.2172/1007397.
7. Feng, Q., Miyai, Y., Katoh, H., Ooi, K. (1992): Li+ extraction/insertion with spinel-type lithium manganese oxides. characterization of redox-type and ion-exchange–type sites, Langmuir 8, 1861–1867.
8. Fijałkowska, A., Kurowski, R., and Czaplicka, M. (2008): "Polska Baza Surowcowa Litu w Kontekście Światowych Tendencji Produkcji Węglanu Litu z Solanek i Litonośnych Wód Termalnych." Rudy i Metale Nieżelazne, no. 9: 548–54 (in Polish).
9. Gao, A., Hou, X., Sun, Z., Li, S., Li, H., (2019): Lithium-desorption mechanism in LiMn2O4, Li1.33Mn1.67O4, and Li1.6Mn1.6O4 according to precisely controlled acidtreatment and density funtional theory calculations, J. Mater. Chem. A 7, 20878–20890.
10. Goonan, T.G. (2012): "Lithium Use in Batteries." US Geological Survey Circular, January, 1–22.
11. Guo, L.-P., Guo, Z.-Y., Wang, J., Zhang, P.-P., Huang, Z.-H., and Ji., Z.-Y. (2024): "Flexible Lithium Selective Composite Membrane for Direct Lithium Extraction from High Na/Li Ratio Brine." Journal of Membrane Science 703: 122843. https://doi.org/https://doi.org/10.1016/j.memsci.2024.122843.
12. Herrmann, L., Ehrenberg, H., Graczyk-Zajac, M., Kaymakci, E., Kölbel, T., Kölbel, L., Tübke, J. (2022): Lithium recovery from geothermal brine – an investigation into the desorption of lithium ions using manganese oxide adsorbents. Energy Advances, 1, 877-885.
13. Kitajou, A., Suzuki, T., Nishihama, S., Yoshizuka, K. (2003): Selective recovery of lithium from seawater using a novel MnO2 type adsorbent. Ars Separatoria Acta, 2: 97–106.
14. Knapik, E., Rotko, G., Marszałek, M., and Piotrowski, M. (2023): "Comparative Study on Lithium Recovery with Ion-Selective Adsorbents and Extractants: Results of Multi-Stage Screening Test with the Use of Brine Simulated Solutions with Increasing Complexity." Energies. https://doi.org/10.3390/en16073149.
15. Knapik, E., and Stopa, J. (2021): "Kinetic Modeling of Biosorption for Hydrocarbons Removal from Wastewater Using Modified Logistic Equation." Journal of Geotechnology and Energy 38 (1): 27–34. https://doi.org/https://doi.org/10.7494/jge.2021.38.1.4334.
16. Li, H., Deng, Y., and Chen, J. (2024): "Recovery of Lithium Resources from Salt Lake Brines Using a Novel Low Dissolution Loss Extractant of DEHEHP with FeCl3." Separation and Purification Technology 341: 126779. https://doi.org/https://doi.org/10.1016/j.seppur.2024.126779.
17. Liu, L., Zhang, H., Zhang, Y., Cao, D., Zhao, X. (2015): Lithium extraction from seawater by manganese oxide ion sieve MnO2 0.5H2O. Colloids Surf A, 468: 280–284.
18. Marthi, R., Smith, Y. (2019): Selective recovery of lithium from the great salt lake using lithium manganese oxide-diatomaceous earth composite, Hydrometallurgy 185, 115–125.
19. Miranda, M.A., Ghosh, A., Mahmodi, G., Xie, S., Shaw, M., Kim, S., Krzmarzick, M.J., Lampert, D.J., and Aichele, C.P. (2022): "Treatment and Recovery of High-Value Elements

from Produced Water." Water. https://doi.org/10.3390/w14060880.
20. Płaziński, W., and Rudziński, W. (2011): "Kinetyka Adsorpcji Na Granicy Faz Roztwór/Ciało Stałe. Znaczenie Równań Pseudo-First Order Oraz Pseudo-Second Order." Wiadomości Chemiczne 65 (11–12): 1055–67 (in Polish).
21. Safari, S., Lottermoser B.G., Alessi, D.S., (2020): Metal oxide sorbents for the sustainable recovery of lithium from unconventional resources, Applied Materials Today, Volume 19, 100638. https://doi.org/10.1016/j.apmt.2020.100638.
22. Shen, X.M., Clearfield, A. (1986): Phase transitions and ion exchange behavior of electrolytically prepared manganese dioxide, J. Solid State Chem. 64, 270–282.
23. Shojaeddini, E., Alonso, E., and Nassar, N.T. (2024): "Estimating Price Elasticity of Demand for Mineral Commodities Used in Lithium-Ion Batteries in the Face of Surging Demand." Resources, Conservation and Recycling 207: 107664. https://doi.org/https://doi.org/10.1016/j.resconrec.2024.107664.
24. Tan, K.L., and Hameed, B.H. (2017): "Insight into the Adsorption Kinetics Models for the Removal of Contaminants from Aqueous Solutions." Journal of the Taiwan Institute of Chemical Engineers 74: 25–48. https://doi.org/10.1016/j.jtice.2017.01.024.
25. Tsalidis, G.A., Panteleaki Tourkodimitri, K., Mitko, K., Gzyl, G., Skalny, A., Posada, J.A., and Xevgenos, D. (2022): "Assessing the Environmental Performance of a Novel Coal Mine Brine Treatment Technique: A Case in Poland." Journal of Cleaner Production 358: 131973. https://doi.org/https://doi.org/10.1016/j.jclepro.2022.131973.
26. Yu, H., Naidu, G., Zhang, C., Wang, C., Razmjou, A., Suk Han, D., He, T., and Shon, H. (2022): "Metal-Based Adsorbents for Lithium Recovery from Aqueous Resources." Desalination 539: 115951. https://doi.org/https://doi.org/10.1016/j.desal.2022.115951.
27. Zavahir, S., Sahar Riyaz, N., Elmakki, T., Tariq, H., Ahmad, Z., Chen, Y., Park, H., Ho, Y.-C., Shon, H.K., and Suk Han, D. (2024): "Ion-Imprinted Membranes for Lithium Recovery: A Review." Chemosphere 354: 141674. https://doi.org/https://doi.org/10.1016/j.chemosphere.2024.141674.
28. Zhang, L., Zhang, T., Lu, S., Song, S., Ojeda Galván, H.J., Quintana, M., and Zhao, Y. (2024): "Adsorbents for Lithium Extraction from Salt Lake Brine with High Magnesium/Lithium Ratio: From Structure-Performance Relationship to Industrial Applications." Desalination 579: 117480. https://doi.org/https://doi.org/10.1016/j.desal.2024.117480.

SAŽETAK

Modeliranje kinetike sorpcije litija na temelju manganskih adsorbenata postignutom rekacijom čvrstog stanja

Pridobivanje litija iz otopine (slojne vode, geotermalne vode, rudničke jalovine) smatra se održivom metodom za pridobivanje litija. Adsorbenti temeljeni na manganu imaju visok kapacitet sorpcije te su stoga često primijenjeni kod proizvodnje litija. Ovdje su prikazana dva adsorbenta na temelju mangana dobivena reakcijama čvrstoga stanja. Ocijenjena je morfologija materijala uporabom skenirajućeg elektronskog mikroskopa (SEM-a) na velikoj površini. Sorbenti su nakon aktivacije reagirali s testnom otopinom, a kako bi se testirala kinetika sorpcije. Uporabljena su tri različita kinetička modela: (1) jednadžbe pseudo-prvoga reda, (2) one pseudo-drugoga reda i (3) logistički model. Svi su podešeni prema eksperimentalnim podatcima. Rezultati su ukazali na najveću podudarnost kod uporabe jednadžbi pseudo-drugoga reda. Ocrtani su povoljni uvjeti za sorpciju, tj. sorbenti su u manje od dva sata dosegli visok kapacitet sorpcije od oko 10-12 mg/g. Daljna istraživanja bit će usmjerena na optimizaciju uvjeta sorpcije (pH, temperatura, regeneracija sorbenata).

Ključne riječi: slojna voda; pridobivanje litija; sorpcija; kinetika; modeliranje

Author's contributions

Ewa Knapik (Assistant Professor, PhD) - conceptualization, methodology, software, validation, investigation, resources, data curation, writing - original draft preparation, visualization, supervision, project administration, funding acquisition. **Grzegorz Rotko** (Assistant Professor, PhD) - conceptualization, investigation, writing - original draft preparation, visualization. **Marek Leszek Solecki** (Assistant, MSc.) - validation, writing - original draft preparation, writing - review and editing. **Katarzyna Chruszcz-Lipska** (Assistant Professor, PhD) - investigation, writing - original draft preparation.

Funding

The research leading to these results has received funding from the National Centre for Research and Development (NCBR) in the frame of Project Contract No. LIDER/34/0174/L-12/20/NCBR/2021 under the LEADER Program and AGH University of Krakow subsidy No. 16.16.190.779 (Faculty of Drilling, Oil and Gas, Department of Petroleum Engineering).

5th Croatian geomathematical congress
UDC: 622.1; category: original scientific paper

Statistical analysis and mapping of imaginary coal layer using inverse distance interpolation, simple case study of recommended methods

Ana Ljubić[1]; Mirta Petrović[1]
[1]University of Zagreb, Faculty of Mining, Geology and Petroleum Engineering, Pierottijeva 6, 10000 Zagreb, Croatia
ORCID: Ana Ljubić: 0009-0007-7753-4608; Mirta Petrović: 0009-0006-6131-5905
Corresponding author: mirta.petrovic@rgn.unizg.hr

Abstract

In order to correctly describe the minerals within a deposit for the purpose of exploitation, a large amount of geological data from the selected deposit is required. In the case of underground exploitation, the amount of necessary data increases. This paper describes an imaginary coal seam using both simulated data and primary research findings. The selected coal seam is located underground, making it difficult to get the necessary data. That is why proper spatial analysis of known data is necessary. Statistical methods are applied to measure spatial diversity with the measured samples. Results are described according to the total variant of estimated points or blocks. The methods used in order to observe the distribution of the data are the Shapiro-Wilk, Kolmogorov-Smirnov tests and the QQ diagram. The inverse distance method was used to create the maps. The goal was to obtain reliable and spatial results and show set of methods for fast and reliable representation of 2D maps of deposits, like coal one. All conducted research provided a large amount of data on the mentioned layer, which was successfully described using statistical methods.

Key words: coal seam; normal distribution; null hypothesis; data analysis

1. Introduction

In many geosciences, but specific to mining industry, it is often necessary to collect a large amount of information about the composition and stability of the subsoil. These informations are not easy to obtain because each specific type of work has a need for unique equipment and large number of workforce. Also, underground researches come with high risks and costs. In these conditions, statistical data analysis is of great help, which simplifies research and greatly reduces the time and costs.

This paper describes an imaginary coal seam, with imagined data on depth and size intended only for the purpose of displaying statistical analyses. The described coal seam is located in the settlement of Siverić, which is located 4 kilometers northeast of the town of Drniš, in the municipality of Promina (**Figure 1-1**). The Promina deposits are groups of sedimentary rocks that are named after the mountain in which they are located. They consist of conglomerate, limestone, marl and coal of Eocene-Oligocene age with a high degree of carbonization. It covers an area of 187 km² and is located at a depth of 500 m (**Zupanič & Babić, 2011**).

Precisely this depth of the deposit represents the mentioned obstacles in the research that would be carried out for the purpose of exploitation. That is why it is necessary to reduce the influence of these obstacles. Specifically, by examining the normal distribution of data on the depth of the top and the bottom area of the deposit, it is possible to visualize the shape of the deposit itself. Since that examination will only give informations whether our data is normally distributed, and it is difficult to conclude with the obtained numerical indicators which data in the data set causes a potential deviation from the normal distribution, statistical tools such as variance and standard deviation will also be used for better interpretation. In order to present the analytical results of the mentioned tests in graphic form, the easiest way is to use the mapping method. The chosen method is inverse distance weighting, which is also used for interpolation of a limited number of known data. The objectives of this paper is to determine how much data can be obtained about the

mentioned imaginary coal seam based on limited data, and what methods are best to use for our purposes.

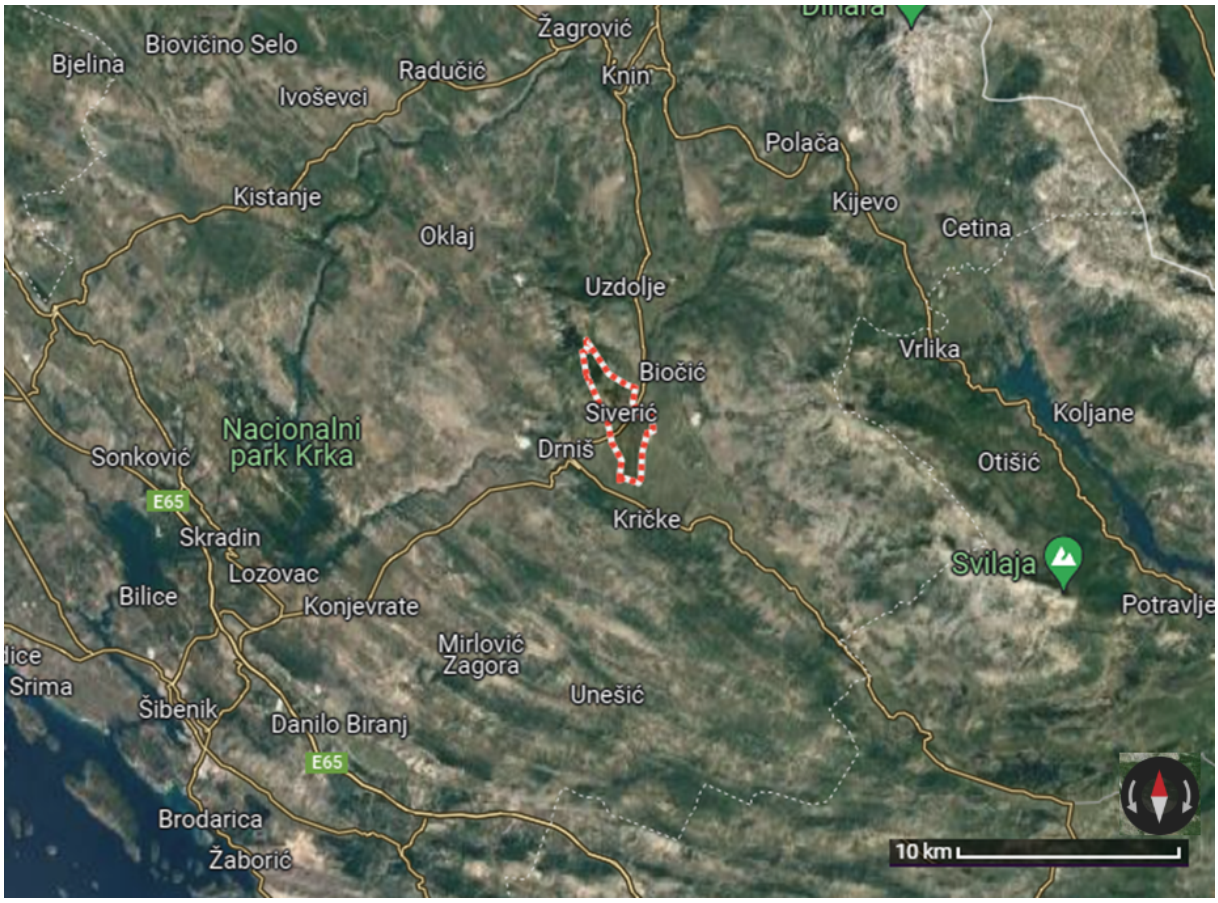

Figure 1-1: Geographical location of the settlement Siverić (**Google Maps**, accessed: 18th December 2023)

2. Materials and methods

To approximate the data of the imaginary coal seam, and to find out whether they are normally distributed, it is necessary to use statistical analysis. In this paper, the collected data were analyzed by Shapiro-Wilk, Kolmogorov-Smirnov test and QQ diagram. For easier data interpretation, they were also described with simple statistical tools.

2.1. Case study

General rule for coal deposition environments is that coal layers usually have a form of a syncline. Based on that, imaginary coal seam in the Siverić settlement is described in the same model. The data on the thickness of the layer i.e., the depth of the top and bottom surfaces are defined by imaginary coal data set, which is shown in **tables 1** and **2**. In said tables it is shown how the thickness of the layers differs and gradually increases approaching the middle of the syncline, where the layer is up to 50 meters thick, while moving away from the centre, towards the edges, the layer becomes thinner. These data sets are imagined based on previous investigations of similar coal deposits in the area, so the x and y variables can be considered as points in the imaginary coordinate system in the area of the Siverić settlement. The entire coal deposit is located approximately 500 meters below the surface, and precisely because of this great depth it is considered that research could be expensive, risky and time-consuming.

2.2. Statistical tools

Some of the statistical tools that form the basis of correct data analysis are the mean value, the minimum and maximum of the measured values, and the median and centiles, which are independent of extreme values and thus provide more detailed information.

Also useful statistical tools are variance and standard deviation which are closely related to each other. Variance can be defined as a measure of the dispersion of measured or random variables, i.e. the average sum of the squares of the deviations of the characteristic values from the arithmetic mean, and was described by **Equation 1**:

$$\sigma^2 = \frac{1}{N}\sum_{i=1}^{N}(x_i - \bar{x})^2 \quad (1)$$

where are:
σ^2 - variance;
x - one of the values from series;
$\bar{x}$ - arithmetic mean;
N - number of values in the series (**Pfaff, 2012**),

while the standard deviation indicates the positive square root of the variance, i.e. the measure of deviation (**URL 1**). Due to this mathematical connection, it can be emphasized that these two statistical tools are closely related.

For data processing, a deep study of the data distribution and statistical parameters are very helpful. The most common and well-known distribution function in statistics is the normal distribution. It is bell-shaped and symmetrical around the ordinate axis, which is shown in **Figure 2-1**. It was described by the function (**Equation 2**):

$$f(x) = \frac{1}{s\sqrt{2\pi}}\exp\left[-\frac{1}{2}\left(\frac{x-\bar{x}}{s^2}\right)^2\right] \text{ for } -\infty < x < \infty \quad (2)$$

where for any „x“ are :
s - standard deviation;
x - measured value;
$\bar{x}$ - mean value.

The function reaches its maximum at a value of 0.4/s, which was valid in the case x=$\bar{x}$, and it was precisely this case that explains the symmetry around the ordinate axis and the bell shape. Due to the central limit axiom, which describes the behavior of a large number of independent measurements and the property that most of the data will be located exactly around x=$\bar{x}$, the use of this type of distribution was frequent. Due to the poor availability of data, the normal distribution approximation was a very useful method in all phases of research (e.g. **Malvić et al., 2015**).

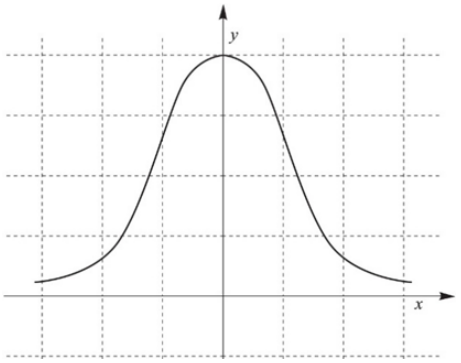

Figure 2-1: Example of normal distribution diagram (**URL 2**)

Three tests, Shapiro-Wilk, Kolmogorov-Smirnov and QQ plot, were used to test normal distribution.

2.3. Examination of the normal distribution

The Shapiro-Wilk test is used for testing normal distribution. It was published by Samuel Sanford Shapiro and Martin Wilk in 1965 (**URL 3**), and was described with **Equation 3**:

$$W = \frac{\left(\sum_{i=1}^{n} a_i x_{(i)}\right)^2}{\sum_{i=1}^{n}(x_i - \bar{x})^2} \quad (3)$$

where are:
W - test statistic
α - level of significance
$x_{(i)}$ - measured values ordered from smallest to largest;
$\bar{x}$ - arithmetic mean.

The null hypothesis of this test was that the data is normally distributed. If the p-values of the test are less than alpha, then we reject the hypothesis and the data are not normally distributed. When the p-value is greater than alpha (α), we do not reject the hypothesis and conclude that the data are normally distributed. In general, there is a possibility that this test will show errors in case of too much data. Therefore, it is necessary to use several different tests for the same data set in order to compare the results. That's how we can consider them more reliable.

An example of the second type of test is the Kolmogorov-Smirnov test (K-S test), which can be defined as a non-parametric test of the equality of one-dimensional probability distributions, and with it we can find out whether a sample comes from a given probability distribution and whether two samples come from the same distribution. It differs from parametric tests because it does not require a defined variance and mean value for data analysis (**URL 4**). Because of this, it is less precise so it is required to do additional tests. K-S test can be calculated using the equation (**equation 4**):

$$D_n = \frac{sup}{x} \left|F_n(x) - F(x)\right| \quad (4)$$

where are:
n - number of values in series;
sup - distance supremum;
F_n - empirical distribution function;
F - theoretical cumulative distribution function (**Bralić et al., 2022**).

While the empirical distribution function F_n was defined by the equation (**Equation 5**):

$$F_n(x)=\frac{number\ of\ values\ in\ series \leq x}{n}=\frac{1}{n}\sum_{i=1}^{n} 1_{<-\infty,x]}(x_i) \quad (5)$$

where are:

$1_{<-\infty,x]}(x_i)$ - an indicator function whose value equals 1 when $x_i \leq x$, while it equals 0 in other cases.

In addition to qualitative tests, the quantitative QQ diagram (quantile-quantile diagram) is also useful for data analysis, which was defined as a graphical method for comparing two probability distributions (**URL5**). With the QQ diagram, we can check whether the assumption that the data set is normally distributed is correct. A scatterplot is obtained by plotting two sets of quantiles, and a 45-degree reference line is also plotted. If the data set is normally distributed, the points should fall approximately along this reference line. The further the data set is from the normal distribution, the greater the deviation from the reference line. The QQ diagram is only a visual representation of the data, and the assessment itself is subjective, which is why this solution is only an aid to analysis (**URL6**).

Data obtained from previous research in the observed area should be interpolated in order to best understand the details of the exploitation field. The method used for this purpose is called the inverse distance weighting method, which is also the simplest interpolation method, and was often used in statistical procedures. This method assigns corresponding weighting coefficients to the control points depending on their distance from the points of the regular spatial mesh. The distance exponent (Power), that is shown in **tables 5** and **8**, is a weighting parameter that determines how quickly the weight will decrease depending on the distance from the nodes of the spatial mesh. The closer the parameter is to zero, the more similar the resulting display is to a horizontal surface, while larger parameter, results in more elaborate topography of the surface (**Medved et al., 2010**).

networks. With the help of a mathematical expression, the value at the selected points was estimated (**6**):

$$z_{IU} = \frac{\frac{z_1}{d_1^p}+\frac{z_2}{d_2^p}+\cdots+\frac{z_n}{d_n^p}}{\frac{1}{d_1^p}+\frac{1}{d_2^p}+\cdots+\frac{1}{d_n^p}} \quad (6)$$

where are:

z_{IU} - estimated value;
$d_1 \ldots d_n$ - distances of locations 1...n from the assessment site z_{IU};
p - distance exponent;
$z_1 \ldots z_n$ - measured values at locations 1...n.

The number of points is determined by the radius of the circle placed around the test location. The influence of each point is inversely proportional to its distance from the location where the value is estimated, which means that the values that are closer to the points will have a greater influence on the interpolation process. (**Malvić, 2008**).

Table 1: Artificial data of coal layer (in meters), a)

x	1	1	1	2	2	2	2	2	2	2	2	3	3	3	3	3	3	3	3	3	3	4	4	4	4
y	10	6	11	4	5	6	7	8	9	10	11	3	4	5	6	7	8	9	10	11	12	3	4	5	6
Thickness of layers	1	0	0	2	3	5	4	2	1	6	5	1	3	12	8	10	6	8	12	8	0	3	10	14	10
Depth of the roof surface	497	493	498	492	494	500	495	496	496	497	499	492	493	494	501	500	495	495	500	497	501	492	496	500	502
Depth of the bottom surface	498	493	498	494	497	505	499	498	497	503	504	493	496	506	509	510	501	503	512	505	501	495	506	514	512

x	4	4	4	4	4	4	5	5	5	5	5	5	5	5	5	5	6	6	6	6	6	6	6	6	6
y	7	8	9	10	11	12	3	4	5	6	7	8	9	10	11	12	3	4	5	6	7	8	9	10	11
Thickness of layers	18	20	18	15	11	4	4	12	25	18	22	27	25	27	15	6	2	10	28	20	28	32	42	30	16
Depth of the roof surface	500	500	499	501	501	506	492	499	500	503	501	501	500	500	502	502	493	499	500	504	503	501	501	501	503
Depth of the bottom surface	518	520	517	516	512	510	496	511	525	521	523	528	525	527	517	508	495	509	528	524	531	533	543	531	519

x	6	6	7	7	7	7	7	7	7	7	7	7	7	8	8	8	8	8	8	8	8	8	8	9	9
y	12	13	3	4	5	6	7	8	9	10	11	12	13	4	5	6	7	8	9	10	11	12	13	4	5
Thickness of layers	7	2	0	9	28	32	35	45	47	28	25	7	1	6	15	30	42	48	50	49	32	12	1	0	18
Depth of the roof surface	500	497	496	497	500	502	504	505	502	505	501	501	492	496	500	503	506	503	506	505	502	498	498	491	497
Depth of the bottom surface	507	499	496	506	528	534	539	550	549	533	526	508	493	502	515	533	548	551	556	554	534	510	499	491	515

Table 2: Artificial data of coal layer (in meters), b)

x	9	9	9	9	9	9	9	9	10	10	10	10	10	10	10	10	10	11	11	11	11	11	11	11	11
y	6	7	8	9	10	11	12	13	5	6	7	8	9	10	11	12	13	4	5	6	7	8	9	10	11
Thickness of layers	29	38	50	50	22	8	4	2	5	17	42	50	47	43	11	2	1	0	6	27	50	50	50	42	13
Depth of the roof surface	503	507	503	506	504	500	498	500	496	502	502	502	501	503	502	500	501	493	496	501	501	500	501	502	499
Depth of the bottom surface	532	545	553	556	526	508	502	502	501	519	544	552	548	546	513	502	502	493	502	528	551	550	551	544	512

x	11	11	12	12	12	12	12	12	12	12	12	12	13	13	13	13	13	13	13	13	13	13	14	14	14
y	12	13	4	5	6	7	8	9	10	11	12	13	3	4	5	6	7	8	9	10	11	12	3	4	5
Thickness of layers	3	1	10	28	32	48	50	40	38	12	3	0	0	8	7	16	30	24	22	25	22	4	0	5	7
Depth of the roof surface	499	500	497	502	500	500	500	501	498	497	502	497	496	500	501	497	497	499	499	499	496	497	497	500	500
Depth of the bottom surface	502	501	507	530	532	548	550	541	536	509	505	497	496	508	508	513	527	523	521	524	518	501	497	505	507

x	14	14	14	14	14	14	14	15	15	15	15	15	15	15	15	15	16	16	16	16	16	17	17	17	17
y	6	7	8	9	10	11	12	3	4	5	6	7	8	9	10	11	4	5	6	7	8	4	5	6	7
Thickness of layers	8	12	8	9	15	8	2	0	3	6	7	10	5	4	4	2	1	3	3	2	2	1	5	4	1
Depth of the roof surface	496	494	499	500	496	496	496	497	497	496	494	493	499	497	496	494	496	497	493	492	496	495	495	492	492
Depth of the bottom surface	504	506	507	509	511	504	498	497	500	502	501	503	504	501	500	496	497	500	496	494	498	496	500	496	493

3. Results

By performing the S-W and K-S test, total of 750 samples were entered that contain values of depths of top and bottom area, thickness of the deposit and artificial positions of known points. (**Table 1** and **2**) Those tests also showed histograms that describe distribution of values of depths. **Figure 3-1** decribes the data for the top area of the deposit, while **Figure 3-2** displays bottom area. In the histograms, the x axis shows the ranges of the depths, while the y axis represents count of samples that fall within each range.

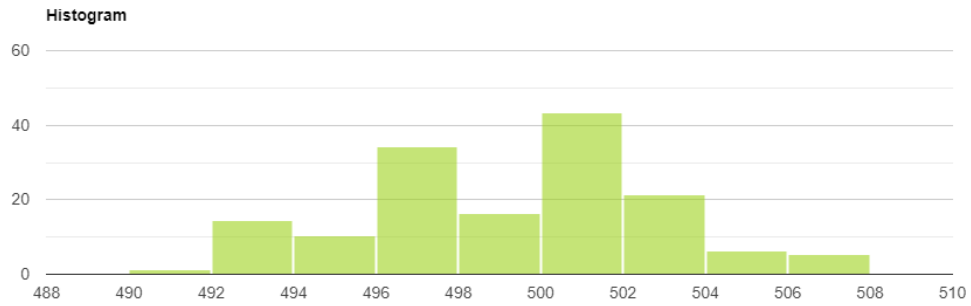

Figure 3-1: Values of depths of top area (**URL7**)

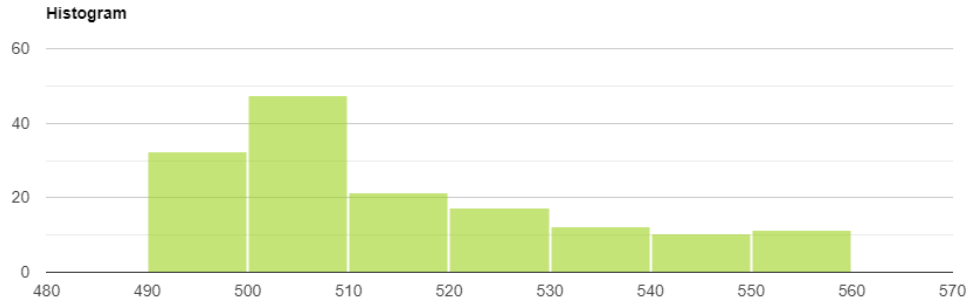

Figure 3-2: Values of depths of bottom area (**URL7**)

Table 3 shows the results of the Shapiro-Wilk test. The initial null hypothesis was that the data are normally distributed. The obtained p-value was 0, also visible from the table (**table 3**), which is a smaller value than alpha (α=0.5). For that reason the null hypothesis was rejected, and it could be concluded that the data were not normally distributed.

Table 3: Presentation of Shapiro-Wilk test results

P-value	<0.001
W	0.66
Number of samples	750
Average	290.33
Median	15
Sample standard deviation (S)	243.41
Skewness	0.41

Due to the amount of alpha (α=0.05), the S-W test allows 5% deviation of the data, and since the p-value was less than α, the data significantly deviate from a normal distribution. The same could be seen with observing the test statistic (W), which was valued at 0.6602. In S-W test, the test statistic (W) close to 1 is desirable, so its obtained value confirmed deviation from the normal distribution.

In the Kolmogorov-Smirnov test, the null hypothesis was also rejected because the obtained p-value was lower than alpha. The test statistic D representing the deviations between the empirical and the theoretical relative cumulative frequency was equal to 0.34. Similar to the S-W test, the test statistic D serves as a confirmation for deviation from the normal distribution, which was also seen with the derived value of 0.34. (**Table 4.**). Also, in **Figure 3-3**, the curve obtained by K-S test is shown, which can be compared with **Figure 2-1** for a better understanding of the results, and how far they deviate from the normal distribution.

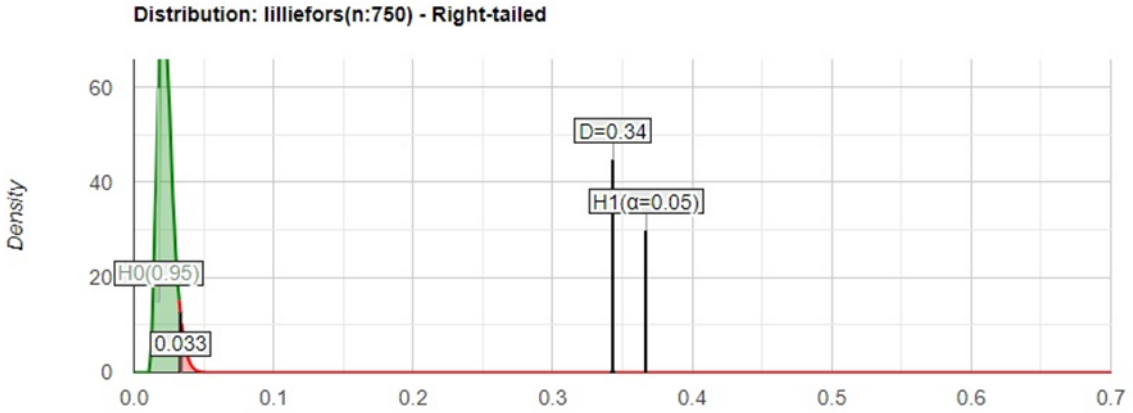

Figure 3-3: Display of the curve obtained by the K-S test (**URL7**)

Table 4: Displaying the results of the Kolmogorov-Smirnov test

P-value	<0.001
D	0.34
Number of samples	750
Average	209.23
Median	15
Sample standard deviation (S)	243.41
Skewness	0.41
K	9.41

Also, a QQ plot can graphically display the dispersion of results. This graphic representation can be obtained with the formula for calculating the quantiles of the entered data (from the **Tables 1** and **2**). Since the points do not follow the blue reference line, it could be concluded that the data do not come from the same distribution and that the assumption of a normal data distribution is wrong (**Figure 3-4**)

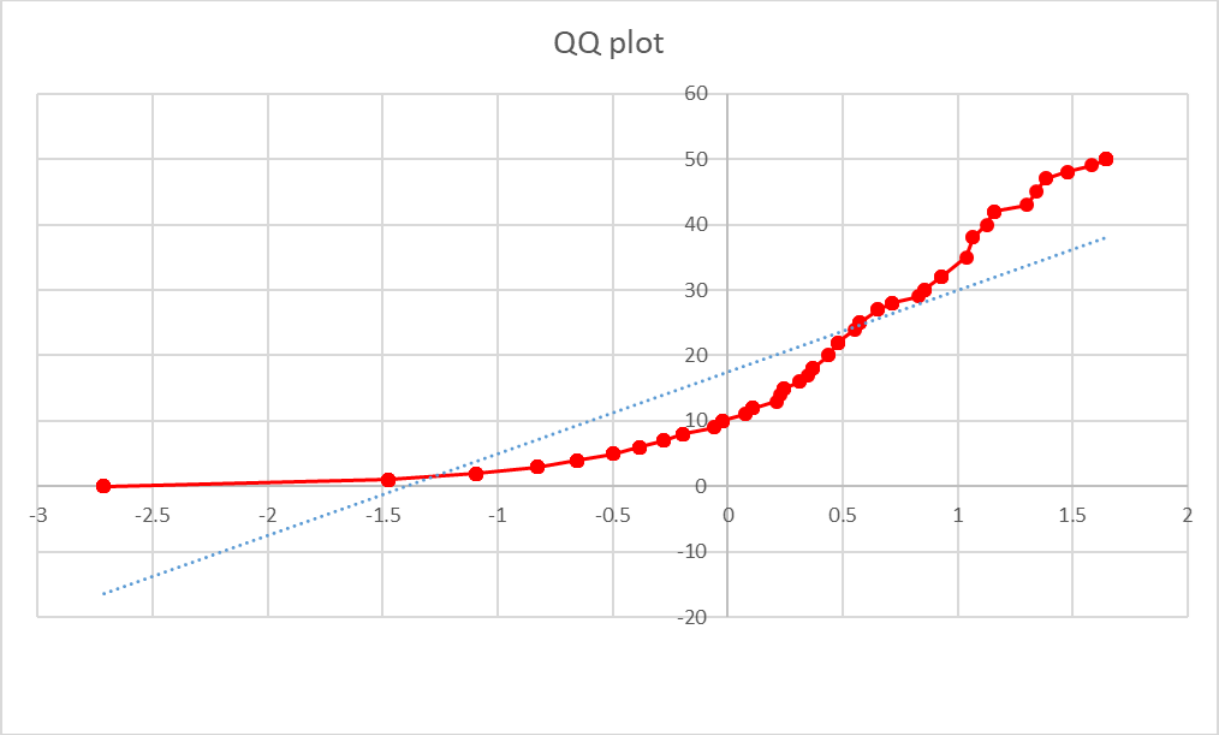

Figure 3-4: Display of QQ diagram (**URL7**)

Using the Surfer 8 program, x and y data, depth of the top and bottom, were entered. The inverse distance method was used for interpolation. The obtained results provide a basic statistical analysis, the size of the network and the number of nodes, which can be seen in **Tables 5**, **6**, **7** and **8**. Limits of the different depth values must be clearly seen, which is why in this paper the distance exponent value equals 2, which shows the simplest form of the map due to properly rounded lines. The map was displayed through 63 rows and 100 columns, which, due to the ratio of the map, shows all the given values of the depths.

Table 5: Data for the top area

Weighting power	2
Smoothing power	0
Anisotropy ratio	1
Anisotropy angle	0
Grid size	63 rows and 100 columns
Total nodes	6300

Table 6: Basic statistical analysis for top area

	x	y	z
Minimum	1	3	491
25%-tile	5	5	496
Median	9	8	500
75%-tile	13	10	501
Maximum	17	13	507
Average	8.83	7.83	498.77
Standard deviation	4.38	2.87	3.54
Variance	19.18	8.26	12.54

Table 7: Basic statistical analysis for bottom area

	x	y	z
Minimum	1	3	491
25%-tile	5	5	501
Median	9	8	509
75%-tile	13	10	527
Maximum	17	13	556
Average	8.83	7.83	514.75
Standard deviation	4.38	2.87	17.95
Variance	19.18	8.26	322.25

Table 8: Data for bottom area

Weighting power	2
Smoothing factor	0
Anisotropy ratio	1
Anisotropy angle	0
Grid size	63 rows and 100 columns
Total nodes	6300

In the Surfer 8 program, maps of the depth of the top and bottom were created. A darker color represents smaller depth, while a lighter color represents deeper surfaces. **Figure 3-5** shows a map of the depth of the top, while **Figure 3-6** shows a map of the depth of the bottom.

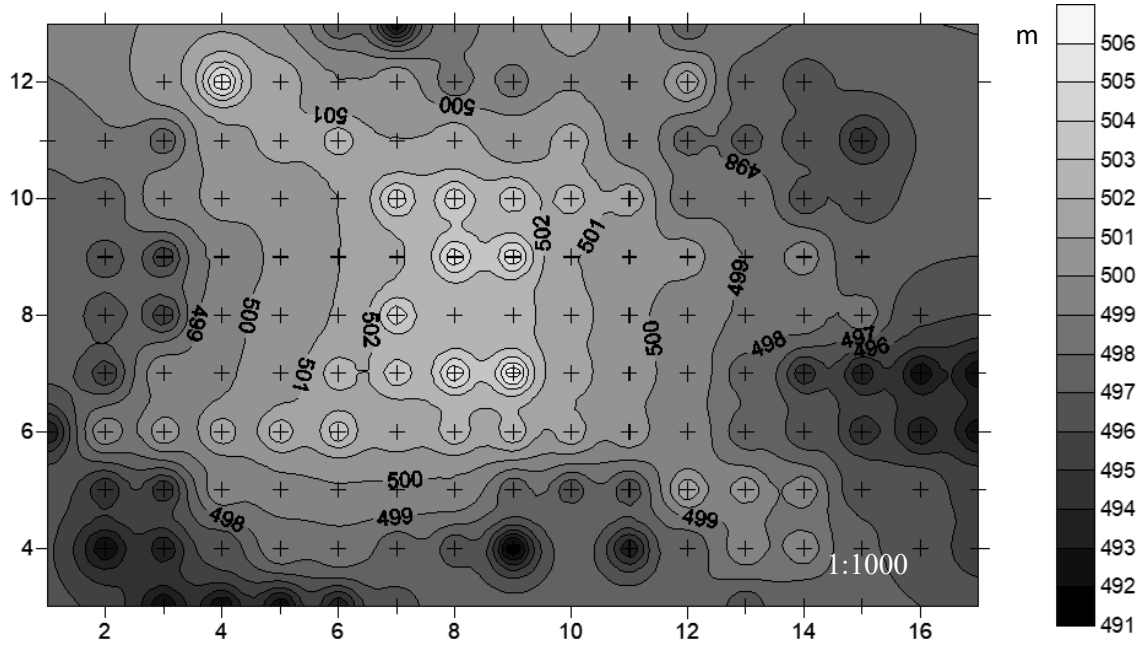

Figure 3-5: Map of the relative depth of the top area

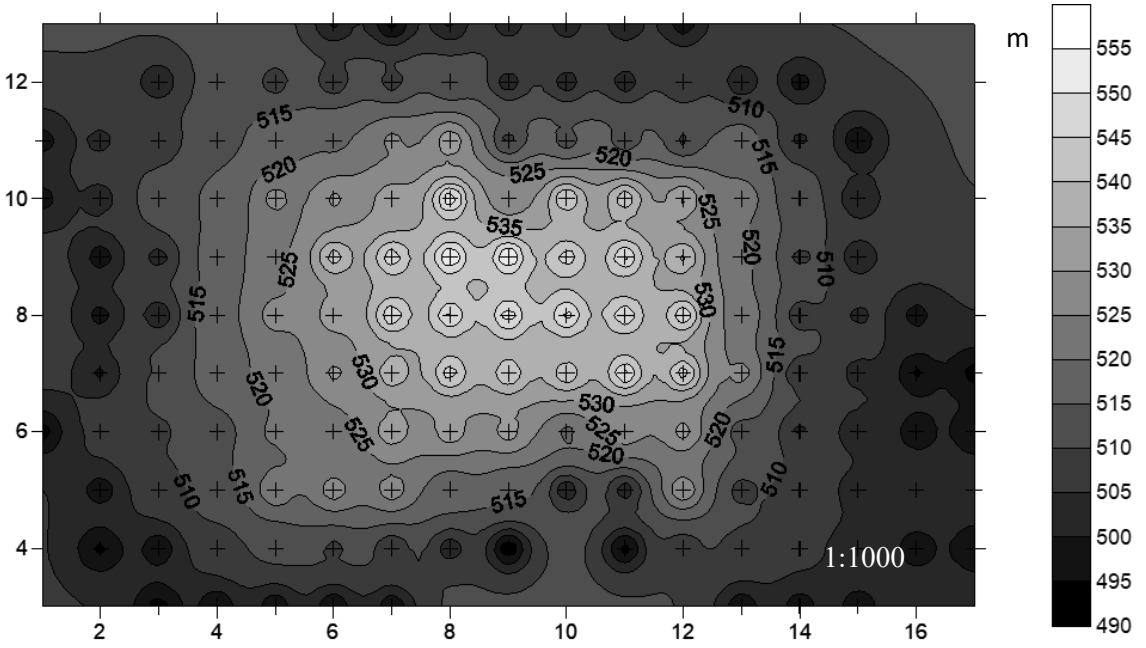

Figure 3-6: Map of the relative depth of the bottom area

4. DISCUSSION AND CONCLUSIONS

Testing for normal distribution was performed using the Shapiro-Wilk, Kolmogorov-Smirnov and QQ plot tests. The inverse distance interpolation method was used when creating the depth map of the top and bottom. The results of the Shapiro-Wilk test showed that the data were not normally distributed because the obtained p-value was less than alpha, which rejects the initial null hypothesis. The coefficient of skewness is 0.4109 and shows an asymmetric curve where most of the data is on the left side, which does not match the Gaussian normal distribution curve. The results of the Kolmogorov-Smirnov test show a p-value less than alpha, which also rejects the null hypothesis that the data are normally distributed, and the coefficient of skewness is equal to the coefficient of skewness as in the Shapiro-Wilk test. Graphical data analysis was performed with the help of QQ diagram. The data were analyzed according to a reference line with a slope of 45°, the trend of which the data should follow, however, the obtained QQ diagram shows a deviation, so it can be concluded that it is not a normal distribution.

The inverse distance method was used because it is cosidered to be one of the most simple method of interpolation as it is originally an exact interpolator, which means that it keeps the input data values fixed even during interpolation. Due to the relatively simple algorithm, speed in the calculation is significant, so for smaller data sets, all available inputs can be used when interpolating (**Medved et al., 2010**).

The reason for using three different methods for the same data set is to eliminate the flaws of each separate test and thus we can get a more realistic interpretation of that data set.

The inverse distance method was used to obtain maps which resulted in variance values, and for the top it was 12.5, and for the bottom 322.3. This confirms the shape of the syncline due to the large mutual difference. Also, taking into account the large value of the variance of the subsurface, it can be concluded that the depths on the bottom differ quite a bit, and that is precisely why the data did not pass the normal distribution tests. It is precisely this dispersion of data on the bottom area and the shape of the syncline of the coal layer that can be observed on the resulting maps of the depth of the top and bottom areas, where the lighter color shows greater and the darker color smaller depths. The map was made according to the ratio of anisotropy of 1 and the angle of anisotropy 0. These coefficients define the shape that encloses the boundaries of the depths. In our maps these boundaries are in the shape of the circle, rather than ellipse because of the proper distribution of data around the chosen points.

All conducted research provided a large amount of data on the mentioned layer, which was successfully described using statistical methods and mapping. If the normal distribution of the measured data is proven by the implemented statistical methods, the behavior of the layer on its unexplored parts can be easily concluded, and mapping results are more reliable. In the case of imaginary coal seam in Siverić, where normal distribution is not proven, with auxiliary statistical analyses it was still possible to obtain a large amount of data which can greatly help with reducing costs and high time consumption of research. So, it can be concluded that all analysis of the data carried out in this paper could be very helpful.

5. References

1. BRALIĆ, N., MALVIĆ, T. (2022): Interpretation of chemical analyses and cement modules in flysch by (geo)statistical methods, example from the southern Croatia. Processes 2022, 10(5), 813, pg. 2, 8-9 p.
2. MALVIĆ, T. (2008): Primjena geostatistike u analizi geoloških podataka (*Application of geostatistics in the analysis of geological data*). Udžbenici Sveučilišta u Zagrebu. Zagreb (*in Croatian, without English abstract*), 16-18 p
3. MALVIĆ, T., MEDUNIĆ, G. (2015): Statistika u geologiji *(Statistics in geology).* Udžbenici Sveučilišta u Zagrebu. Zagreb *(in Croatian, without English abstract),* 12 p
4. MEDVED, I., PRIBIČEVIĆ B., MEDAK, D., KUZMANIĆ, I. (2010.) Usporedba metoda interpolacije batimetrijskih mjerenja za praæenje promjena volumena jezera (*Comparison of bathymetric interpolation methods measurements to monitor lake volume changes)* Geod. list 2010, 2, 71–86, Zagreb *(in Croatian, with English abstract),* 74-75 p
5. PFAFF, S., (2012): Osnove statistike (*Basics of statistics*). Zagreb: Element. (*in Croatian, without English abstract*), 23 p
6. ZUPANIČ, J., BABIĆ, LJ., (2011): Sedimentary evolution of an inner foreland basin margin: Palaeogene Promina Beds of the type area, Mt. Promina *(Dinarides, Croatia)* 102 p

Internet sources:

1. URL 1: https://www.enciklopedija.hr/clanak/63913 (accessed 18th January 2024)
2. URL 2: https://www.enciklopedija.hr/natuknica.aspx?ID=21410 (accessed 9th January 2024)
3. URL 3: https://builtin.com/data-science/shapiro-wilk-test (accessed 12th January 2024)
4. URL 4: https://www.itl.nist.gov/div898/handbook/eda/section3/eda35g.htm (accessed 20th January 2024)
5. URL 5: https://www.itl.nist.gov/div898/handbook/eda/section3/qqplot.htm (accessed 18th January 2024)
6. URL 6: https://library.virginia.edu/data/articles/understanding-q-q-plots (accessed 18th January 2024)
7. URL 7: https://www.statskingdom.com/shapiro-wilk-test-calculator.html (accessed 12th January 2024)

SAŽETAK

Statistička analiza i kartiranje metodom inverzne udaljenosti zamišljenog sloja ugljena, jednostavna studija slučaja preporučenih metoda

Za ispravno opisivanje ležišta mineralnih sirovina u svrhu eksploatacije potrebna je velika količina geoloških podataka o navedenom ležištu. U slučaju podzemne eksploatacije povećava se količina potrebnih podataka, a sama istraživanja su složenija. Ovaj rad opisuje zamišljeni ugljeni sloj koristeći simulirane podatke i rezultate primarnog istraživanja. Navedeni sloj ugljena nalazi se duboko ispod površine, što otežava dobivanje potrebnih podataka, zbog čega je potrebna pravilna prostorna analiza. Za mjerenje prostorne raznolikosti mjerenim uzorcima, primjenjuju se statističke metode istraživanja, a rezultati se opisuju prema nesigurnosti procijenjenih točaka ili blokova. Također je potrebno promotriti vrstu distribucije podataka, za što su korišteni Shapiro-Wilkov, Kolmogorov-Smirnovljev test i QQ dijagram, koji se međusobno nadopunjavaju. Za izradu karata i interpolaciju podataka korištena je metoda inverzne udaljenosti, a sam cilj rada je dobiti pouzdane analitičke rezultate te pokazati skup metoda za brz i pouzdan prikaz 2D karata ležišta. Postizanjem tog cilja, moguće je smanjiti troškove te vrijeme istraživanja. Sva provedena istraživanja dala su veliku količinu podataka o navedenom sloju koji je uspješno opisan statističkim metodama.

Ključne riječi: ugljeni sloj; normalna distribucija; nul-hipoteza; analiza podataka

Acknowledgment

This research is made under motivation of Tomislav Malvić, tenure Full Professor on University of Zagreb, Faculty of Mining, Geology and Petroleum Engineering, whose knowledge on geostatistics has made vast contribution.

Author's contribution

Mirta Petrović (graduate student) has contributed with a description of research goal mentioned in abstract as well as in introduction. In her involment in this research, she described methods that were used for the interpretation. **Ana Ljubić** (graduate student) provided and edited results obtained from Surfer 8 program, in written and graphic form, while designing the maps, as well as conveying discussion and conclusions, were done by both authors.